Investigation of the Effects of
Non-Thermal Plasma and Microwaves
on Mordenite

by

Alice May Halman

A thesis submitted in partial fulfilment for the requirements for the degree of
Doctor of Philosophy at the University of Central Lancashire

February 2020

STUDENT DECLARATION FORM

Type of Award

        Doctor of Philosophy

School

        Forensic and Applied Sciences

1.   Concurrent registration for two or more academic awards

I declare that while registered as a candidate for the research degree, I have not been a registered candidate or enrolled student for another award of the University or other academic or professional institution

2.   Material submitted for another award

I declare that no material contained in the thesis has been used in any other submission for an academic award and is solely my own work

3.   Collaboration

Where a candidate's research programme is part of a collaborative project, the thesis must indicate in addition clearly the candidate's individual contribution and the extent of the collaboration. Please state below:

N/A

4.   Use of a Proof-reader

No proof-reading service was used in the compilation of this thesis.

Signature of Candidate: _____A Halman_____

Print name: ___ALICE HALMAN_____

i

ABSTRACT

Zeolites constitute a multi-billion pound industry, with no indication of diminishing in value. Preliminary studies at the University of Central Lancashire discovered that the regeneration of a sample of coked mordenite via microwave plasma extended the catalytic life of the zeolite when used in the toluene disproportionation reaction. As a joint-venture between the University of Central Lancashire and Johnson Matthey, this research was designed with the purpose of investigating the effects of microwaves and plasma to determine whether they could be used as novel methods of zeolite modification.

The application of microwaves in synthetic zeolite chemistry is well established, however the application of microwaves for post-synthesis modification of zeolites is much more limited. Microwave regeneration has been reported to display higher efficiencies and reduced regeneration times compared to conventional regeneration. However, there are, to this author's knowledge, no studies performed on the regeneration of coked zeolites using microwaves. Dealumination of zeolites using microwaves is also very limited, with results reporting faster dealumination rates and a more pronounced decrease in crystallinity compared with conventional methods.

The application of plasma in zeolite chemistry is limited to zeolite calcination, regeneration and surface modification. Plasma regeneration of a coked zeolite is, to this author's knowledge, limited to a single study, where focus was on removing the carbon. There are limited studies on the effect of plasma on zeolite acidity. Results suggest plasma can be used to increase the density of Brønsted acid sites, which can alter product selectivity within a reaction.

This research investigated the effects of microwaves and plasma on the zeolite mordenite. Microwaves, microwave plasma and dielectric barrier discharge plasma were applied to samples of virgin and coked mordenite. Using toluene disproportionation as the probe reaction, changes in catalytic activity were observed. Characterisation methods including pyridine and collidine infrared studies, ammonia temperature programmed desorption and solid state nuclear magnetic resonance were used to explain the changes in catalytic activity. Results showed microwave plasma regeneration extended the catalytic life of mordenite due to the destruction of Brønsted

acid sites caused by dealumination, without loss of crystal structure. Whilst the loss of Brønsted acid sites was also seen in microwave treated mordenite and microwave plasma treated virgin mordenite, it was accompanied by the loss of catalyst crystallinity.

These results have shown that microwave plasma can be used to fully regenerate coked mordenite and can dealuminate the sample without loss of catalyst crystallinity. In the toluene disproportionation reaction, this reduces the amount of cracking which occurs, subsequently leading to less coke deposition and therefore an extended catalytic life.

TABLE OF CONTENTS

ACKNOWLEDGEMENTS

LIST OF TABLES

LIST OF FIGURES

LIST OF EQUATIONS

ABBREVIATIONS

BAS	Brønsted Acid Sites
BET	Brunauer, Emmett and Teller
BTX	Benzene, Toluene and Xylene
B/X	Benzene to Xylene Ratio
CCD	Charge Coupled Device
DBD	Dielectric Barrier Discharge
DCM	Dichloromethane
EFAL	Extra-framework Aluminium Species
FCC	Fluid Catalytic Cracking
FINA	Petrofina
GC	Gas Chromatography
GC-MS	Gas Chromatography Mass Spectrometry
HF	Hydrogen Fluoride
h-peak	High Temperature Peak
IR	Infrared Spectroscopy
JM	Johnson Matthey
LAS	Lewis Acid Sites
l-peak	Low Temperature Peak
MAS	Magic Angle Spinning
MS	Mass Spectrometry
MSTDP	Mobil Selective Toluene Disproportionation Process

MTPX	Mobil Toluene to ParaXylene
MTP-3	Mobil Toluene Disproportionation Process Version 3
m-Xylene	*meta*-Xylene
MW	Microwave Heating
MWP	Microwave Plasma
MWPR	Microwave Plasma Regeneration
m/z	Mass to Charge Ratio
NH$_3$ TPD	Ammonia Temperature Programmed Desorption
NMR	Nuclear Magnetic Resonance
o-Xylene	*ortho*-Xylene
p-Xylene	*para*-Xylene
Si/Al	Silicon to Aluminium Ratio
ssNMR	Solid State Nuclear Magnetic Resonance
STP	Standard Temperature and Pressure
TDP	Toluene Disproportionation
T.E.	Thermodynamic Equilibrium
TGA	Thermogravimetric Analysis
UCLan	University of Central Lancashire
UOP	Universal Oil Products
XPS	X-ray Photoelectron Spectroscopy
XRD	X-ray Diffraction

CHAPTER 1: INTRODUCTION

1.1. BACKGROUND TO THE STUDY

Zeolites constitute a multi-billion pound industry, with no indication of diminishing in value (1). Preliminary studies at the University of Central Lancashire (UCLan) discovered that the regeneration of a sample of coked mordenite via microwave plasma extended the catalytic life of the zeolite when used in the toluene disproportionation reaction. As a joint-venture between UCLan and Johnson Matthey (JM), this research was designed with the purpose of investigating the effects of microwaves and plasma to determine whether they could be used as novel methods of zeolite modification.

The primary focus of this research was to understand the cause of the extended catalytic life produced upon microwave plasma regeneration. The application of microwaves in the regeneration of zeolites has been performed (2-4), reportedly achieving higher efficiencies, reduced regeneration times and requiring less energy. However, reports of microwave regeneration of coked zeolites have, to this author's knowledge, not been published. This is also true of microwave plasma. Whereas limited studies of regeneration of coked zeolites have been performed using other types of plasma (e.g. glow discharge, dielectric barrier discharge), the results were focused on achieving 100 % coke removal (5) or as a tool for identifying the type of coke formed during a reaction (6). If any modifications to the zeolites were seen, they were not reported.

To understand the cause of the extended catalytic life seen from microwave plasma regeneration of a sample of coked mordenite, this research explores other novel methods of regeneration including microwave heating and dielectric barrier discharge plasma. It links the source of reduced coking to changes seen in the structural and/or acidic properties of the regenerated catalyst samples. It then extends the study to the pre-treatment of mordenite by microwave heating, dielectric barrier discharge plasma and microwave plasma. Finally, the research

concludes with a preliminary study of microwave plasma optimisation, specifically the effect of increasing the input microwave power.

1.2. AIMS

This research will address:

(1) The regeneration of mordenite, coked during the toluene disproportionation reaction, via novel methods involving microwaves, microwave plasma and dielectric barrier discharge plasma

(2) The pre-treatment of mordenite, via novel methods involving microwaves, microwave plasma and dielectric barrier discharge plasma

(3) The investigation of optimising microwave power input during microwave plasma regeneration of mordenite, coked during the toluene disproportionation reaction.

1.3. LAYOUT OF THE THESIS

As described above, this thesis investigates the effects of microwaves and plasma on the zeolite mordenite, to explore their potential for zeolite regeneration and pre-treatment, as well as probing the possibility for optimisation of these processes. The effects of which are measured via catalyst characterisation techniques and the impact on the activity of the zeolite in the probe reaction, toluene disproportionation. As such, the thesis is divided into 12 chapters.

Chapters 1-3 aim to introduce the reader to the subject matter and current research. **Chapter 4** is a description of the methods and techniques used in this research. **Chapters 5-10** are the results and discussion chapters, separating regeneration (**Chapters 5-6**), pre-treatment (**Chapters 7-8**), and modification of power **(Chapters 9-10)** into three parts. **Chapter 11** consists of an overall discussion, bringing together all the findings from this research, before **Chapter 12** explores where these new discoveries might lead to next.

1.4. REFERENCES

(1) Acumen Research and Consulting. Zeolite Catalysts Market. 2019; Available at: https://www.acumenresearchandconsulting.com/press-releases/zeolite-catalysts-market. Accessed 7/19, 2019.

(2) Polaert I, Ledoux A, Estel L, Huyghe R, Thomas M. Microwave Assisted Regeneration of Zeolite. International Journal of Chemical Reactor Engineering 2007;5:1-10.

(3) Piunchukova NA, Voloshko AY, Baumer VN, Shishkin OV, Chebanov VA. The use of Microwave Irradiation for Zeolite Regeneration in a Continuous Ethanol Dewatering Process. Chemical Engineering and Processing: Process Intensification 2015;95:151-158.

(4) Chowdhury T, Shi M, Hashisho Z, Kuznicki SM. Indirect and Direct Microwave Regeneration of Na-ETS-10. Chemical Engineering Science 2013;95:27-32.

(5) Khan MA, Al-Jalal AA, Bakhtiari IA. 'Decoking' of a 'Coked' Zeolite Catalyst in a Glow Discharge. Analytical and Bioanalytical Chemistry 2003;377(1):89-96.

(6) Bibby D, Milestone NB, Patterson JE, Aldridge LP. Coke Formation in Zeolite ZSM-5. Journal of Catalysis 1986;97:493-502.

CHAPTER 2: LITERATURE REVIEW

2.1. CATALYSIS

2.1.1. Introduction

The first use of the term catalysis is often attributed to the Swedish chemist Berzelius, who in 1835 described it as the decomposition of chemical bodies by a "catalytic force" (1). It was almost 60 years later before Ostwald provided the more familiar definition of "the acceleration of a slow chemical process by the presence of a foreign material" (2). Today we understand this "foreign material" is a catalyst, and the acceleration of a slow, or even thermodynamically improbable reaction is achieved by reducing the activation energy via chemical interactions with the reactants (3). Ideally, the catalyst is not consumed within the reaction, but is instead restored to its original state after each catalytic cycle, whereby small amounts will catalyse large quantities (2). More than 90 % of chemical industry production is based on catalysis (3).

2.1.2. Heterogeneous Catalysis

Catalysis is often categorised by the form the catalyst takes compared to the reactants it is transforming. When catalyst and reactants take the same state (i.e. liquid, solid or gas) as the reactants, it is referred to as homogeneous catalysis. Heterogeneous catalysis is where the states of catalyst and reactants differ (i.e. gas-solid, liquid-solid, or liquid-gas).

Where heterogeneous catalysis involves a solid catalyst, the reaction takes place on the catalyst surface, therefore large surface areas are likely to improve efficiency. Porous materials are particularly interesting as, despite their typically large surface areas, the catalytic active sites may include pores and exterior surfaces, or may be restricted to the outer surface, depending on transport limitation of the reactants and products (2). Fundamentally, catalysis can be reduced to the interaction of reactants with the active centre of the catalyst (3). Heterogeneous catalysis can be described as a three-step process: (i) substrate adsorption, (ii) catalytic reaction, (iii) product desorption (2).

2.1.3. Zeolites

Zeolites are 3-dimensional microporous crystalline alumino-silicate structures. Built from tetrahedral aluminium and silicon building blocks bridged via oxygen atoms, their framework comprises of a 3-dimensional network of channels, intersections and cavities, with a pore diameter often comparable to the cross-section of molecules (4,5). The structure of each zeolite (formula given in Equation 2.1.) is unique, with a variety of channel, intersection and cavity sizes, providing the basis of their shape-selectivity and leading to their identity as molecular sieves (2). In 2007 there were 176 discrete zeolite frameworks which had been identified (6), with new structures being reported every year, including three new frameworks (AVE, SOV, PWN) in April of 2019 (7). These should not be confused with zeotypes. Whilst characteristically similar, zeotypes are formed from the incorporation of alternative atoms, e.g. phosphorus or gallium; producing structures such as aluminophosphates or gallosilicates (4).

Equation 2.1. - Structural Formula of a Zeolite

$$xM_{2/n}O.xAl_2O_3.ySiO_2.wH_2O$$
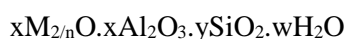
Where:	M	is a group I or II cation
	n	is the valence of the cation
	w	is the water contained in the zeolite voids

Zeolites are derived from the incorporation of aluminium into a silicate (SiO_4) framework by replacement of the silicon atoms (3). As aluminium is tetrahedrally co-ordinated, it is electron deficient, and thus creates a negatively charged framework. In order to balance this charge, readily exchangeable cations are present, and where these are exchanged by hydrogen atoms, it leads to the formation of Brønsted acid sites (2). Therefore, the number of acid sites generated is equal to the number of Al^{3+} ions, with their strength dependent on the type of framework and number of sites (3).

The tetrahedra may be linked to different structural frameworks, producing zeolites of different shapes and sizes, which by careful control can lead to specifically designed shape-selectivity.

Furthermore, by careful control of the chemical composition of the framework and exchangeable ions, zeolites of specific acid site strength and distribution can be produced (3). With that said, there are limitations on the degree of control permitted during zeolite modification or synthesis as dictated by Löwenstein's rule. Löwenstein's rule states that where oxygen bridges two tetrahedral species, only one of the centres can be aluminium; the other can be silicon or a similarly small ion with a valence ≥4 (8). Should oxygen possess two aluminium ion neighbours, at least one aluminium requires a coordination number greater than 4. This limits the silicon-to-aluminium ratio (Si/Al) of a zeolite to ≥1. Dempsey (9) attributed Löwenstein's rule to instability in the formation of Al-O-Al due to electrostatic effects; where aluminium ions assume positions as far from each other as possible. Whilst Löwenstein's rule holds true in most cases, the formation of non-Löwensteinian distributions in sodalite materials have been published, albeit under high temperatures (10).

2.1.4. Zeolite Acidity

If a zeolite only contained SiO_2 tetrahedral units, the material would be electrically neutral and possess no acidity on its surface. The Brønsted acidity of zeolites arises from the substitution of the Si^{4+} with the isomorphic trivalent Al^{3+}, and the resulting formation of a negative charge in the lattice which is compensated by a proton. The proton is attached to an oxygen atom connected to neighbouring silicon and aluminium atoms, forming what is referred to as a bridging hydroxyl group and is the site responsible for the Brønsted acidity of zeolites (4,11) (Figure 2.1.).
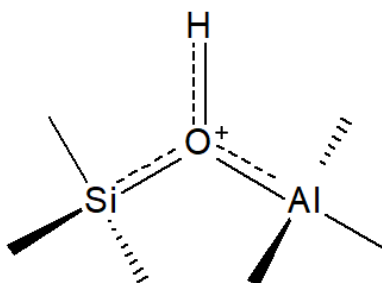
Figure 2.1. - Zeolite Brønsted Acid Site

In synthesised zeolites, the negative charge present on the Al-substituted framework is compensated by organic and inorganic alkaline cations. As a consequence, these zeolites possess no Brønsted acidity. However, the application of zeolites as catalysts often requires the acidic form of the zeolite. Therefore, to produce acidic zeolites, calcination (thermal treatment) is required to remove any organic cations and the alkaline cations are removed via ion exchange followed by calcination. The ion exchange is typically carried out using ammonium or lanthanum ions (Figure 2.2) (12). Consequently, the Brønsted acidity of a zeolite catalyst will depend on the framework silicon-to-aluminium ratio. Theoretically by careful control of the Si/Al, it should be possible to prepare a zeolite with a specific acid strength required for a given reaction. However, one drawback is that during zeolite treatments, e.g. activation, regeneration etc., dealumination can occur, generating extra-framework aluminium species and altering the Si/Al ratio (4).

$$NH_4^+ + Na^+ Z^- \xrightarrow[-Na^+]{} NH_4^+ Z^- \xrightarrow[-NH_3]{\Delta} H^+ Z^- \qquad (a)$$

$$[La(H_2O)_n]^{3+} + 3Na^+ Z^- \xrightarrow[-3Na^+]{} [La(H_2O)_n]^{3+} Z^- \qquad (b)$$

$$\xrightarrow[-(n-2)H_2O]{\Delta} [(LaOH)(H_2O)]^{2+} H^+ (Z^-)_3$$

$$\xrightarrow{} [(LaOH)_2]^+ (H^+)_2 (Z^-)_3$$
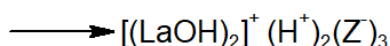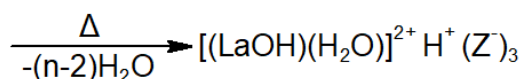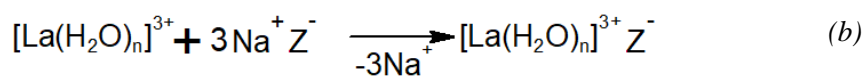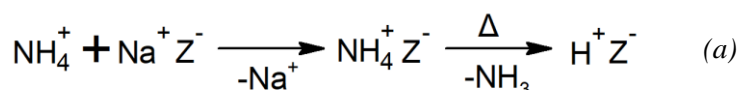
Figure 2.2. - Reaction Schemes of (a) Ammonium Ion Exchange; (b) Lanthanum Ion Exchange
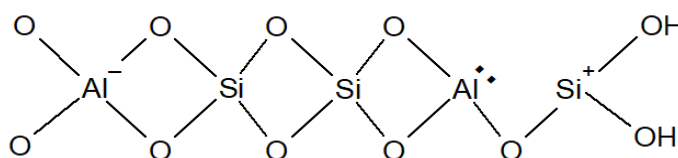
Figure 2.3. - Proposed Framework Lewis Acid Site

Both Bronsted and Lewis acid sites occur in zeolites, however there has been some debate on the nature of how Lewis acid sites arise. The simplest explanation for the production of Lewis acid sites is the dehydroxylation of Brønsted acid sites, creating framework Lewis acid sites via the formation of positively charged tri-coordinated silicon (13) (Figure 2.3.). However, it was reported that after the dehydroxylation of Brønsted acid sites, the silicon remained tetra-

coordinated (12). From this it was suggested that Lewis acid sites arise from unsaturated extra-framework aluminium species, formed by cation exchange or steaming, including species such as $Al(OH)_2^+$, $Al(OH)^{2+}$ and Al^{3+} (14-16).

Catalytic activity in zeolites was widely understood to be attributed to Brønsted rather than Lewis acidity (12). However, reports have emerged claiming that a synergistic interaction occurs between Brønsted and Lewis acid sites, which enhances zeolite acidic activity (16). This was also reported to occur in the toluene disproportionation reaction (17). Nevertheless, the nature of this remains an area for discussion.

Two prominent theories exist: (i) Lewis acid sites directly participate in the reaction (16), and (ii) there is an electron density transfer from Brønsted to Lewis acid sites, increasing the acid strength of Brønsted acid sites (16,18,19), forming what has been referred to as 'super acid' sites (18).

Research in this area is ongoing and it is apparent that although extra-framework aluminium will affect each different reaction individually, there are some common features. The effects of Lewis acid sites on toluene disproportionation has been studied using ZSM-5 (15,20) and HY (17,21) modified zeolites. In the modified ZSM-5 study (15), the increase in Lewis acid sites led to an increase in *p*-xylene selectivity, attributed to a decrease in the zeolite inner volume. In another modified ZSM-5 study (20) however, no significant effect of Lewis acid sites on toluene disproportionation was seen. In the HY zeolite studies, the modified zeolite removed the activation period seen in the unmodified zeolite, allowing the reaction to proceed immediately (17). An increase in initial conversion was also reported (21). However, in all four studies, the increased presence of Lewis acid sites elevated the deactivation rate via coking and promoted dealkylation as a by-product. Similar side effects were also reported in Lewis acid site studies of other zeolite-catalysed reactions including *m*-xylene transformation (22), and ethylene alkylation (16).

Studies focusing solely on Lewis acid sites are scarce, and where an attempt has been made, it was unsuccessful (21). Further research is required to demonstrate the impact of Lewis acid sites on acid-catalysed reactions. However, current knowledge suggests that increasing the

concentration of Lewis acid sites possesses the disadvantages of increasing catalyst deactivation and side reactions, outweighing the benefits of a slight increase in selectivity or initial activity.

2.1.5. Zeolites Within Industry

The application of zeolites as industrial catalysts developed heavily after the production of synthetic zeolites had been realised, ca. 1948-1955 (12). One of the largest impacts being the application of synthetic faujasites in fluid catalytic cracking (FCC) of heavy petroleum distillates in 1963. In recent years, FCC still makes up over half of the zeolite application within industry (23,24), with other applications for zeolites including isomerisation and transalkylation of aromatics (5,23). The development of using zeolites for toluene disproportionation is discussed in Chapter 3.

The added value to industrial processes from the use of early synthetic zeolites, by increasing activity and product yields, remains a focus in modern development of novel zeolite catalysts. Therefore, it is unsurprisingly to find that today's global market predicts an increase of 4.8 % in zeolite catalysts by 2025 with an expected market value of over £6 billion (25).

2.1.6. Mordenite

Mordenite zeolites are important catalysts for many industrial applications, including alkylation, transalkylation and disproportionation reactions (26,27). As such, it is the catalyst of choice used within this research. Mordenite is a naturally occurring zeolite, consisting of 8- and 12- membered oxygen containing rings with pore openings of 2.6 x 5.7 Å and 6.5 x7.0 Å, respectively (Figure 2.4) (5). The chemical structure for mordenite is given as:

Equation 2.2. - Structural Formula of Mordenite (6)

$$Na_8[Al_8Si_{40}O_{96}] \cdot 24H_2O$$
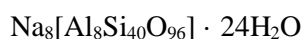
Despite its dual pore system, it is often considered as a one-dimensional large pore zeolite, with a single 12-membered oxygen containing ring channel. This is a result of the 8-membered oxygen containing ring often being too small to transport most molecules and therefore referred to as a "side pocket" (26,28). As such, the transport of molecules within the zeolite can only occur along

the c axis, therefore making this type of zeolite highly susceptible to pore blockage via coking (2,26).
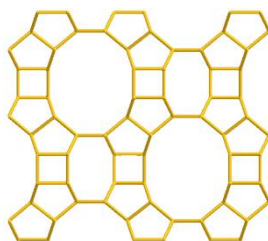
Figure 2.4. - Structure of Mordenite Viewed Along the c Axis (102)

2.1.7. Catalytic Deactivation

Catalyst deactivation is the process by which catalytic activity is reduced over time during a reaction. Deactivation can be a lengthy process, where the catalyst remains active for many years, or a rapid one, where the catalyst lasts minutes or even seconds (29). The nature of the deactivation may be chemical, physical or thermal, each proceeding via numerous mechanisms. However, it is often categorised into poisoning, coking, sintering and phase transformation (30).

Poisons are species (often reactant impurities) present within the reaction system, which chemically bond to the catalyst. Deactivation occurs as the poison directly competes with the reactants for active sites, and when bound, they can alter the reactivity of nearby sites, reducing the absorptivity of the reactants (30). Sintering is the structural modification of the catalyst, caused by high temperatures and results in the reduction of active surface area (30,31). In supported metal catalysts, this occurs via the formation of larger, more stable crystallites from the migration of metal atoms in smaller crystallites. Typically, a metal begins to sinter at a temperature half of its melting point (32). Phase transformation can be considered as a severe form of sintering, whereby very high temperatures transform crystal phases from one form into another, leading to the collapse of the crystal structure, and a decrease in active surface area (30,32). The fourth category, coking is the mechanical deposition of carbonaceous material (commonly referred to as 'coke'), formed from hydrocarbon side reactions (30,31). It is the method by which mordenite is known to deactivate during the toluene disproportionation reaction (33).

2.1.8. Coking

Carbon deposition is one of the fundamental challenges for industrial processes. Coke can build up on internal equipment surfaces, reducing the flow of gas in pipes or changing the heat transfer of heat exchangers (34). Furthermore, carbon deposition on a catalyst can block the accessibility of reactants to the active sites, leading to catalyst deactivation (35).

Catalyst deactivation via coking has been reported to occur via different mechanisms, including external methods such as pore mouth plugging, and internal methods such as acid site coverage (31,36,37). Pore mouth plugging involves the deposition of coke at the pore mouth, resulting in a reduction of reactant diffusivity to and from the active sites (37,38), whereas acid site coverage typically refers to the deposition of coke covering the acid sites, reducing the available acid site number (30,37). Acid site coverage has also been suggested to involve the adsorption of coke, poisoning the catalyst (31). However, the method of coking which occurs is dependent on reaction type, operating conditions, catalyst structure and acidity (31,37,39,40).

Gates et al. (41) suggested coke formation may comprise of olefins which have undergone dehydrogenation, polymerization or cyclization, or of benzene (or aromatics) forming polynuclear aromatics. These mechanisms have been suggested to proceed via carbonium intermediates, catalysed by Bronsted acid sites (30). Strong Bronsted acid sites have been reported to deactivate first (37), with the coke deposited on them held responsible for the rapid decrease in initial catalytic activity (42).

The type of coke formed has been categorised in various ways, including reaction temperature used to produce the coke (43), temperature at which the coke is removed via TGA (37) and the composition of coke by ratio of hydrogen to carbon (44). It has been proposed that coke formed at lower temperatures is more susceptible to hydrogenation, forming methane and thus leaving the catalyst surface at relatively low temperatures (38). At high temperatures however, the coke formed will gradually become inert, graphitic carbon (29).

Reports suggesting coke composition is dependent on the space available for its formation (31), and coke yield being linked to pore size (29), lead to the wide understanding that coking is a

shape-selective process. As such, zeolites, with their porous nature, are especially susceptible to deactivation by coke (45), with rapid deactivation more common in zeolites with a mono-dimensional structure, such as mordenite (46). Zeolite deactivation via coking is mainly attributed to the formation and retention of heavy aromatics within their pores or pore intersections (29). Acid-site poisoning predominantly occurs at high temperatures, with low coking rates and coverage (<2 % by weight), whereas pore blocking is known to predominantly occur at high reaction rates at low temperatures with high coke coverage (29). As such, where pore size and structure are likely to be more important than acid strength and density under typical commercial conditions (29), the conditions used in this thesis, mean it will consider both, with a slight emphasis on the latter.

However, it must be recognised, not all coke is harmful. Coke deposition may not affect catalytic activity (spectator coke), and contrarily, some coke may be beneficial to a reaction, altering selectivity towards a desired product (38,47). Therefore, the amount of coke present on a catalyst is not necessarily as important as the structure, morphology or location of it (38).

2.1.9. Catalytic Regeneration

When a catalyst is deactivated, activity for the reaction needs to be restored. This can be accomplished by replacing the catalyst, however it is an expensive and time-consuming process, involving the temporary shut-down of the operating plant (48). For this reason, catalyst regeneration, whenever possible, is preferred.

As this thesis is concerned with the deactivation and regeneration of mordenite by toluene disproportionation, this section will exclusively focus on the regeneration of coked catalysts.

When regenerating a catalyst, changes to the internal structure are often undesirable as it will change the activity of the catalyst towards the reaction (35). The typical industrial regeneration process involves the thermal regeneration of the catalyst via combustion – removing the coke as carbon dioxide and water (44). This can be a periodic or continuous process (40), with temperatures ranging from 400-800°C (35,48), however under these conditions, the exothermic

process can lead to sintering of the catalyst, loss of crystal integrity and thus catalytic activity (40,44).

Novel methods of catalyst regeneration which do not affect the internal structure of the catalyst are therefore sought after. Alternative regeneration methods which have been explored include the use of ozone (49,50) , solvent extraction (51) and gas stripping (44). Hutchings et al. (49,50) demonstrated the successful regeneration of coked pentasil zeolites deactivated by the conversion of methanol to hydrocarbons. They reported a rapid regeneration process of 80 minutes under mild temperature conditions (150°C) with an ozone/oxygen mixture, fully restoring catalytic activity to that displayed by the virgin catalyst. With that said, they also reported the presence of some coke remaining post-regeneration. Liang et al. (51) studied the application of solvent extraction as a successful means of removing coke on zeolite HY from the alkylation of benzene with dodecane. However, the alkylation process was in liquid-phase, resulting in the carbonaceous deposits being "liquid coke", which could be easily extracted. Tsai et al. (44), investigated gas stripping as a regeneration treatment of coked mordenite deactivated via toluene disproportionation. They found that by regenerating under hydrogen at a temperature 30°C above the reaction temperature, the zeolite could be successfully regenerated. They also reported that the limitations of this were at reaction temperatures of 420°C, after which the regeneration treatment became increasingly less effective. There are limited studies which have been performed to regenerate coked zeolites using microwaves and/or plasma. These will be discussed in their respective sections.

2.2. MICROWAVES

2.2.1. Fundamentals

Microwaves are a form of electromagnetic radiation, with frequencies ranging from 0.3 to 30 GHz, and wavelengths between 1 mm and 1 m, placing them amidst IR and radio waves on the electromagnetic spectrum (52) (Figure 2.5.). The application of microwaves for domestic use began in 1950 with the patent filed by Arthur Welch (53), but it was in the 1980s when research involving the use of microwaves for chemistry applications began to significantly develop. Today this includes chemical synthesis (54,55), drying (56,57) and microwave-assisted reactions (58,59).
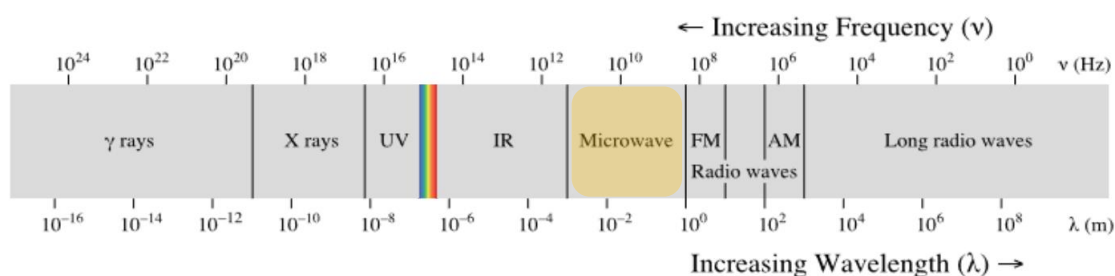
Figure 2.5. - Electromagnetic Spectrum (60)

Microwave Heating

The heating effect of microwave radiation proceeds through dielectric loss processes, namely the absorption and conversion of electromagnetic energy by a material into heat (61,62). If a material is an electrical insulator and can also be polarised, it is called a dielectric material. Different materials have different dielectric properties, based on their ability to absorb and convert electromagnetic energy to heat (dissipation factor), the efficiency of this energy conversion (dielectric loss factor) and the ability of a molecule to be polarised by the electromagnetic field (dielectric constant) (52,61). The quantification of these properties can be expressed as shown in Equation 2.3..

Equation 2.3. - Dielectric Loss Tangent

$$\tan \delta = \varepsilon'' / \varepsilon'$$

Where: $\tan \delta$ is the dissipation factor

            ε'' is the dielectric loss factor

            ε' is the dielectric constant

The total polarisation of any particular material is the sum of the components given in Equation 2.4..

Equation 2.4. - Polarisation of a Material

$$\alpha_T = \alpha_e + \alpha_a + \alpha_d + \alpha_i$$

Where: α_T is the total polarisation

            α_e is the electronic polarisation

            α_a is the atomic polarisation

            α_d is the dipolar polarisation

            α_i is the interfacial polarisation

When a dielectric material is exposed to an applied electromagnetic field, the atoms or molecules within the material attempt to align and realign with the oscillation of the electromagnetic field. In the case of atom and electron polarisation and depolarisation, microwave frequencies are comparably much slower, therefore atom and electron polarisation does not contribute to microwave dielectric heating (63). However, microwave frequencies are comparable to the polarisation associated with permanent dipole moments and some interfacial processes.

In dipolar polarisation, low frequencies are too slow, where the resulting energy generated is too small to heat the material. At high frequencies, the oscillation rate is too fast, and the dipole is unable to realign, therefore no heat is produced (64). However, when the oscillation rate is

comparable to the response time of the dipole, a phase lag develops between the polarisation of the material and the electric field, which causes thermal energy to be produced (61).

Interfacial polarisation (also known as Maxwell-Wagner polarisation) occurs between the interface of two materials with different dielectric properties, resulting in the build-up of charge due to a difference between the charge carrier relaxation times of the materials (65).

The processing of industrial materials within the microwave frequency range is a result of both dipolar and interfacial polarisation (66).

Types of Microwaves

The application of microwaves for heating purposes requires an applicator to focus the microwaves. Two common applicators are multi-mode and single-mode (61). Multi-mode microwaves possess non-uniform electric field distribution, e.g. domestic microwave oven. The dimensions of the cavity are carefully controlled and often accompanied by a mechanical mode stirrer to prevent any standing wave pattern from forming inside the cavity. This results in the heating of microwave absorbing materials anywhere inside the cavity and allows for multiple materials to be irradiated simultaneously (63) (Figure 2.6.). In contrast, single-mode microwaves produce a single standing wave within the cavity, typically focused using waveguides. The dimensions of the cavity are carefully controlled to correspond to the wavelength of the microwave at the frequency used (for 2.45GHz the length of a single full wave is 12.24 cm) (52). Whilst the radiation from a single mode cavity is typically at a much higher field strength which makes it ideal for research purposes, the area of irradiation is much smaller. Careful placement of materials for irradiation is required to avoid standing wave nodes (areas where no heating will occur) and to ensure the standing wave is not disrupted by the material to be treated. As such, only a single material is typically irradiated at any one time (63) (Figure 2.7.).

Although microwave frequencies range from 0.3-30 GHz, industrial applications typically utilise microwaves in the 2.45, 5.8, 9.15, and 22.13 GHz region, with academic research often conducted using 2.45 GHz microwaves (52).
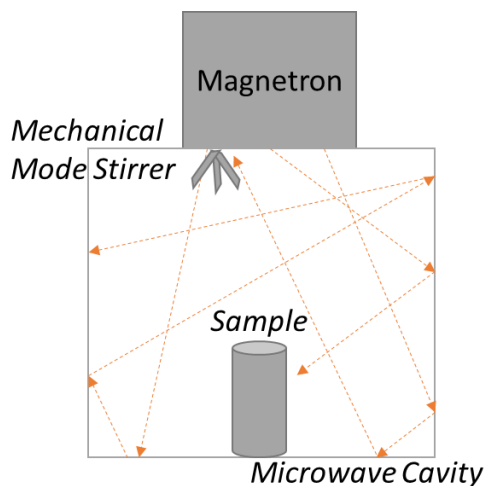
Figure 2.6. - Multi-mode Microwave
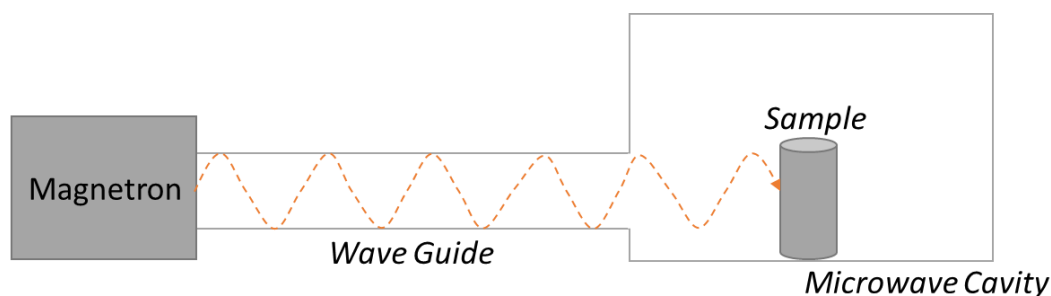
Figure 2.7. - Single-mode Microwave

Benefits of Using Microwaves

Microwaves are becoming more desirable within academic research over conventional methods as their advantages include rapid internal heating, direct energy transfer from source to reaction molecules, uniform heating (for homogeneous samples), and selective heating (for heterogeneous samples) (52,55,67). In terms of results, these features lead to reduced side reactions, reduced reaction times, and enhanced yields with improved conversion and higher selectivity (55,64). Additionally, reduced reaction times (often at lower temperatures) equate to less input energy required and consequently reduce the cost of the process (55,62,68). It should be recognised however, that the energy of a microwave photon (~1 J mol^{-1}) is significantly smaller than the energy needed to break a typical chemical bond (~ >300 J mol^{-1}), and so any effect seen during a microwave-assisted process is most likely due to thermal processes and not microwave radiation (52). Finally, one drawback of microwave heating is thermal runaway, which in zeolites, results in the loss of crystal structure (69).

2.2.2. Zeolites and Microwaves

The application of microwaves in zeolite chemistry dates back to the 1980s, where the dehydration of zeolite 13X was first reported (70). However, it was in 1990s with zeolite synthesis, where the benefits of microwave heating were most effective (59). Today, a search for microwave zeolite synthesis will render over 700 results on Web of Science (accessed 06/2019), with syntheses including zeolites A (71), X (72), Y (73), MFI (74), CHA (75) and MOR (54) to name but a few.

Post Synthesis Modification of Zeolites

Microwave post-synthesis modification of zeolites, however, is much less common, with limited studies published on microwave ion exchange, desilication, regeneration, and dealumination.

Examples of studies on ion exchange of zeolites which have been performed, include nickel or copper exchanged mordenite (76,77), and sodium exchanged ZSM-12 (78). Limitations should be recognised where not all studies performed have been compared with conventional counterparts, however, those that were, reported faster exchange rates over conventional methods (76,77), the formation of new weak acid sites not seen in conventional methods (76) and enhanced dealumination (without framework destruction) (77).

Desilication studies have primarily involved microwave assisted treatments of zeolites including mordenite and ZSM-5 with NaOH or NH_4OH (79,80). Benefits included reduced reaction times, lower energy consumptions without affecting zeolite crystallinity, acid strength or density. Moreover, narrow pore size distribution was found to be produced irrespective of the base used (80).

Microwave regeneration has been compared with conventional regeneration of zeolite A (68) and X (62), and compared as a direct versus indirect regeneration treatment of ETS-10 (81). Results on zeolite A reported higher efficiency, reduced regeneration time and reduced energy inputs (68), zeolite X was considered for industrial scale regeneration (62) and the direct versus indirect regeneration, concluded that direct regeneration at a constant microwave power was more

efficient than prior water desorption followed by microwave drying (81). However, there are, to this author's knowledge, no studies performed on the regeneration of coked zeolites solely using microwaves.

Studies of using microwaves for the dealumination of zeolites is very limited and has so far only included the use of microwaves with HCl on mordenite (82), zeolite Beta and ZSM-5 (83,84), and the use of microwaves with toluene-4-sulphonic acid on BEA (85). The results of these studies have reported faster dealumination times and a more pronounced decrease in crystallinity compared with conventional methods. An increase in surface area for mordenite was also seen (82), (produced as a result of higher mesoporosity from the loss of structural aluminium). However, for all dealuminated samples (microwave-assisted and conventional alike), similar amounts of BAS were seen (82-84).

2.3. PLASMA

2.3.1. Introduction

Plasma is often referred to as the "fourth state of matter". Just as an increase in energy will transform a solid into a liquid, or a liquid into a gas, if the energy supplied is sufficient, the collision processes will become strong enough for gaseous atoms to break apart into their charge-bearing sub-atomic particles (86-88). This ionised gas may be partially or fully ionised, containing electrons, ions, and neutral atoms or molecules. However plasmas are quasi-neutral, meaning the concentration of positively and negatively charged ions is equal (88,89). The free electric charges make plasma electrically conductive, internally interactive and strongly responsive to electromagnetic fields (88).

Plasma was first discovered as far back as the 18th Century when G.C. Lichtenberg observed brush like patterns on insulating surfaces following discharges from a pointed electrode. Although Sir William Crookes was able to produce plasma and understood it to be due to the existence of electrically charged particles, and Werner von Siemens may have been the first person to apply plasma for chemical applications, it was only after the discovery of electrons by Sir J.J. Thomson

in 1897, that plasma could be fully understood (86). The scientist attributed to naming plasma, is Irving Langmuir, who in 1928 described plasma as an "ionised gas…containing balanced charges of ions and electrons", in his paper entitled, "oscillations in ionised gases"(90).

Plasma is thought to constitute more than 99 % of the visible universe (88), including the interior of stars or intergalactic space. However, plasma does not occur naturally on Earth, with some exceptions, e.g. lightning and the aurora borealis (86).

On Earth, plasmas are man-made, produced in a laboratory or industrial environment by subjecting a gas to an electric field, either of constant or alternating amplitude (87). The plasma can be produced over a wide range of pressures, electron temperatures and densities, where the temperature of the plasma can range from ambient to temperatures comparable with stars (88). Plasma can be produced from various energy sources including thermal, electric, and microwave frequencies, where the type of plasma formed is dependent on the conditions used to produce it (86,87).

2.3.2. Types of Plasma

Plasma is often categorised into two types: thermal and non-thermal plasma.

Thermal plasma is typically produced at under high temperature and pressure conditions and it is characterised by a single temperature across the plasma (86,88,91). It is considered the more powerful of the two types, and has applications within materials processing amongst others (91), but as it is not the type of plasma used within this research, further information on this type of plasma is not provided.

Non-thermal plasma typically produced under reduced pressure and comparatively lower temperatures (88). Unlike thermal plasma, non-thermal plasma does not exist in local thermodynamic equilibrium. The temperature of the electrons far exceeds the temperature of the "heavy" particles, i.e. the gas molecules and ions, and it is these energetic electrons which are responsible for initiating chemical reactions through collision-induced energy transfer (86). As a

result, they tend to be more selective than thermal plasmas, which makes them more attractive for chemistry applications (88).

The main benefit of non-thermal plasma for chemistry applications is the ability to produce very high concentrations of chemically active species, where energy density and electron temperature can significantly exceed conventional methods, whilst retaining an ambient bulk temperature (88). In zeolite chemistry, maintaining a low bulk temperature is highly desirable as high temperatures lead to the loss of catalyst structure which can severely affect activity and selectivity (44).

This research will utilise two different types of non-thermal plasmas, categorised by the nature of their energy input. These are: microwave plasma and dielectric barrier discharge (DBD) plasma.

2.3.3. The Role of Plasma in Catalysis

The application of plasma in catalysis primarily involves plasma-assisted catalysis. This typically involves the use of plasma in a known catalytic reaction to provide advantages over conventional methods. Often these advantages include lower reaction temperatures or enabling thermodynamically unfavourable reactions (92). Examples of plasma-assisted reactions include: CO oxidation over Au/TiO_2 catalyst (93), oxidative methane coupling over Ag/SiO_2 catalyst (94), and catalytic dry reforming of butane over Ni-γ-alumina (92).

Often these reactions are accompanied by deactivation, which has led to plasma being applied in the regeneration process of these catalysts. Mok et al. (92) regenerated a deactivated Ni-γ-alumina catalyst using a DBD plasma for 120 minutes at 500°C. This was reported to have fully restored both the surface area of the catalyst and its original activity. Kim et al. (93) successfully regenerated Au/TiO_2 catalyst deactivated by volatile organics. An oxidative DBD plasma treatment of up to 120 minutes at 15 Watts was able to restore the catalyst to its original activity. Lee et al. (94) used a DBD plasma to regenerate an Ag/SiO_2 catalyst deactivated by oxidative coupling of methane. A successful plasma treatment of 30 minutes at 375°C was compared with thermal regeneration, where a minimum regeneration temperature of 500°C was required.

Plasma has also been applied in the preparation or pre-treatment of catalysts. Examples of this include: a novel method of producing supported catalysts via plasma torch (95), an alternative method of calcining catalysts (96) and the promotion of catalytic activity on CuO/TiO_2 catalysts towards NO_x reduction via exposure to microwave plasma (97).

2.3.4. Plasma and Zeolites

The application of plasma in zeolite chemistry is relatively similar to the plasma-catalysis applications previously described. Plasma has been utilised for zeolite calcination (98), regeneration (36,48) and additionally for surface modification (99).

Furukawa et al. (99) explored the effects of radiofrequency plasma on H-Y zeolite, subjecting the catalyst to a 30 minute plasma treatment of 75 Watts with a temperature of 450°C and carbon tetrafluoride as the gas. The results indicated the plasma had destroyed some of the crystallinity of the catalyst via dealumination, however the treatment had also increased the hydrophobic character of the zeolite, via the replacement of surface OH- groups by CF_n or F- groups.

Bibby et al. (36) applied an oxidative plasma to selectively remove surface coke as a tool to exploring coke formation on ZSM-5 and Khan et al. (48) exposed a coked zeolite to a glow discharge to evaluate its success at regeneration, which they found under their conditions to be 60 %.

Although very few, there are studies which have explored the effect of plasma treatment on the acidity of a zeolite. Zhu et al (100) applied a glow discharge to a Mo-Fe/H-ZSM-5 zeolite to improve the catalytic activity for methane aromatisation. Their results exhibited a change in the products produced after treatment with plasma. There was no apparent change to the structure seen, however the density of Brønsted acid sites had increased, which was attributed to the shift in products produced.

Plasma has been shown to dealuminate zeolites (99), and induce changes to acidity (100). However, to this author's knowledge, there are currently no studies which investigate how plasma

regeneration on a zeolite may not only restore catalytic activity, but also impacts the acidity of the zeolite.

The application of microwave plasma in zeolites is extremely limited, with this author knowing of a single study (101). The findings of this study however reported the benefits of microwave plasma as a technique for the zeolite activation, producing higher activity, stability and selectivity.

2.4 REFERENCES

(1) Robertson AJB. The Early History of Catalysis. Platinum Metals Rev 1975;19(2):65-69.

(2) Roduner E. Understanding Catalysis. Chem Soc Rev 2014;43:8226-8329.

(3) Haber J. Catalysis - where science and industry meet. Pure and Applied Chemistry 1994;66(8):1597-1620.

(4) Corma A. Inorganic Solid Acids. Chemical Reviews 1995;95:559-614.

(5) Tsai T, Liu S, Wang I. Disproportionation and transalkylation of alkylbenzenes over zeolite catalysts. Applied Catalysis A: General 1999 5/17;181(2):355-398.

(6) Baerlocher C, McCusker LB, Olson DH. Atlas of Zeolite Framework Types. Sixth ed.: Elsevier; 2007.

(7) Baerlocher C, McCusker LB. Database of Zeolite Structures. 2019; Available at: http://www.iza-structure.org/databases/. Accessed 07/17, 2019.

(8) Löwenstein W, Löwenstein M, Löwenstein C. The Distribution of Aluminium in the Tetrahedra of Silicates and Aluminates. American Mineralogist 1954;39(1):92-96.

(9) Szostak R. Structural Aspects. In: Szostak R, editor. Molecular Sieves: Principles of Synthesis and Identification. 2nd ed. London: Thomson Science; 1998. p. 29-31.

(10) Fletcher RE, Ling S, Slater B. Violations of Löwenstein's Rule in Zeolites. Chemical Science 2017;8:7483-7491.

(11) White JL, Beck LW, Haw JF. Characterisation of Hydrogen Bonding in Zeolites by Proton Solid-State NMR Spectroscopy. Journal of the American Chemical Society 1992;114(15):6182-6189.

(12) Weitkamp J. Zeolites and Catalysis. Solid State Ionics 2000;131:175-188.

(13) De S, Dutta S, Saha B. Critical Design of Heterogeneous Catalysts for Biomass Valorization: Current Thrust and Emerging Prospects. Catalysis Science and Technology 2016;6:7364-7385.

(14) Huang J, Jiang Y, Marthala VRR, Thomas B, Romanova E, Hunger M. Characterisation and Acidic Properties of Aluminium-Exchanged Zeolites X and Y. Journal of Physical Chemistry 2008;112:3811-3818.

(15) Cejka J, Vondrova A, Whichterlova B, Jerschkewitz HG, Lischke G, Schreier E. The Effect of Extra-Framework Aluminum in Dealuminated ZSM-5 Zeolites on the Transformation of Aromatic Hydrocarbons. Collection of Czech Chemical Communications 1994;60:412-420.

(16) Cejka, J. & Wichterlova, B. Acid-Catalysed Synthesis of Mono- and Dialkyl Benzenes Over Zeolites: Active Sites, Zeolite Topology, and Reaction Mechanisms. Catalysis Reviews: Science and Engineering 2002;44(3):375-421.

(17) Mavrodinova V, Popova M, Mihalyi MR, Pal-Borbely G, Minchev C. Influence of the Acidity Modification on the Reactions of Toluene and Ethyl Benzene Disproportionation. Effect

of Lewis Acidic InO+ Species Introduced into Y Zeolite. Applied Catalysis A: General 2004;262:75-83.

(18) Mirodatos C. Superacid Sites in Zeolites. Journal of the Chemical Society-Chemical Communications 1981;0(2):39-40.

(19) Rhodes NP, Rudham R. Catalytic Studies with Dealuminated Y Zeolite - Part 2. - Disproportionation of Toluene. Journal of the Chemical Society Faraday Transactions 1994;90(5):809-814.

(20) Cejka J, Zikova N, Tvaruzkova Z, Wichterlova B. Contribution of Framework and Extraframework Al and Fe Cations in ZSM-5 to Disproportionation and C3 Alkylation of Toluene. Studies in Surface Science and Catalysis 1995;97:401-408.

(21) Mavrodinova V, Popova M, Mihalyi MR, Pal-Borbely G, Minchev C. Toluene Disproportionation and Coking on Zeolites Y Modified with Lewis-Connected InO+ Acid Sites. Journal of Molecular Catalysis A: Chemical 2004;220:239-246.

(22) Mavrodinova VP, Popova MD, Neinska YG, Minchev CI. Influence of the Lewis Acidity of Indium-Modified Beta Zeolite in the m-xylene Transformation. Applied Catalysis A: General 2001;210:397-408.

(23) Perego C. Industrial Applications of Zeolites. 2005; Available at: https://www.researchgate.net/publication/237076666_Industrial_applications_of_Zeolites. Accessed 07/19, 2019.

(24) Yilmaz B, Muller U. Catalytic Applications of Zeolites in Chemical Industry. Topics in Catalysis 2009;52:888-895.

(25) Acumen Research and Consulting. Zeolite Catalysts Market. 2019; Available at: https://www.acumenresearchandconsulting.com/press-releases/zeolite-catalysts-market. Accessed 7/19, 2019.

(26) Lobo R. Chapter Three - Introduction to the Structural Chemistry of Zeolites. In: Auerbach SM, Carrado KA, Dutta PK, editors. Handbook of Zeolite Science and Technology. First ed. New York, U.S.A.: Marcel Dekker; 2003. p. 65-98.

(27) Huo H, Peng L, Gan Z, Grey CP. Solid-State MAS NMR Studies of Bronsted Acid Sites in Zeolite H-Mordenite. Journal of the American Chemical Society 2012;134(23):9708-9720.

(28) Hayashi S, Kojima N. Acid Properties of H-type Mordenite Studied by Solid-State NMR. Microporous and Mesoporous Materials 2011;141:49-55.

(29) Bartholomew CH. Mechanisms of catalyst deactivation. Applied Catalysis A: General 2001 4/30;212(1–2):17-60.

(30) Forzatti P, Lietti L. Catalyst deactivation. Catalysis Today 1999 9/14;52(2–3):165-181.

(31) Bhatia S, Beltramini J, Do DD. Deactivation of zeolite catalysts. Catalysis Reviews: Science and Engineering 2008;31(4):431-480.

(32) Rothenberg G. Catalysis - Concepts and Green Applications. First ed. Weinheim, Germany: Wiley-VCH Verlag GmbH & Co.; 2008.

(33) Wu J, Leu L. Toluene Disproportionation and Transalkylation Reaction Over Mordenite Zeolite Catalysts. Applied Catalysis 1983;7:283-294.

(34) Blaikley DCW, Jorgensen N. Studies of Catalytically Enhanced Carbon Deposition and Removal Using a Gas Plasma System. Catalysis Today 1990;7:277-286.

(35) HafezKhiabani N, Fathi S, Shokri B, Hosseini SI. A novel method for decoking of Pt–Sn/Al2O3 in the naphtha reforming process using RF and pin-to-plate DBD plasma systems. Applied Catalysis A: General 2015 3/5;493:8-16.

(36) Bibby D, Milestone NB, Patterson JE, Aldridge LP. Coke Formation in Zeolite ZSM-5. Journal of Catalysis 1986;97:493-502.

(37) Tsai TC, Chen WH, Lai CS, Liu SB, Wang I, Ku CS. Kinetics of toluene disproportionation over fresh and coked H-mordenite. Catalysis Today 2004 NOV 3 2004;97(4):297-302.

(38) Menon PG. Coke on Catalysts - Harmful, Harmless, Invisible and Beneficial Types. Journal of Molecular Catalysis 1990;59:207-220.

(39) Meshram NR, Hegde SG, Kulkarni SB. Active Sites on ZSM-5 Zeolites for Toluene Disproportionation. Zeolites 1986;6:434-438.

(40) D'Ippolito SA, Especel C, Epron F, Marécot P, Pieck CL. O2 and O3 regeneration of PtReSn/Al2O3 and PtReGe/Al2O3 naphtha reforming catalysts prepared by catalytic reduction. Applied Catalysis A: General 2010 11/20;388(1–2):272-277.

(41) Gates BC, Katzer JR, Schuit GCA. Chapter 1: Cracking. In: Gates BC, Katzer JR, Schuit GCA, editors. Chemistry of Catalytic Processes New York: McGraw-Hill; 1979. p. 1-111.

(42) Chen WH, Huang SJ, Lai CS, Tsai TC, Lee HK, Liu SB. Effects of binder, coking and regeneration on acid properties of H-mordenite during TDP reaction. Research on Chemical Intermediates 2003 2003;29(7-9):761-772.

(43) Lange JP, Gutsze A. Coke Formation Through the Reaction of Ethene over Hydrogen Mordenite III. IR and 13CNMR Studies. Applied Catalysis 1988;45:345-356.

(44) Tsai T. Reactivation of acidic sites in mordenite used in toluene disproportionation. Applied Catalysis A: General 2006 2/24;301(2):292-298.

(45) Gnep NS, Martin de Armando ML, Marcilly C, Ha BH, Guisnet M. Toluene Disproportionation and Coke Formation on Mordenites - Effect of Catalyst Modifications and of Operating Conditions. Studies in Surface Science and Catalysis 1980;6:79-89.

(46) Guisnet M, Magnoux P, Martin D. Roles of Acidity and Pore Structure in the Deactivation of Zeolites by Carbonaceous Deposits. In: Bartholomew CH, Fuentes GA, editors. Catalyst Deactivation: Elsevier; 1997. p. 1-19.

(47) Haag WO, Olson DH, inventors. Mobil Oil Corportation, assignee. Selective Disproportionation of Toluene. United States of America patent 4097543. 1978 1977.

(48) Khan MA, Al-Jalal AA, Bakhtiari IA. 'Decoking' of a 'coked' zeolite catalyst in a glow discharge. Analytical and Bioanalytical Chemistry 2003 SEP 2003;377(1):89-96.

(49) CARLTON L, COPPERTHWAITE R, HUTCHINGS G, REYNHARDT E. Characterization of Carbonaceous Residues on the Pentasil Zeolite Zsm-5 Following Reactivation - a Solid-State C-13 Nmr Spectroscopic Study. J Chem Soc -Chem Commun 1986 JUL 1(13):1008-1009.

(50) Copperthwaite RG, Hutchings GJ, Johnston P, Walter Orchard S. Regeneration of Pentasil Zeolite Catalysts Using Ozone and Oxygen. Journal of the Chemical Society Faraday Transactions 1: Physical Chemistry in Condensed Phases 1986;82(3):1007-1017.

(51) Liang W, Jin Y, Yu Z, Wang Z, Han B. Alklation of Benzene with Dodecene Over HY Zeolite: Deactivation, Regeneration, and Product Distribution. Zeolites 1996;17:297-303.

(52) Li Y, Yang W. Microwave Synthesis of Zeolite Membranes: A Review. Journal of Membrane Science 2008;316:3-17.

(53) Welch AE, inventor. Baytheon Manufacturing Company, assignee. Method of Treating Foodstuffs. Massachusetts, United States of America patent 2495435. 1947 1950.

(54) Li G, Hou H, Lin R. Rapid Synthesis of Mordenite Crystals by Microwave Heating. Solid State Sciences 2011;13(3):662-664.

(55) Priya SS, Selvakannan PR, Chary KVR, Kantam ML, Bhargava SK. Solvent-free Microwave-assisted Synthesis of Solketal from Glycerol Using Transition Metal Ions Promoted Mordenite Solid Acid Catalysts. Molecular Catalysis 2017;434:184-193.

(56) Auvray X, Thuault A. Effect of Microwave Drying, Calcination and Aging of Pt/Al2O3 on Platinum Dispersion. Catalysts 2018;8(9):348.

(57) Taketoshi A, Ishida T, Ohashi H, Honma T, Haruta M. Preparation of Gold Clusters on Metal Oxides by Deposition-Precipitation with Microwave Drying and Their Catalytic Performance for CO and Sulfide Oxidation. Chinese Journal of Catalysis 2017;38:1888-1898.

(58) Gui J, Liu D, Zhang X, Song L, Sun Z. Aromatization of n-Hexane Under Microwave Irradiation. Petroleum Science and Technology 2008;26(5):506-513.

(59) Whittington BI, Milestone NB. The Microwave Heating of Zeolites. Zeolites 1992;12:815-818.

(60) Wikipedia Commons. EM Spectrum Revised. 2019; Available at: https://commons.wikimedia.org/wiki/File:EM_spectrumrevised.png. Accessed 06/19, 2019.

(61) Cundy CS. Microwave Techniques in the Synthesis and Modification of Zeolite Catalysts. A Review. Collection of Czechoslovak Chemical Communications 1998;63(11):1699-1723.

(62) Polaert I, Ledoux A, Estel L, Huyghe R, Thomas M. Microwave Assisted Regeneration of Zeolite. International Journal of Chemical Reactor Engineering 2007;5:1-10.

(63) D. Shorrock. Microwave Assisted Remediation of Organic Waste in Aqueous Effluent Streams. University of Central Lancashire: University of Central Lancashire; 2003.

(64) Sun Z, Yan Y, Li G, Zhang Y, Tang Y. Microwave Influence on Different M-O Bonds During MFI-Type Heteroatom (M) Zeolite Preparation. Industrial & Engineering Chemistry Research 2017;56(39):11167-11174.

(65) Iwamoto M. Maxwell-Wagner Effect. In: Bhushan B, editor. Encyclopedia of Nanotechnology Dordrecht: Springer; 2015.

(66) Metaxas AC, Meredith RJ. Dielectric Loss. In: Johns AT, Ratcliff G, Platts JR, editors. Industrial Microwave Heating. Third ed. London: Peter Peregrinus Ltd.; 1983. p. 5-25.

(67) Ramesh S, Prakash BSJ, Bhat YS. Enhancing Bronsted Acid Site Activity of Ion Exchanged Montmorillonite by Microwave Irradiation for Ester Synthesis. Applied Clay Science 2010;48:159-163.

(68) Piunchukova NA, Voloshko AY, Baumer VN, Shishkin OV, Chebanov VA. The use of Microwave Irradiation for Zeolite Regeneration in a Continuous Ethanol Dewatering Process. Chemical Engineering and Processing: Process Intensification 2015;95:151-158.

(69) Ohgushi T, Nagae M. Durability of Zeolite Against Repeated Activation Treatments with Microwave Heating. Journal of Porous Materials 2005;12:265-271.

(70) Roussy G, Chenot P. Selective Energy Supply to Adsorbed Water and Nonclassical Thermal Process During Microwave Dehydration of Zeolite. Journal of Physical Chemistry 1981;85(15):2199-2203.

(71) Xu X, Yang W, Liu J, Lin L. Synthesis of a High-Permeance NaA Zeolite Membrane by Microwave Heating. Advanced Materials 2000;12(3):195-198.

(72) Ozdemir OD, Piskin S. A Novel Synthesis Method of Zeolite X From Coal Fly Ash: Alkaline Fusion Followed by Ultrasonic-Assisted Synthesis Method. Waste and Biomass Valorization 2017;10(1):143-154.

(73) Le T, Wang Q, Pan B, Ravindra AV, Ju S, Peng J. Process Regulation of Microwave Intensified Synthesis of Y-type Zeolite. Microporous and Mesoporous Materials 2019;284:476-485.

(74) Cai R, Liu Y, Gu S, Yan Y. Ambient Pressure Dry-Gel Conversion Method for Zeolite MFI Synthesis Using Ionic Liquid and Microwave Heating. Journal of the American Chemical Society 2010;132(37):12776-12777.

(75) Nasser G, Muraza O, Nishitoba T, Malaibari ZO, Yamani ZH, Al-Shammari TK, et al. Microwave-Assisted Hydrothermal Synthesis of CHA Zeolite for Methanol-to-Olefins. Industrial & Engineering Chemistry Research 2018;58(1):60-68.

(76) Bergada O, Boix E, Salagre P, Cesteros Y, Medina F, Sueiras JE. Acidity Properties of Ni-Exchanged Mordenites Prepared with and without Microwaves. Applied Catalysis A: General 2009;368:163-169.

(77) Zhukov YM, Shelyapina MG, Zvereva IA, Efimov AY, Petranovskii V. Microwave Assisted Versus Convention Cu2+ Exchange in Mordenite. Microporous and Mesoporous Materials 2018;259:220-228.

(78) Muraza O, Sanhoob MA, Siddiqui MAB. Fabrication of Desilicated MTW Zeolite and its Application in Catalytic Cracking of n-Heptane. Advanced Powder Technology 2016;27:372-378.

(79) Paixao V, Monteiro R, Andrade M, Fernandes A, Rocha J, Carvalho AP, et al. Desilication of MOR Zeolite: Conventional Versus Microwave Assisted Heating. Applied Catalysis A: General 2011;402:59-68.

(80) Hasan Z, Jun JW, Kim C, Jeong K, Jeong S, Jhung SH. Desilication of ZSM-5 Zeolites for Mesoporosity Development using Microwave Irradiation. Materials Research Bulletin 2014;61:469-474.

(81) Chowdhury T, Shi M, Hashisho Z, Kuznicki SM. Indirect and Direct Microwave Regeneration of Na-ETS-10. Chemical Engineering Science 2013;95:27-32.

(82) Gonzalez MD, Cesteros Y, Salagre P, Medina F, Sueiras JE. Effect of Microwaves in the Dealumination of Mordenite on its Surface and Acidic Properties. Microporous and Mesoporous Materials 2009;118:341-347.

(83) Gonzalez MD, Cesteros Y, Salagre P. Comparison of Dealumination of Zeolites Beta, Mordenite and ZSM-5 by Treatment with Acid under Microwave Irradiation. Microporous and Mesoporous Materials 2011;144(1-3):162-170.

(84) Gonzalez MD, Cesteros Y, Salagre P. Effect of Microwaves on the Surface and Acidic Properties of Dealuminated Zeolites. Physics Procedia 2010;8:104-108.

(85) Shekara BMC, Prakash BSJ, Bhat YS. Dealumination of Zeolite BEA under Microwave Irradiation. ACS Catalysis 2011;1(3):193-199.

(86) d'Agostino R, Favia P, Oehr C, Wertheimer MR. Low-Temperature Plasma Processing of Materials: Past, Present, and Future. Plasma Processes and Polymers 2005;2(1):7-15.

(87) Thirumdas R, Sarangapani C, Annapure US. Cold Plasma: A Novel Non-Thermal Technology for Food Processing. Food Biophysics 2015;10(1):1-11.

(88) Fridman A. Plasma Chemistry. second ed. United States of America: Cambridge University Press; 2008.

(89) Panel on Plasma Processing of Materials, Plasma Science Committee, Board on Physics and Astronomy, Mathematics, and Applications Commission on Physical Sciences, Division on Engineering and Physical Sciences, National Research Council. Plasma Processing and Low-Energy Plasma Science. Plasma Processing of Materials: Scientific Opportunities and Technological Challenges: National Academies Press; 1991. p. 6-12.

(90) Langmuir I. Oscillations in Ionized Gases. Proceedings of the National Academy of Sciences of the United States of America PNAS, Proceedings of the National Academy of Sciences 1928;14(8):627-637.

(91) HEBERLEIN J. Generation of Thermal and Pseudo-Thermal Plasmas. Pure Appl Chem 1992 MAY;64(5):629-636.

(92) Mok YS, Jwa E, Hyun YJ. Regeneration of C4H10 dry reforming catalyst by nonthermal plasma. Journal of Energy Chemistry 2013 MAY 2013;22(3):394-402.

(93) Kim HH, Tsubota S, Date M, Ogata A, Futamura S. Catalyst Regeneration and Activity Enhancement of Au/TiO2 by Atmospheric Pressure Nonthermal Plasma. Applied Catalysis A: General 2007;329:93-98.

(94) Lee H, Lee D, Ha JM, Kim DH. Plasma Assisted Oxidative Coupling of Methane (OCM) over Ag/SiO2 and Subsequent Regeneration at Low Temperatures. Applied Catalysis A: General 2018;557:39-45.

(95) Phillips J, inventor. The Penn State Research Foundation, assignee. Plasma Generation of Supported Metal Catalysts. United States of America patent 5989648. 1999 23/11/1999.

(96) Chen G, Georgieva V, Godfroid T, Synders R, Delplancke-Ogletree M. Plasma Assisted Catalytic Decomposition of CO2. Applied Catalysis B: Environmental 2016;190:115-124.

(97) Gao F, Liu B, Sun W, Wu Y, Dong L. The Influence Of Microwave Plasma Pretreated CuO/TiO2 Catalysts in NO + CO Reaction. Catalysis Today 2011;175:34-39.

(98) Maesen TLM, Bruinsma DSL, Kouwenhoven HW, Van Bekkum H. USe of Radiofrequency Plasma for Low-temperature Calcination of Zeolites. Journal of Chemical Society Chemical Communications 1987;17:1284-1285.

(99) Furukawa H, Tian SR, Yamauchi H, Yamazaki S, Ijiri H, Ariga K, et al. Characterisation of H-Y Zeolite Modified by a Radio-Frequency CF4 Plasma. Chemical Physics Letters 2000;318:22-26.

(100) Zhu X, Yu K, Cheng D, Zhang Y, Xia Q, Liu C. Modification of Acidity of Mo-Fe/HZM-5 Zeolite via Argon Plasma Treatment. Frontiers of Chemical Engineering in China 2008;2(1):55-58.

(101) Lishchiner II, Malova OV, Krasheninnikov EG. Microwave Plasma Treatment as an Effective Technique for Activation of Zeolite Catalysts. Studies in Surface Science and Catalysis 2001;135:210.

(102) International Zeolite Association. Framework Type MOR. 2007; Available at: https://europe.iza-structure.org/IZA-SC/framework.php?STC=MOR. Accessed 07/19, 2019.

CHAPTER 3: TOLUENE DISPROPORTIONATION

3.1. FUNDAMENTALS

Toluene disproportionation (TDP) is an acid-catalysed reaction, converting two molecules of toluene into benzene and a mixture of xylene isomers in equimolar quantities (Figure 3.1.) (1-4).
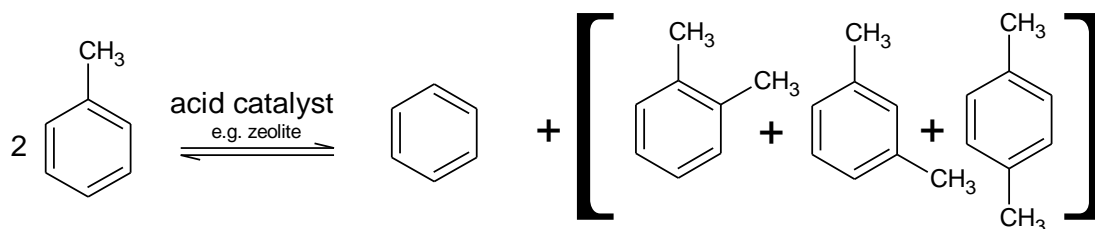
Figure 3.1. - Reaction Scheme for Toluene Disproportionation

Benzene, toluene and xylene (often referred to as BTX) are raw materials used in the production of commodity and fine chemicals in industry (2). They are predominantly formed from catalytic naphtha reforming and naphtha pyrolysis, however as these are typically thermodynamically controlled, there is often a mismatch between production and market demand, creating a surplus of toluene (Figure 3.2.) (2,5). Therefore, transforming toluene into benzene and xylene is more economically favourable.

Xylenes are used to manufacture polyesters, plasticisers and engineering plastics, and of the three, *para*-xylene (*p*-xylene) is the most valuable. *p*-Xylene is converted into terephthalate and polyester, *meta*-xylene (*m*-xylene) is an additive in polyester as well as a key material in the synthesis of isophthalic acid, and *ortho*-xylene (*o*-xylene) is used to produce phthalic anhydride - a component in plasticisers. Their relevance within industry has led to research and modifications of conditions and catalysts for this reaction, with a focus on increasing rate of reaction, reducing deactivation and shifting xylene selectivity in favour of the *para* isomer (2).

THERMODYNAMIC EQUILIBRIUM
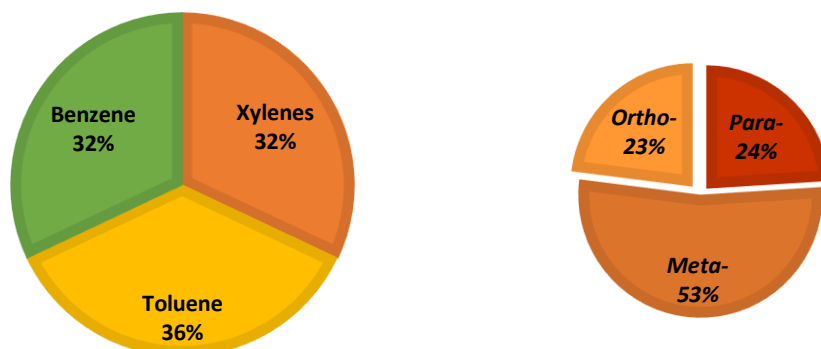
MARKET DEMAND
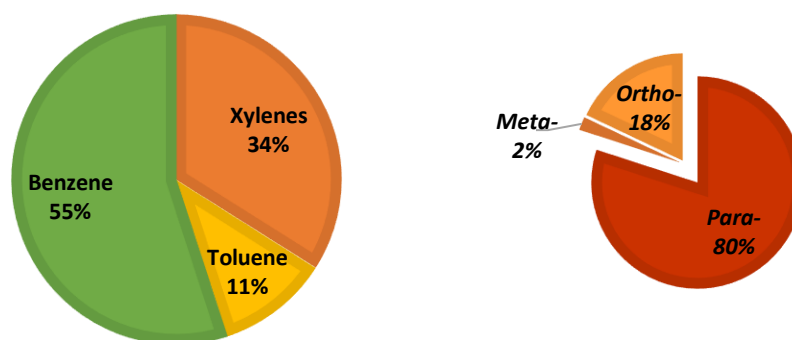
Figure 3.2. - Comparison of Thermodynamic Equilibrium with Market Demand for BTX (2)

3.2. MECHANISM OF TOLUENE DISPROPORTIONATION

The mechanism for toluene disproportionation has been suggested to operate either via an intermolecular methyl transfer (Figure 3.3.) or a bimolecular reaction involving a carbonium ion intermediate (Figure 3.4.) (6-8). It is believed that toluene disproportionation proceeds via the intermolecular methyl transfer over ZSM-5, but via the bimolecular reaction mechanism when carried out over most 12-membered oxygen ring zeolites (9).

It is thought p-xylene is the primary product leaving the zeolite pore mouth, where isomerisation to m- and o-xylene occurs on the external surface of the zeolite, generating the thermodynamic equilibrium that is produced (Figure 3.2.) (2,10).
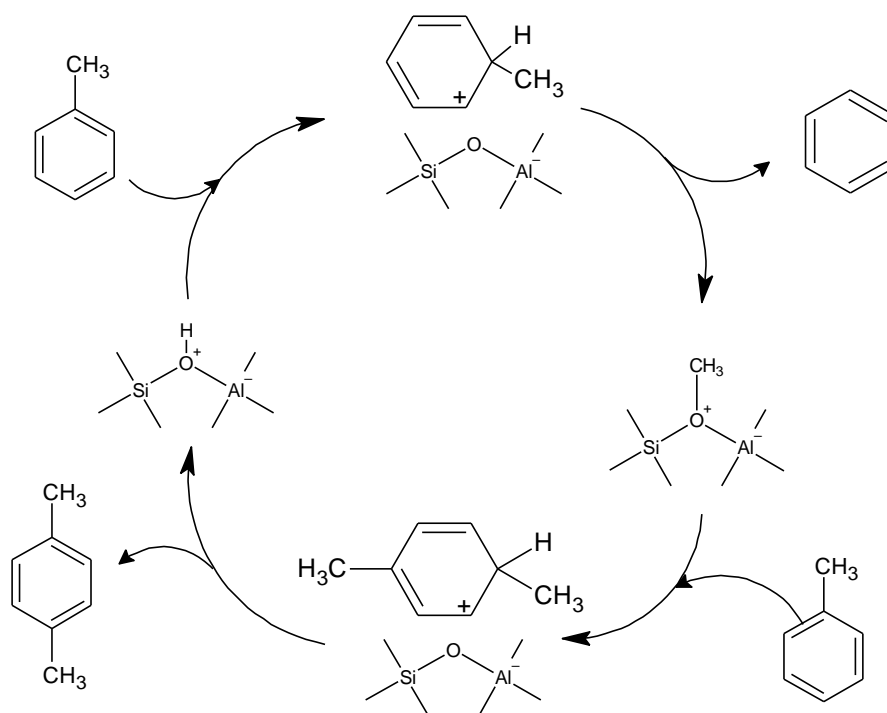
Figure 3.3. – Intermolecular Methyl Transfer Mechanism (8)
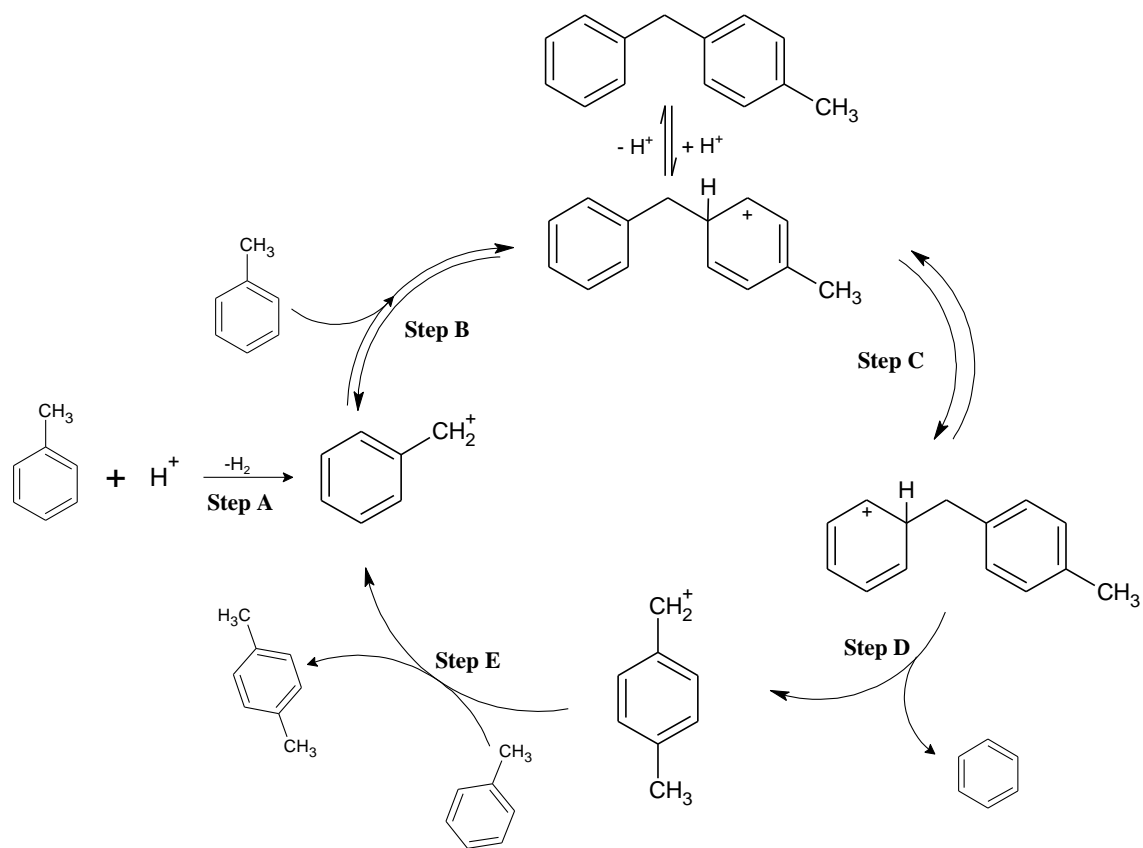
Figure 3.4. – Bimolecular Reaction Mechanism (8)

3.3. CATALYSTS USED IN TDP

Historically, toluene disproportionation was carried out in the liquid phase using Friedel-Crafts catalysts such as $AlCl_3$-HCl. However, these carried many drawbacks as they were corrosive, difficult to handle, and often used as slurries which generated mechanical problems during use (1,2). These difficulties brought about research into alternative acid catalysts, including but not exclusively alumina-boria (6,11), silica-alumina (11,12), and zeolites (1-5,13).

Studies undertaken on alumina-boria however, highlighted disadvantages including low catalytic activity towards toluene disproportionation, carbon deposition and subsequently a short catalytic life; ultimately finding the catalyst to be unsuitable for commercial use (11).

Alkali containing zeolites have been found to have no activity towards toluene disproportionation, however when replaced with divalent or trivalent cations, zeolites show significant activity for disproportionation reactions (14). Large pore zeolites such as faujasite and mordenite have shown to be more favourable for toluene disproportionation than amorphous silica-alumina catalysts (3). Studies have been carried out on cation exchanged Linde 13X zeolites, using cadmium and lanthanum (1). From this cadmium was found to be unsuitable as when toluene disproportionation was carried out under H_2, the cations were sublimed from the catalyst – something that has been reported to happen with reducible metals such as mercury, zinc and cadmium (15). In the lanthanum exchanged zeolite however, an increase in toluene conversion was seen, attributed to the acidity of the catalyst and availability of cations in accessible sites (1), demonstrating in order to catalyse toluene disproportionation, some acidity is imperative. Nevertheless, mordenite was reported to show a higher activity towards toluene disproportionation than Y-faujasite (16).

Zeolites are the catalysts currently used in the commercial toluene disproportionation process. Of these, mordenite is the large-pore zeolite favoured and ZSM-5 is the medium-pore zeolite used (4). However, due to mordenite's large pore size, it can suffer from lower selectivity due to dealkylation and cracking as well as being prone to deactivation via coking (3), thus commercial use may favour ZSM-5 (2).

3.4. DEVELOPMENT OF THE TDP PROCESS

3.4.1. Development of Industrial Catalysts for the TDP Process

As an industrial process, there has been a focus on improving the efficacy of toluene disproportionation. Early attempts focused on improving purity, yield and minimising coke deposition. To achieve this, modifications or syntheses of novel catalysts have often been the focal point.

Sato et *al.* (11) filed a patent on toluene disproportionation, with claims of improved conversion and minimised coke deposition, by performing the process using a dealkylated mordenite catalyst containing aluminium fluoride. Mitsche et *al.* (17) filed a patent on an improved process for transalkylation using a novel catalyst composition, where the catalyst contains a 60-90 % by weight mordenite crystal structure combined with alumina.

In contrast, Otani et *al.* (18) filed a patent using catalysts typical of toluene conversion, such as silica-alumina, boria-alumina and mordenite, instead focusing on the process itself. They proposed a toluene conversion to benzene and xylene process, claiming to have improved purity and yield, by carrying out both disproportionation and dealkylation as separate steps whose products could be separated out and then combined. Toluene produced could then be recycled back into the feed and the process could be performed several times.

3.4.2. *p*-Xylene Selectivity

As the isomer with the highest market value, it was inevitable that later research of toluene disproportionation would focus on selectively producing *para*-xylene. This has led to an increased understanding of the factors involved and the development of novel selective toluene disproportionation processes.

It has been proposed that there are two key factors in achieving *p*-xylene selectivity: diffusivity and the deactivation of external surface sites (2). Diffusivity of zeolites is dependent on molecular structure, such as crystal size or tortuosity (19). By increasing the diffusion resistance, the more

mobile *p*-xylene, with a reported 1000 times faster diffusion rate than the other isomers (2), will be selectively produced. The external surface sites are the location for *p*-xylene isomerisation, producing *m*- and *o*- isomers (2,10), therefore deactivating the external surface sites would inhibit this reaction, leading to preferential *p*-xylene formation.

Research into producing novel selective toluene disproportionation processes often focuses on the development of a modified catalyst; patents including silica (20-24), magnesium (25), phosphorus (26) and pre-coking (27) modifications to zeolites have been filed, all claiming to preferentially produce *p*-xylene over the other xylene isomers. To-date, both silica-modified and pre-coking-modified ZSM-5 catalysts have been used in commercial toluene disproportionation (2).

The silica-modified catalysts include patents from Chang et *al.* (20), Rodewald et *al.* (21,22), and Beck et *al.* (23,24). They all claim to have successfully synthesised various zeolites and have tested their modification techniques on ZSM-5. Chang et *al.* (20) proposed combining a zeolite with an organosilicon compound by dissolving the organosilicon compound in an organic solvent, adding the zeolite and then heating the mixture to boil off the solvent whilst calcining the residue. Rodewald et *al.* (21,22) proposed depositing a silica coating on the external zeolite surface by treating the zeolite with a silicone compound with a molecular size incapable of entering the zeolite pores, followed by heating in an oxygen-containing atmosphere. Beck et *al.* (23,24) proposed a selectivation sequence involving multiple impregnations of the zeolite with a compound such as silicon, where after each impregnation, the catalyst is calcined. The catalyst could then be further modified to enhance the *p*-xylene selectivity by subsequent steaming or *in-situ* trim-selectivation – the process of using either a silicon compound or a thermally decomposable organic compound to be fed simultaneously on-stream with the reactant, until the desired selectivity is attained. Despite their different methods of incorporating silica into the zeolite, all the patents described above achieve *p*-xylene selectivity by the same means: deactivation of the external surface sites.

Similarly, a *p*-xylene selective toluene disproportionation method via pre-coking the zeolite was filed by Haag et *al*. (27). It describes a methodology of pre-coking the surface of a zeolite by exposing it to a thermally decomposable organic compound (preferably the feed source) under conditions that enable a deposit of at least 2 % coke on the surface of the catalyst. In contrast, Haag et *al*. (28) filed a patent claiming to achieve *p*-xylene selectivity by modifying the diffusivity of the zeolite. This could be achieved by combining the catalyst with small amounts (2-30 % by weight) of a reducible oxide such as antimony, boron, phosphorus or magnesium.

3.5. INDUSTRIAL PROCESSES

One of the leading companies for research into and commercialisation of selective toluene disproportionation was, and still is: Mobil Oil Corporation (now ExxonMobil). The company was the assignee for all the patents referenced previous in the *p*-xylene selectivity section, and developed the commercial processes known as Mobil Selective Toluene Disproportionation Process (MSTDP), Mobil Toluene to ParaXylene (MTPX) and Toluene Disproportionation Process Version 3 (TDP-3) (2).

ExxonMobil (at time of writing) currently offer two methods of toluene disproportionation on their website (29). Their older MTDP-3 toluene disproportionation process that has been licensed for over twenty years (30) and their revolutionary PxMax[SM] selective toluene disproportionation process replacing their MTPX and MSTDP processes (31,32).

The MTDP-3 process is not *p*-xylene selective and so uses an unmodified ZSM-5 catalyst. The operation instead focuses on a high yield of benzenes and xylenes, claiming to achieve a 99.9 % benzene purity, superior xylene/benzene ratio and concentrates on keeping costs down (30).

The MSTDP process was introduced in 1991 (33), using a pre-coked catalyst to achieve a *p*-xylene selectivity of 82 % (34). One drawback of the MSTDP catalyst was that after each regeneration the catalyst had to undergo pre-coking selectivation. However, this also allowed for a level of control over *p*-xylene selectivity, as the amount of coke deposited on the zeolite could be adjusted (27), resulting in a range of *p*-xylene selectivity up to 90 % (34), but at the cost of a

shorter catalytic life. In contrast, the MTPX process which was originally commercialised in 1996 (35), used a silica-modified ZSM-5 catalyst in order to selectively produce *p*-xylene at a rate of 90 % (2). The silica modification was permanent (20), and so eradicated the need for *in-situ* selectivation after regeneration.

The current PxMax[SM] process was made available for licensing in 2000 (36). It claims a *p*-xylene selectivity of 96 %, a catalytic life of 15 years (31), and uses the same fixed-bed silica-modified ZSM-5 catalyst developed in the MTPX process (32). Further information on the process and the conditions used is limited.

Other companies such as Universal Oil Products (UOP, now Honeywell UOP) and Petrofina (FINA) have developed their own commercial toluene disproportionation processes: PX-Plus and T2BX respectively (2). The T2BX process, developed in the 1980s by FINA was not *p*-xylene selective, but instead produced high amounts of C_9 aromatics with a selectivity of up to 14 % (2). The Px-Plus process developed by UOP is a *p*-xylene selective toluene disproportionation process that achieves a *p*-xylene selectivity of up to 90 % (37). However, as with the PxMax[SM] process, information on these commercial processes is not readily available to the general public. The reaction conditions known about the processes mentioned are given in Table 3.1..

3.6. LAB SCALE CONDITIONS

Although toluene disproportionation is an industrial process, operating under the scale of a commercial process is outside of the remit of this research. Factors such as a 3-15-year catalytic cycle length and quantities of catalyst known to be up to 3700 Kg (34) are understandably impractical when conducting bench-top scale experiments. Therefore, it is important to understand the conditions used in lab-scale experiments published in the literature.

Experiments reported in the literature include (but are not limited to) studies on the effects of toluene disproportionation due to catalyst composition, including factors such as catalyst binder, cation exchange, impregnation and dealumination of the catalyst (1,3,5,38,39). There have been studies on the effect zeolite structure and acidity may have on toluene disproportionation (39,40),

as well as the contribution framework and extra-framework aluminium and iron cations may have on the reaction when using ZSM-5 (41). The scale and duration of these experiments was varied, and reaction conditions were often diverse, with parameters such as temperature ranging between 250°C and 550°C, and pressures of 1.03-29.2 Kg cm^{-2} being used. The conditions used in a selection of reported literature is given in Table 3.2..

Table 3.1. - Commercial Toluene Disproportionation Process Conditions (2)

	Toluene Disproportionation Process					
	TDP-3	MSTDP	MTPX	PxMax[SM]	Px-Plus	T2BX
Developer	Mobil	Mobil	Mobil	Mobil	UOP	FINA
Catalyst	ZSM-5	ZSM-5 pre-coked	ZSM-5 silica-modified	ZSM-5 silica-modified	Not disclosed	Not disclosed
Cycle length / years	>3	>1.5	-	15	-	>1
Reaction Conditions						
Reactor Type	Fixed bed	Fixed bed	Fixed bed	Fixed bed	Fixed bed	Fixed bed
Temperature / °C	435	455-470	~420	-	-	390-495
Pressure / kgcm^{-2}	24.5-28.2	21.1-42.3	~21.1-42.3	-	-	49.3
H$_2$/HC / mol	1-2	2-4	~2-4	-	-	4
WHSV / h^{-1}	6	2-4	-	-	-	1.2-2.3
Conversion / %	45-50	30	30	-	30	44
Product Selectivity / %						
C$_5^-$ gas	2.7	6.6	3.7	-	5.3	8.1
Benzene	42.3	44.9	44.7	-	46.4	35.0
Xylenes	50.4	43.5	48.0	-	44.7	40.8
EB	1.3	2.5	2.0	-	1.9	2.4
C$_9^+$ aromatics	3.3	2.5	1.6	-	1.7	13.7
Xylene Distribution / %						
p-xylene	25.2	82.2	89.8	96	90.2	25.1
m-xylene	52.8	15.1	8.2	-	8.5	50.1
o-xylene	22.0	2.7	2.0	-	1.4	24.8
B/(X+EB) / mol	1.1	1.3	1.2	-	1.4	1.1

Table 3.2. - *Literature Toluene Disproportionation Process Conditions*

	Toluene Disproportionation Process						
Author	Chen, W-H., et *al.* (2003)[a] (39)	Wu, J-C. & Leu, L-J. (1983) (3)	Bawa, J.S., et *al.* (1973) (1)	Yashima, T., et *al.* (1969) (5)	Rhodes, N.P. & Rudham, R. (1994) (38)	Cejka, J., et *al.* (1995) (41)	Odedairo, T., et *al.* (2011) (40)
Catalyst	Mordenite	Mordenite	13 X	Mordenite	Zeolite Y	ZSM-5	Mordenite ZSM-5 SSZ-33 TNU-9
Reaction Conditions							
Reactor Type	Fixed bed	Fixed bed	Fixed bed	Fixed bed	Fixed bed	Fixed bed	Fluidised bed
Temperature / °C	280-470	370-550	450-525	250-450	280-450	497	300-400
Pressure / Kg cm^{-2}	21.4	8.1-29.2	5-40	1.03[b]	1.03[b]	1.03[b]	9.25
H$_2$/HC / mol	3.0	2-3	3.8-10.94	0.2[c]	-	-	-
WHSV / h^{-1}	0.8-5.6	1.7	-	-	-	2.7	-
Carrier Gas	H$_2$	H$_2$	H$_2$	N$_2$	He	N$_2$	H$_2$

[a] TDP carried out in a commercial pilot plant

[b] Atmospheric pressure

[c] N$_2$ as carrier gas so molar ratio is of N$_2$/HC rather than H$_2$/HC

The effect of temperature on toluene disproportionation has been reported for a variety of catalysts. Yashima et *al.* (5), described an increase in toluene conversion with increase in temperature over synthetic mordenite within a certain temperature range. Temperatures of 250°C and below did not produce sufficient reaction, and temperatures of 450°C and above suffered from a decrease in xylene yield as more dealkylation and cracking occurred. Bawa et *al.* (1) studied the effect of temperature on conversion and selectivity over Linde 13X catalysts. They reported an increase in conversion between 475-500°C from 27-30.9 %, but a decrease in

conversion between 500-525°C falling from 30.9-26 %. This may be linked to the linear increase of hydrodealkylation with temperature that was described. Wu and Leu (3) studied the effect of temperature on conversion and selectivity over copper impregnated mordenite. They observed an increase in toluene conversion over temperatures between 420-550°C, and a decrease in selectivity over these temperatures. Table 3.3. shows that although there is a significant increase in conversion between 420°C and 480°C, the increase in conversion between 480°C and 550°C is not as significant. Similarly, for selectivity there is a smaller decrease between 420°C and 480°C and a slightly larger decrease between 480°C and 550°C, however this is not as significant as the changes in conversion.

Table 3.3. - Toluene Disproportionation Conversion and Selectivity Values at Different Temperatures (3)

Reaction Temperature / °C	Toluene Conversion / %	Reaction Selectivity / %
420	18	94
480	45	92
550	50	85

The effect of pressure on toluene disproportionation was also considered in the studies of Bawa et *al*. (1) and Wu, J-C. and Leu, L-J. (3), previously described. Bawa et *al*. (1), reported a beneficial increase in pressure between 5-40 Kg cm^{-2}, with toluene conversion increasing from 23.2-38.5 % by weight at 500°C. Wu and Leu (3), also reported an increase in toluene conversion with pressure, where 7-28 Kg cm^{-2} produced an increase in toluene conversion from 12-48 % at 480°C.

The effect of carrier gas on toluene disproportionation was reported by Schulz-Ekloff and Jaeger (42) over HZSM-5. The study investigated hydrogen, argon, nitrogen and helium as potential carrier gases at temperatures of 299-324°C, and pressures of 1.02-10.20 Kg cm^{-2}. From their research, they found toluene disproportionation activity decreased in order of argon > nitrogen > helium > hydrogen. They surmised the effect of carrier gas on toluene disproportionation activity could be associated with the size of the carrier gas molecules, with activity decreasing with decreasing diameter of the gas molecule or atom. A possible explanation was physical shielding

of catalytic active sites, where the smaller molecules can approach closest to the sites, rendering them inaccessible. With respect to selectivity, xylene isomer distribution was close to thermodynamic equilibrium under all conditions used, however they reported a benzene deficit with a B/X ratio of ~0.8, attributing this to possible further reactions of a benzenium ion intermediate (42). It is important to note however, Schulz-Ekloff and Jaeger (42) operated under extremely low conversion rates of 2-15 % to minimise coke deposition. In other studies, Yashima et *al*. (5) reported that over mordenite, under their toluene disproportionation conditions, choice of carrier gas (H_2 or N_2) did not appear to make a difference. Gnep and Guisnet (43) however, reported hydrogen having a stabilising effect on mordenite during toluene disproportionation when under pressure, as it inhibited coke deposition and produced spectator coke or coke with less deactivating properties.

In summary, there are a wide range of conditions used within the literature for carrying out toluene disproportionation, as would be expected in studies investigating effects of catalyst modification. There appears to be a trend in temperature across the studies, whereby an increase in conversion is seen within a specific temperature range, dependent on other conditions and the catalyst used. Lower temperatures are unable to facilitate a reaction, and higher temperatures promote competing side reactions. An increase in pressure is suggested to improve conversion over the range reported regardless of catalyst type. However, effect of carrier gas appears to be dependent on the specific reaction conditions and catalyst used, with literature reporting contradictory effects.

3.7. REFERENCES

(1) Bawa JS, Shanker U, Rawat DS, Dabral RP, Bhattacharyya KK. Disproportionation of Toluene to Benzene and Xylenes. Indian Institute of Petroleum 1973;41(1):55-62.

(2) Tsai T, Liu S, Wang I. Disproportionation and Transalkylation of Alkylbenzenes Over Zeolite Catalysts. Applied Catalysis A: General 1999;181(2):355-398.

(3) Wu J, Leu L. Toluene Disproportionation and Transalkylation Reaction Over Mordenite Zeolite Catalysts. Applied Catalysis 1983;7:283-294.

(4) Tsai T. Reactivation of Acidic Sites in Mordenite Used in Toluene Disproportionation. Applied Catalysis A: General 2006;301(2):292-298.

(5) Yashima T, Moslehi H, Hara N. Disproportionation of Toluene on Synthetic Mordenites. Bulletin of the Japan Petroleum Institute 1970;12(May):106-111.

(6) Izumi Y, Shiba T. Characterisation of the Alumina-Boria Catalyst. Bulletin of the Chemical Society of Japan 1964;37(12):1797-1809.

(7) Cejka, J. & Wichterlova, B. Acid-Catalysed Synthesis of Mono- and Dialkyl Benzenes Over Zeolites: Active Sites, Zeolite Topology, and Reaction Mechanisms. Catalysis Reviews: Science and Engineering 2002;44(3):375-421.

(8) Xlong Y, Rodewald PG, Chang CD. On the Mechanisms of Toluene Disproportionation in a Zeolite Environment. J Am Chem Soc 1995;117:9427-9431.

(9) Tsai TC, Chen WH, Lai CS, Liu SB, Wang I, Ku CS. Kinetics of Toluene Disproportionation Over Fresh and Coked H-mordenite. Catalysis Today 2004;97(4):297-302.

(10) Olson DH, Haag WO. Structure-Selectivity Relationship in Xylene Isomerisation and Selective Toluene Disproportionation. In: Whyte TEJ, Betta RAD, Derouane EG, Baker RTK, editors. Catalytic Materials: Relationship Between Structure and Reactivity United States of America: American Chemical Society; 1984. p. 275-307.

(11) Sato M, Otani K, Otani S, Ohtsu-shi, inventors. Toyo Rayon Kabushiki Kaisha, assignee. Method of the Disproportionation of Toluene. United States patent 3,553,277. 1967 1971.

(12) Given PH, Hammick DL. Some Catalysed Gas-Phase Reactions of Aromatic Hydrocarbons. Part V. Interconversion of Alkylbenzene. Disproportionation and Cracking Reactions. Journal of the Chemical Society 1949;0:1779-1783.

(13) Matsumoto H, Morita Y. The Activities of Zeolite Catalysts for the Reaction of Aromatic Hydrocarbons. Bulletin of the Chemical Society of Japan 1968;10:8-13.

(14) Venuto PB, Landis PS. Organic Catalysis Over Crystalline Aluminosilicates. Advances in Catalysis. 18th ed. New York: Academic Press Inc.; 1968. p. 319-340.

(15) Yates DJC. The Stability of Metallic Cations in Zeolites. Journal of Physical Chemistry 1965;69:1676-1683.

(16) Benesi HA. Relationship Between Catalytic Activity and Nature of Acidity of the Crystalline Zeolites, Mordenite and Y Faujasite. Journal of Catalysis 1967;8:368-374.

(17) Mitsche RT, Michalko E, inventors. Universal Oil Products Company, assignee. Transalkylation of Alkylaromatic Hydrocarbons in Contact with a Zeolite Catalyst Composition. United States of America patent 3720726. 1972 1973.

(18) Otani S, Iwamura T, Hayashi S, Ogawa D, Kanaoka M, inventors. Toyo Rayon Kabushiki Kaisha, assignee. Process for Converting Toluene to Benzene and Xylene. Japan patent 3597492. 1969 1971.

(19) Kareem A, Chand S, Mishra I. Disproportionation of Toluene to Produce Benzene and p-Xylene - A review. J Sci Ind Res 2001;60(4):319-327.

(20) Chang CD, Shihabi DS, inventors. Mobil Oil Corporation, assignee. Catalyst and Process for the Selective Production of Para-dialkyl Substituted Benzenes. United States of America patent 5243117. 1993 1990.

(21) Rodewald PG, inventor. Mobil Oil Corporation, assignee. Process for Selective Production of Para Dialkyl Substituted Benzenes. United States of America patent 4127616. 1978 1978.

(22) Rodewald PG, inventor. Mobile Oil Corporation, assignee. Catalyst for Selective Production of Para Dialkyl Substituted Benzenes. United States of America patent 4090981. 1978 1976.

(23) Beck JS, McCullen SB, Olson DH, inventors. Mobil Oil Corporation, assignee. Selective Toluene Disproportionation Process (STDP) with Ex Situ Selectivated Zeolite Catalysis. United States of America patent 5365004. 1994 1993.

(24) Beck JS, Olson DH, McCullen SB, inventors. Mobil Oil Corporation, assignee. Selective Toluene Disproportionation Process (STDP) with Ex Situ Selectivated Zeolite Catalyst. United States of America patent 5367099. 1994 1993.

(25) Kaeding WW, Young LB, inventors. Mobil Oil Corporation, assignee. Selective Production of Para-xylene. United States of America patent 4034053. 1977 1975.

(26) Kaeding WW, inventor. Mobil Oil Corporation, assignee. Disproportionation of Toluene. United States of America patent 4016219. 1977 1975.

(27) Haag WO, Olson DH, inventors. Mobil Oil Corporation, assignee. Selective Disproportionation of Toluene. United States of America patent 4097543. 1978 1977.

(28) Haag WO, Olson DH, inventors. Mobil Oil Corporation, assignee. Selective Production of Para Dialkyl Substituted Benzenes. United States of America patent 4117026. 1978 1977.

(29) ExxonMobil Corporation. Xylenes Production. 2017; Available at: https://www.exxonmobilchemical.com/en/products-and-services/technology-licensing-and-services/xylenes-production. Accessed 01/05, 2019.

(30) ExxonMobil Corporation. ExxonMobil's State-of-the-Art Processes for Toluene Disproportionation. 2018; Available at: https://www.exxonmobilchemical.com/~/media/chemicals/kl-media-assets/2017/08/24/09/56/aromatics_processes_mtdp_3pdf.pdf. Accessed 09/24, 2018.

(31) ExxonMobil Corporation. Unmatched PX Selectivity and Catalyst Cycles in STDP Service. 2018; Available at: https://www.exxonmobilchemical.com/en/library/Asset/7AB8134F64AA41BA83B95B7C55B2E298. Accessed 09/24, 2018.

(32) ExxonMobil Corporation. PxMax[SM] - Selective Toluene Disproportionation Technology from ExxonMobil. 2002; Available at: https://www.researchgate.net/profile/Rick_Manner/post/How_can_I_find_the_rate_expressions_kinetics_for_reactions_of_tatoray_process/attachment/5a5d3d654cde266d58834b12/AS%3A583212088532992%401516060005510/download/ExxonMobil+transalky+-+TDP+process+info+from+website.pdf. Accessed 01/05, 2019.

(33) Ramaswamy AV. Catalysis and Production of Petrochemicals. In: Riswanathan B, Sivasanker S, Ramaswamy AV, editors. Catalysis Principles and Applications New Delhi: Narosa Publishing House; 2002. p. 245-246.

(34) Gorra F, Breckenridge LL, Guy WM, Sailor RA. Selective Toluene Disproportionation Process Proven at Italian Refinery. Oil & Gas Journal 1992;90(41):09/24/2018.

(35) ICIS. PxMax Process Licensed. 2000; Available at: https://www.icis.com/resources/news/2000/10/02/123294/pxmax-process-licensed/. Accessed 09/24, 2018.

(36) Axens. PxMax. 2017; Available at: https://www.axens.net/product/process-licensing/10041/pxmax.html. Accessed 09/24, 2018.

(37) UOP LLC. Aromatics and Derivatives - The PX-Plus[TM] Process. 1999; Available at: pxplus+tech+sheet.pdf. Accessed 01/06, 2019.

(38) Rhodes NP, Rudham R. Catalytic Studies with Dealuminated Y Zeolite - Part 2. - Disproportionation of Toluene. Journal of the Chemical Society Faraday Transactions 1994;90(5):809-814.

(39) Chen WH, Huang SJ, Lai CS, Tsai TC, Lee HK, Liu SB. Effects of Binder, Coking and Regeneration on Acid Properties of H-mordenite During TDP Reaction. Research on Chemical Intermediates 2003 2003;29(7-9):761-772.

(40) Odedairo T, Balasamy RJ, Al-Khattaf S. Toluene Disproportionation and Methylation over Zeolites TNU-9 SSZ-33, ZSM-5, and Mordenite Using Different Reactor Systems. Industrial & Engineering Chemistry Research 2011;50:3169-3183.

(41) Cejka J, Zikova N, Tvaruzkova Z, Wichterlova B. Contribution of Framework and Extraframework Al and Fe Cations in ZSM-5 to Disproportionation and C3 Alkylation of Toluene. Studies in Surface Science and Catalysis 1995;97:401-408.

(42) Schulz-Ekloff G, Jaeger NI. Effects of Carrier Gases in the Toluene Disproportionation on HZSM-5 Zeolite. Applied Catalysis 1987;33:73-81.

(43) Gnep NS, Guisnet M. Toluene Disproportionation over Mordenites - II. Kinetic Study. Applied Catalysis 1981;1:329-342.

CHAPTER 4: CHARACTERISATION AND EXPERIMENTAL METHODS

The characterisation and experimental methods provided in this chapter appear in their final form for ease of replication. However, during research challenges occur and methods are often optimised to improve accuracy and replicability to achieve best possible results. Details of where this has occurred within this research, and the optimisation processes implemented are given at the end of the chapter for reference.

4.1. EXPERIMENTAL METHODS

4.1.1. Toluene Disproportionation

Toluene disproportionation was carried out via two different methods, referred to within this thesis as small-scale and large-scale. Both processes were performed at bench-scale, with small-scale toluene disproportionation producing approximately 700 mg and large-scale producing approximately 3 g of coked catalyst. All activity data contained herein was measured under small-scale toluene disproportionation. The large-scale method was introduced in order to rapidly produce greater quantities of coked catalyst for dielectric barrier discharge regeneration and microwave regeneration. Differences between the methods and apparatus used are given in Table 4.1..

Materials

All catalyst samples consisted of commercially available extruded (1.6 mm cylinders) ammonium mordenite (Zeolyst CBV21A), with a silicon to aluminium ratio (Si/Al ratio) of 20 and contained ~ 20 % alumina binder. The samples were provided by Johnson Matthey. Prior to use, they underwent size modification at UCLan (cutting extrudate to ≤ 0.5 cm) to minimise dead space in the reactor. The toluene feed was analytical grade (99.99 % purity) manufactured by Acrôs Organics and was used as supplied by the manufacturer. Nitrogen gas was supplied by Energas and was used as supplied by the manufacturer.

Table 4.1. - Laboratory Toluene Disproportionation Apparatus and Conditions

	Small-Scale	Large-Scale
Apparatus		
Furnace	Leco Laboratory Equipment Corporation furnace; Vertex VT4830 temperature controller	Carbolite VST 12/60/200 clamshell furnace; Eurotherm 2408 temperature controller
Mass Flow Controller	MKS type 1179A Mass Flo® controller; MKS type 247D four-channel readout)	
Heating Tape and Controller	Electrothermal MC227 one-way heating controller	
Gas Line	Swagelok rubber core hose rayon fiber reinforced hose	
Swagelok Fittings	¼ inch	¾ inch
Reaction Conditions		
Mass of Catalyst / g	0.6	3
Carrier Gas	N_2	N_2
Flow Rate / mL min^{-1}	20	85[a]
Calcination Temperature / °C	300	300
Calcination Duration / hours	1	1
Temperature / °C	500	500
Duration / hours	16.5	46
Total Reactor Bed Volume / cm^3	1.79	7.85
Coke Content / %	3.89 ± 0.63	2.91 ± 0.64

[a] 85 mL min^{-1} used to produce the same space velocity as the small-scale reaction

Small-Scale

Virgin mordenite (~700 mg) was packed into a fixed-bed borosilicate microreactor containing a thermocouple well and plugged with glass wool (total reactor bed volume: 1.79 cm^3) (Figure 4.1.). The microreactor was enclosed within a temperature programmed furnace and connected to a gas line regulated by a mass flow controller via Swagelok stainless steel vacuum fittings with O-ring seals. The output gas line was heated using heating tape (to 150°C ± 3°C) which was connected to a controller. A Pyrex® gas saturator fitted with a sinter (Figure 4.2.) was attached to the gas line before the microreactor, so that toluene could be fed over the catalyst when the valves V_a and V_b were opened (Figure 4.3..). During the reaction, the saturator was submerged in an ice bath to regulate the temperature of the toluene. A schematic of the small-scale toluene disproportionation set-up is given in Figure 4.3..
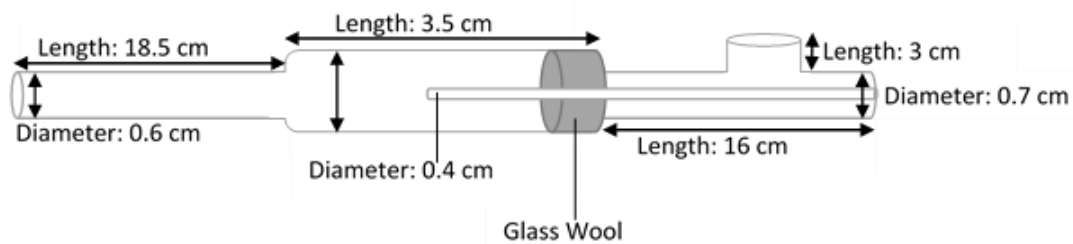
Figure 4.1. - Microreactor for Small-Scale TDP
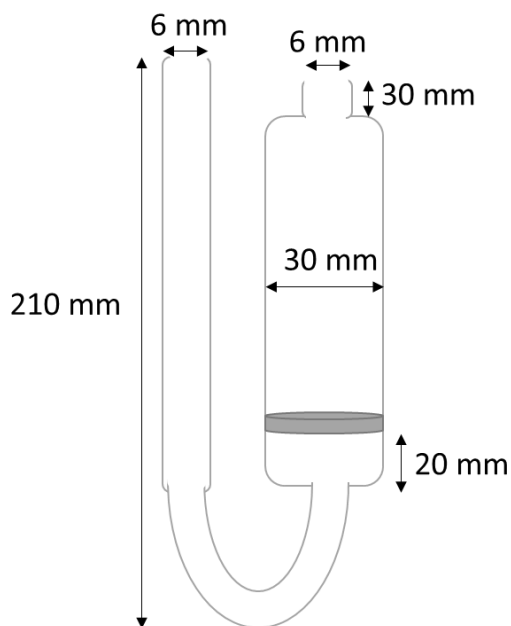
Figure 4.2. - Schematic of Gas Saturator for TDP
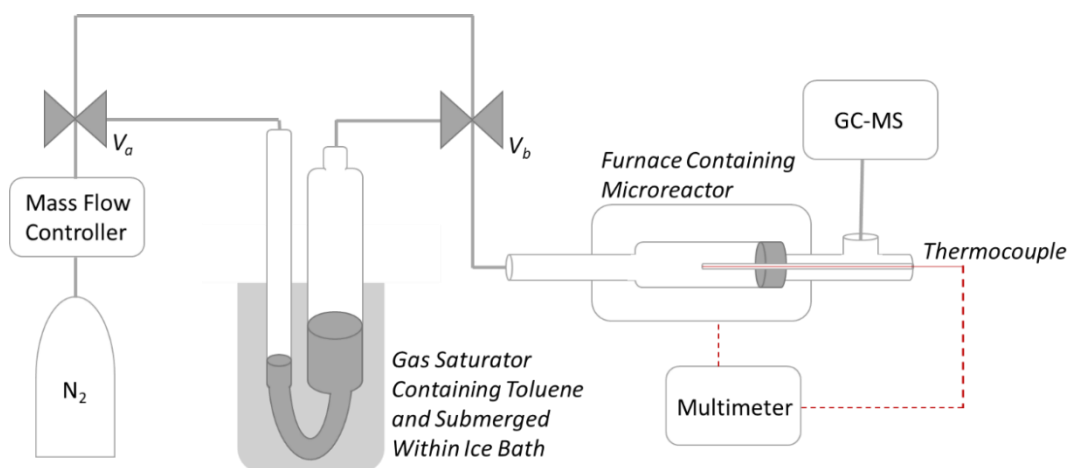
Figure 4.3. - Schematic of Small-Scale TDP

V_a and V_b designate two-way valves that can be opened to allow gas to travel over the toluene contained in the gas saturator or closed to divert gas flow directly from source to microreactor.

Large-Scale

Virgin mordenite (~3 g) was packed into a fixed-bed borosilicate reactor tube plugged with glass wool (total reactor bed volume: 7.85 cm^3) (Figure 4.). The reactor tube was enclosed within a temperature programmed furnace and connected to a gas line regulated by a mass flow controller via Swagelok stainless steel vacuum fittings with O-ring seals. The output gas line was heated using heating tape (to 150°C ± 3°C) which was connected to a controller. A Pyrex® gas saturator fitted with a sinter (Figure 4.2.) was attached to the gas line before the reactor, so that toluene could be fed over the catalyst when the valves V_a and V_b were opened (Figure 4.5.). During the reaction, the saturator was submerged in an ice bath to regulate the temperature of the toluene. A schematic of the large-scale toluene disproportionation set-up is given in Figure 4.5..

Figure 4.4. – Reactor for Large-Scale TDP
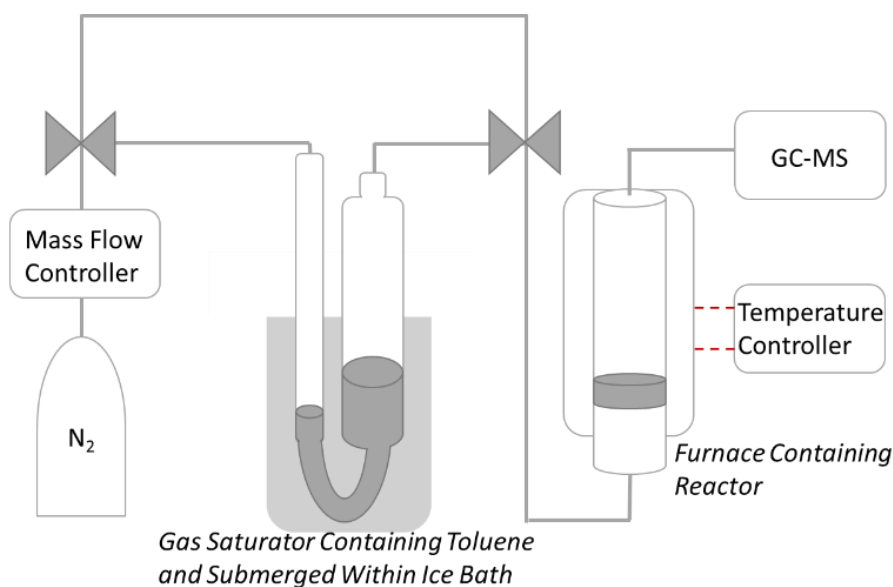
Figure 4.5. - Schematic of Large-Scale TDP

4.1.2 Regeneration Methods

Three regeneration methods involving microwaves and plasma were undertaken. A thermal regeneration method was also employed, acting as a facsimile to industrial regeneration methods, although on a much smaller scale. This allowed for a like-with-like comparison between the commonly used thermal regeneration with the novel microwave, plasma and combined methods.

Materials

All coked catalyst samples were produced from deactivating the virgin catalyst supplied via toluene disproportionation (as previously described in Section 4.1.1.). All gases were supplied by Energas and were used as supplied by the manufacturer.

Thermal

Coked mordenite (~700 mg) was packed into a fixed-bed borosilicate reactor tube plugged with glass wool (total reactor bed volume: 1.79 cm^3). The reactor was enclosed within a temperature programmed furnace and connected to a gas line regulated by a mass flow controller via Swagelok stainless steel vacuum fittings with O-ring seals. Regeneration was performed under air (20 mL min^{-1}) at 500°C (heating rate: 60°C per minute) for a period of 24 hours. The furnace was then switched off and the sample was left in the furnace to cool (approximate cooling rate: 0.13°C per minute). A schematic of the thermal regeneration equipment is given in Figure 4.6..
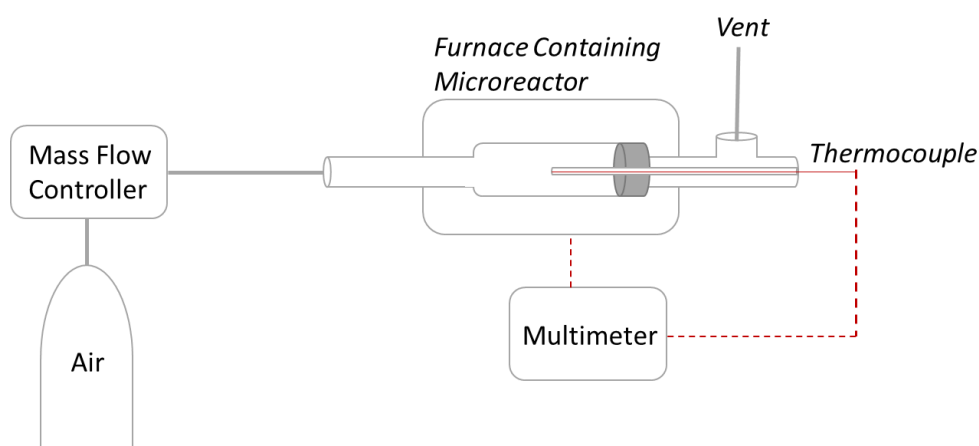
Figure 4.6. - Schematic of Thermal Regeneration

Microwave

The apparatus for microwave regeneration and microwave plasma regeneration are largely identical and details can be found in Table 4.2..

Table 4.2. - Microwave and Microwave Plasma Regeneration Apparatus and Conditions

	Microwave Regeneration		Microwave Plasma Regeneration	
Apparatus				
Microwave Generator	2.45 GHz half-wave rectified, supplied by Industrial Microwave Systems Ltd.			
Wave Guide Aperture Dimensions / cm	9.0 x 4.7		3.1 x 2.1[a]	
Mass Flow Controller	MKS type 1179A Mass Flo® controller; MKS type 247D four-channel readout)			
Gas Line	Swagelok rubber core hose rayon fiber reinforced hose			
Swagelok Fittings	½ inch		¾ inch	
Vacuum Pump	N/A		Vacuubrand PC3001 VARIO Pro vacuum pump fitted with Vacuubrand CVC3000 Detect compact vacuum controller	
Thermocouple	Omega Precision I/R Thermocouple with k-type output signal			
Multimeter	TENMA® Dual Input Thermometer			
Reactor Tube	Quartz		Quartz	
Reaction Conditions				
Mass of Catalyst / g	3.5		0.7	
Total Reactor Bed Volume / cm^3	5.5		1.57	
Gas(es) Used	Argon	Oxygen	Argon	Oxygen
Flow Rate / mL min^{-1}	10	5	20	10
Power[b] / Watts	~200		~200	
Temperature /°C	250 ± 50		230 ± 10	
Pressure / mbar	1013.25 (Atmospheric)		5	
Reflective Power / %	25 ± 5		10 ± 5	
Duration / hours	7		7	

[a] Wave guide aperture was minimised for microwave plasma to focus the microwaves for ease in producing the plasma.

[b] Power was altered to maintain temperature because the total energy of the system was affected by the catalyst; i.e. amount of coke remaining in the system. For further information on challenges and considerations when carrying out this experiment, please refer to Section 4.3.2 at the end of this chapter.

Coked mordenite (~3.5 g) was packed into a fixed-bed quartz reactor tube plugged with glass wool (total reactor bed volume: 5.50 cm^3). The reactor tube was enclosed within a cavity with a viewing port and connected to a gas line regulated by a mass flow controller via Swagelok stainless steel vacuum fittings with O-ring seals. The cavity was part of the microwave apparatus, consisting of a 2.45 GHz half-wave rectified microwave generator connected to a variable power

supply (max: 1 kW), wave guide, water cooled circulator and manual tuning stage. A reflective power meter and infrared thermocouple were used to measure reflected power and temperature respectively. In order to ensure homogeneity of the treatment across the sample, the reactor tube was periodically removed and rotated 90°. A schematic of the experimental apparatus is given in Figure 4.7..
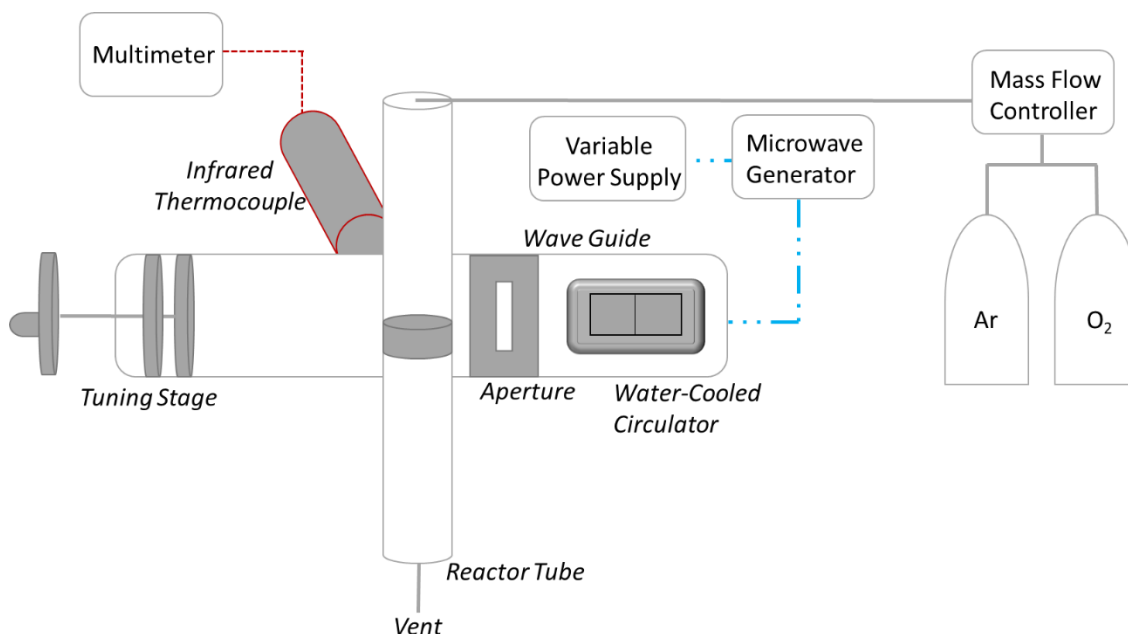
Figure 4.7. - Schematic of Microwave Regeneration

Microwave Plasma

The apparatus for microwave regeneration and microwave plasma regeneration are largely identical and details can be found in Table 4.2..

Coked mordenite (~700 mg) was packed into a fixed-bed quartz reactor tube containing a glass sinter (total reactor bed volume: 1.57 cm^3). The reactor tube was enclosed within a cavity with a viewing port and connected to a gas line regulated by a mass flow controller via Swagelok stainless steel vacuum fittings with O-ring seals and connected to a vacuum pump. The cavity was part of the microwave apparatus, consisting of a 2.45 GHz half-wave rectified microwave generator connected to a variable power supply (max: 1 kW), wave guide, water cooled circulator and manual tuning stage. Reflected power and temperature were measured using a reflective

power meter and infrared thermocouple respectively. A schematic of the experimental equipment is given in Figure 4.8.. In order to ensure homogeneity of the treatment across the sample, the reactor tube was periodically removed and vigorously shaken.
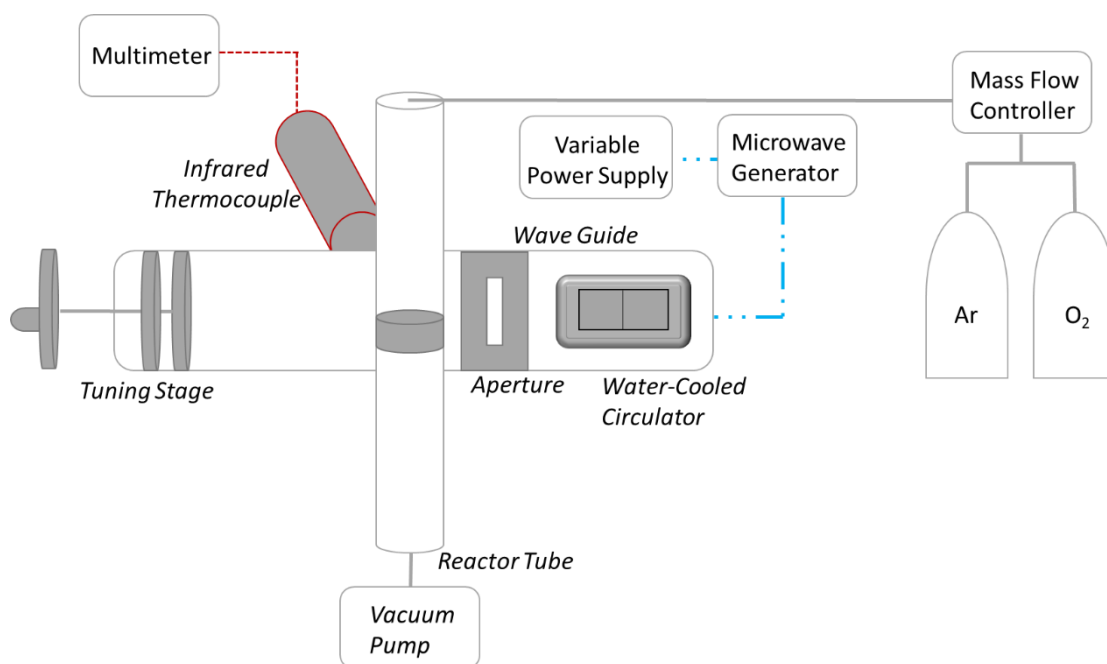
Figure 4.8. - Schematic of Microwave Plasma Regeneration

Dielectric Barrier Discharge Plasma

Experiments using dielectric barrier discharge plasma were performed at Johnson Matthey Technology Centre, Chilton by Dr. Vladimir Demidyuk, Dr. Alkis Gkelios and Dr. Peter Hinde. Conditions of the DBD treatment are given in Table 4.3..

Coked mordenite (~1 g) was packed into a quartz reactor tube (total reactor bed volume: 50 cm^3). The reactor tube was enclosed within the plasma chamber that contained the stainless-steel mesh electrodes, dielectric barriers and gas inlet and outlet. A schematic of the dielectric barrier discharge apparatus is given in Figure 4.9..

Table 4.3. - Conditions Used in DBD Regeneration

Mass of Catalyst / g	1	
Total Reactor Bed Volume / cm^3	50	
Gas(es) Used	Argon	Oxygen
Flow Rate / mL min^{-1}	80	20
Power / Watts	14	
Pressure / mbar	1013.25 (Atmospheric)	
Voltage / kV (peak-to-peak)	20	
Frequency / kHz	10	
Discharge Gap / mm	5	
Duration / hours	8	
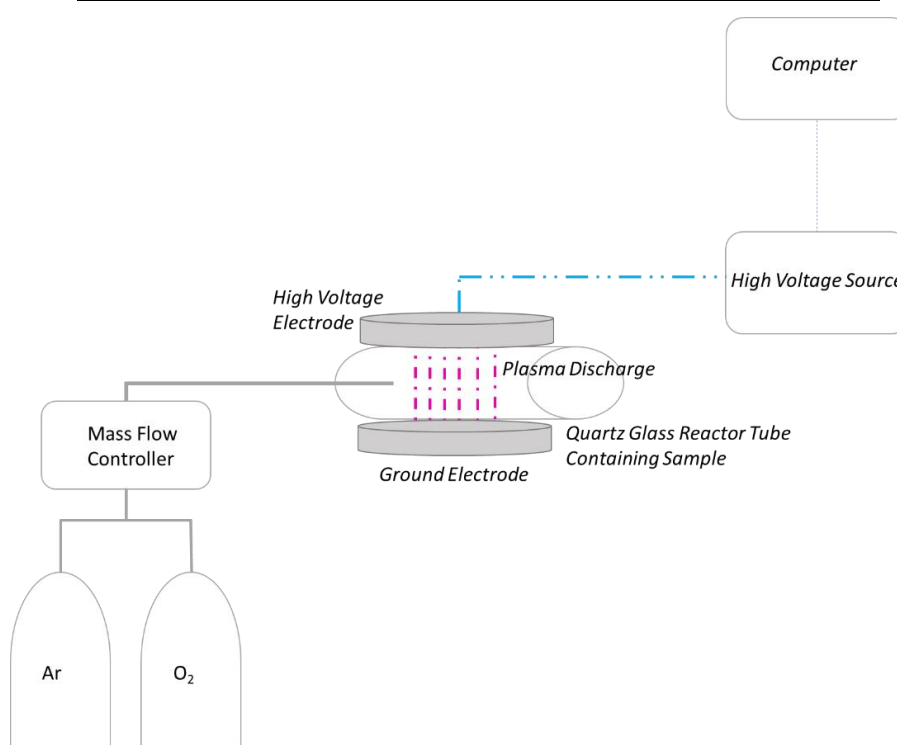
Figure 4.9. - Schematic of Dielectric Barrier Discharge Regeneration

4.1.3 Pre-Treatment

Pre-treatment involved the exposure of size-modified virgin catalyst to microwaves, plasma or a combination of the two. Methods of pre-treatment were, for all practical purposes, identical to their regeneration counterparts, allowing for a comparison between the two. Any observed differences between the pre-treatment methods with their corresponding regeneration experiments are discussed in the challenges and optimisation section at the end of this chapter (Section 4.3.3.).

4.2. CHARACTERISATION TECHNIQUES

4.2.1. Gas Chromatography Mass Spectrometry

Background

Gas Chromatography Mass Spectrometry (GC-MS) is the amalgamation of two analytical techniques, combining the separation technique of Gas Chromatography (GC) with the structural identification properties of Mass Spectrometry (MS) (1). GC uses a stationary phase (e.g. the silica coating on the GC column) and an inert mobile phase (typically hydrogen or helium), in order to separate a mixture of compounds (2). The mobile phase carries the sample to the column, where the affinity for a compound to remain on it (determined by its properties) is different between species; leading each compound to elute at a different time. Detection of these eluted compounds was performed by a mass spectrometer and displayed as a function of time, resulting in production of the chromatogram. MS works by ionising gaseous species (leading to fragmentation) and then measuring the mass-to-charge ratio *(m/z)* of these ions (3). Identification is then made by matching the fragmentation patterns to those stored in a library. By combining the two techniques, identifying a mixture of compounds can be performed quickly and efficiently and when calibrated against known standards, these compounds can be quantified (1). A schematic of a GC-MS is given in Figure 4.10..
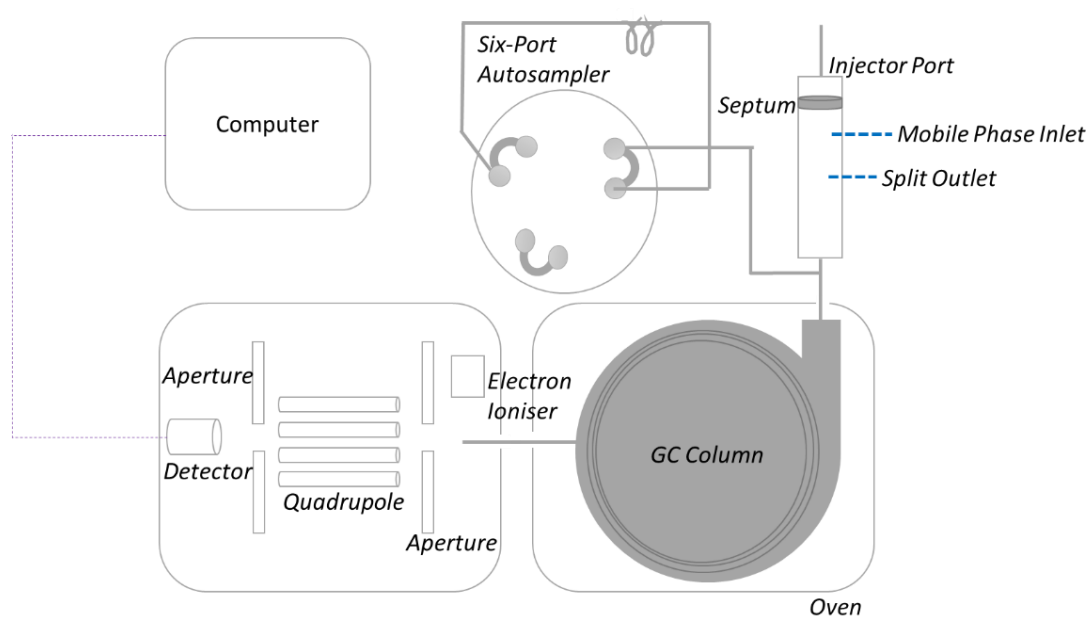
Figure 4.10. - Schematic of GC-MS

Application and Procedure

GC-MS was used to periodically monitor the catalyst activity during toluene disproportionation. By calibrating toluene and the disproportionation products, the technique could be used to quantify the amount of products (and unreacted toluene) to determine catalytic activity throughout the experiment. The detector was calibrated over a range of concentrations comparable with those observed during the toluene disproportionation experiments. A multi-point calibration using 5 concentrations was performed to produce calibration curves. This multi-point calibration procedure was carried out periodically, however two-point calibrations were performed daily to maintain accurate quantification and compensate for small changes in detector sensitivity. The GC-MS apparatus and conditions used is given in Table 4..

Table 4.4. - GC-MS Apparatus and Conditions

GC	Thermo Scientific Focus GC
MS	Thermo Scientific DSQ II
Column	Supelco Supelcowax™ 10 fused silica capillary column
Column Dimensions	30 m x 0.2 mm x 0.2 μm
GC Gas	He
Flow Rate / mL min^{-1}	1.5
GC Inlet Temperature / °C	200
Split Ratio	200
Injector Loop / mL	1
Transfer Line Temperature / °C	250
Ion Source Temperature / °C	200

The GC was coupled to an MS and fitted with a column specifically chosen for its resolution of xylene isomers. The GC operated under constant flow and samples were injected via an autosampler (Figure 4.11.) at 0.10 mins for 0.50 mins into the injector loop. The GC programme operated as described in

Table 4.5.. The programme was set to run a total of 50 times in order to monitor samples throughout the duration of the experiment.
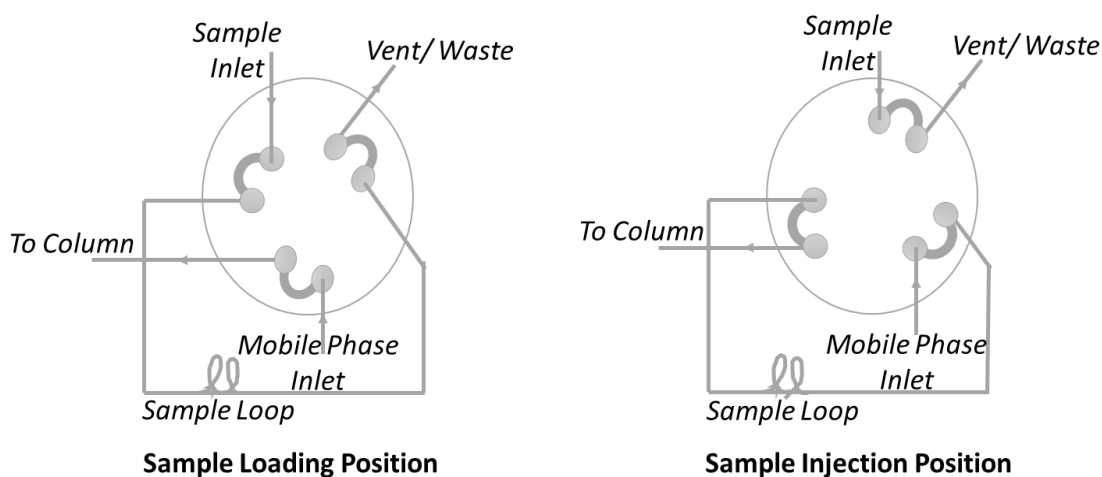
Figure 4.11. - Schematic of Autosampler

Table 4.5. - GC Programme

	Ramp Rate / °C min^{-1}	Initial Temperature / °C	Final Temperature / °C	Hold Time / mins
Isotherm	n/a	40	40	2
Ramp 1	3	40	70	0
Ramp 2	20	70	200	0

Under these conditions, base line separation (Figure 4.12.) was obtained for products from toluene disproportionation: toluene, benzene, and *para- meta-* and *ortho-* xylenes. Common side reaction products – ethylbenzene and trimethylbenzene – were also recorded.

Products from the GC were transferred via a line to the MS. The MS ran a full scan with a mass range of 15-400 at a scan rate of 1.2610 scans per second with a total scan time of 0.79 seconds. The output from the detectors was recorded using Thermo Scientific XCalibur^{TM} software (Version 2.0.7.) and transferred to Microsoft Excel for data analysis.
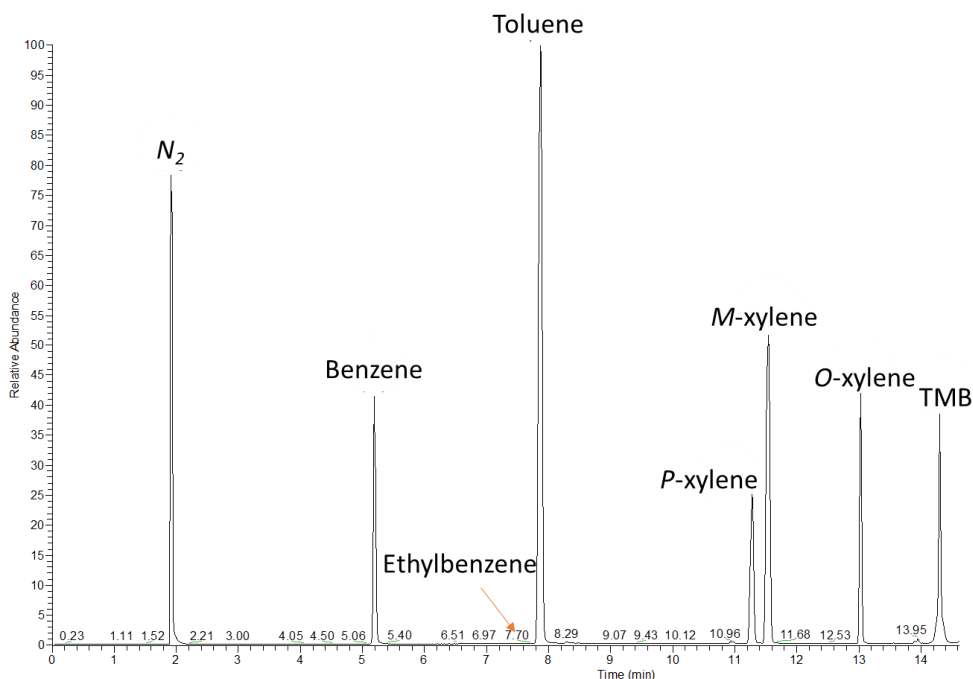
Figure 4.12. - Example of a TDP Chromatogram

4.2.2. Thermogravimetric Analysis

Background

Thermal analysis operates under the principle that the physical and/or chemical properties of a material can change as a product of temperature. Thermogravimetric analysis (TGA) is a type of thermal analysis which measures the change in mass as a function of temperature (4). The apparatus consists of a sensitive recording balance housed inside a temperature-controlled furnace, connected to a computer. The atmosphere is controlled via a gas inlet and can either be inert (e.g. N_2) or reactive (e.g. O_2). When heating a compound under a controlled temperature programme, phase transitions, drying (i.e. loss of solvent) or oxidation reactions may occur, leading to a recorded mass loss. As such, this apparatus is commonly used in thermal stability studies. A schematic of TGA apparatus is given in Figure 4.13..
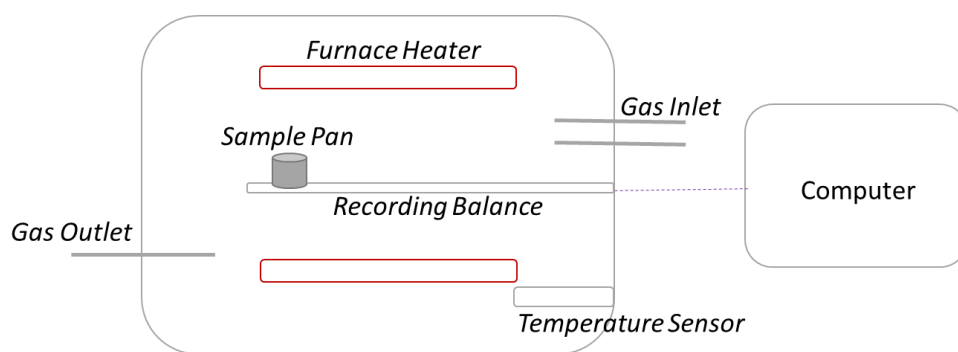
Figure 4.13. - Schematic of TGA

Application and Procedure

Carbon content of deactivated and regenerated catalysts was determined using TGA, with the mass loss at 500°C attributed to loss of coke. Details of apparatus and conditions is given in Table 4.6.. The TGA operated under constant flow of purge gas and oxidising carrier gas regulated by rotameters. Extrudate samples were heated in an open alumina pan. The TGA programme operated as given in Table 4.7. - TGA Programme.. Under these conditions, all visible carbon was removed. Blank TGA runs were subtracted to minimise any buoyancy effects. Mass loss was recorded using Mettler STARe Software (Version 13.00.) and transferred to Microsoft Excel for data analysis.

Table 4.6. - TGA Apparatus and Conditions

TGA	Mettler Toledo TGA1 STARe System	
Rotameters	CT Platon NG Series GTF1CHD-5-100 cm^3 min^{-1}	
Pan	Mettler Toledo TGA Crucible Set, Alumina Crucible 51140843, 70 µL	
Gases	Purge	Oxidising
	N$_2$	Compressed Air
Flow Rate / mL min^{-1}	20	20

Table 4.7. - TGA Programme

	Ramp Rate / °C min^{-1}	Initial Temperature / °C	Final Temperature / °C	Hold Time / mins
Ramp 1	10	25	400	n/a
Isotherm 1	n/a	400	400	30
Ramp 2	5	400	500	n/a
Isotherm 2	n/a	500	500	300
Ramp 3	5	500	600	n/a
Isotherm 3	n/a	600	600	120
Ramp 4	5	600	800	n/a
Isotherm 4	n/a	800	800	60

4.2.3. Powder X-ray Diffraction

Background

Powder X-ray diffraction (XRD) is an analytical technique that can be used to identify and characterise crystalline materials. When X-rays meet an obstacle, the electron cloud surrounding the atoms causes the x-ray beam to scatter (5). The resulting constructive beams give a unique diffraction pattern specific to that material. Bragg's law applies this theory, introducing an integer to ensure all waves are constructive (thus producing a diffraction pattern), and by measuring the angle of incidence (ϴ), interlayer spacing *(d)* can be calculated. Bragg's law can be expressed as Bragg's equation given in Equation 4.1. (6).

XRD apparatus consists of an X-ray source focused onto a sample, a detector connected to a computer that records diffracted X-rays from the sample, and a method of varying angle θ. In the Bruker D2 Phaser, this is accomplished via movement of the detector through 2θ in an arc. A schematic of XRD apparatus taken from Powder Diffraction: Theory and Practice (7) is given in Figure 4.14..

Equation 4.1. - Bragg's Law

$$n\lambda = 2d\sin\theta$$

Where: n is an integer

λ is the wavelength of the X-ray

d is the interlayer spacing of the atoms

θ is the X-ray angle of incidence
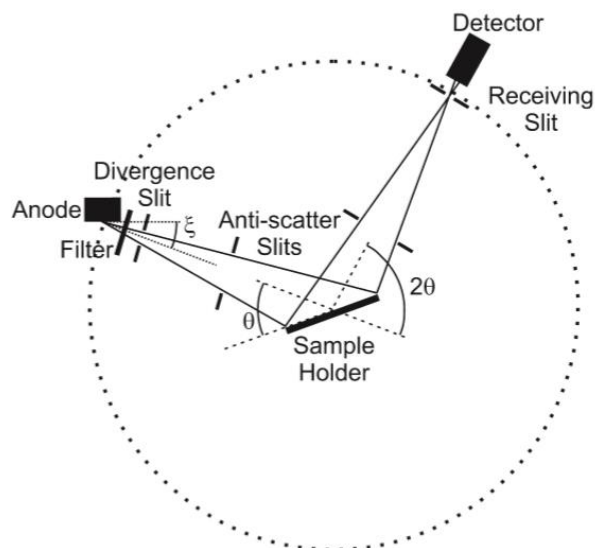
Figure 4.14. - Schematic of XRD (7)

Application and Procedure

XRD analysis was carried out on catalyst samples to determine any crystalline changes that regeneration or pre-treatment may have had on the sample. Details of apparatus and conditions used is given in Table 4.8..

Catalyst samples were ground from extrudate into a fine powder before being packed into a specimen holder. The prepared sample was loaded into the XRD instrument, where the X-ray generator produced Kα 1 and 2 X-rays. Measurements were taken between 5-80° at 2.5° per minute and recorded by the detector. Data was analysed using Bruker DIFFRAC.EVA (V3.0.) software.

Table 4.8. - XRD Apparatus and Conditions

XRD	Bruker D2 Phaser
Detector	Bruker Lynexeye
Specimen Holder	PMMA 8.5 mm height, sample reception ø 25 mm
Source	Cu
Wavelength / Å	1.5418
Filter	Ni
Measurement range / °	5-80
Measurement rate / ° min⁻¹	2.5

4.2.4. Gas Adsorption

Background

Gas adsorption is one of the fundamental techniques used to determine surface area and pore size of porous materials. It involves the interaction between an adsorbent (solid) and an adsorbate (gas) at the gas/solid interface (8). The amount adsorbed on a solid surface is dependent on temperature, pressure and the interaction potential between the surface with the gas. Adsorption can be a chemical or physical process, depending on the strength of the interaction between adsorbent and adsorbate (8). Chemisorption is irreversible and involves the chemical bonding of the gas with the solid. In contrast, physisorption is reversible, and occurs whenever an absorbable gas is brought into contact with the surface of the solid. Physisorption may involve multilayer coverage, can completely fill pores and absorbed molecules are not site specific, allowing for surface area measurements to be made (8).

IUPAC have published six isotherms illustrating the possible sorption profiles arising from different materials with various pore sizes (Figure 4.15.) (9). It is not within the remit of this thesis to discuss the isotherms in detail, but a brief description of each isotherm and the conditions involved to produce them is given in Table 4.9..
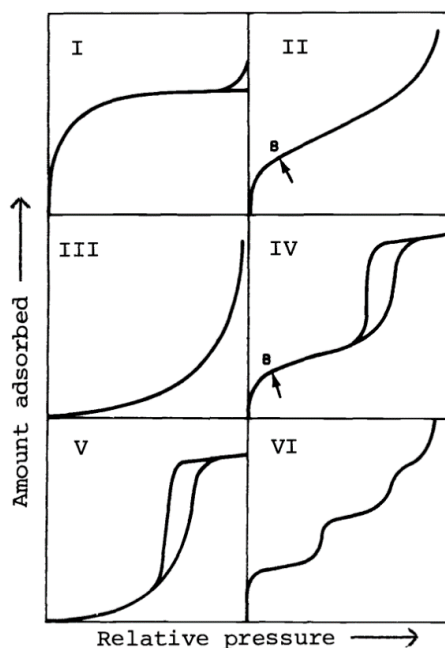
Point B represents full monolayer coverage and the beginning of multilayer adsorption

Figure 4.15. - IUPAC Classification of Sorption Isotherms (9)

Table 4.9. - Description of Isotherm Profiles (8)

Isotherm	Adsorption	Found In
I	Few Monolayers	Microporous Materials
II	Unrestricted monolayer-multilayer adsorption	Non-porous Materials Macroporous Materials
III	Weak adsorbate-adsorbent interactions Adsorbate-adsorbate interactions important	Uncommon
IV	Initial monolayer-multilayer adsorption as in Type II Hysteresis loop associated with pore condensation Limiting uptake over a range of high P/P_o results in a plateau indicating complete pore filling	Mesoporous Materials
V	Hysteresis loop associated with pore condensation At lower relative pressures profile relates to adsorption isotherms of type III indicating relatively weak attractive interactions between adsorbent and adsorbate	Water on Charcoal
VI	Stepwise multi-layer adsorption where sharpness of steps is dependent on homogeneity of adsorbent surface, adsorptive and temperature.	Uniform non-porous surface, particularly spherically symmetrical non-polar adsorptives

Langmuir developed a theory for monolayer adsorption which described the Type I isotherms (8). This was then built upon by Brunauer, Emmett and Teller (BET) to extend to multilayer adsorption. The BET equation (Equation 4.2.) enables the experimental determination of the number of molecules required to form a monolayer, by assuming the uppermost adsorbed molecules are in dynamic equilibrium with the vapour (8). This dynamic equilibrium means that although the surface sites covered by one or more layers may vary, the number of molecules in each layer will remain constant. Plotting P/V $(P_o – P)$ vs P/P_o for values of P/P_o between 0.05 and 0.35 should give a linear relationship, with a gradient of $C-1/V_mC$ and a y-intercept of $1/V_mC$. The volume of gas needed to form a monolayer can therefore be written as $1/(gradient + intercept)$ (8).

Correcting the volume of the monolayer to STP, the number of adsorbate molecules contained within it can be calculated. Density can be used to calculate the effective area occupied by each adsorbed molecule, assuming a close-packed sphere model. The total area of the monolayer can

hence be calculated, which, when divided by the mass of the adsorbent, will give the specific surface area of the solid.

Equation 4.2. - BET Equation

$$1/V\ [P/P_o-1] = 1/V_mC + C-1/V_mC(P/P_o)$$

Where: V   is total volume adsorbed at pressure

V_m is the volume of gas needed to form a monolayer

P   is the pressure

P_o is the saturation vapour pressure of the adsorbate

C   is a constant

Application and Procedure

Gas adsorption was used to determine the amount of surface area lost during coking or restored during regeneration, and any changes in pore size that may impact active site availability. The BET method was used to determine surface area of the catalyst. The measurements were carried out using a Micromeritics ASAP2020 Accelerated Surface Area and Porosimetry System. A schematic of the apparatus is given in Figure 4.16.. The sample was evacuated at 90°C for 60 minutes and for a further 360 minutes at 250°C. It was backfilled with helium before subsequent measurements and analysis was run. The adsorbate used was N_2.
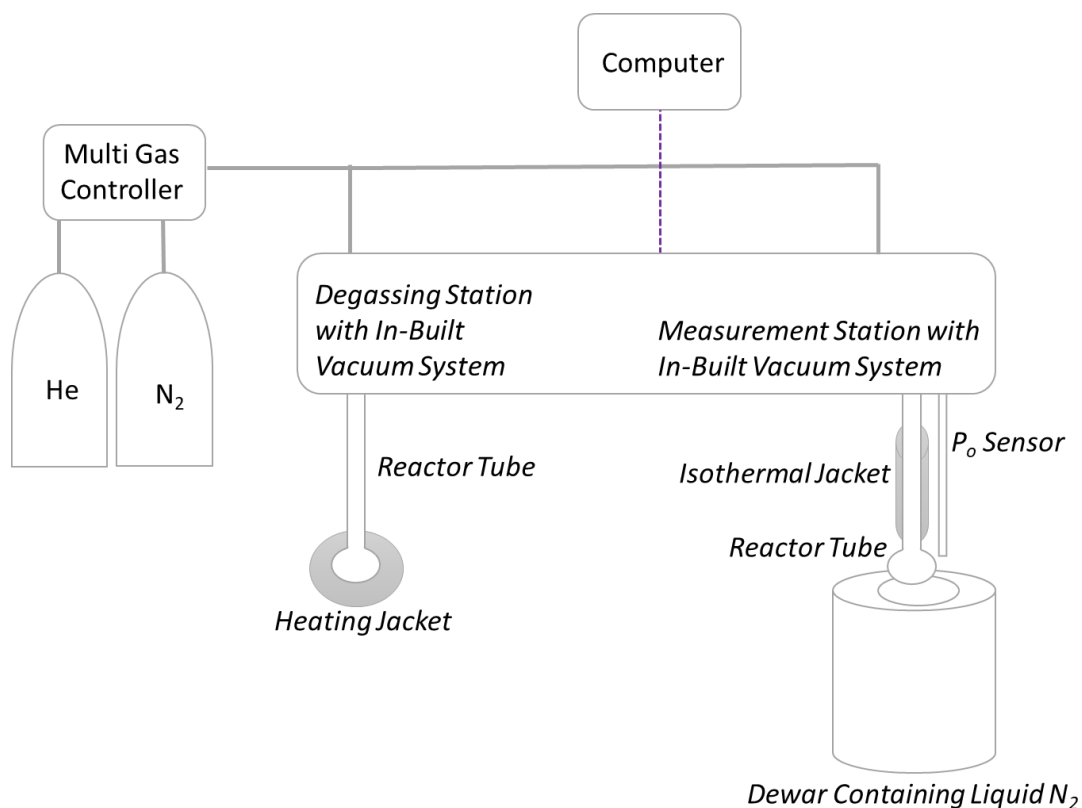
Figure 4.16. - Schematic of Gas Adsorption Apparatus

4.2.5. Raman Spectroscopy

Background

Raman spectroscopy is an analytical technique used to study molecular vibrations, often to determine the identity of a compound from its unique structural fingerprint (10). Whenever light meets matter, the light may be absorbed, scattered or pass straight through it. The fundamental interaction in Raman spectroscopy is scattering.

Scattering involves the distortion of the electron cloud and can be categorised into three types: Rayleigh, Stokes and anti-Stokes. Rayleigh scattering is elastic – there is no net change in energy. Stokes and anti-Stokes scattering however, is inelastic as it involves the transfer of energy either from photon to molecule (Stokes scattering), or molecule to photon (anti-Stokes scattering) (10).

Raman spectroscopy records the shift in energy of inelastic scattering, the intensity of the scattered light is proportional to the amount of material present. Fundamentally, Raman apparatus consists of a monochromatic light source (often a laser), a focussing lens and a detector. Modern equipment often uses a microscope as the optic lens, a charge coupled device (CCD) detector, mirrors, and notch filters or additional monochromators to aid separation of incident and scattered light, which subsequently focuses the scattered light (10). A schematic of Raman apparatus is given in Figure 4.17..
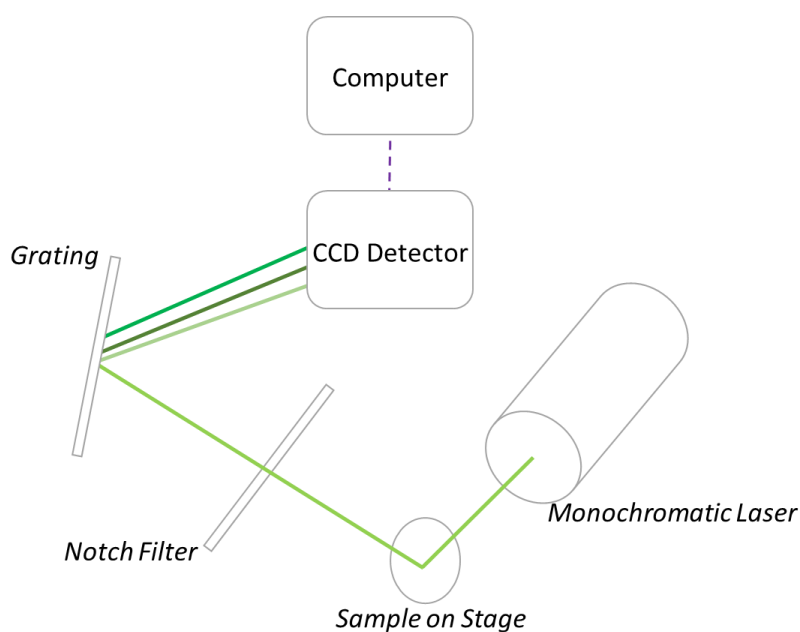
Figure 4.17. - Schematic of Raman Apparatus

Carbon, with its symmetric covalent bonds and lack of dipole makes it especially sensitive to Raman spectroscopy. Each band in the Raman spectrum corresponds to a specific vibrational frequency of a bond within a molecule. This technique is therefore particularly useful to carbon, as carbon allotropes, composed entirely of C-C bonds, can be differentiated using Raman spectroscopy (11). The carbon atoms in diamond give a signature band at 1332 cm^{-1}. In comparison, graphite has several bands in the Raman spectrum, and instead of a band at 1332 cm^{-1} the main band has shifted to 1582 cm^{-1} (11). This shifted band is known as the G band (as a reference to graphitic carbon) and the shift occurs because graphite is composed of sp^2 bonded

carbon rather than sp^3 bonded carbon which is present in diamond. The sp^2 bonds in graphite have a higher bond energy. This pushes the vibrational frequency and consequently the frequency of the Raman spectrum higher. The presence of additional bands in graphite indicates different bond energies within the sample, which is a result of the non-uniformity of graphite. Another common band observed with carbonaceous materials appear around 1350 cm^{-1} and is referred to as the D band (11). This band originates from defects or disorder within a graphitic structure.

Application and Procedure

Raman spectroscopy was used to investigate the type of carbon formed on the regenerated catalysts and to identify any changes in carbon formation post-regeneration. The analysis was carried out on a Horiba Jobin Yvon LabRAM HR800 confocal Raman microscope. The conditions and apparatus used are given in Table 4.10.. The apparatus was calibrated daily using a silicon wafer reference. Data was recorded using the Horiba LabSpec 6 software before being transferred to Microsoft Excel for analysis.

Table 4.10. - Conditions and Apparatus for Raman Spectroscopy

Apparatus	
Laser Power Supply	Laser Quantum DPSS Laser System With mpc6000 Power Supply
Optic Light Source	Euromex Holland Fiber Optic Light Source Ek-1
Instrument Setup	
Objective	x50
Grating / gr mm^{-1}	600
Filter / %	25
Laser / nm	532
Slit	200
Hole	200
Acquisition Parameters	
Range / cm^{-1}	400-4000

4.2.6. Infrared Spectroscopy

Background

Infrared spectroscopy (IR) is an analytical technique used for structural identification based on the characteristic absorption bands of specific functional groups. It measures the change in intensity when light is absorbed. When a molecule is irradiated by a photon with the exact energy corresponding to the difference between a lower energy level (often the ground state) and a higher energy level (excited state), the photon may be absorbed (12). This absorption causes the molecules to vibrate in a specific manner determined by the identity of the molecule. The various vibrational modes and their corresponding infrared bands at specific wave numbers have been recorded, enabling rapid identification of functional groups. Additionally, infrared spectroscopy can also be used for quantitative analysis by applying Beer-Lambert's law (Equation 4..) (12).

Equation 4.3. - Beer-Lambert's Law

$$A = \varepsilon cl$$

Where: A is the absorption

     ε is the molar coefficient

     c is the concentration of the sample

     l is the path length

When light is absorbed by a sample, the amount absorbed is dependent on how many molecules it interacts with and the identity of the molecule. By applying Beer-Lambert's law, absorption of different samples can be directly compared, and the amount of a specific compound or molecule can be quantified.

In catalysis, acid sites are often of great importance. Infrared spectroscopy is beneficial to catalysis as it can be used to determine the number of Brønsted and Lewis acid sites within a sample. By introducing a known concentration of a base to the catalyst sample, an infrared spectrum can determine the number of acid sites and their type, Lewis Acid Sites or Brønsted Acid Sites (13). Two common bases used are pyridine and collidine. Pyridine (5.7 Å) is a

relatively small molecule and so can easily fit into the pores of medium- and large-pore zeolites, such as ZSM-5 and mordenite. Collidine (7.4 Å) is bigger and so often cannot fit inside the pores, instead interacting with the surface acid sites (14). This is beneficial as carrying out infrared spectroscopy using the two probe molecules can help to identify not only how many acid sites are present on the catalyst, but also give an indication of their specific locations. A schematic of the infrared apparatus for zeolite characterisation is given in Figure 4.18..
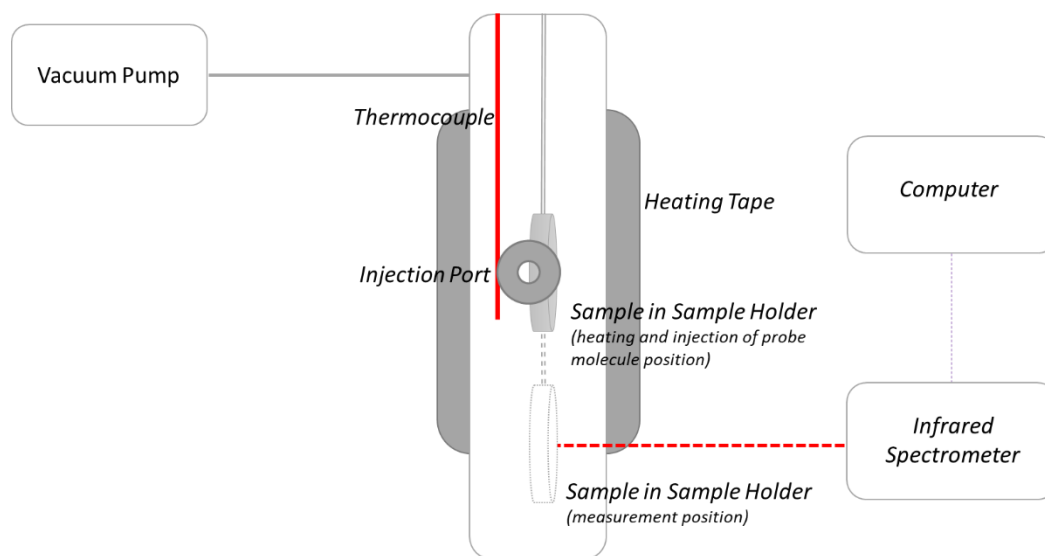
Figure 4.18. - Schematic of IR Apparatus

Application and Procedure

Pyridine and collidine infrared spectroscopy experiments were carried out at Keele University with the help of Dr. Vladimir Zholobenko. Calibration experiments and preliminary calculations were carried out by Dr. Vladimir Zholobenko, with calculations and identification of acid sites for pre-treatment being carried out by the author. Apparatus of the infrared studies are given in Table 4.11.

Table 4.11. - Infrared Spectroscopy Apparatus

Infrared Spectrometer	Thermo Scientific Nicolet iS10 FT-IR Spectrometer
Vacuum Pump	Pfeiffer HiCube 80 Eco, DN 63 ISO-K, MVP 015-4
Infrared Cell	Quartz
Number of Scans	64
Resolution	4

Catalyst samples (~10 mg) were ground into a fine powder before being pressed into self-supporting discs (~0.05 mm thickness). The sample was placed inside a sample holder and enclosed within the infrared cell. The sample was pre-treated in situ at 450°C for 5 hours under vacuum. Following this the temperature was lowered to 150°C whereupon an infrared spectrum was collected before an excess of the probe molecule (1μL) was injected into the cell. After 10 minutes the cell was evacuated removing any unbound or physisorbed probe molecules and the infrared spectrum inclusive of the probe molecule was collected. The obtained infrared data was analysed (including integration, subtraction and determination of peak positions) using Thermo OMNIC software (Version 9.).

To determine the concentration of acid sites, Beer-Lambert's law (Equation 4.3.) was modified because the pathlength of the sample is undefined (Equation 4.4.).

Equation 4.4. - Modified Beer-Lambert's Law

$$n = A \times S / \varepsilon$$

Where n is the number of moles per sample

            A is the absorption

            S is the physical sample size

            ε is the molar absorptivity coefficient

The molar absorptivity coefficient is dependent upon the type of acid site and type of zeolite used. For the calculations carried out in this research and contained within this thesis, the molar absorptivity coefficients used were provided by Dr. Vladimir Zholobenko from Keele University and are not currently published in the literature. For absorption values, 1544 cm^{-1} is used to calculate BAS and 1453 cm^{-1} is used to calculate LAS when using pyridine as the probe molecule, and 1636 cm^{-1} is used to calculate BAS when collidine is the probe molecule [15,16]. A copy of the calculations for the results produced herein are found in the Appendix.

4.2.7. Solid State Nuclear Magnetic Resonance

Background

Nuclear Magnetic Resonance (NMR) is an analytical technique that applies the principle of nuclear spin to determine the composition of a material (17). When an external magnetic field is applied to a nucleus with a nuclear spin, the magnetic moment of the nucleus will align or oppose the external field. NMR utilises this property by introducing electromagnetic radiation in the form of radio waves to cause the nuclei to undergo energy transitions, where the energy absorbed in the spin-flips is re-emitted as the nuclei undergo relaxations back to their more thermodynamically stable state (17). This process is referred to as nuclear magnetic resonance, and it is this re-emitted energy that is measured by the detector to form the NMR spectrum.

Solid State NMR (ssNMR) differs from classical NMR, where samples are typically liquids or in solution. Various interactions between nuclei exist in both types of NMR, however where in classical NMR the molecules can rotate freely and so act isotropically, in solid samples the nuclei are more restricted (17). As a result, the nuclei interactions in liquid samples cancel each other out, but in solid samples they remain dominant and create broad, unintelligible spectra. To overcome this, the magic angle spinning (MAS) technique was introduced. By rotating the sample at high velocity at a critical angle of 54.74° to the applied magnetic field, the interactions that are geometrically dependent (i.e. chemical shift anisotropy and dipolar interactions) are negated (17). In practical terms, using MAS, ssNMR produces clearer, more defined peaks.

Application and Procedure

ssNMR was performed in order to determine the composition of the catalyst, specifically concerning the ratio between silicon and aluminium. ^{1}H, ^{27}Al and ^{29}Si MAS ssNMR was performed. The experiments were carried out at Johnson Matthey Technology Centre, Sonning Common, by Dr. Nathan Barrow and Dr. Johnathon Bradley, and they subsequent produced reports on the results (found in the Appendix). Details of the apparatus and conditions used is given in Table 4.12..

Table 4.12. - Conditions and Apparatus used in ssNMR

Apparatus				
NMR Apparatus	Bruker Avance III		Bruker Avance NEO	
Software	TopSpin Version 3.1		TopSpin Version 4.0	
Reaction Conditions				
Magnetic Field Strength / T	9.5		14.1	
Nuclei Detected	^{1}H	^{27}Al		^{29}Si
Probe Frequency / MHz	400.16 600.22	104.27 156.41		79.49
Reference Material	D16 Adamantane	YAG		Kaolinite
Reference Material Chemical Shift / ppm	1.73	0.0		-91.2

Powdered samples (~100 mg) were packed into zirconia MAS rotors with Kel-F caps, with mass being recorded before and after the experiment. The rotors were spun using room-temperature purified compressed air. Data was recorded on TopSpin (Version 3.1. or 4.0.).

4.2.8. X-ray Photoelectron Spectroscopy

Background

X-ray photoelectron spectroscopy (XPS) is a surface analysis technique used to determine the elemental composition and chemical environment of the outer 10 nm of a material (18). By irradiating a sample with X-rays, photons with sufficient energy are able to eject an electron bound to an atom or ion, and even from the material itself. The electrons emitted from the material are detected and their remaining kinetic energy is measured. It is the kinetic energy of the electron which can determine the atom and chemical environment which it came from, as electron binding energy is element and environment specific (18). The binding energy can be calculated, assuming the element exists at >0.05 atomic %, as shown in Equation 4.5..

Equation 3.5. - XPS Binding Energy Equation

$$K.E._{xps} = E_{ph} - \Phi_{xps} - B.E._{xps}$$

Where $K.E._{xps}$ is the kinetic energy of the emitted electron

E_{ph} is the energy of the photon

Φ_{xps} is the work function of the instrument

$B.E._{xps}$ is the binding energy of the electron

In order to obtain accurate results, XPS is carried out under high vacuum. As such, it is usually limited to solid samples, although it is possible to run liquid or gaseous samples using specialist equipment (18). A schematic of XPS apparatus is given in Figure 4.19..
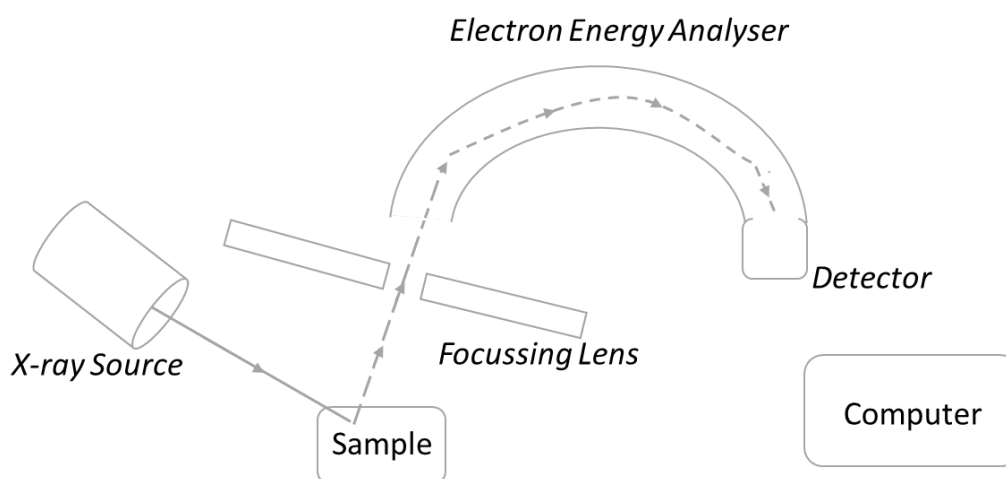
Figure 4.19. - Schematic of XPS Apparatus

Application and Procedure

XPS was carried out on regenerated catalysts to investigate any changes to the catalyst surface. The procedure and data analysis were carried out at Johnson Matthey by Dr. Tuğçe Eralp Erden, using Johnson Matthey's standard procedure. Details of this were not disclosed. A copy of the report produced by Dr. Tuğçe Eralp Erden can be found in the Appendix.

4.2.9 Ammonia Temperature Programmed Desorption

Background

Ammonia Temperature Programmed Desorption (NH_3 TPD) is a widely used analytical technique for the determination of acid site strength in zeolites (19). It operates by exposing a small amount of clean catalyst to ammonia and monitoring the desorption of the gas as a function of temperature (20). The temperature at which the ammonia desorbs can be used as an indicated of the relative strength of the acid site (21). Typically, in H-zeolites such as mordenite, two peaks are observed.

These represent low (l-peak) and high (h-peak) temperature desorbed ammonia. However, only the h-peak is a result of directly bound NH_3, whereas the l-peak corresponds to weakly adsorbed NH_4^+ species (22). The intensity of such peaks is dependent on experimental conditions such as the contact time of the carrier gas. This can be referred to as W/F, the mass of the sample / the flow rate of the carrier gas (22). Therefore, to directly compare results, mass and flow rate should be the same. A schematic of NH_3 TPD apparatus is given in Figure 4.20..
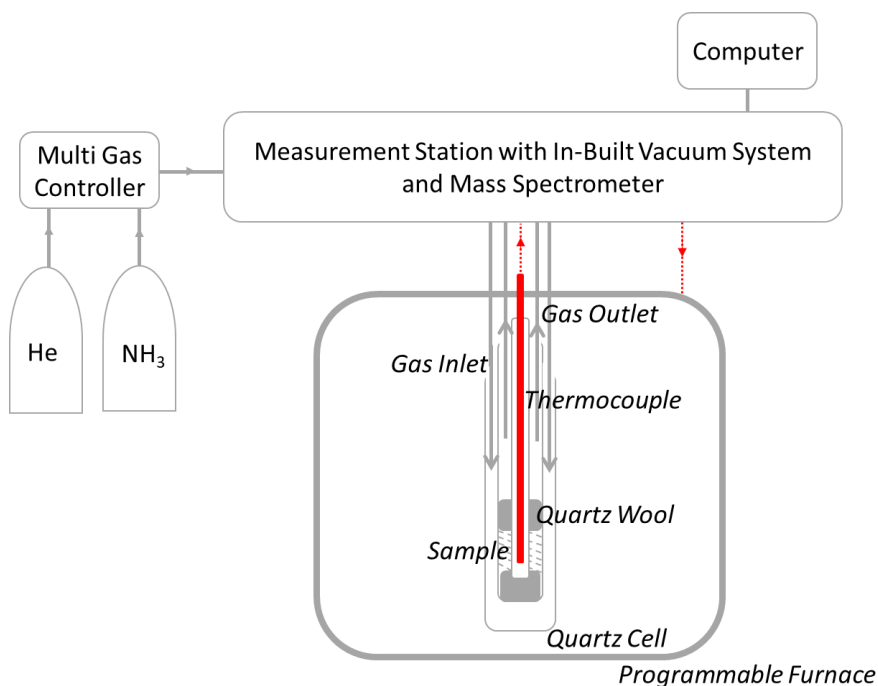
Figure 4.20. – Schematic of NH₃ TPD Apparatus

Application and Procedure

NH_3 TPD was carried out on regenerated and pre-treated catalysts to determine any changes to the distribution of acid site strength on the mordenite samples. The procedure and data analysis were carried out at Johnson Matthey by Dr. John West. Details of the programme used as provided by Johnson Matthey are given in Table 4.13.. No sample preparation was carried out. Samples of 100 mg were used, and the procedure was carried out under helium at a constant flow rate of 40 mL min^{-1}.

Table 4.13. – Temperature Programme for NH₃ TPD

Table 4.13. – Temperature Programme for NH$_3$ TPD

	Ramp Rate / °C min^{-1}	Initial Temperature / °C	Final Temperature / °C	Hold Time / mins
Ramp 1	10	25	400	n/a
Isotherm 1	n/a	400	400	120
Cooldown 1	n/a	400	40	n/a
Isotherm 2ª	n/a	40	40	240
Isotherm 3	n/a	40	40	240
Ramp 2	10	40	1000	n/a

ª Addition of NH$_3$ (5000 ppm) over this period

4.3. CHALLENGES AND OPTIMISATION

The following section details the optimisation and modification processes which occurred in order to produce the final experimental procedures detailed in this chapter.

4.3.1. Toluene Disproportionation

Toluene disproportionation was originally carried out under small-scale conditions detailed at the beginning of this chapter. Therefore, the following optimisations and modifications were performed at small-scale, however the final conditions and experimental set-up was applied to large-scale toluene disproportionation where possible.

The main challenge for toluene disproportionation was preventing toluene and the products from condensing along the apparatus, causing an inconsistent amount of products reaching the GC-MS for detection. This was first seen under the original conditions, where the gas saturator was not temperature controlled, the line was not heated, and the results were very much dependent upon the weather and temperature of the laboratory of any particular day. To overcome this challenge, heating tape was applied from the end of the reactor tube to the GC-MS detector at a temperature of 150°C. The gas saturator was temperature controlled using a water bath set to 35°C, however this led to detector saturation, so the water bath was instead replaced with an ice bath.

Other modifications included:

- Using the same amount of toluene in each reaction to prevent change in the degree of saturation

- Routine leak testing

- For large-scale TDP, the flow rate was altered to match the space velocity of the small-scale reactor

4.3.2. Regeneration

Thermal

In order to determine the required regeneration time, initially thermal regeneration was performed for durations of 1, 2, 4, 8, 12, 16, 20, and 24 hours. Visual observation was used as a first measure of regeneration and final confirmation was determined by TGA.

Microwave

Microwave regeneration proved difficult initially, as the microwaves had to be focussed on a small section of reactor tube containing the catalyst. Modifications made to overcome this challenge included: using a smaller aperture to narrowly focus the microwaves and using a reactor tube with a smaller diameter to increase reactor bed height.

These modifications enabled the microwaves to heat the catalyst sufficiently for regeneration (confirmed via TGA), however upon removal of the catalyst post-regeneration, it was apparent that the microwaves were directional and not all the catalyst had regenerated (Figure 4.1.). For this reason, rotating the reactor tube every 105 minutes was introduced.
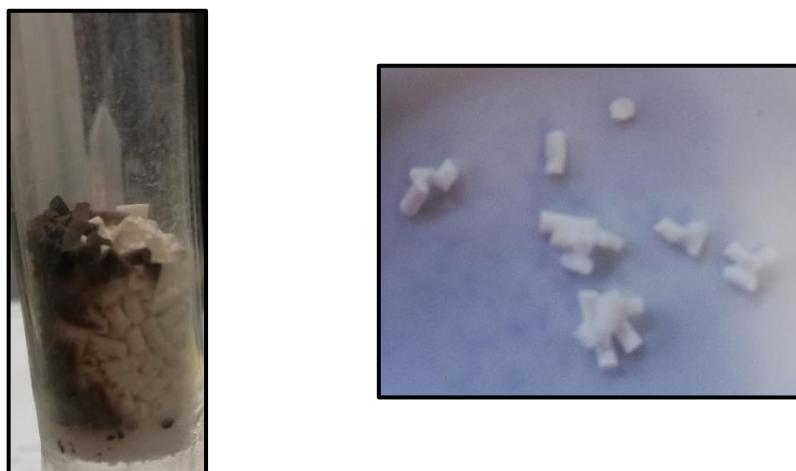
Figure 4.21. – Photos of Incomplete Microwave Regeneration (Left); Fused Microwave Treated Catalyst (Right)

The final challenge, and probably the most detrimental to the microwave studies, was temperature control. The power was controlled manually, and the amount of coke or water within the reactor tube had a large impact on the energy within the system. This meant temperature could fluctuate by over 100°C using the same power in under 30 seconds. The result of this was ultimately catalyst destruction, with parts of the sample losing crystallinity, some to the point where the sample fused together (Figure 4.21.). Therefore, to produce sufficient quantities of sample for activity testing, a larger amount of catalyst was used in the microwave studies. The sample was then manually separated after treatment before further testing.

Microwave Plasma

By using a non-equilibrium plasma in microwave plasma regeneration, it was unsurprising to see that initial regenerations produced samples where the majority of the regeneration was complete, but not absolute. This was because the plasma was not uniform across the reactor tube, so parts of the reactor would have plasma of a lower energy than others. To overcome this, vigorous shaking of the reactor tube was introduced.

To determine the sufficient power required for microwave plasma regeneration, experiments were undertaken at various powers ranging from 50-500 Watts. 200 Watts was decided on as the standard power, as below this did not guarantee full regeneration within a reasonable time-frame, and above this led to partial destruction of the catalyst. Similarly to other regeneration methods, complete regeneration was initially determined visually before final confirmation via TGA.

4.3.3. Pre-Treatment

Pre-treatment was carried out after the modifications of the regeneration techniques had been applied. However, it is worth mentioning for the microwave and microwave plasma pre-treatments, the water content of virgin catalyst had an impact on initial temperature control of the treatment. Furthermore, restarting the experiments after the rotation/vigorous shaking of the reactor tube became progressively more difficult. In this author's understanding, this was likely due to a lack of water and coke, both of which readily absorb microwaves.

4.3.4. Gas Chromatography Mass Spectrometry

As the method used to monitor catalytic activity, it was imperative to ensure clear separation of the products, especially the xylene isomers. Programme optimisation and testing was carried out using a mixture of the products. Initially an Omegawax® column was used, which displayed a clear separation for most of the products with the exception of *p-* and *m-* xylene (Figure .22.). This persisted during the development of various programmes involving changes to split ratio and temperature profile (Table 4.14.). Therefore, the column was replaced with a Supelco Supelcowax™ column, specifically advertised to separate xylene isomers. Once fitted, optimisation of split ratio and temperature profile was repeated, producing a distinct base line separation.
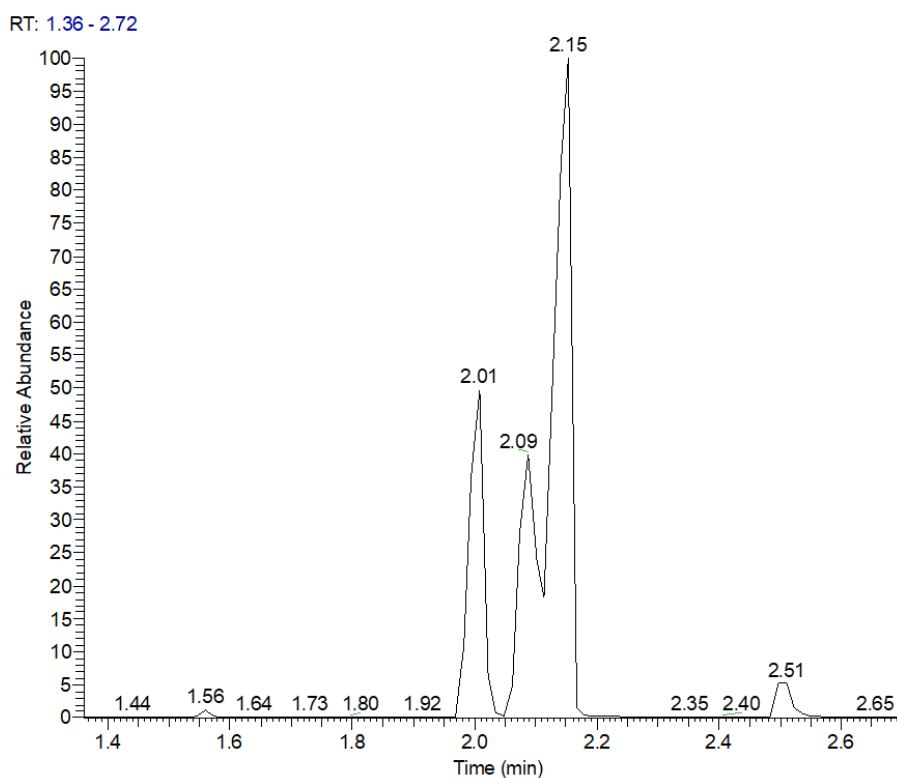
Figure 4.22. - Chromatograph of Unresolved Xylene Peaks (2.01, 2.09 & 2.15 mins)

Table 4.13. - Conditions of GC Programmes Tested During Optimisation

Method	Initial Temperature / °C	Hold Time at Initial Temperature /°C	Ramp Rate / °C min⁻¹	Final Temperature / °C	Split Ratio
1	60	8	8	130	40
2	40	2	5	130	40
3	40	2	5	130	100
4	40	2	3	130	100
5	40	2	3	70	40
	70	0	20	200	
6	40	2	3	70	200
	70	0	20	200	
7	40	2	3	70	300
	70	0	20	200	
8	40	2	3	70	200
	70	0	20	200	

4.3.5. Thermogravimetric Analysis

Often in TGA, a linear temperature programme is used to reduce time and give general results on the thermal stability of a compound. However, when a scan-type programme was used for the coked catalyst samples, it was apparent the coke had not been fully removed (Figure 4.3.). For this reason, various programmes of different length isotherms were tested to create a temperature programme which could determine the mass of any carbon oxidised at 500°C.
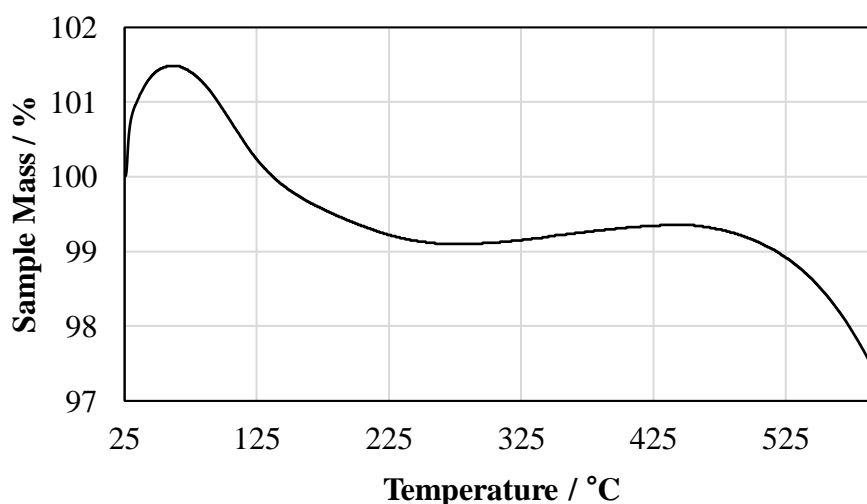
Figure 4.23. – Linear Programme TGA (Temp: 25-600°C; Ramp Rate: 10°C min⁻¹) of Coked Sample

4.4. REFERENCES

(1) Sparkman OD, Penton ZE, Kitson FG. The Fundamentals of GC/MS. In: Sparkman OD, Penton ZE, Kitson FG, editors. Gas Chromatography and Mass Spectrometry A Practical Guide. Second ed.: Elsevier; 2011. p. 3-218.

(2) Robinson JW, Skelly Frame EM, Frame II GM. Gas Chromatography. Undergraduate Instumental Analysis. Seventh ed. U.S.A.: CRC Press; 2014. p. 873-919.

(3) Robinson JW, Frame EMS, Frame II GM. Mass Spectrometry I: Principles and Instrumentation. In: Robinson, J.W., Frame, E.M.S., Frame II, G.M., editor. Undergraduate Instrumental Analysis. Seventh ed.: CRC Press; 2014. p. 705-761.

(4) Kett VL, Price DM. Thermogravimetry. In: Gaisford S, Kett V, Haines P, editors. Principles of Thermal Analysis and Calorimetry. Second ed. Cambridge, United Kingdom: Royal Society of Chemistry; 2016. p. 18-46.

(5) Clearfield A, Reibenspies J, Bhuvanesh N. Principles and Applications of Powder Diffraction. first ed. Oxford: Wiley-Blackwell; 2008.

(6) West AR. Crystallography and Diffraction Techniques. Solid State Chemistry and its Applications. Second ed. West Sussex, United Kingdom: Wiley; 2014. p. 229-270.

(7) Cockcroft JK, Fitch AN. Experimental Setups. In: Dinnebier RE, Billinge SJL, editors. Powder Diffraction: Theory and Practice London: RSC Publishing; 2008. p. 20-57.

(8) Lowell S, Shields JE, Thomas MA, Thommes M. Characterization of Porous Solids and Powders: Surface Area, Pore Size and Density. 1st ed. United States of America: Springer; 2010.

(9) Sing KSW. Reporting Physisorption Data for Gas/Solid Systems with Special Reference to the Determination of Surface Area and Porosity. Pure and Applied Chemistry 1982;54(11):2201-2218.

(10) Smith E, Dent G. Introduction, Basic Theory and Principles & The Raman Experiment - Raman Instrumentation, Sample Presentation, Data Handling and Practical Aspects of Interpretation. In: Smith E, Dent G, editors. Modern Raman Spectroscopy: John Wiley & Sons, Ltd.; 2005. p. 1-70.

(11) Hodkiewicz J. Characterizing Carbon Materials with Raman Spectroscopy. 2010; Available at: https://tools.thermofisher.com/content/sfs/brochures/D19504~.pdf. Accessed March, 16th, 2018.

(12) Mitsuo T, Sakamoto A, Ochiai S. Fundamentals of Infrared Spectroscopic Measurements. In: Mitsuo T, editor. Introduction to Experimental Infrared Spectroscopy - Fundamentals and Practical Methods: John Wiley & Sons, Ltd.; 2015. p. 32-271.

(13) Kondo JN, Nishitani R, Yoda E, Toshiyuki Y, Tatsumi T, Domen K. A Comparative IR Characterisation of Acidic Sites on HY Zeolite by Pyridine and CO Probes with Silica-Alumina and Gamma-Alumina References. Physical Chemistry Chemical Physics 2010;12(37):11576-11586.

(14) Holm MS, Svelle S, Joensen F, Beato P, Christensen CH, Bordiga S, et al. Assessing the Acid Properties of Desilicated ZSM-5 by FTIR using CO and 2,4,6-Trimethylpyridine (Collidine) as Molecular Probes. Applied Catalysis A: General 2009;356(1):23-30.

(15) Freitas C, Barrow NS, Zholobenko V. Accessibility and Location of Acid Sites in Zeolites as Probed by Fourier Transform Infrared Spectroscopy and Magic Angle Spinning Nuclear Magnetic Resonance. Johnson Matthey Technology Review 2018;62(3):279-290.

(16) Lonstad Bleken B, Mino L, Giordanino F, Beato P, Svelle S, Lillerud KP, et al. Probing the Surface of Nanosheet H-ZSM-5 with FTIR Spectroscopy. Physical Chemistry Chemical Physics 2013;15(32):13363-13370.

(17) West AR. Nuclear Magnetic Resonance (NMR) Spectroscopy. In: West AR, editor. Solid State Chemistry and its Applications. Second ed. United Kingdom: Wiley; 2014. p. 298-300.

(18) Van der Heide P. Introduction & Atoms, Ions, and Their Structure & XPS Instrumentation. In: Van der Heide P, editor. X-ray Photoelectron Spectroscopy - An Introduction to Principles and Practices. First ed.: Wiley; 2012. p. 1-60.

(19) Niwa M, Katada N. New Method for the Temperature Programmed Desorption (TPD) of Ammonia Experiment for Characterisation of Zeolite Acidity: A Review. The Chemical Record 2013;13(5):432-455.

(20) Ishii T, Kyotani T. Temperature Programmed Desorption. In: Inagaki M, editor. Materials Science and Engineering of Carbon: Characterisation. First ed. Oxford, United Kingdom: Elsevier Inc.; 2016. p. 287-305.

(21) Karge HG. Comparative Measurements on Acidity of Zeolites. In: Ohlmann G, Pfeifer H, Fricke R, editors. Catalysis and Adsorption by Zeolites. First ed. Amsterdam: Elsevier Science Publishers; 1991. p. 133-156.

(22) Niwa M, Katada N, Okumura K. Solid Acidity of Zeolites. In: Hull R, Jagadish C, Osgood RM, Jr., Parisi J, Wang Z, Warlimont H, editors. Characterisation and Deisgn of Zeolite Catalysts. First ed. Heidelberg: Springer; 2010. p. 9-28.

CHAPTER 5: REGENERATION STUDIES I - RESULTS

5.1. INTRODUCTION

Using toluene disproportionation as a probe reaction and as a means of providing carbon lay down, virgin mordenite samples were deactivated (as described in Section 4.1.1.). Three novel regeneration methods were proposed. Studies were then performed in order to evaluate the efficacy of these processes, namely microwave heating (MW), microwave plasma (MWP) and dielectric barrier discharge (DBD) plasma. These novel regeneration technologies were compared to conventional heating (referred herein and henceforth as thermal regeneration). Details of these processes are given in Section 4.1.2.. This chapter presents the findings of these studies which will be discussed in the following chapter (Chapter 6).

5.2. CATALYST TESTING

5.2.1 Toluene Conversion as a Function of Time

Regenerated mordenite was subjected to a second toluene disproportionation. The regenerated activity represented as toluene conversion as a function of time has been plotted in Figures 5.1.-5.4.. The data for each regeneration treatment has been plotted alongside virgin mordenite in order to assist in the visualisation of any differences which may have resulted.

As can be seen in Figure 5.1., the initial toluene conversion over the virgin catalyst was 60 %, which decreased over time. After 450 minutes, catalytic activity had dropped to a 10 % conversion and remained in a *pseudo*-steady state with activity only reducing a further 4 % after an additional 500 minutes. Rapid deactivation occurred between 180 minutes and 325 minutes at a rate of 0.30 % min^{-1}.

The activity data for a sample of spent mordenite which had undergone thermal regeneration is also shown in Figure 5.1.. Whilst the catalyst exhibits very similar activity to the virgin material,

including the same rate of deactivation (0.30 % min^{-1}), it should be noted the initial activity is slightly reduced (58 %).
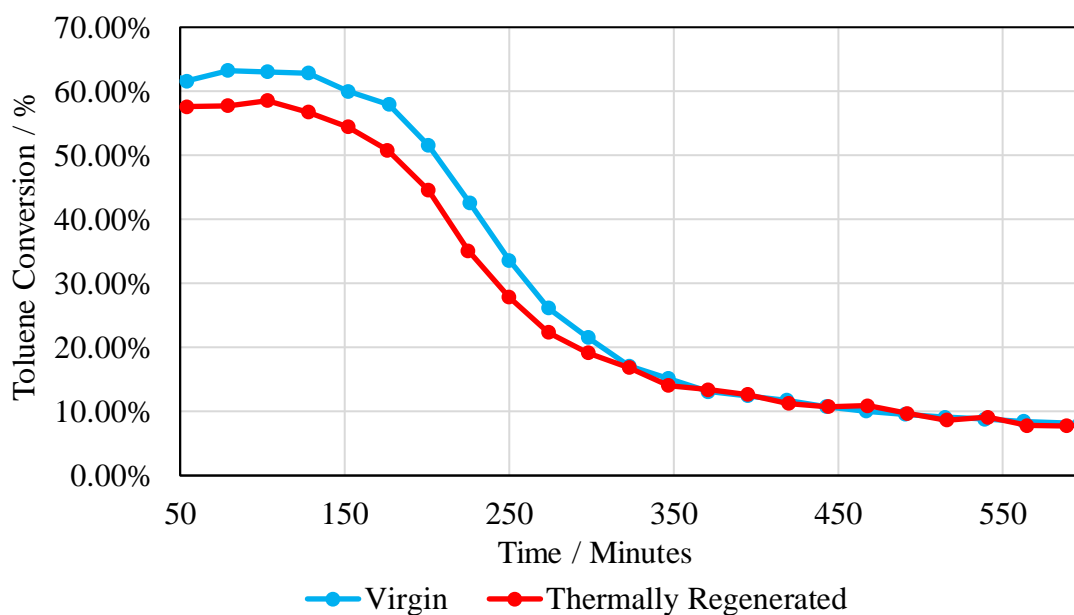
Figure 5.1. - Activity Plot of Virgin Catalyst Compared with Thermally Regenerated Catalyst

In contrast, the deactivation profile of a sample of spent mordenite which had undergone microwave regeneration (Figure 5.2.), was significantly different from both the virgin and the thermally regenerated materials. In terms of toluene conversion, the sample did not undergo a rapid deactivation. In contrast, the profile displays a much more gradual deactivation with a rate of 0.088 % min^{-1}, when measured over the same period as the virgin material.

The sample of spent mordenite which had undergone microwave plasma regeneration displayed an activity profile for toluene disproportionation (Figure 5.3.) very similar to the microwave regenerated sample. The initial activity was slightly reduced compared with the virgin material (58 %) and the rate of deactivation over the measured period (180-350 mins) was calculated to be 0.085 % min^{-1}.

The sample of spent mordenite which had undergone DBD plasma regeneration (Figure 5.4.) proceeded to deactivate rapidly, similar in profile but even more pronounced than the virgin and thermally regenerated catalysts. Rapid deactivation occurred between 71-214 minutes with a rate of deactivation of 0.523 % min^{-1}, reaching a *pseudo*-steady state where toluene conversion was 5 %.
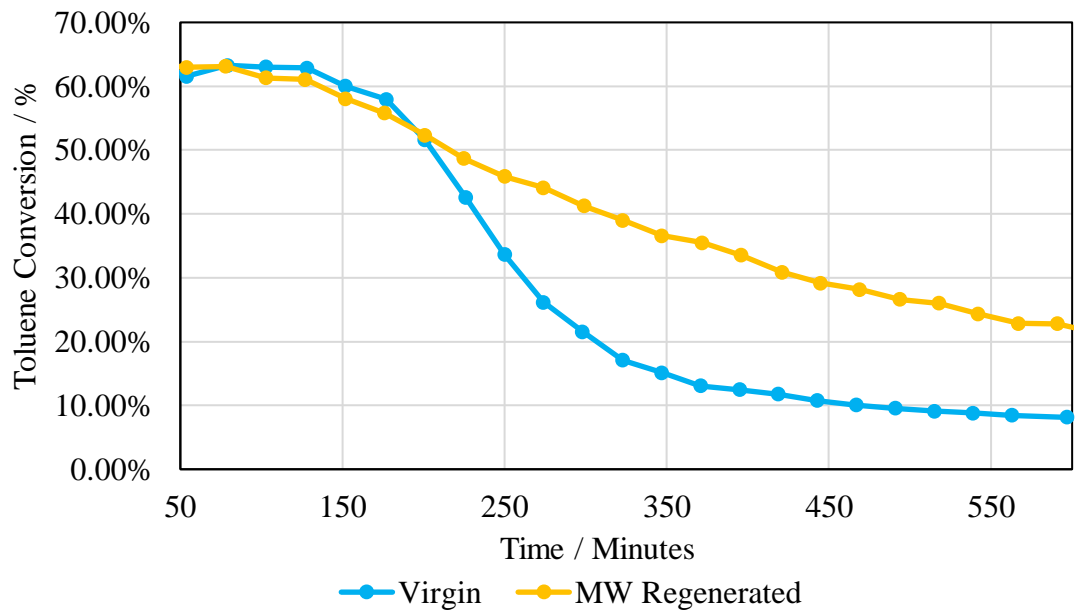
Figure 5.2. - Activity Plot of Virgin Catalyst Compared with Microwave Regenerated Catalyst
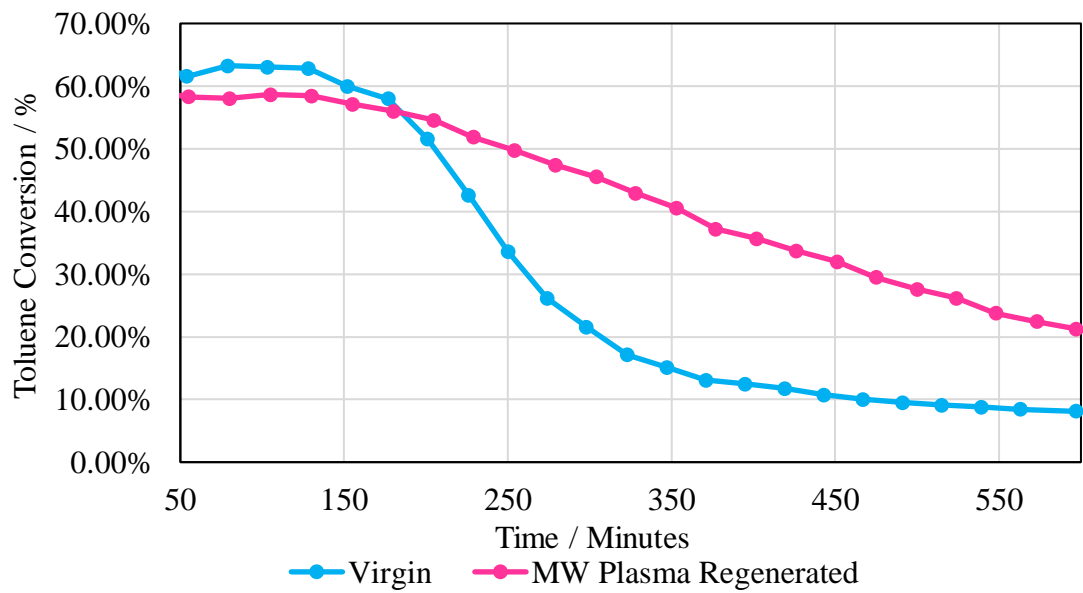
Figure 5.3. - Activity Plot of Virgin Catalyst Compared with Microwave Plasma Regenerated Catalyst
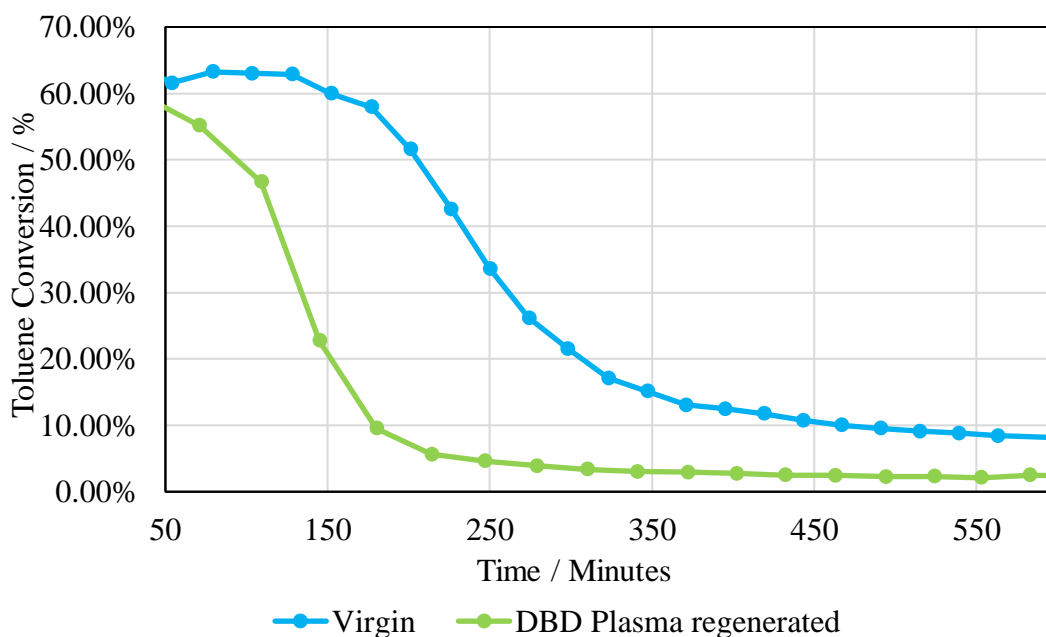
Figure 5.4. - Activity Plot of Virgin Catalyst Compared with Dielectric Barrier Discharge Plasma Regenerated Catalyst

5.2.2 Effect of Regeneration on Catalyst Selectivity

When investigating how the regeneration treatments have affected catalyst selectivity, both the more desirable toluene disproportionation and the competing toluene dealkylation (cracking) need to be considered. Reaction selectivity between disproportionation and cracking can be studied through observation of the benzene-to-xylene ratio (B/X), whereas the product selectivity of disproportionation can be examined through xylene isomer selectivity, in terms of quantities of the individual isomers produced.

The B/X as a function of reaction time for the regenerated catalysts is shown in Figure 5.5., excluding the initial data point, which is instead provided in Table 5.1.. As can be seen in Figure 5.5., the B/X decreases as a function of reaction time, reducing to a *pseudo*-steady state of ~0.2 for all samples. From Table 5.1. it can be seen that the initial B/X of the samples is significantly higher than their subsequent values, and therefore the reason the initial data point for each sample was excluded from Figure 5.5.. The virgin catalyst had an initial B/X of 0.57, whereas the regenerated catalysts (with the exception of the DBD plasma regenerated sample) had lower B/X values. The initial B/X of the thermally regenerated sample had decreased by 14 %, whereas the microwave and microwave plasma regenerated samples had both decreased by a third compared

with the virgin sample. In contrast the initial B/X of the DBD plasma regenerated sample had increased by 7 % compared with the virgin sample.

Table 5.1. - Initial B/X of Regenerated Catalysts

Regeneration Method	Initial B/X
None (Virgin)	0.57
Thermal	0.48
Microwave	0.36
Microwave Plasma	0.35
DBD Plasma	0.61

- Virgin
- Thermal Regeneration
- Microwave Regeneration
- Microwave Plasma Regeneration
- Dielectric Barrier Discharge Plasma Regeneration
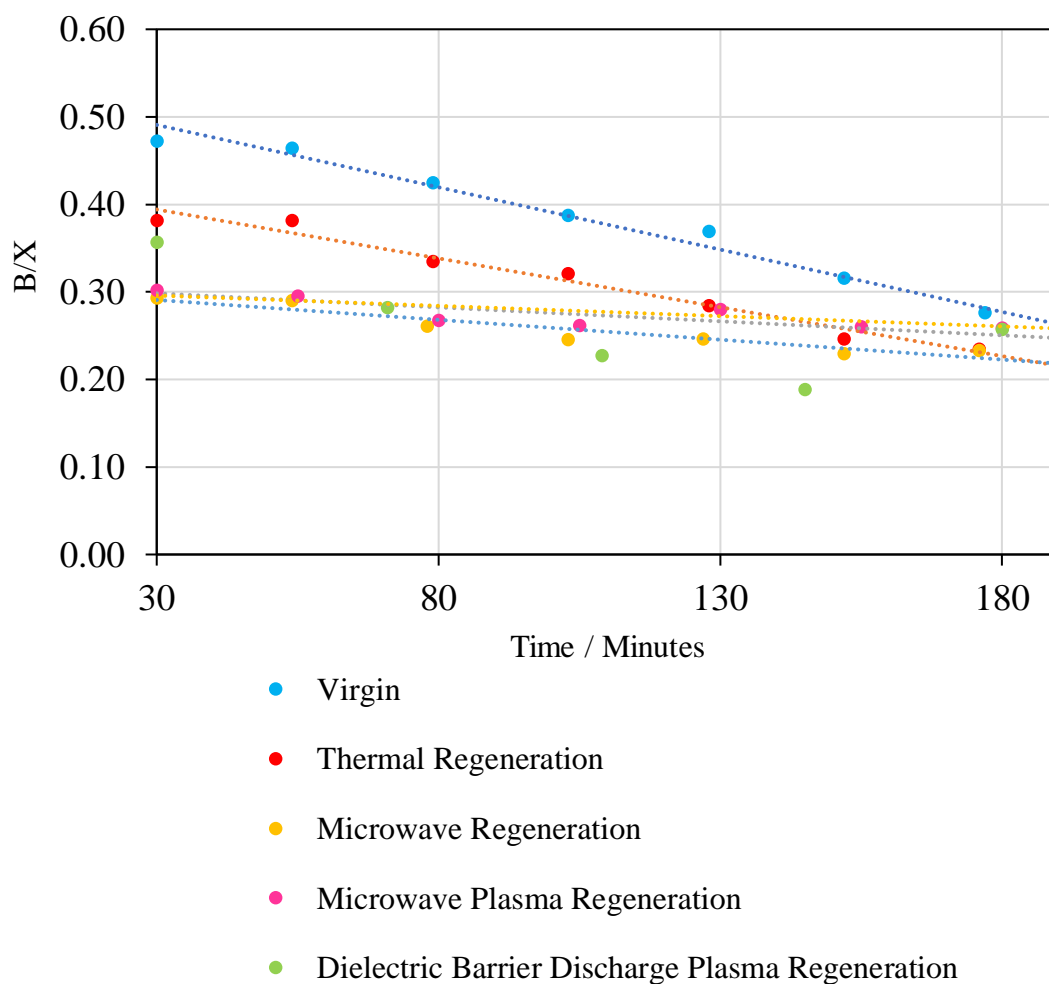
Figure 5.5. - B/X of Regenerated Catalysts

The individual xylene isomer selectivities as a function of reaction time for the regenerated catalysts are given in Figures 5.6.-5.8.. The data has been plotted alongside the thermodynamic equilibrium (T.E.) and grouped by similarity of xylene selectivity profiles for ease of discussion and interpretation.

Figure 5.6. presents the individual xylene isomer selectivities for a sample of virgin and a sample of thermally regenerated mordenite. Initial values of *p-* and *o*-xylene are slightly higher than the thermodynamic equilibrium. During the first 400 minutes, the amount of *p-* and *o*-xylene slowly decreases (whilst the amount of *m*-xylene correspondingly increases) towards thermodynamic equilibrium. However, after this period, the amount of *p*-xylene begins to move away from thermodynamic equilibrium, slowly increasing for the remainder of the reaction, whilst *m-* and *o*-xylene values slowly decrease accordingly.
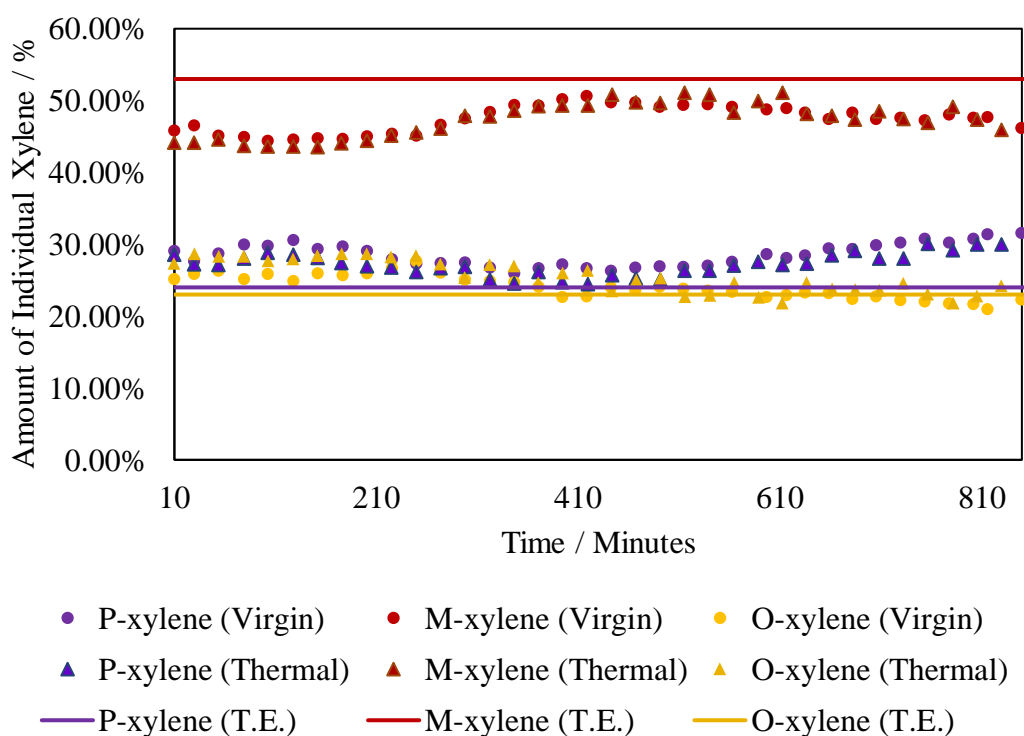
Figure 5.6. - Plot of Individual Xylene Isomer Selectivities for Virgin and Thermally Regenerated Catalysts

Figure 5.7. presents the individual xylene isomer selectivities for a sample of microwave regenerated and a sample of microwave plasma regenerated mordenite. Similar to the virgin and

thermally regenerated samples, the initial amounts of *p*- and *o*-xylene are slightly elevated compared with the thermodynamic equilibrium, whilst the amount of *m*-xylene is lower accordingly. Over the duration of the first 400 minutes, the amount of *p*-xylene decreases slightly, moving towards thermodynamic equilibrium, after which it remains constant for the remainder of the reaction. *m*-Xylene increases throughout the duration of the reaction towards thermodynamic equilibrium, almost reaching it by 800 minutes. *o*-Xylene remains relatively constant throughout the reaction, before slowly decreasing after 630 minutes proportionately in accordance with changes in *p*- and *m*-xylene.
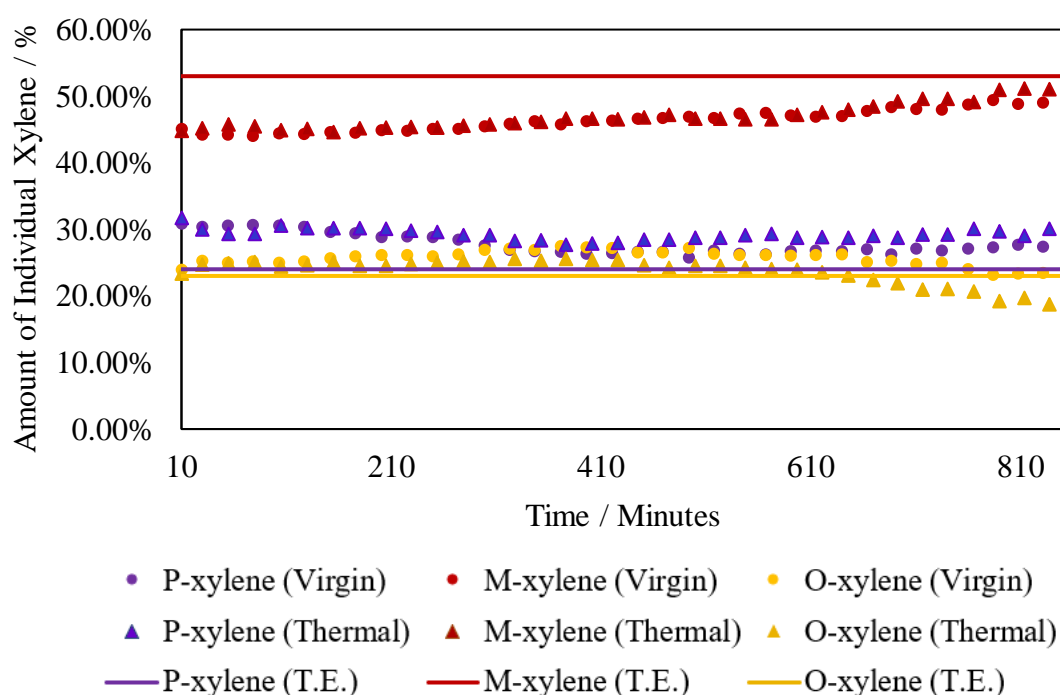
Figure 5.7. - Plot of Individual Xylene Isomer Selectivities for Microwave and Microwave Plasma Regenerated Catalysts

Figure 5.8. presents the individual xylene isomer selectivities for a sample of DBD plasma regenerated mordenite. Initially the xylene isomer selectivities of the DBD plasma regenerated sample are in thermodynamic equilibrium. However, after 200 minutes, the xylene isomers move away from thermodynamic equilibrium, with a slight increase in *p*-xylene and corresponding decrease in *m*- and *o*-xylene.
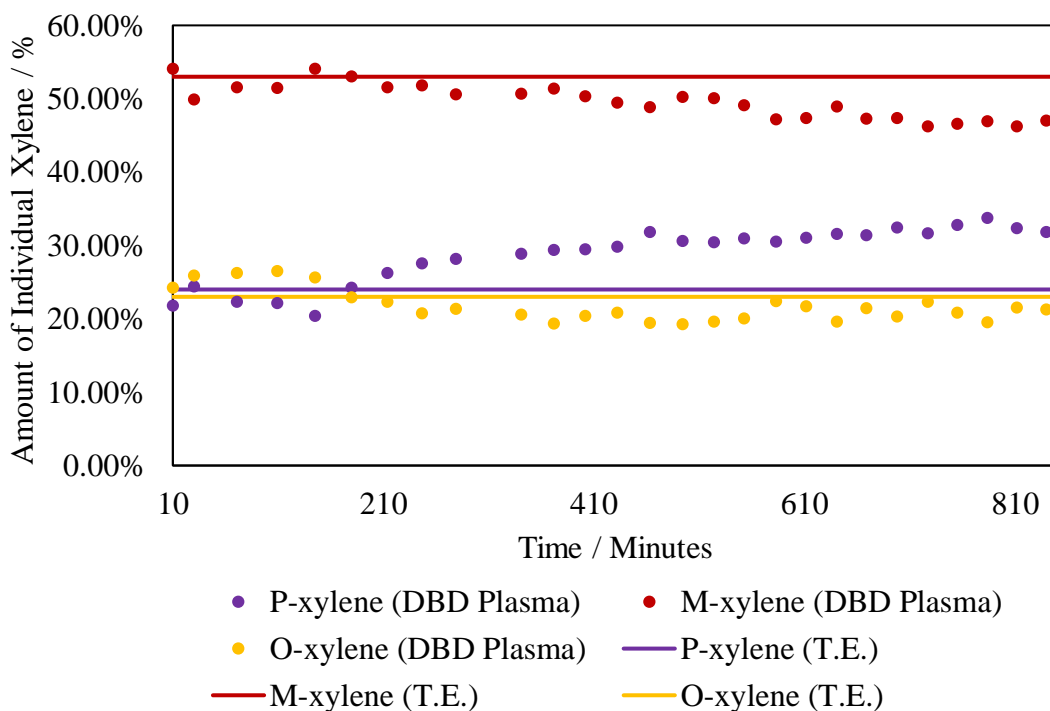
Figure 5.8. - Plot of Individual Xylene Isomer Selectivities for DBD Plasma Regenerated Catalyst

5.3. SURFACE AREA AND AMOUNT OF COKE

The surface area and coke present for each of the coked and uncoked catalysts was determined according to the method described in Section 4.2.4. and is given in Table 5.2..

Table 5.2. - Surface Area and Coke Present on Regenerated Catalysts

	BET Surface Area / m^2g^{-1}		Coke Present / weight %	
	Uncoked	Coked	Uncoked	Coked
Virgin	348	189	0.30	4.55
Thermal Regenerated	352	190	0.36	3.37
Microwave Regenerated	259	210	0.19	2.39
Microwave Plasma Regenerated	333	158	0.32	3.05
DBD Plasma Regenerated	290	186	2.20	4.49

As can be seen from Table 5.2., the BET surface area of the catalysts is reduced upon coking, with virgin mordenite losing almost half of its surface area post-deactivation. Upon regeneration, a large proportion of surface area is recovered, ranging between 74-100 % depending on the regeneration method. Both the thermally and microwave plasma regenerated catalysts recovered

over 95 % of their surface area, with the DBD plasma regenerated mordenite having recovered 83 % and the microwave regenerated sample recovered the least surface area (74 %). Post-deactivation, the regenerated catalysts lost similar amounts of surface area to virgin deactivation (54 %), with microwave plasma losing the most surface area with respect to virgin (45 %).

From the coke data given in Table 5.2., it can be seen that the amount of coke deposited on the regenerated catalysts during toluene disproportionation was significantly less than the virgin, with the exception of DBD plasma regenerated mordenite, where the difference is negligible. There is only a slight decrease in the amount of coke formed in the thermally regenerated sample, however, the microwave and microwave plasma regenerated coked samples show considerably less coke, with values approximately half or two thirds respectively, when compared with virgin.

5.4. COKE COMPOSITION

The deactivation of the catalyst in this reaction is attributed to coking. Therefore, determination of the coke composition may offer an insight into whether the regeneration process affects the coking mechanism. Raman and solvent extraction (coupled with GC-MS) were used to aid identification of any structural alterations which may be present in the coke.

5.4.1. Raman Spectroscopy

Raman spectra of virgin (both coked and uncoked), coked thermally regenerated and coked microwave plasma regenerated samples are given in Figure 5.9.. However, Raman studies involving zeolites and/or coke are known to suffer interference due to fluorescence of the sample (1). This drawback can affect the interpretation of the Raman data, leading to higher intensities than would be seen with no interference. The (uncoked) virgin sample exhibits a significant amount of fluorescence between 2000-1200 cm^{-1}. In contrast, fluorescence does not appear to be present on the coked virgin sample, however it is present on the thermally and microwave plasma regenerated coked samples, most noticeably in the 2000-1700 cm^{-1} region. Therefore, to interpret the Raman data taking fluorescence into consideration, the (uncoked) virgin sample was subtracted from the thermally and microwave plasma regenerated coked samples between 2000-

1200 cm^{-1}. The subtraction result plotted with the unaltered coked virgin sample are given in Figure 5.10..
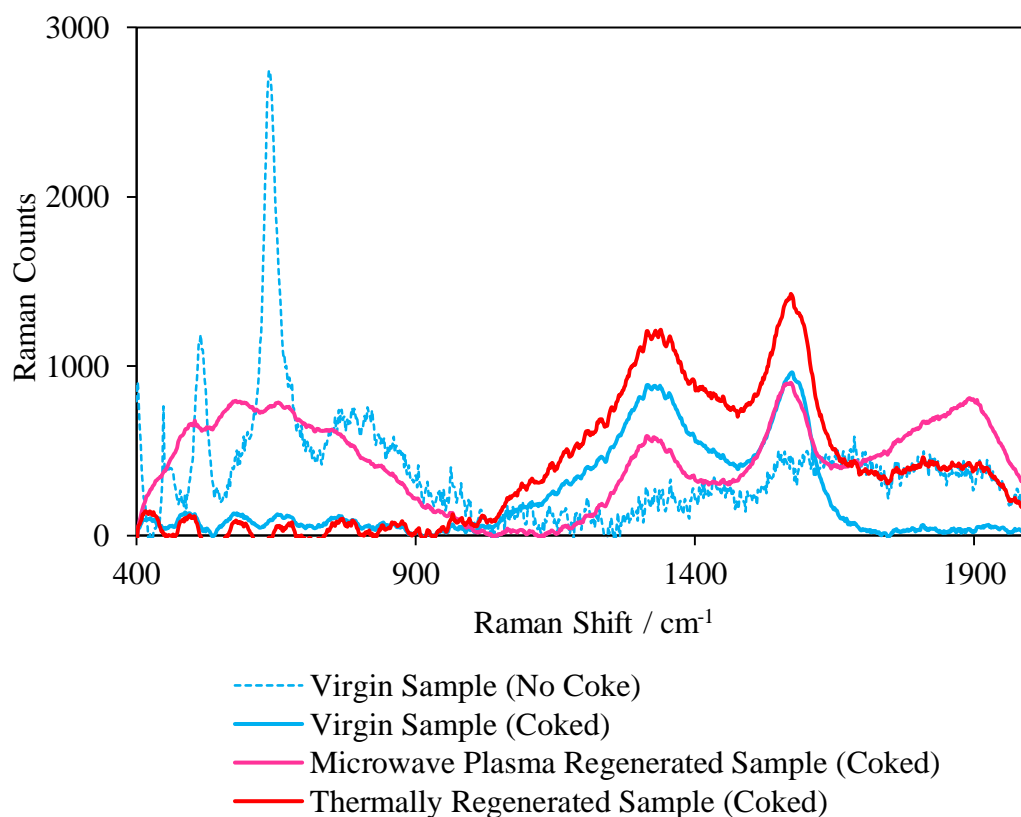
Figure 5.9. - Raman Spectrum of Regenerated Coked Catalysts
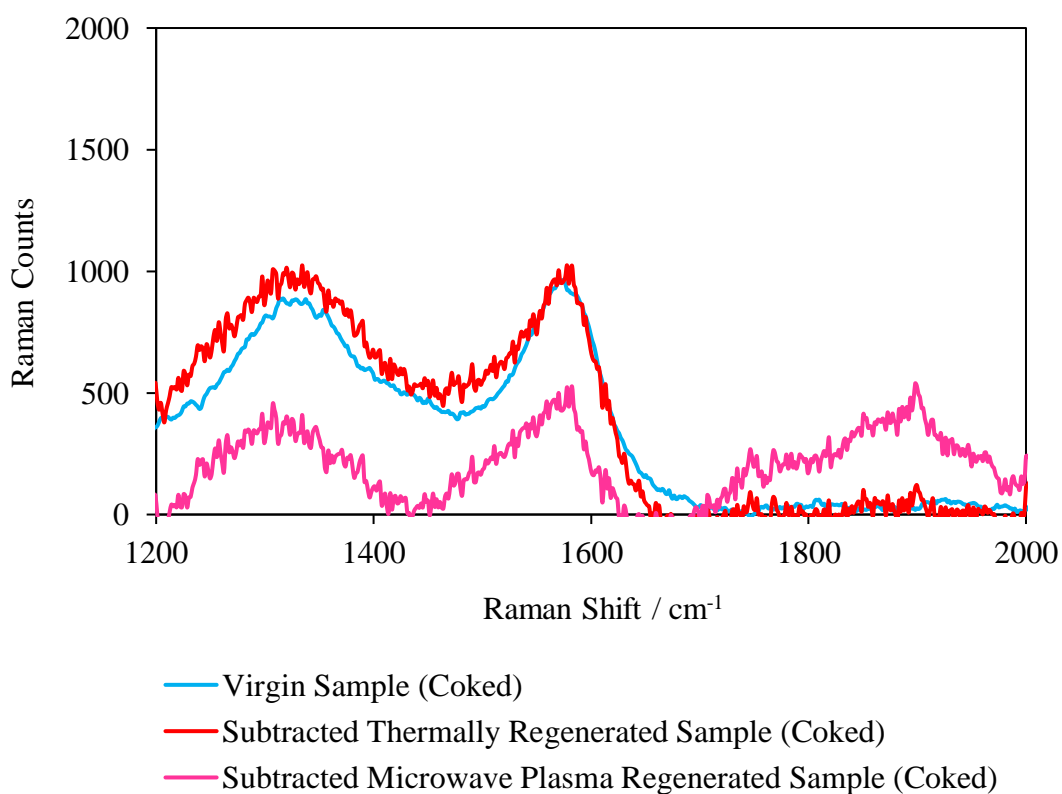
Figure 5.10. – Subtracted Raman Spectrum of Regenerated Coked Catalysts

In the 2000-1200 cm^{-1} region (Figure 5.10.), three distinct peaks can be identified at 1350 cm^{-1} (D-band), 1575 cm^{-1} (G-band) and 1900 cm^{-1} (2), although the latter only appears in the microwave plasma regenerated sample. The intensity of the microwave plasma regenerated sample is significantly lower in the d- and g-bands compared with the virgin and thermally regenerated samples. In Figure 5.9., the (uncoked) virgin sample exhibits peaks in the lower wavenumber region <1000 cm^{-1} characteristic of the crystallinity of the zeolite (3). These appear broader and less defined in the microwave plasma regenerated sample, whereas in the coked virgin and thermally regenerated samples, the peaks become broad and muted, with very low intensities. This is due to coverage of the zeolite by the carbonaceous species.

5.4.2. Solvent Extraction

Identification of carbonaceous species is often determined using solvent extraction (4). Studies have shown coke deposited during toluene disproportionation to consist of various hydrocarbons, some readily soluble and others insoluble to common solvents such as dichloromethane (DCM) (5). A typical solvent extraction performed on a zeolite can involve multiple extraction stages, ultimately leading to treatment with hydrogen fluoride (HF), resulting in the destruction of the zeolite (5). For this research, a milder solvent extraction involving DCM was performed, to investigate any difference in the proportion or type of DCM soluble coke species upon regeneration. The solvent extraction process was as follows: 100 mg coked catalyst was submerged in 20 mL DCM and vigorously shaken for a period of 72 hours. Following this, the samples were removed, and the effluent was injected into the GC-MS for analysis. Figure 5.11. gives a photograph of the effluent post-extraction, and Figure 5.12. gives the results of the GC-MS analysis.
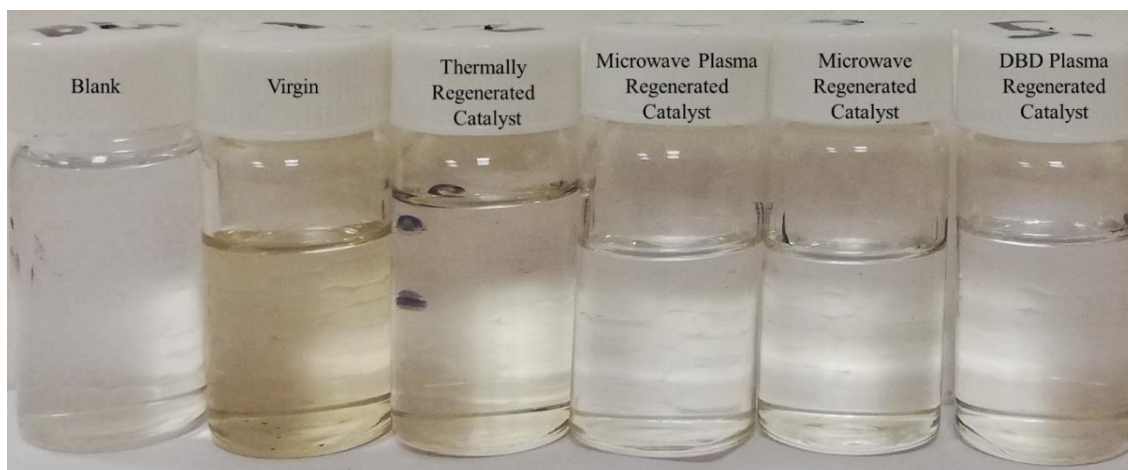
Figure 5.11. - Photo of the Effluent Post-Extraction

Whilst all the catalyst samples post-DCM extraction were still completely black, Figure 5.11. shows some colouration of the effluent compared with the blank (solely DCM), illustrating some DCM soluble species. In particular, the virgin and thermally regenerated effluent showed a darker colour compared with the microwave and plasma samples.

Figure 5.12. presents the GC-MS data of the effluent, with relative abundance referenced to the solvent. The GC-MS programme used was the same used for the detection of TDP products on-stream during the deactivation process and the species elucidated were preliminarily identified through the NIST library.

There were no significant peaks below 15 minutes with the exception of the solvent. All the samples appeared to have DCM soluble species. The virgin sample exhibits a similar amount of DCM soluble coke to the thermally regenerated sample, both of which appear to have less DCM soluble coke present than microwave plasma and DBD plasma samples. The microwave regenerated sample exhibits almost no DCM soluble coke.

The preliminary identification of the DCM soluble coke species using the NIST library, determined the carbonaceous species to be similar in structure, with up to 3 rings and molecular weights ranging from 165-340 g mol^{-1}, similar to those reported by Magnoux et *al.* (6).
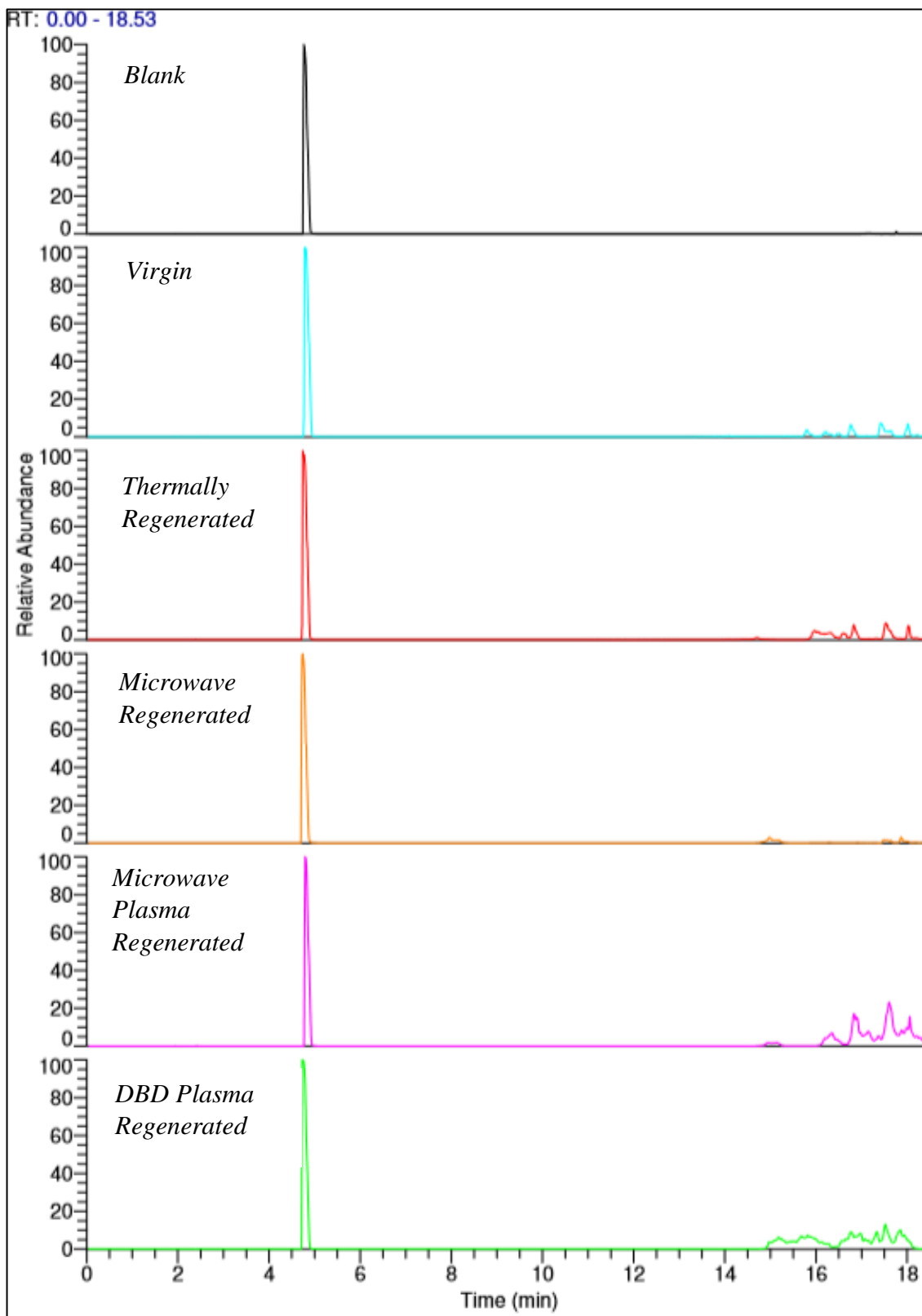
Figure 5.12. – Chromatogram of DCM Soluble Coke

5.5. X-RAY DIFFRACTION

One of the main concerns of catalytic regeneration is loss of crystallinity during the process, which often results in heavily reduced activity, selectivity or both (7-9). XRD was carried out on the regenerated samples to determine whether the microwave, microwave plasma and DBD plasma regeneration processes had any significant effect on the catalytic crystal structure. The results of this are given in Figures 5.13.-5.16., with the regenerated samples laid over virgin mordenite to aid in visualisation of any changes which may have occurred.

There is little difference in the diffractograms of the virgin and regenerated samples, with the exception of microwave regenerated mordenite. All the diffractograms show characteristic mordenite peaks (10), with negligible change in peak position and very little peak broadening. Loss of relative intensity is suggestive of a loss in crystallinity or less sample present in the beam. Whilst difficult to determine where only marginal losses are seen (i.e. thermal, microwave plasma and DBD plasma regenerated samples), the considerable loss in relative peak intensity of the microwave regenerated sample compared with the virgin sample suggests a loss of crystallinity to be more likely in this case. This would elude to changes in the cell coordinates or composition. However further analysis such as Rietveld refinement would need to be performed to confirm this.
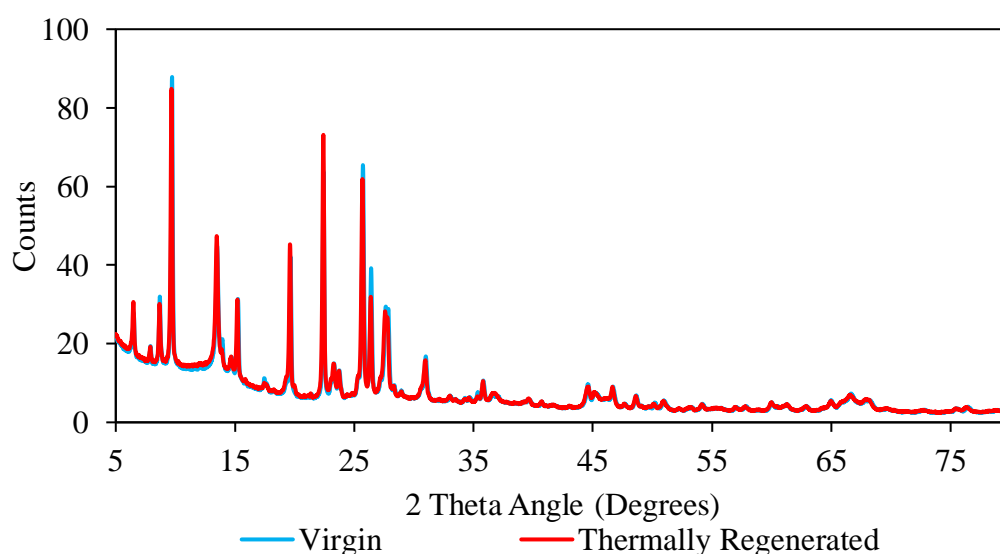
Figure 5.13. - XRD Diffractogram of Thermally Regenerated Mordenite
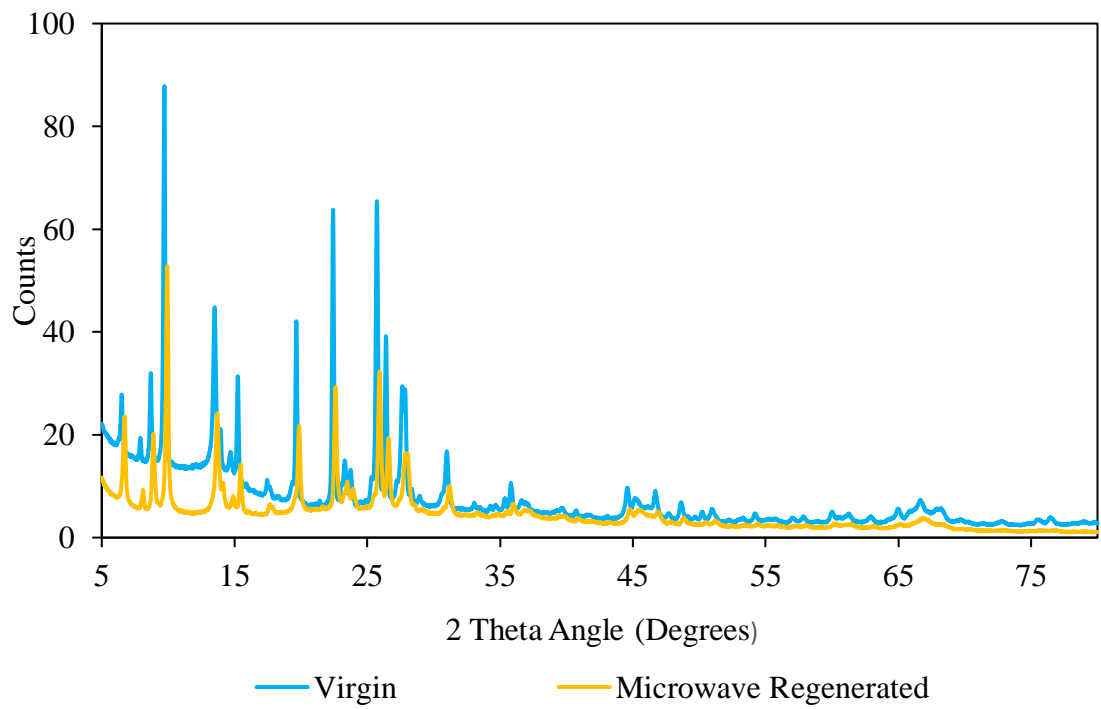
Figure 5.14. - XRD Diffractogram of Microwave Regenerated Mordenite
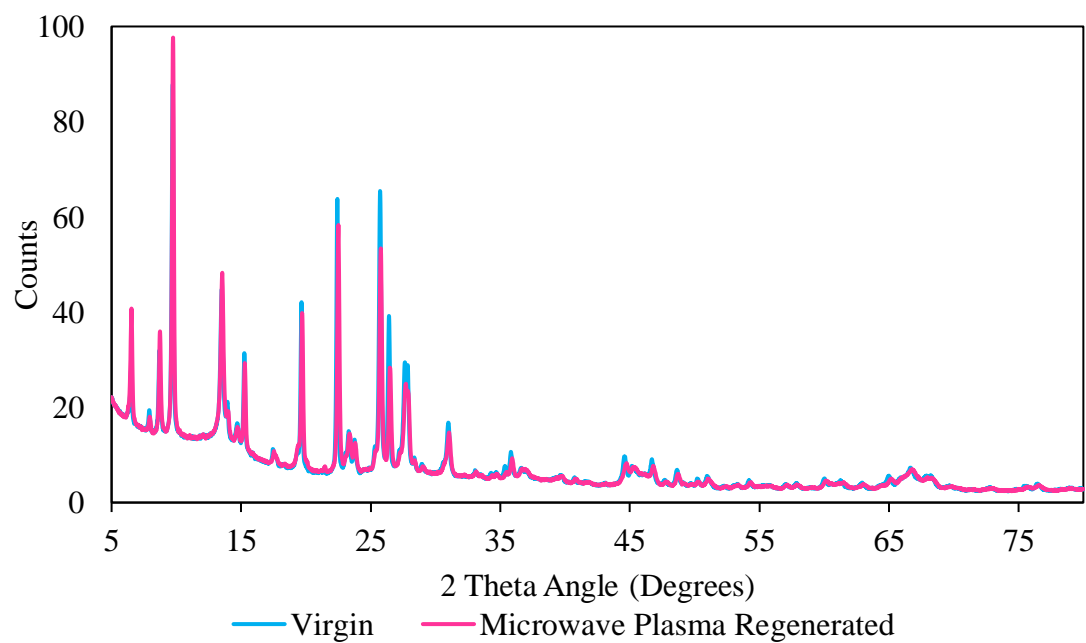
Figure 5.15. - XRD Diffractogram of Microwave Plasma Regenerated Mordenite
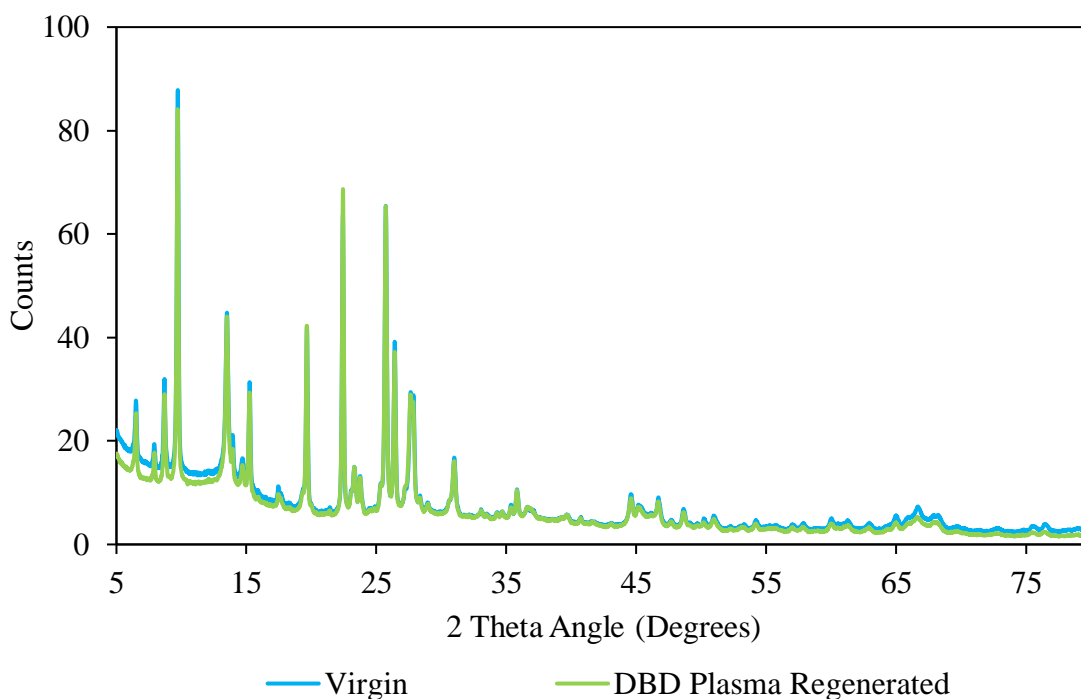
Figure 5.16. - XRD Diffractogram of DBD Plasma Regenerated Mordenite

5.6 X-RAY PHOTOELECTRON SPECTROSCOPY

XPS was carried out to determine any changes in the surface structure which may have been caused by the regeneration processes. The results are given in Table 5.3..

Table 5.3. - Surface Composition (Surface Atom %) of Regenerated Catalysts

Element	Virgin	Thermally Regenerated	Microwave Plasma Regenerated
Oxygen	60.5	59.2	60.4
Aluminium	25.5	24.9	22.7
Silicon	7.9	8.5	11.6

From Table 5.3., a change in the number of aluminium and silicon surface composition can be seen between the virgin and regenerated catalysts. There is a minor decrease from 25.5 % to 24.9 % for the thermally regenerated catalyst and a slightly more pronounced decrease to 22.7 % for the microwave plasma regenerated catalyst. There is also a corresponding increase in silicon, although no significant change in the amount of oxygen present.

5.7. CATALYST ACIDITY

5.7.1. Magic Angle Spinning Solid State Nuclear Magnetic Resonance

As an acid catalyst, the activity of mordenite is heavily linked to availability and strength of its acid sites. ssNMR and IR studies were carried out to determine any impact the microwave or plasma regeneration processes may have had on catalytic acidity. Figures 5.17., 5.18. and 5.19. depict the results of ^{29}Si, ^{27}Al, and ^{1}H MAS ssNMR on the regenerated catalysts respectively.

The ^{29}Si NMR in Figure 5.17. displays three peaks in the region of -95 and -115 ppm. These are characteristic of mordenite, representing the oxygen bridged tetrahedrally bound silicon to aluminium atoms. Typically, these peaks are -100 ppm (2 bound Al atoms), -106 ppm (1 bound Al atom) and -113 ppm (0 bound Al atoms) [11]. The most significant of the three peaks is the peak at -106 ppm, as this has been recognised as highly sensitive to the presence of aluminium and the change in intensity can be correlated to the amount of dealumination occurring on a given mordenite sample [11]. The -106 ppm peak in Figure 5.17. shows a decrease of intensity in both the thermally regenerated and microwave plasma regenerated samples compared with virgin.

The ^{27}Al NMR in Figure 5.18. exhibits two peaks: 54 ppm and 0 ppm, representing framework and extra-framework aluminium (EFAl) respectively [12]. The shoulders seen to the left of both peaks are attributed to the γ-alumina binder [12]. Figure 5.18. shows a decrease in framework aluminium for both thermal and microwave plasma regenerated samples, however there is still less EFAl for both samples than seen in the virgin.

The ^{1}H NMR in Figure 5.19. displays 4 peaks: 4.0, 2.6, 1.8 and 0.0 ppm. The peaks at 4.0 and 1.8 ppm are widely known to represent Brønsted acid sites and silanol group protons respectively [13-16]. The peaks at 2.6 and 0.0 ppm are less established within the literature as results can often produce broad peaks, where resolution of individual peaks can be difficult to identify [13]. What is present in the literature attributes these peaks to EFAl species [15]. Figure 5.19. shows a decrease in Brønsted acid sites for the regenerated samples compared to virgin, with the

microwave plasma sample losing significantly more Brønsted acid sites. There is an increase in

EFAl at 2.6 ppm (although this is not seen at 0.0 ppm).
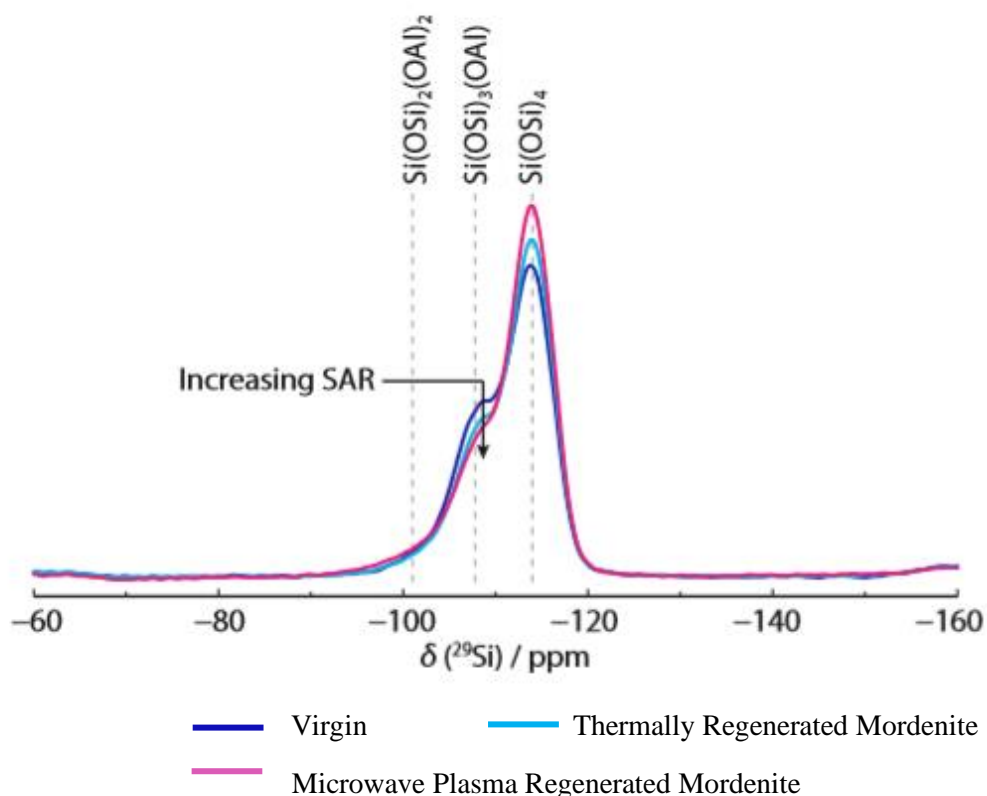
Figure 5.17. - ^{29}Si MAS ssNMR of Regenerated Catalysts
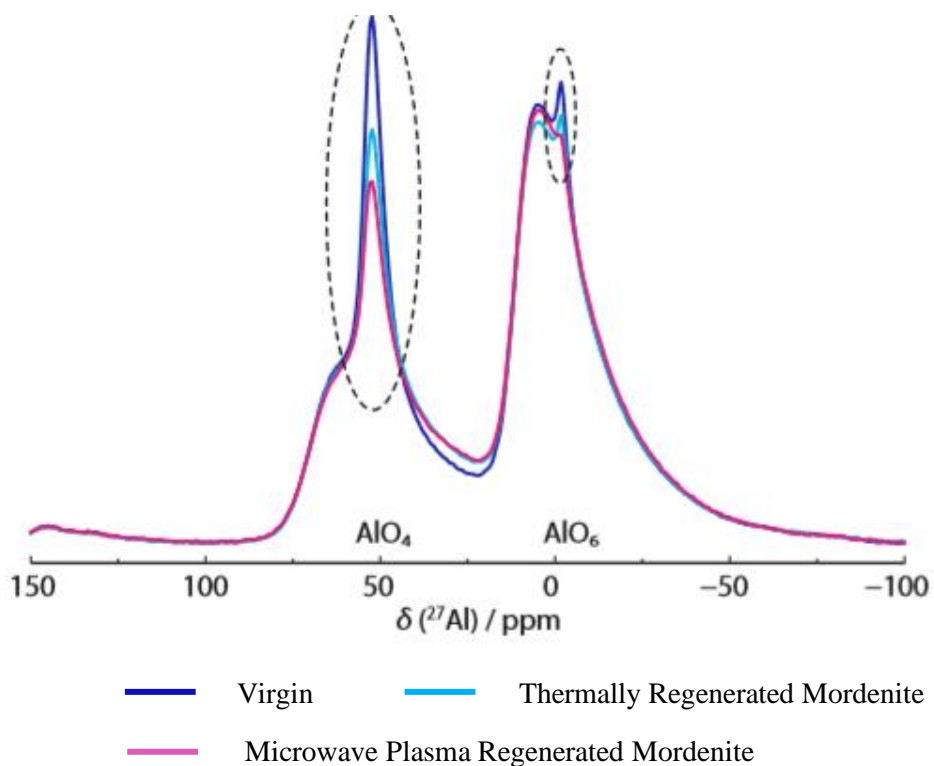
Figure 5.18. – ^{27}Al MAS ssNMR of Regenerated Catalysts

Brønsted
4.0

AlOH
2.6

SiOH
1.8

AlOH?
0.0

δ (^{1}H) / ppm

— Virgin   — Thermally Regenerated Mordenite

— Microwave Plasma Regenerated Mordenite
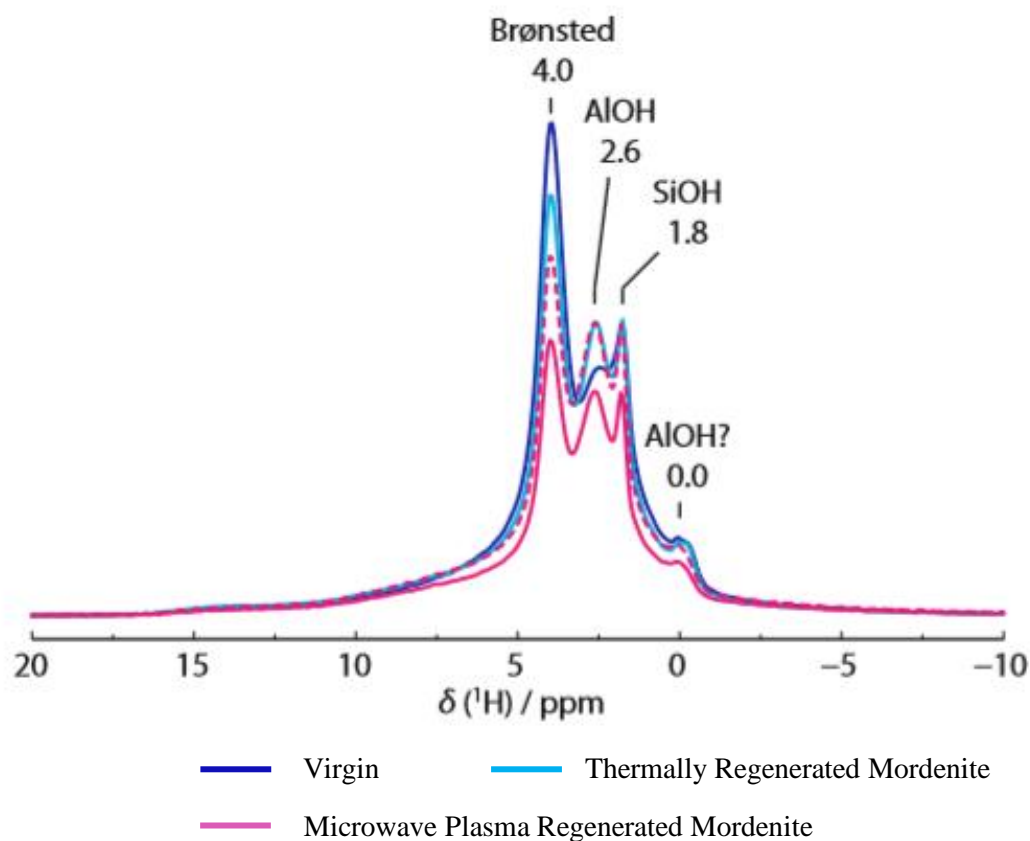
- - - The dashed line represents the microwave plasma scaled to the SiOH peak height of the other samples.

Figure 5.19. - ^{1}H MAS ssNMR of Regenerated Catalysts

5.7.2 Infrared Spectroscopy

Results from the infrared studies using probe molecules are given in Figures 5.20.-5.25.. Figure 5.20. depicts the IR spectra of the virgin sample prior to and post pyridine adsorption in the 4000-3500 cm^{-1} region where the O-H stretching frequencies appear (17). Peaks of interest include 3742 cm^{-1}, 3653 cm^{-1} (Si-OH and Al-OH groups) and 3606 cm^{-1} (acidic Al-OH-Si groups). The additional peak at 3775 cm^{-1} is a result of the γ-Al$_2$O$_3$ in the binder. These peaks were also present in the regenerated samples but were omitted for simplification.

The subtraction result ((spectrum of the sample after pyridine adsorption) – (the spectrum of the activated sample prior to adsorption)) of the regenerated samples is given in Figure 5.21.. The interaction of pyridine with the catalyst samples can be seen from the presence of negative peaks appearing at 3608 cm^{-1}, 3660 cm^{-1}, 3744 cm^{-1} and 3775 cm^{-1}.
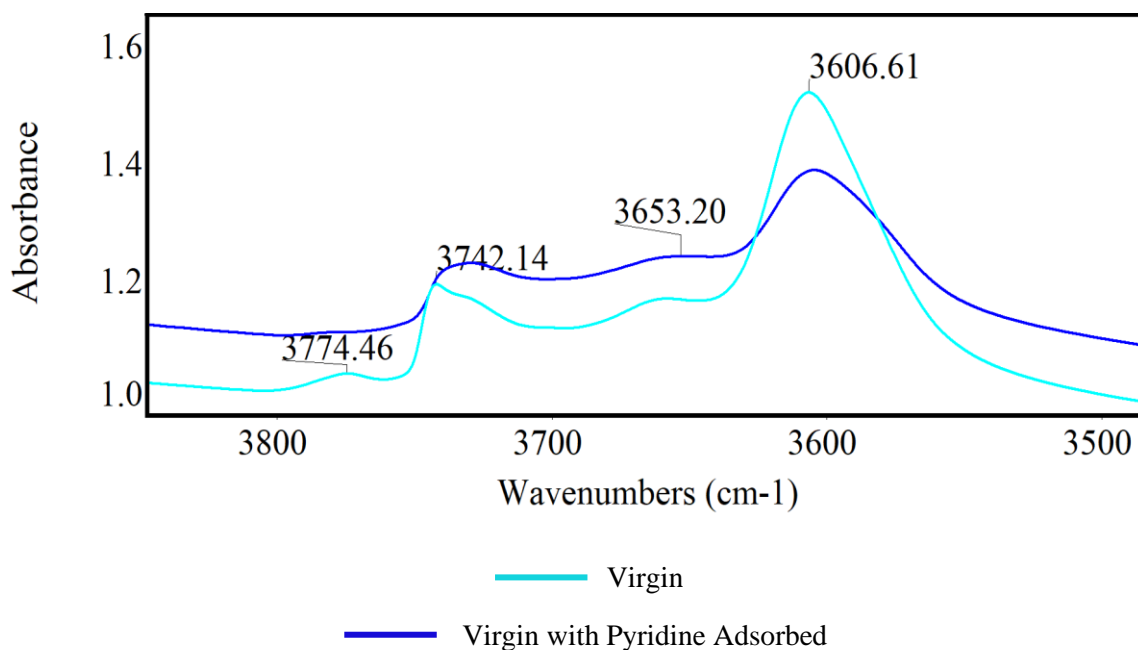
Figure 5.20. – IR Spectra of Virgin Sample Pre- and Post-Pyridine Adsorption
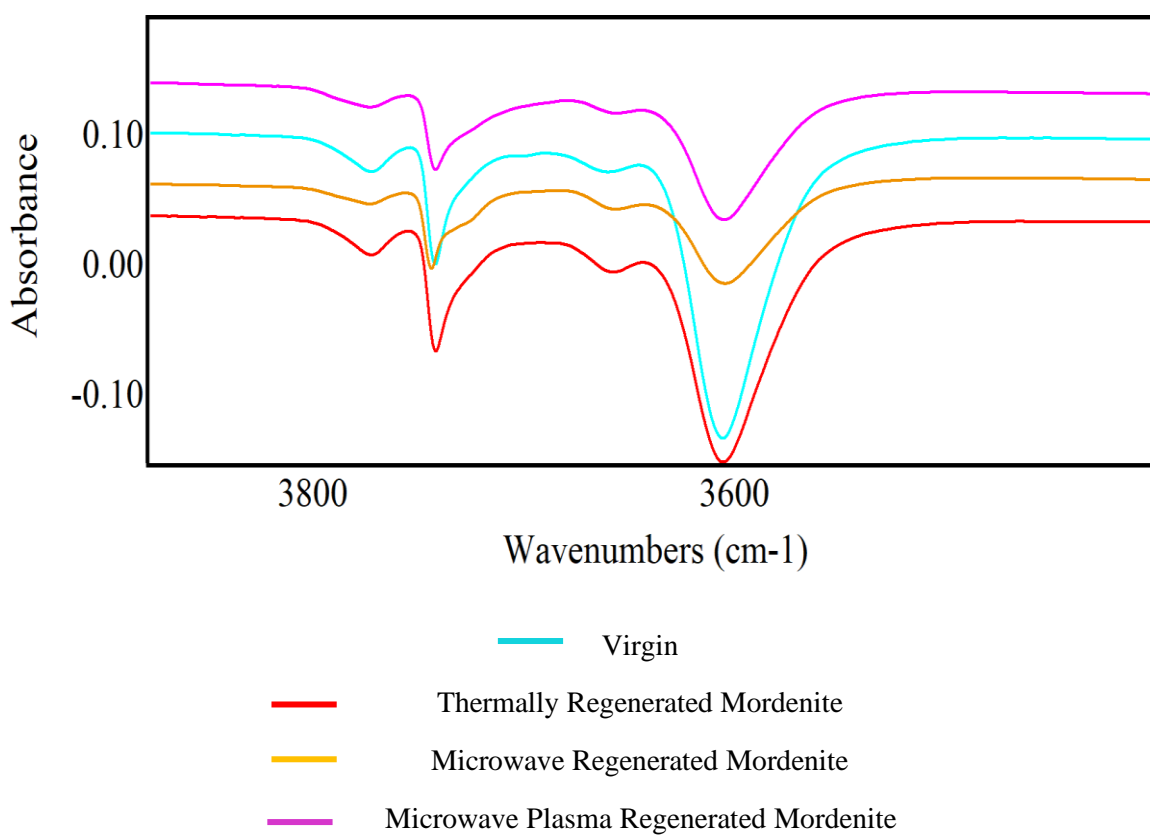
Figure 5.21. – IR Spectra Subtraction Result of Pyridine Adsorbed Regenerated Catalysts

(4000-3400 cm^{-1})

Figure 5.22. depicts the IR subtraction result of the regenerated catalysts in the 1700-1400 cm^{-1} region where the pyridine frequencies appear (17). Peaks of interest include 1454 cm^{-1} (strong LAS), 1489 cm^{-1} (BAS and LAS), 1544 cm^{-1} (BAS), 1621 cm^{-1} and 1633 cm^{-1}. The peaks at 1544 cm^{-1} and 1454 cm^{-1} were used to calculate the concentration of Brønsted and Lewis acid sites (as described in section 4.2.6) respectively (Table 5.4).
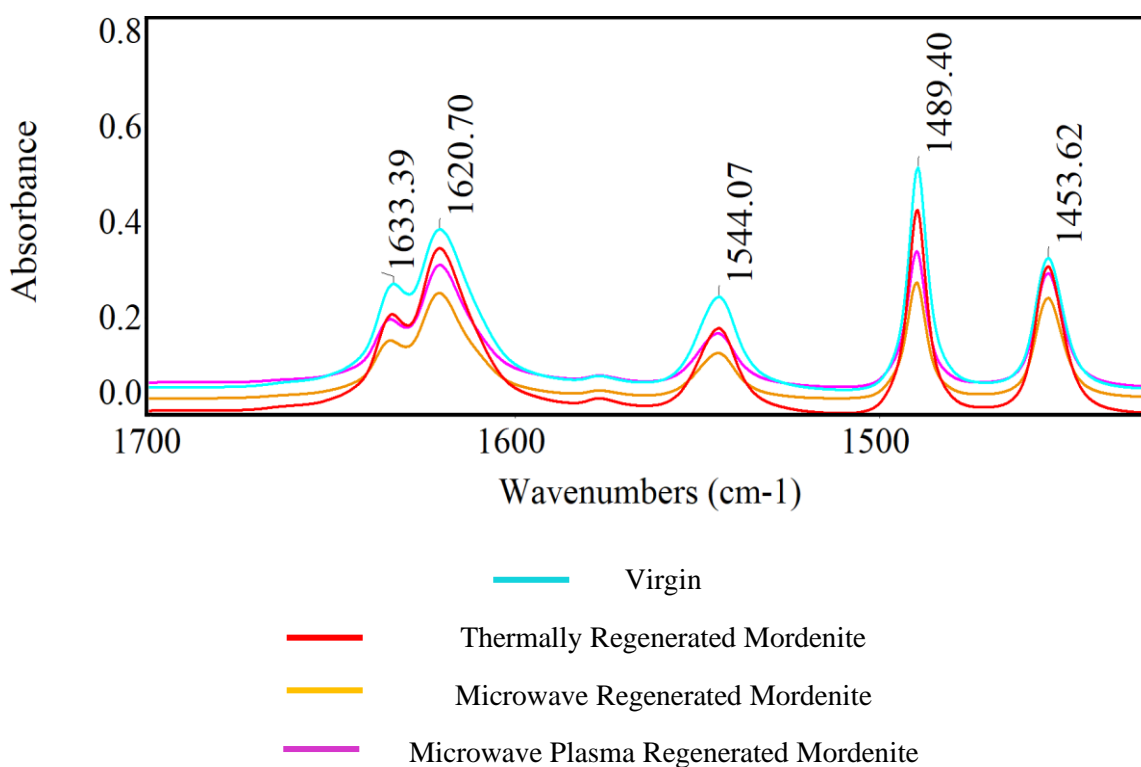
Figure 5.22. – IR Spectra Subtraction Result of Pyridine Adsorbed Regenerated Catalysts

(1700-1400 cm^{-1})

Figure 5.23. depicts the IR spectra of the virgin sample prior to and post collidine adsorption in the 4000-3500 cm^{-1} region where the O-H stretching frequencies appear (18). Peaks of interest include 3743 cm^{-1}, 3657 cm^{-1} (Si-OH and Al-OH groups) and 3607 cm^{-1} (acidic Al-OH-Si groups). The additional peak at 3775 cm^{-1} is a result of the γ-Al$_2$O$_3$ in the binder. The subtraction result of the regenerated samples is given in Figure 5.24.. The interaction of collidine with the catalyst samples can be seen from the presence of negative peaks appearing at 3608 cm^{-1}, 3663 cm^{-1}, 3745 cm^{-1} and 3775 cm^{-1}.
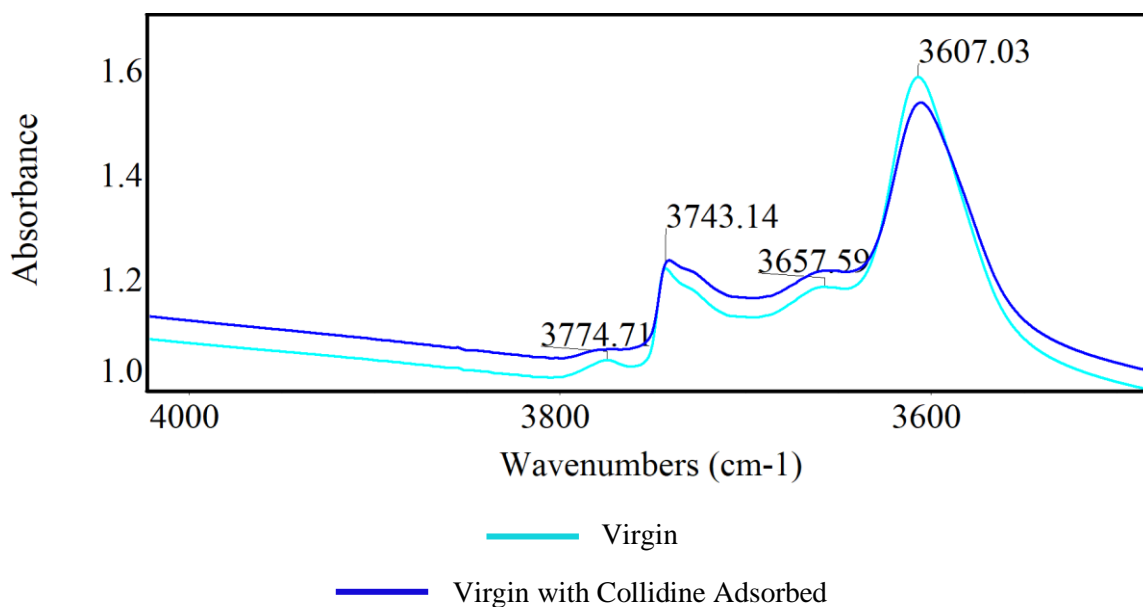
Figure 5.23. – IR Spectra of Virgin Sample Pre- and Post-Collidine Adsorption
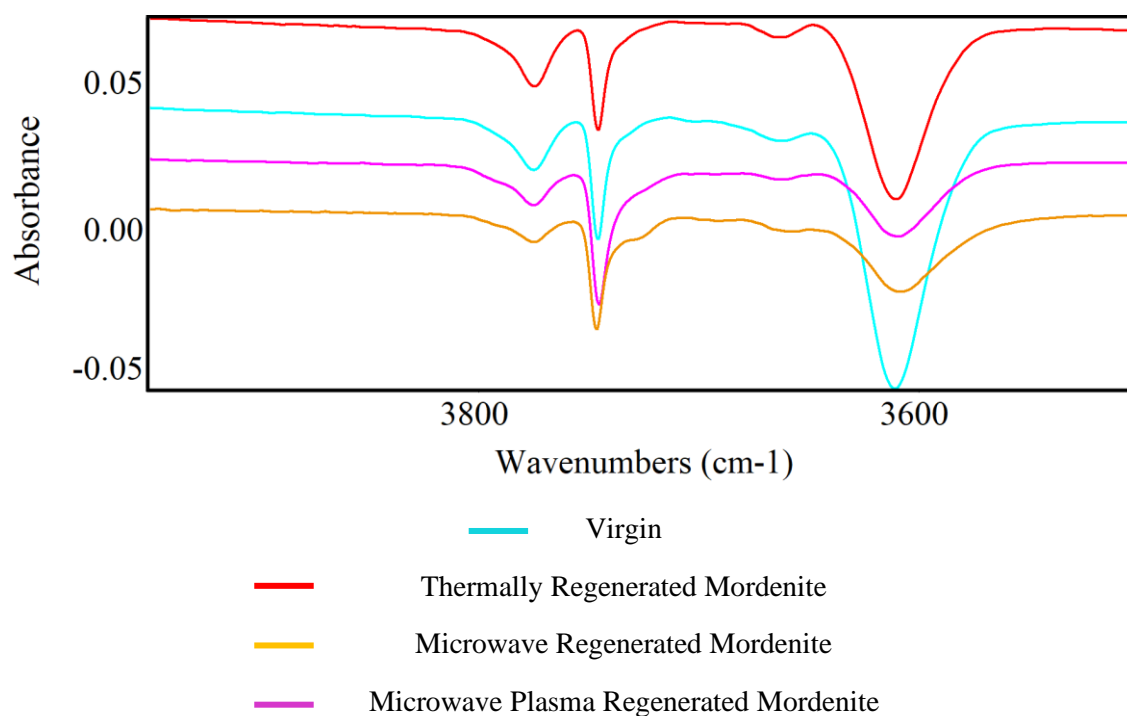
Figure 5.24. – IR Spectra Subtraction Result of Collidine Adsorbed Regenerated Catalysts

(4000-3400 cm^{-1})

Figure 5.25. depicts the IR subtraction result of the regenerated catalysts in the 1800-1500 cm^{-1} region where the collidine frequencies appear (19). The peak of interest appears at 1636 cm^{-1}, corresponding to the BAS present (19). This peak was used (as described in Section 4.2.6.) to calculate the concentration of Brønsted acid sites (Table 5.4.).

1635.79

Virgin
Thermally Regenerated Mordenite
Microwave Regenerated Mordenite
Microwave Plasma Regenerated Mordenite
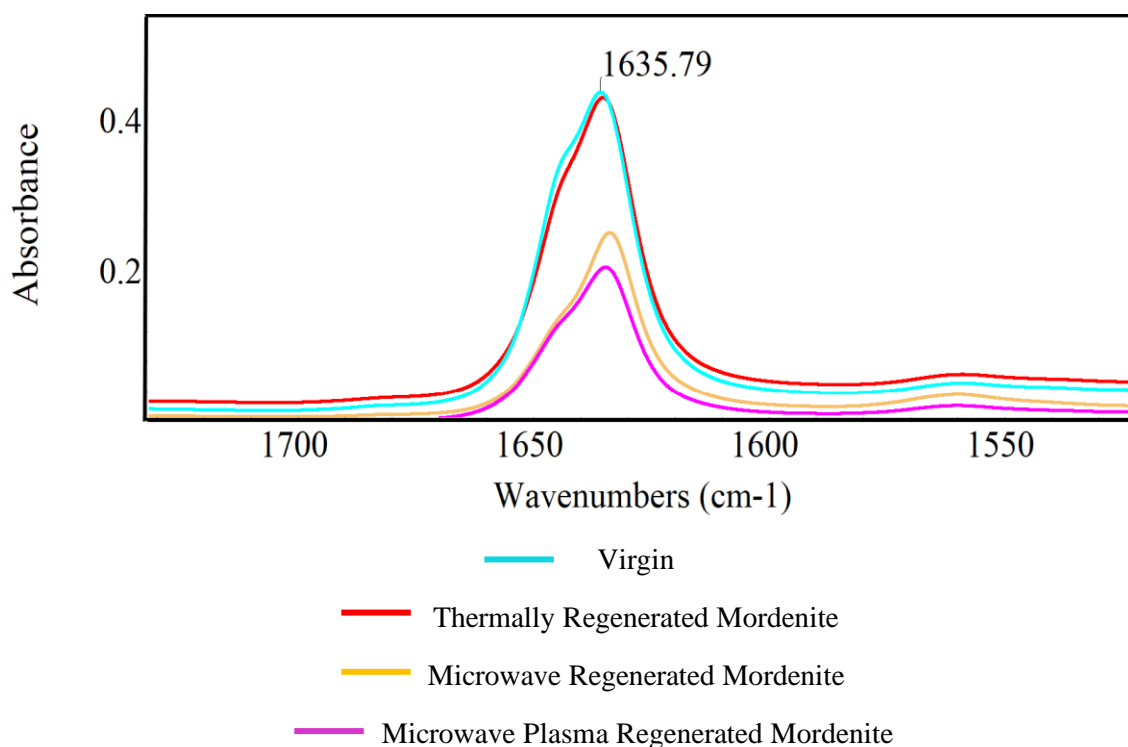
Figure 5.25. – IR Spectra Subtraction Result of Collidine Adsorbed Regenerated Catalysts

(1700-1400 cm^{-1})

The concentration of Brønsted and Lewis acid sites determined using the probe molecules is reported in Table 5.4., taking surface area into account. As can be seen from Table 5.4., virgin mordenite possessed the highest number of total Brønsted acid sites, followed by thermally, microwave plasma and microwave regenerated mordenite. In comparison, microwave plasma regenerated mordenite had the most Lewis acid sites, followed by thermally regenerated, virgin and microwave regenerated mordenite. The collidine data (also shown in Table 5.4.), illustrates virgin mordenite has the most surface Brønsted acid sites, decreasing by 25 % for thermally regenerated mordenite and decreasing by ~40 % for both microwave and microwave plasma regenerated samples.

Table 5.4. - Number of Acid Sites (μmol m^{-2} g^{-1}) in Regenerated Catalysts

		Virgin	Thermally Regenerated	Microwave Regenerated	Microwave Plasma Regenerated
Pyridine	**BAS**	0.5	0.42	0.32	0.37
	LAS	0.45	0.47	0.43	0.50
	B/L	1.1	0.9	0.7	0.7
Collidine	**BAS**	0.24	0.18	0.15	0.13

5.7.3 Ammonia Temperature Programmed Desorption

Results of the NH$_3$ TPD studies of the regenerated catalysts are given in Figures 5.26-5.28, plotted alongside a sample of virgin mordenite to assist in the visualisation of any differences which may have arisen. Typically, relative acid site strength can be determined by peak temperature, where increasing temperatures are indicative of stronger acid sites (20).
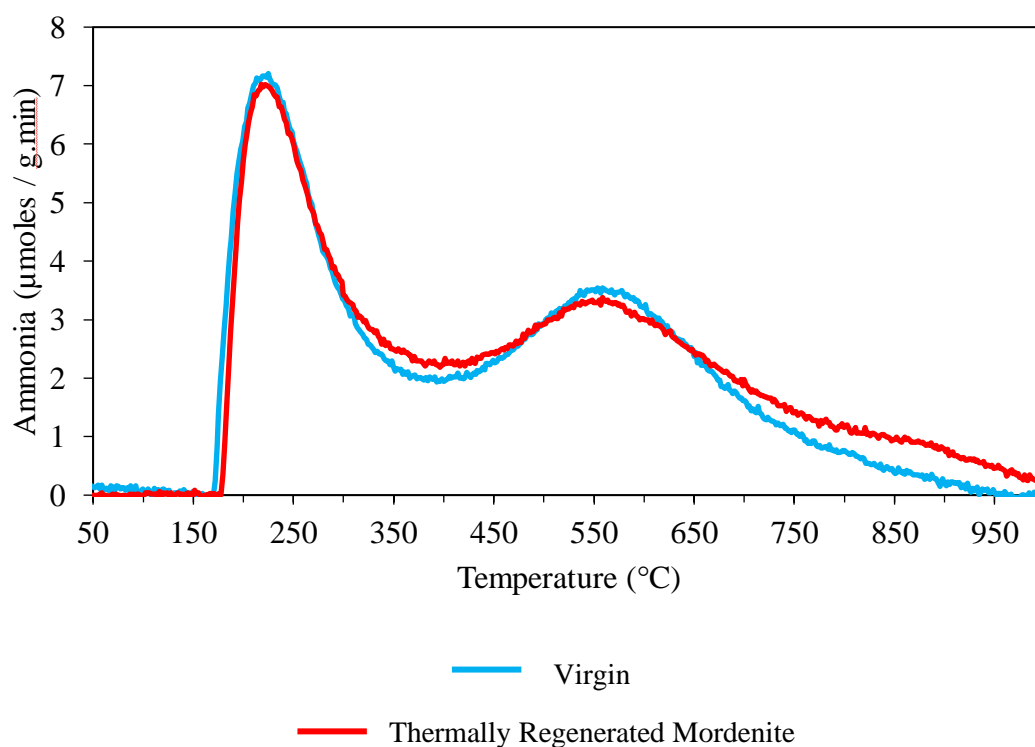
Figure 5.26. – NH$_3$ TPD Spectra of Virgin Catalyst Compared with Thermally Regenerated Catalyst

The NH$_3$ TPD data for a sample of virgin mordenite, given in Figure 5.26., displays two peaks; the first at 225°C and the second at 560°C. The peak at 225°C exhibits a peak maximum of 7 µmoles g^{-1} min^{-1} ammonia, twice as much as the peak at 560°C (3.37 µmoles g^{-1}min^{-1} ammonia).

The NH$_3$ TPD data for a sample of thermally regenerated mordenite is also shown in Figure 5.26. and exhibits two peaks in the same region as the virgin sample. However, there is a minor decrease (~0.5 µmoles g^{-1}min^{-1}) in the intensity of the two peaks.
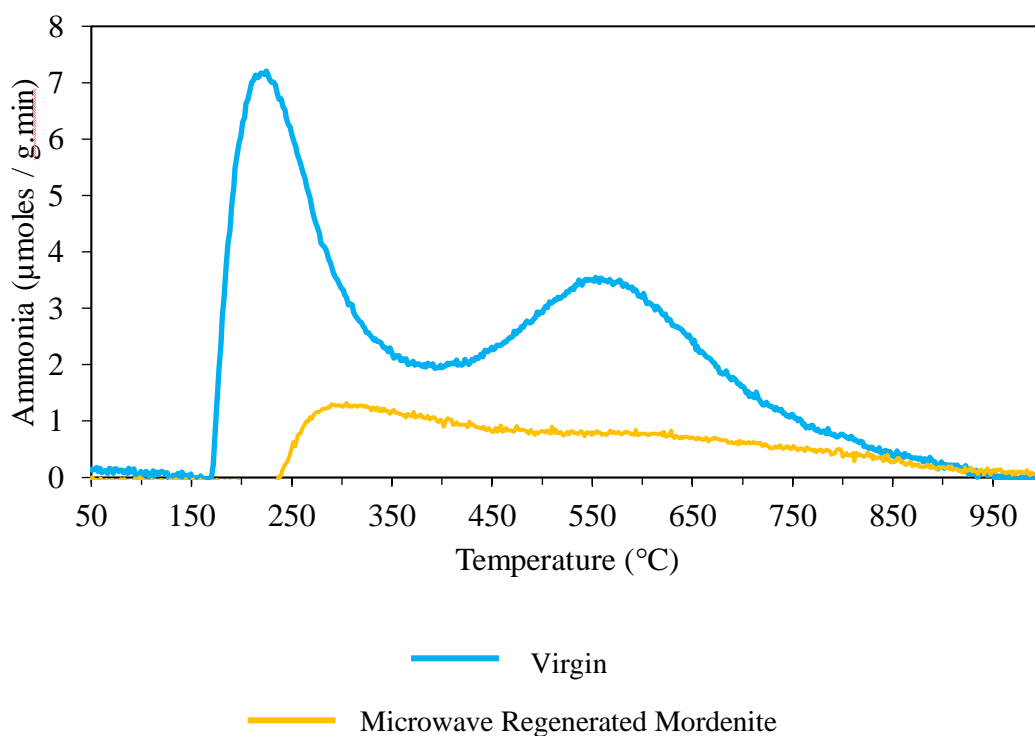
Figure 5.27. – NH₃ TPD Spectra of Virgin Catalyst Compared with Microwave Regenerated Catalyst

The NH$_3$ TPD data for a sample of microwave regenerated mordenite is given in Figure 5.27.. In contrast to the virgin sample, the microwave regenerated sample exhibits a single broadened peak at 300°C peak maximum ~ 1.25 µmoles g^{-1} min^{-1} which reduces to 0 µmoles g^{-1} min^{-1} at 950°C.
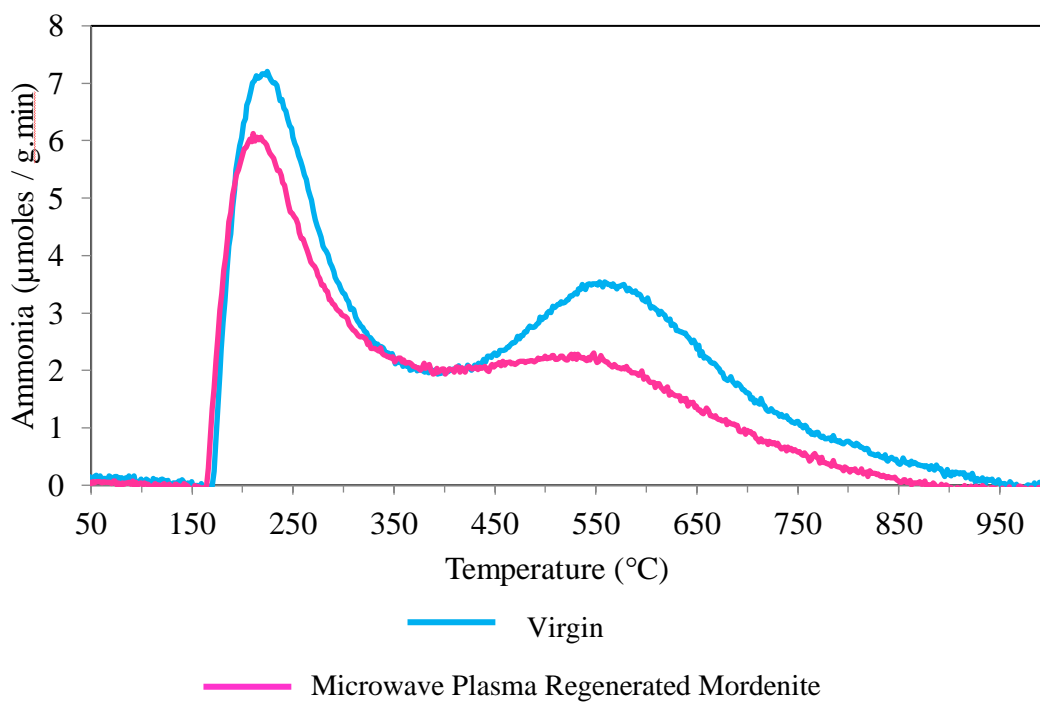
Figure 5.28. – NH₃ TPD Spectra of Virgin Catalyst Compared with Microwave Plasma Regenerated Catalyst

The NH$_3$ TPD for a sample of microwave plasma regenerated mordenite is given in Figure 5.28.. This sample is similar to the virgin and thermally regenerated samples, as it exhibits two peaks, however the position of these have shifted slightly, appearing at 215°C and 555°C. The intensity of these peaks is slightly lower than the virgin sample, with the 215°C peak displaying a concentration of 6 µmoles g^{-1}min^{-1} ammonia, and the 555°C displaying a concentration of 2 µmoles g^{-1}min^{-1} ammonia.

5.8. REFERENCES

(1) Angell CL. Raman Spectroscopic Investigation of Zeolites and Adsorbed Molecules. The Journal of Physical Chemistry 1973;77(2):222-227.

(2) Chua YT, Stair PC. An Ultraviolet Raman Spectroscopic Study of Coke Formation in Methanol to Hydrocarbons Conversion Over Zeolite H-MFI. Journal of Catalysis 2003(213):39-46.

(3) Russel PE, editor. Raman Spectroscopy of Zeolites: Characterization of Natural Zeolites with the Laser Raman Microprobe. Microbeam Analysis 1989: Proceedings of the 24th Annual Conference of the Microbeam Analysis Society; 16-21 July; San Francisco: San Francisco Press Inc.; 1989.

(4) Abdullah HA, Hauser A, Ali FA, Al-Adwani A. Optimal Conditions for Coke Extraction of Spent Catalyst by Accelerated Solvent Extraction Compared to Soxhlet. Energy and Fuels 2006;20:320-323.

(5) Holmes SM, Garforth M, B., Dwyer J. A Solvent Extraction Method to Study the Location and Concentration of Coke Formed on Zeolite Catalysts. Applied Catalysis A: General 1997;151:355-372.

(6) Magnoux P, Canaff C, Machado F, Guisnet M. Coking Aging and Regeneration of Zeolites XIII. Composition of the Carbonaceous Compounds Responsible for the Deactivation of USHY Zeolite during Toluene Disproportionation. Journal of Catalysis 1992;134:286-298.

(7) HafezKhiabani N, Fathi S, Shokri B, Hosseini SI. A Novel Method for Decoking of Pt–Sn/Al$_2$O$_3$ in the Naphtha Reforming Process Using RF and Pin-to-Plate DBD Plasma Systems. Applied Catalysis A: General 2015 3/5;493:8-16.

(8) Tsai T. Reactivation of Acidic Sites in Mordenite Used in Toluene Disproportionation. Applied Catalysis A: General 2006 2/24;301(2):292-298.

(9) D'Ippolito SA, Especel C, Epron F, Marécot P, Pieck CL. O$_2$ and O$_3$ Regeneration of PtReSn/Al$_2$O$_3$ and PtReGe/Al$_2$O$_3$ Naphtha Reforming Catalysts Prepared by Catalytic Reduction. Applied Catalysis A: General 2010 11/20;388(1–2):272-277.

(10) Lafuente B, Downs RT, Yang H, Stone N. Mordenite R061118. 2015; Available at: http://rruff.info/Mordenite/R061118. Accessed 02/28, 2019.

(11) Hays GR, van Erp WA, Alma NCM, Couperus PA, Huis R, Wilson AE. Solid-State Silicon NMR Studies of the Zeolite Mordenite and its Dealumination. Zeolites 1984;4(4):377-383.

(12) Hannus I, Fonseca A, Kiricsi I, Nagy JB, Fejes P. 29Si and 27Al MAS NMR Investigation of H-mordenite Dealuminated with Phosgene. Studies in Surface Science and Catalysis 1995;94:155-162.

(13) Huo H, Peng L, Gan Z, Grey CP. Solid-State MAS NMR Studies of Brønsted Acid Sites in Zeolite H-Mordenite. Journal of the American Chemical Society 2012;134(23):9708-9720.

(14) Hajjar R, Millot Y, Man PP, Che M, Dzwigaj S. Two Kinds of Framework Al Sites Studies in BEA Zeolite by X-ray Diffraction Fourier Transform Infrared Spectroscopy, NMR Techniques and V Probe. The Journal of Physical Chemistry C 2008;112(51):20167-20175.

(15) Li S, Zheng A, Yongchao S, Fang H, Shen W, Yu Z. Extra-Framework Aluminium Species in Hydrated Faujasite Zeolite as Investigated by Two-Dimensional Solid-State NMR Spectroscopy and Theoretical Calculations. Physical Chemistry Chemical Physics 2010;12(15):3895-3903.

(16) White JL, Beck LW, Haw JF. Characterisation of Hydrogen Bonding in Zeolites by Proton Solid-State NMR Spectroscopy. Journal of the American Chemical Society 1992;114(15):6182-6189.

(17) Hadjiivanov K. Identification and Characterisation of Surface Hydroxyl Groups by Infrared Spectroscopy. Advances in Catalysis 2014;57:99-318.

(18) Braeuer P, Ng PL, Situmorang O, Hitchcock I, D'agostino C. Effect of Al Content on Number and Location of Hydroxyl Acid Species in Zeolites: a DRIFTS Quantitative Protocol Without the Need for Molar Extinction Coefficients. RSC Advances 2017;7:52604-52613.

(19) Lonstad Bleken B, Mino L, Giordanino F, Beato P, Svelle S, Lillerud KP, et al. Probing the Surface of Nanosheet H-ZSM-5 with FTIR Spectroscopy. Physical Chemistry Chemical Physics 2013;15(32):13363-13370.

(20) Karge HG. Comparative Measurements on Acidity of Zeolites. In: Ohlmann G, Pfeifer H, Fricke R, editors. Catalysis and Adsorption by Zeolites. First ed. Amsterdam: Elsevier Science Publishers; 1991. p. 133-156.

CHAPTER 6: REGENERATION STUDIES II - DISCUSSION

6.1. SURFACE AREA AND AMOUNT OF COKE

Catalyst deactivation is by definition the loss of catalytic activity. In toluene disproportionation, deactivation can be produced via the deposition of carbonaceous material on the surface, in the channel intersections and cavities of the zeolite (1-3). Deposition of coke has been shown to result in a loss of surface area (4-7). This study confirms these findings as can be seen from the data in Table 5.2.. A virgin sample of mordenite exhibited a surface area of approximately 350 $m^2\,g^{-1}$, which reduced to 189 $m^2\,g^{-1}$ during the course of the reaction, with a deposition of approximately 4.5 % by weight of carbonaceous material. Both the thermal and microwave plasma regenerations resulted in almost complete restoration of the initial surface area, 352 and 333 $m^2\,g^{-1}$ respectively, with less than 0.5 % by weight of carbon remaining in the zeolite structure.

The microwave regenerated sample exhibits significantly different results. While the carbon appears to be removed effectively by the regeneration process, the surface area does not appear to be restored. The reason behind this can be seen from the X-ray diffraction data (Figures 5.13.-5.16.). While the other regeneration techniques do not appear to have any significant effect of the zeolite structure, the microwave regeneration shows significant loss of zeolite structure. This was seen despite attempts to select sample which visually appeared unaltered. The microwave regeneration is a harsh regeneration technique due to the significant thermal gradients that are established within the catalyst bed during the regeneration. Control of temperature is difficult, this is exacerbated by rapid exothermic loss of carbon and the loss of the high dielectric loss carbon means there are sudden changes in the dielectric properties of the sample, and hence the microwave power required to maintain controlled heating changes dramatically. This is coupled with the increase in the dielectric loss tangent as a function of temperature. The result of all these competing factors is a sample which is difficult to maintain at a constant temperature. The

excessive local temperatures generated in the sample lead to loss of structural integrity and hence loss of surface area.

Dielectric barrier discharge plasma did not appear to be an effective means of regenerating the sample under the test conditions employed. While the coke appeared to have been removed effectively from the exterior of the sample, sectioning the catalyst pellet showed the centre remained black due to ineffective removal of the carbon (Figure 6.1.). This manifested itself in that after regeneration 2.2 % by weight of carbon remained in the sample and had a surface area of 290 $m^2 g^{-1}$. The reason for this could be that at atmospheric pressure and using only 14 Watts of power the active radicals may not have been generated deep within the structure of the zeolite, resulting in only surface regeneration.

Figure 6.1. - Photo of Cross-Section of DBD Plasma Regenerated Catalysts

Figure 6.2. indicates there is a correlation between surface area and the amount of carbon deposition, with certain exceptions (shown by red circles). The first of those being the microwave regenerated sample where there is loss of zeolite structure. The second being samples where there are high amounts of carbon, virgin (4.55 % by weight) and DBD (4.49 % by weight). This may result from the carbon being present in sufficient quantities to form its own porous structure resulting in an unexpected increase in the observed surface area (189 and 186 $m^2 g^{-1}$ respectively).

However, perhaps the most interesting phenomenon is the rate of deactivation. The DBD plasma sample deactivates rapidly (0.5 % min^{-1}) (Figure 5.4.) which is as would be expected as the initial surface area is reduced (Table 5.2.) and hence consequently the number of active sites. However, the results of most interest are those produced from the microwave regenerated and microwave plasma regenerated samples. These catalysts deactivate much slower than might have been predicted. The following sections will discuss possible origins of this reduced rate of deactivation.
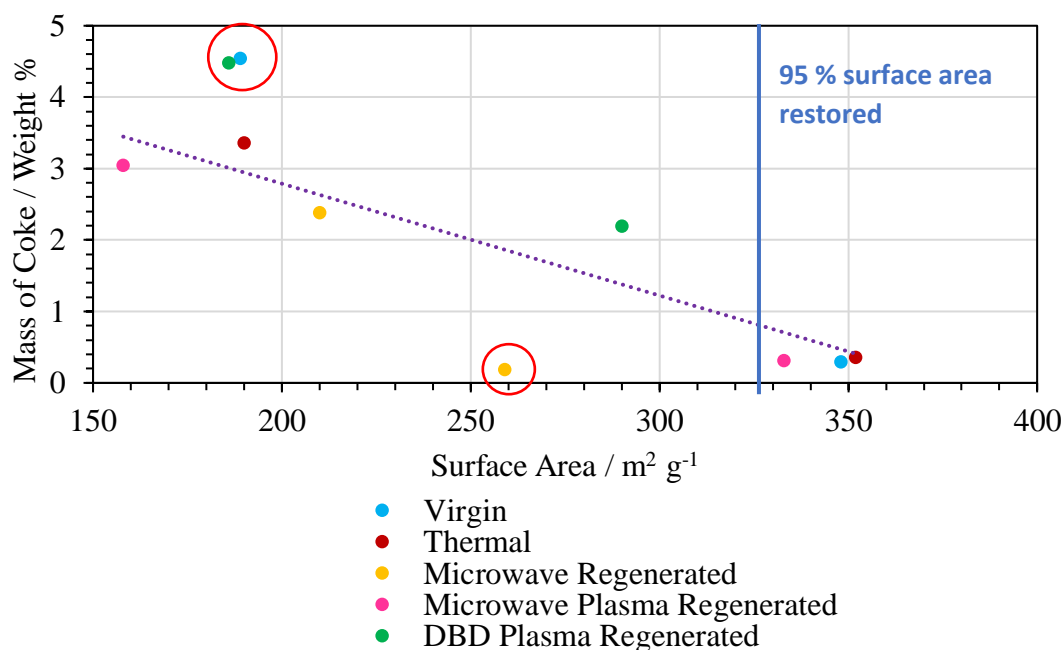
Figure 6.2. - Coke Present on Regenerated Samples as a Function of Surface Area

6.2. COKE COMPOSITION

Table 5.2. expressed the total amount of coke present on the regenerated catalysts pre- and post-deactivation. However, studies have shown coke deposited during toluene disproportionation to consist of various hydrocarbons (8), some readily soluble and others insoluble to common solvents such as DCM (9). Those readily soluble have often been identified, whereas the insoluble species are presumed to be bulkier aromatics (10). The solvent extraction studies of coke performed (as described in Section 5.4.2.) identify only the DCM soluble carbon present on the regenerated catalysts (Figure 5.10.). As would be expected, there is a difference between the total amount of coke and the amount of DCM soluble coke.

The microwave regenerated sample possessed almost no DCM soluble coke despite having a total amount of 2.39 % by weight of coke. This is probably due to sintering of the catalyst, seen by the significant loss of zeolite structure in the X-ray diffraction (Figure 5.14.) and surface area data (Table 5.2.). Coke deposition on the sintered catalyst is likely to be produced at the external surface, where the absence of shape selectivity allows for the formation of bulkier, insoluble coke species.

Whilst the virgin sample possessed the highest total amount of coke, this was not reflected in the amount of DCM soluble coke present. The highest concentration of DCM soluble coke was detected in the microwave plasma sample, closely followed by the DBD plasma sample. In contrast, minimal amounts of DCM soluble coke were seen in the virgin and thermally regenerated samples. The increase in soluble coke exhibited by the DBD and microwave plasma regenerated samples, may indicate a shift in the type of coke deposited. In the Raman studies (Figure 5.10.), the microwave plasma regenerated sample exhibited lower intensity D- and G- band peaks than the virgin and thermally regenerated samples, but an additional peak appeared in the 1900 cm^{-1} region. The origin of this additional band has not, to this author's knowledge, been previously identified, but the position of the peak would suggest it may be due to polyaromatic species and considering the solvent extraction data, this peak might be attributed to DCM soluble coke species.

The decrease in the intensity of the D- and G-bands for the microwave plasma regenerated sample, may explain the retention of crystalline character seen in the lower wavenumber region (Figure 5.9.). Although a reduced coking rate leads to less deactivation, and therefore less coverage of the crystalline structure (seen in the 1000-400 cm^{-1} region on the Raman spectrum), the difference in coke deposited on the virgin (4.55 weight %) and thermally regenerated (3.37 weight %) samples compared with the microwave plasma regenerated sample (3.05 weight %), does not account for the difference seen. If a 1.18 % by weight difference between virgin and thermally regenerated catalysts appears to have no effect on the intensity of the crystalline structural region of the Raman spectra, why would a 0.32 % by weight difference in coke deposited between the thermally and microwave plasma regenerated samples have such an effect as is seen? It is more likely, that some of the coke deposited on the microwave regenerated catalyst, possibly the species seen at 1900 cm^{-1} is non-deactivating or spectator coke. This would still be identified by TGA but would not have an effect on the rate of reaction, and therefore explains why some crystalline character is still seen on the Raman spectrum.

6.3. CATALYST ACIDITY

6.3.1. Magic Angle Spinning Solid State Nuclear Magnetic Resonance

The MAS ssNMR studies performed on the regenerated catalysts (Figures 5.17.-5.19.) display a shift in the amount of aluminium present compared with the virgin sample.

^{29}Si NMR

The three peaks displayed on the ^{29}Si NMR represent the silicon environments containing 2 (-100 ppm), 1 (-106 ppm), and 0 (-113 ppm) bound aluminium atoms [11]. Whilst there appears to be little to no change in the number of $Si(OSi)_2(OAl)_2$ species, there is a difference in both the number of $Si(OSi)_3(OAl)$ and $Si(OSi)_4$ environments. The -106 ppm peak is recognised to be highly sensitive to aluminium and changes of its intensity are often correlated to the amount of dealumination occurring [11]. Therefore, the decrease of intensity for $Si(OSi)_3(OAl)$ species exhibited in the regenerated samples indicates dealumination has taken place, and occurs more prominently in the microwave plasma regenerated sample. This is supported by the XPS results (Table 5.3.), which show a decrease in aluminium for the regenerated catalysts, with more aluminium lost from the microwave plasma regenerated sample.

^{27}Al NMR

The ^{27}Al MAS ssNMR data (Figure 5.18.) exhibits two peaks arising from framework (54 ppm) and extra-framework (0 ppm) aluminium [12]. There is a significant decrease in framework aluminium seen in the microwave plasma regenerated catalyst, and to a lesser extent, in the thermally regenerated catalyst. During dealumination, tetrahedral aluminium is removed and a proportion of it is known to be deposited in the pores as octahedral extra-framework species [13]. Therefore, it is surprising to see less EFAl in the microwave plasma and thermally regenerated samples than present in the virgin, raising the question of its location. Upon careful consideration of the ^{27}Al ssNMR spectra, a perceptible increase of intensity can be seen at ~30 ppm in the regenerated samples. Although this does not exhibit a peak-like structure, EFAl has been reported to develop here under conditions such as steaming [14,15]. Whilst EFAl at 0 ppm is attributed to

octahedral species (14,16,17), there are conflicting reports of the type of EFAl located at 30 ppm (14,17,18). These differences aside, EFAl is recognised as the source of Lewis acidity (19), and with the limited understanding of its impact in acid-catalysed reactions (Section 2.1.4.) it may be overlooked. Instead, focus is often given to the reduction of framework aluminium and changes in activity are therefore linked to the reduction of Brønsted acid sites. However, consideration of the impact the regeneration process has had on the concentration of both Brønsted and Lewis acid sites in this research, will be looked at in more depth when discussing the infrared spectroscopy data.

^{1}H NMR

The ^{1}H MAS ssNMR data (Figure 5.19.) exhibits a decrease in Brønsted acid sites for the regenerated catalysts, shown as a reduction of the 4.0 ppm peak (20). This is more pronounced in the microwave plasma regenerated sample. The peaks attributed to EFAl species (2.6 and 0.0 ppm) (17), might therefore be expected to increase in intensity, corresponding to the amount of dealumination occurring. However, this only occurs for the peak at 2.6 ppm, with the regenerated catalysts exhibiting a less intense peak at 0.0 ppm than virgin. This result may support the absence of EFAl seen in the [27]Al data at 0 ppm, whilst the ^{1}H peak at 2.6 ppm may correspond to the EFAl suggested at ~30 ppm in the [27]Al data. This would appear to confirm the expected increase in EFAl species; however, the nature of these species remains to be agreed upon (14,15,18).

6.3.2. Infrared Spectroscopy

The infrared spectroscopy data for both pyridine and collidine studies (Figures 5.20.-5.25.) provided an insight to the concentration of BAS and LAS present in the different regenerated catalysts. A preliminary inspection of the OH-stretching region (4000-3500 cm^{-1}) can identify which of the acid sites are available to the probe molecule, before quantification of the concentration of acid sites is performed using the 1700-1400 cm^{-1} region where the pyridinium and collidinium ions appear.

OH Region

In the OH-stretching frequency region (4000-3500 cm^{-1}), the IR spectra of the samples (Figures 5.20.-5.24.), exhibited four peaks prior to the adsorption of the probe molecule. The peaks at ~3742 cm^{-1} and ~3655 cm^{-1} are readily identified as Si-OH and Al-OH groups respectively, and the ~3606 cm^{-1} peak corresponds to acidic Al-OH-Si groups (21). The ~3775 cm^{-1} peak is attributed to the γ-Al$_2$O$_3$ in the binder (21). Interactions of the probe molecule with the zeolite acid sites reduces the peak intensities. The extent of such interaction across the regenerated samples can be seen in the subtraction result (Figures 5.21. and 5.24.). There appears to be a stronger interaction between the probe molecules and the acidic Al-OH-Si groups (3600 cm^{-1}) of the virgin and thermally regenerated samples compared to the microwave and microwave plasma regenerated samples. This may be indicative of the presence of more Brønsted acid sites in the virgin and thermally regenerated samples.

Acid Site Concentration

The 1700-1400 cm^{-1} region of the IR spectra using pyridine as the probe molecule (Figure 5.22.) exhibited five peaks. The peaks appearing at 1633 cm^{-1} and 1544 cm^{-1} correspond to the pyridinium ion (PyH$^+$) and the peaks appearing at 1620 cm^{-1} and 1453 cm^{-1} correspond to pyridine co-ordinated to Lewis acid sites. The peak exhibited at 1489 cm^{-1} is a result of interactions between both PyH$^+$ and LAS. To calculate BAS and LAS concentration, the 1544 cm^{-1} and 1453 cm^{-1} peaks are used (as described in Section 4.2.6.). The results are given in Table 5.4..

The 1700-1400 cm^{-1} region of the IR spectra using collidine as the probe molecule (Figure 5.25.) exhibited a peak at 1636 cm^{-1}. This peak is attributed to the collidinium ion (CollH$^+$) (22) and is used to calculate the concentration of Brønsted acid sites (as described in Section 4.2.6). The results are given in Table 5.4..

The results (Table 5.4.) display more BAS in the virgin and thermally regenerated samples, as suggested previously from the IR spectra in the OH-stretching frequency (Figures 5.21. and 5.24.). Furthermore, it distinguishes between the samples, showing the virgin sample to have the

highest number of BAS (0.5 µmol m^{-2} g^{-1}) and the microwave regenerated sample to have the least (0.32 µmol m^{-2} g^{-1}). Interestingly, the order of decreasing BAS correlates to the rate of deactivation, and amount of coke deposited, where a higher concentration of BAS present in the zeolite, leads to a higher concentration of coke deposited and hence a faster rate of deactivation (Table 6.1.). The single exception to this is the thermally regenerated sample, where the rate of deactivation has not been effected, however when referring back to the activity profile (Figure 5.1.), a decrease in the initial activity can be seen, which can be attributed to the slight decrease in BAS present in the sample.

Table 6.1. - Summary Table of BAS, Rate of Deactivation and Amount of Coke

	BAS$_{py}$ / µmol m^{-2} g^{-1}	Rate of Deactivation / % min^{-1}	Coke Present (Coked) / Weight %
Virgin	0.5	0.30	4.55
Thermally Regenerated	0.42	0.30	3.37
Microwave Plasma Regenerated	0.37	0.085	3.05
Microwave Regenerated	0.32	0.088	2.39

Additionally, the pyridine results (Table 5.4.) provide the concentration of LAS present in the regenerated catalysts. Whilst the concentration of BAS has decreased upon regeneration, the number of LAS has remained relatively similar to the virgin sample (0.45 µmol m^{-2} g^{-1}). Although, the microwave plasma regenerated sample (0.50 µmol m^{-2} g^{-1}) may be considered to have a slight increased concentration of LAS compared with the virgin sample, suggesting the formation of EFAl (23).

The collidine data should provide only the number of surface BAS (24), which for a porous zeolite, should only form a proportion of the catalytic active sites. Whereas the more mobile pyridine would be expected to access all the BAS (24).

Considering the previous two statements:

$$BAS_{Total} - BAS_{external} = BAS_{internal}$$

If
$$BAS_{Total} = BAS_{py}$$

And
$$BAS_{external} = BAS_{coll}$$

$$BAS_{internal} = BAS_{py} - BAS_{coll}$$

Where:　　　　BAS_{py}　　　　is the concentration of BAS determined using pyridine

as the probe molecule

BAS_{coll}　　　　is the concentration of BAS determined using collidine

as the probe molecule

Table 6.2. - Concentration of Internal and External BAS

	BAS_{Total} / μmol m^{-2} g^{-1}	$BAS_{external}$ / μmol m^{-2} g^{-1}	$BAS_{internal}$ / μmol m^{-2} g^{-1}
Virgin	0.50	0.24	0.26
Thermal	0.42	0.18	0.24
Microwave Regenerated	0.32	0.15	0.17
Microwave Plasma Regenerated	0.37	0.13	0.24

From the Table 6.2., it can be suggested the dealumination caused by the regeneration process was surface specific, with the exception of the microwave regenerated sample. The reason for this exception is most likely due to the harsh nature of the regeneration process, seen from the loss of crystal structure by XRD (Figure 5.14.) and surface area data (Table 5.2.). Reasons for the surface specificity of the thermal and microwave plasma regeneration processes may lie in the amount of energy used and/or its penetration depth. Whilst both regeneration methods appeared to have sufficient energy to oxidise the carbonaceous deposits, there was not ample energy to remove the aluminium from the bulk of the catalyst. In the case of the microwave plasma regeneration process

where the plasma may penetrate the catalyst (25), the presence of coke may have affected the exposure of the zeolite to the plasma energy. This is something which will be discussed in further detail in the forthcoming chapters regarding pre-treatment.

6.3.3. Ammonia Temperature Programmed Desorption

The ammonia TPD results (Figures 5.26.-5.28.) of the regenerated catalysts give an insight into possible changes of acid site strength due to the regeneration process. The virgin, thermal and microwave plasma samples exhibited two peaks, one at a lower temperature (215-225°C) and one at a higher temperature (555-560°C), corresponding to l- (lower temperature) and h- (higher temperature) peaks (26). Whilst the h-peak is attributed to directly adsorbed ammonia on the zeolite, the l-peak is attributed to weakly adsorbed NH_4^+ species and is therefore not quantifiable (26). However, from the h-peak, it can be seen that there is a similar strength of acid sites between virgin and thermally regenerated mordenite samples (Figure 5.26.). In contrast, there is a decrease and slight shift in the h-peak of the microwave plasma sample when compared with the virgin sample (Figure 5.28.). This is indicative of a reduction of acid site strength, as weaker bound ammonia will desorb at lower temperatures (27). The decrease in peak area supports the reduction of BAS concentration in the microwave regeneration seen from the IR data (Figure 6.2.). The surface specificity seen by the IR explains why, although there is a shift in desorption temperature and peak height, only minor changes to acid strength have been seen. From this, it might be presumed that the internal acid site strength of the microwave plasma regenerated sample has not changed.

The microwave regenerated sample (Figure 5.27.) expresses a different profile from the other samples as upon initial observation there is only one peak identifiable. However, due to the desorption temperature of the peak, it is more than likely that the h-peak has overlapped with the l-peak. Whilst this makes it extremely difficult to differentiate between the two peaks, the overlapping of the peaks heavily indicates that there is a considerable reduction in acid site strength. When considering the heavy reduction of acid site concentration seen from the IR data

(Table 5.4. and 6.2.), this further supports that the regeneration process has destroyed the acidity of the catalyst.

6.3.4. Summary

Overall, the acidity data suggested the regeneration process had resulted in dealumination of the catalyst samples. The MAS ssNMR data of the regenerated catalysts (Figures 5.17.-5.19.) exhibited a decrease in framework aluminium, and the formation of EFAl species, consistent with dealumination. The XPS results (Table 5.3.) supported this, showing a decrease in aluminium for the regenerated catalysts with more aluminium lost from the microwave plasma regenerated sample, as was seen in the NMR data. The infrared data (Table 5.4.) exhibited a higher concentration of BAS for the virgin sample, which decreased in accordance with the amount of dealumination seen in the NMR and XPS data, i.e. virgin > thermal > microwave plasma. With that said, there was no significant difference in the concentration of LAS. If the slight increase in LAS concentration for the microwave plasma regenerated sample was to be considered significant, it only further supports the presence of EFAl and thus dealumination. The regeneration processes were found to be surface specific, with no significant change in the concentration of internal BAS, with the exception of the microwave regenerated catalyst. This decrease was attributed to the harsh conditions of the regeneration process, resulting in the destruction of the crystal structure. The concentration of external BAS was consistent with the NMR and XPS data, where virgin > thermal > microwave plasma. Finally, the strength of the acid sites seen by NH_3 TPD, demonstrated that whilst the thermally regenerated sample remained similar to virgin, the microwave and microwave plasma regenerated catalysts exhibited changes in acid site strength. The surface specificity of the microwave plasma regeneration process seen by the XPS and IR data indicates the slight shift in the acid site strength exhibited by the NH_3 TPD, may also be surface specific. In contrast, the penetrating destruction microwave regeneration process, was seen by NH_3 TPD to significantly weaken the acid site strength of any acid sites remaining.

6.4. CATALYST ACTIVITY

6.4.1. Thermal Regeneration

The activity of the thermally regenerated catalyst (Figure 5.1.) was similar in profile and deactivation rate to the virgin sample. This was expected, as the method was a replication of the regeneration process typically used within industry (8), although on a much smaller scale. The thermal regeneration process undertaken in this research was shown to restore the surface area lost upon coking (Table 5.2.) with no loss to catalytic structure (Figure 5.13.). Raman and solvent extraction data (Figures 5.10. and Figure 5.12. respectively) indicated no change in coke composition compared with the virgin sample and the TGA results (Table 5.2.) confirmed the majority of the coke had been successfully removed, albeit some residual carbon may have remained. This residual coke may have contributed to the minor loss of initial activity seen in the thermally regenerated activity profile (Figure 5.1.).

As the NH_3 TPD results (Figure 5.26.) exhibited no change in acid site strength, the decrease of initial B/X (Table 5.1) is most likely explained as a result of the reduction of BAS (Table 5.4.), as fewer acid sites are available for cracking. This would also give rise to the slightly lower coking rate exhibited by the TGA results (Table 5.2.), as cracking is a major contributor to coking (28). The regeneration process probably produced the decrease of BAS, as the thermal treatment is known to suffer from hot spots which lead to dealumination of the catalyst (8,29). The NMR results demonstrated a shift in the type of aluminium present, with the loss of framework aluminium seen (Figures 5.17.-5.19.) and the formation of EFAl species identified in the ^{1}H NMR (Figure 5.19), consistent with dealumination. The ^{1}H NMR also exhibited a decrease of intensity for the 4.0 ppm peak attributed to BAS (20). The XPS data (Table 5.3.) supported the NMR results, exhibiting a decrease in aluminium and corresponding increase in silicon, for the thermally regenerated sample compared with the virgin sample. As XPS is surface specific, the results indicated the dealumination occurred on the catalyst surface. This, in conjunction with the combination of pyridine and collidine infrared results (Table 6.2.), demonstrates the reduction of BAS to be surface specific.

Given the reduction of Brønsted acidity in the thermally regenerated catalyst is surface specific, a shift in individual xylene selectivity might be expected. As *p*-xylene is predominantly formed during TDP before being rapidly isomerised to *m*- and *o*-xylene on the surface (30,31), less BAS on the surface should lead to an increase in *p*-xylene selectivity. However, as shown by Figure 5.6., this is not the case. A possible explanation for this is, whilst the concentration of BAS has decreased, there remain BAS on the surface of the catalyst available for isomerisation. Furthermore, the absence of change in coke composition seen by the Raman and solvent extraction results (Figures 5.10. and 5.12. respectively), and only minor decrease in coking rate (Table 5.2.), would suggest the remaining strength of the acid sites has not changed, and would therefore be strong enough to isomerise the xylenes. The NH_3 TPD results (Figure 5.26.) confirm this.

6.4.2. DBD Plasma Regeneration

The activity of the DBD plasma regenerated catalyst (Figure 5.4.) was similar in profile but with a much faster deactivation rate compared to the virgin sample. The rapid deactivation rate was not unexpected, as although during a preliminary inspection of the sample it appeared white, the regeneration process had not fully restored the surface area of the catalyst (Table 5.2.), and remaining coke had been measured by TGA (Table 5.2.). Furthermore, a cross-section of the sample had shown there to be internal coke (Figure 6.1.). As the majority of remaining coke appeared to be on the internal surface, initially the reaction proceeded the same as the virgin sample. There was a minor loss of initial activity, but this was also seen in the thermally regenerated sample and can be attributed to residual coke on the external surface. However, as coke formation is known to proceed via a nucleation-pathway (32), the presence of coke on the internal surface of the catalyst exacerbated the coking rate compared to the virgin and thermally regenerated samples, producing the rapid deactivation seen (Figure 5.4.). The shape of the activity profile was unlikely to differ from the virgin and thermally regenerated samples, as the XRD results (Figure 5.16.) demonstrated the regeneration process had not damaged the crystal structure.

With coke deposited on the internal surface of the catalyst, a shift in xylene selectivity may be expected. As the surface is known to be where *p*-xylene rapidly isomerises into *m*- and *o*-xylene (30), a catalyst with a coked surface would be expected to produce an increased amount of *p*-xylene, as seen in Figure 5.8.. Initially the rate of *p*-xylene is approximately at thermodynamic equilibrium, as the external surface appeared to be uncoked and is available for isomerisation. However, as this rapidly becomes coked, the concentration of *p*-xylene increases.

6.4.3. Microwave Regeneration

In contrast to the thermally and DBD plasma regenerated catalysts, the activity of the microwave regenerated sample (Figure 5.2.) greatly differed in both profile and deactivation rate compared to the virgin sample. The deactivation rate for the microwave regenerated sample was approximately 3.5 times slower than the virgin sample. This is reflected in the amount of coke deposited seen in the TGA data (Table 5.2.). Unlike the virgin, thermally and DBD plasma regenerated catalysts, the microwave regenerated sample deactivated gradually. This is probably caused by the harsh nature of the regeneration process. Whereas the removal of coke during the other regeneration methods had restored surface area, in the microwave regeneration a significant proportion of surface area was lost. This was despite the TGA data determining the success of the method in removing all the coke (Table 5.2.), hence why initial activity was the same as the virgin sample. The other regeneration processes appeared to leave the crystal structure intact, however, the XRD corresponding to the microwave regenerated sample (Figure 5.14.) exhibited a significant loss of crystalline character. Furthermore, and what was most likely the direct cause of the gradual deactivation and reduced deactivation rate, the microwave regeneration process destroyed a significant proportion of the BAS, and the remaining acidity was shown to be significantly weaker. Unlike the thermal and microwave plasma regeneration methods which appeared to be surface specific, the microwave regeneration process included the destruction of both internal and external BAS, determined by the infrared data (Table 6.2.). Furthermore, the NH$_3$ TPD results displayed an overlapping of the l- and h-peaks indicative of a significant loss of

acid site strength for the remaining acid sites. Without acid sites, cracking and therefore coking will not occur.

In accordance with the considerable loss of Brønsted acidity, the initial B/X of the microwave regenerated sample was correspondingly lower than the virgin sample, as can be seen in Figure 6.3.. Additionally, the lack of DCM soluble coke present on the coked microwave regenerated sample, determined by solvent extraction is likely to be due to the change of acid site strength, exhibited by the NH_3 TPD results (Figure 5.27.).

Figure 6.3.- Summary of B/X and Total BAS for Virgin and Microwave Regenerated Catalysts

	B/X at t=0	% Difference	BAS_{Total} / $\mu mol\ m^{-2}\ g^{-1}$	% Difference
Virgin	0.57		0.5	
		37		36
Microwave Regenerated	0.36		0.32	

In terms of individual xylene selectivity, as there is less coke deposited on the microwave regenerated catalyst, no preference of any individual isomer would be expected, which is the case. However, the absence of selectivity could also be attributed to the loss of some pore structure, as *p*-xylene is known to rapidly diffuse out of the zeolite channels at a rate 1000 times faster than the other isomers due to steric effects (30). With the destruction of some of the crystal structure, seen by the XRD (Figure 5.14.) and supported by the loss of surface area upon regeneration (Table 5.2.), the steric constraints may be significantly reduced, and would therefore increase the rate of diffusion for the *m-* and *o-* xylene isomers.

6.4.4. Microwave Plasma Regeneration

In comparison to the virgin and other regeneration methods, the activity of the microwave plasma regenerated sample (Figure 5.3.) is very similar in both profile and deactivation rate to the microwave regenerated sample. The deactivation rate for the microwave plasma regenerated sample was also approximately 3.5 times slower than the virgin sample, which was reflected in the amount of coke deposited seen in the TGA data (Table 5.2.). Unlike the virgin sample, but as

was the case with the microwave regenerated catalyst, the microwave plasma regenerated sample deactivated gradually. However, whilst this is probably caused by the regeneration method, it was not as destructive as the microwave regeneration process.

Similar to the thermal and DBD regeneration processes, the removal of coke during the microwave plasma regeneration process resulted in the restoration of the surface area (Table 5.2.), with no loss to catalytic structure (Figure 5.15.). In contrast to the thermal regeneration process however, the Raman and solvent extraction data (Figures 5.10. and 5.12. respectively), indicated a change in the coke composition. There were lower amounts of D- and G-band carbon for the microwave plasma regenerated catalyst compared with the virgin sample, and the presence of an additional peak at ~1900 cm^{-1} (Figure 5.10.). The identity of this peak was suggested to be the formation of a DCM soluble, less-deactivating or spectator coke, which would explain the gradual deactivation and slower deactivation rate seen for this regeneration process. The cause of this change in coke formation is most likely linked to the change in catalyst acidity, with the NH_3 TPD data (Figure 5.28.) indicating a slight change in acid site strength.

The NMR (Figures 5.17.-5.19.) and XPS (Table 5.3.) results were strongly indicative of dealumination having had occurred. Although this was seen in the thermally regenerated catalyst, the loss of framework aluminium and formation of EFAl was much more prominent in the microwave plasma regenerated sample, as was the decrease in aluminium seen in the XPS data (Table 5.3.). The surface specific XPS indicated dealumination on the catalyst surface, which was confirmed by the combination of pyridine and collidine infrared results (Table 6.2.), which expressed a reduction of external BAS, whilst the concentration of internal BAS remained the same. Compared with the virgin sample, the decrease in external BAS was almost half. A combination of the reduction of external BAS (Table 6.2.) and the partial shift in remaining acid site strength (Figure 5.28.) also had a significant impact on the initial B/X (Table 5.1.), with fewer acid sites available or strong enough for cracking, reducing the coking rate seen by the TGA results (Table 5.2.).

Additionally, with less coke laydown, individual xylene isomerisation would not be expected as the surface is available to isomerise *p*-xylene to *m*- and *o*-xylene, which is what is seen (Figure 5.7.). Yet, the lack of selectivity may also arise from a reduction of coke in the channels and cavities, reducing the steric effects and thus increasing the rate of diffusion for the *m*- and *o*-xylene isomers.

6.5. SUMMARY

The regeneration studies found that by regenerating coked mordenite using microwave heating, DBD plasma or microwave plasma, this could affect the coking rate when the catalyst was used in toluene disproportionation. Whilst the different regeneration methods had varying levels of success in removing carbonaceous deposits, the microwave and microwave plasma regeneration methods were also shown to affect the concentration of BAS via dealumination. This was also shown to have an effect on the strength of the remaining acid sites. In reducing the concentration and strength of external BAS, a reduced rate of cracking can be achieved, which leads to a reduction in the coking rate of regenerated mordenite in toluene disproportionation. This is beneficial as it extends the catalytic life of the zeolite, and toluene disproportionation is more favourable than cracking, however the drawback is that the lack of coke also removes *p*-xylene selectivity of the reaction.

6.6. REFERENCES

(1) Bhatia S, Beltramini J, Do DD. Deactivation of Zeolite Catalysts. Catalysis Reviews: Science and Engineering 2008;31(4):431-480.

(2) Bibby D, Milestone NB, Patterson JE, Aldridge LP. Coke Formation in Zeolite ZSM-5. Journal of Catalysis 1986;97:493-502.

(3) Tsai TC, Chen WH, Lai CS, Liu SB, Wang I, Ku CS. Kinetics of Toluene Disproportionation over Fresh and Coked H-Mordenite. Catalysis Today 2004 NOV 3 2004;97(4):297-302.

(4) Querini CA. Chapter 4 - Coke Characterization - 13 - Sorption Capacity: Surface Area and Pore Volume. In: Spivey JJ, Roberts GW, editors. Catalysis. First ed. United Kingdom: RSC; 2004. p. 197-199.

(5) Soni HS, Samuel V, Ramaswarmy AV. Locartion of Coke in ZSM-5 and HY Zeolite Catalysts used in Ethylation Reaction from Micropore Size Distribution Analysis. Indian Journal of Chemistry 1994;33:844-846.

(6) Gao Y, Zheng B, Wu G, Ma F, Lui C. Effect of the Si/Al Ratio on the Performance of Hierarachical ZSM-5 Zeolites for Methanol Aromatization. RSC Advances 2016;6(87):83581-83588.

(7) Chua LM, Hitchcock I, Fletcher RS, Holt EM, Lowe J, Rigby SP. Understanding the Spatial Distribution of Coke Deposition Within Bimodal Micro-/Mesoporous Catalysts Using a Novel Sorption Method in Combination with Pulsed-Gradient Spin-Echo NMR. Journal of Catalysis 2012;286:260-265.

(8) Tsai T. Reactivation of Acidic Sites in Mordenite used in Toluene Disproportionation. Applied Catalysis A: General 2006 2/24;301(2):292-298.

(9) Holmes SM, Garforth M, B., Dwyer J. A Solvent Extraction Method to Study the Location and Concentration of Coke Formed on Zeolite Catalysts. Applied Catalysis A: General 1997;151:355-372.

(10) Magnoux P, Canaff C, Machado F, Guisnet M. Coking Aging and Regeneration of Zeolites XIII. Composition of the Carbonaceous Compounds Responsible for the Deactivation of USHY Zeolite during Toluene Disproportionation. Journal of Catalysis 1992;134:286-298.

(11) Hays GR, van Erp WA, Alma NCM, Couperus PA, Huis R, Wilson AE. Solid-State Silicon NMR Studies of the Zeolite Mordenite and its Dealumination. Zeolites 1984;4(4):377-383.

(12) Hannus I, Fonseca A, Kiricsi I, Nagy JB, Fejes P. 29Si and 27Al MAS NMR Investigation of H-mordenite Dealuminated with Phosgene. Studies in Surface Science and Catalysis 1995;94:155-162.

(13) Debras G, Nagy JB, Gabelica Z, Bodart P, Jacobs PA. Determination of Silicon-Aluminium Orderings in Mordenite and its Aluminium Deficient Forms Using High-Resolution Magic-Angle-Spinning 29Si-NMR. Chemistry Letters 1983;12(2):199-202.

(14) Miller JT, Hopkins PD, Meyers BL, Ray GJ, Roginski RT, Zajac GW, et al. The Effect of Nonfamework Aluminium on Acidity in Dealuminated Mordenite. Journal of Catalysis 1992;138(1):115-128.

(15) Feng D, Yong Y, Chaohui Y. "NMR Invisible" Aluminium Species in Dealuminated Mordenite Zeolite: a ^{1}H/^{27}Al TRAPDOR NMR Study. Science in China: B 1998;41(2):149-155.

(16) Fyfe CA, Gobbi GC, Hartman JS. Solid-State Magic-Angle Spinning Aluminium-27 Nuclear Magnetic Resonance Studies of Zeolites Using a 400-MHz High-Resolution Spectrometer. Journal of Physical Chemistry 1982;86:1247-1250.

(17) Li S, Zheng A, Yongchao S, Fang H, Shen W, Yu Z. Extra-Framework Aluminium Species in Hydrated Faujasite Zeolite as Investigated by Two-Dimensional Solid-State NMR Spectroscopy and Theoretical Calculations. Physical Chemistry Chemical Physics 2010;12(15):3895-3903.

(18) Corma A, Fornes V, Martinez A, Sanz J. Tetrahedral and Octahedral Extraframework Aluminium in Ultrastable Y Zeolites - Implications in the Cracking of Gas Oil. Fluid Catalytic Cracking 1988;375:17-33.

(19) Wu P, Komatsu T, Yashima T. Acidic and Catalytic Properties of Aluminated Mordenite Zeolite: Effect of Extraframework Aluminium. Journal of the Chemical Society Faraday Transactions 1996;92:861-870.

(20) Huo H, Peng L, Gan Z, Grey CP. Solid-State MAS NMR Studies of Bronsted Acid Sites in Zeolite H-Mordenite. Journal of the American Chemical Society 2012;134(23):9708-9720.

(21) Hadjiivanov K. Identification and Characterisation of Surface Hydroxyl Groups by Infrared Spectroscopy. Advances in Catalysis 2014;57:99-318.

(22) Lonstad Bleken B, Mino L, Giordanino F, Beato P, Svelle S, Lillerud KP, et al. Probing the Surface of Nanosheet H-ZSM-5 with FTIR Spectroscopy. Physical Chemistry Chemical Physics 2013;15(32):13363-13370.

(23) Maier SM, Jentys A, Lercher JA. Steaming of Zeolite BEA and Its Effect on Acidity: A Comparative NMR and IR Spectroscopic Study. The Journal of Physical Chemistry C 2011;115(16):8005-8013.

(24) Holm MS, Svelle S, Joensen F, Beato P, Christensen CH, Bordiga S, et al. Assessing the Acid Properties of Desilicated ZSM-5 by FTIR using CO and 2,4,6-Trimethylpyridine (Collidine) as Molecular Probes. Applied Catalysis A: General 2009;356(1):23-30.

(25) Jia LY, Pinard L, Hedan S, Comparot J, Dufour A, Tayeb KB, et al. New Routes for Complete Regeneration of Coked Zeolite. Applied Catalysis B: Environmental 2017;219:82-91.

(26) Niwa M, Katada N, Okumura K. Solid Acidity of Zeolites. In: Hull R, Jagadish C, Osgood RM, Jr., Parisi J, Wang Z, Warlimont H, editors. Characterisation and Deisgn of Zeolite Catalysts. First ed. Heidelberg: Springer; 2010. p. 9-28.

(27) Karge HG. Comparative Measurements on Acidity of Zeolites. In: Ohlmann G, Pfeifer H, Fricke R, editors. Catalysis and Adsorption by Zeolites. First ed. Amsterdam: Elsevier Science Publishers; 1991. p. 133-156.

(28) Wu J, Leu L. Toluene Disproportionation and Transalkylation Reaction Over Mordenite Zeolite Catalysts. Applied Catalysis 1983;7:283-294.

(29) D'Ippolito SA, Especel C, Epron F, Marécot P, Pieck CL. O_2 and O_3 Regeneration of PtReSn/Al_2O_3 and PtReGe/Al_2O_3 Naphtha Reforming Catalysts Prepared by Catalytic Reduction. Applied Catalysis A: General 2010 11/20;388(1–2):272-277.

(30) Tsai T, Liu S, Wang I. Disproportionation and Transalkylation of Alkylbenzenes over Zeolite Catalysts. Applied Catalysis A: General 1999 5/17;181(2):355-398.

(31) Olson DH, Haag WO. Structure-Selectivity Relationship in Xylene Isomerisation and Selective Toluene Disproportionation. In: Whyte TEJ, Betta RAD, Derouane EG, Baker RTK, editors. Catalytic Materials: Relationship Between Structure and Reactivity United States of America: American Chemical Society; 1984. p. 275-307.

(32) Guisnet M, Magnoux P, Martin D. Roles of Acidity and Pore Structure in the Deactivation of Zeolites by Carbonaceous Deposits. In: Bartholomew CH, Fuentes GA, editors. Catalyst Deactivation: Elsevier; 1997. p. 1-19.

CHAPTER 7: PRE-TREATMENT STUDIES I - RESULTS

7.1. INTRODUCTION

Following the novel regeneration studies of microwave heating, microwave plasma and DBD Plasma on deactivated mordenite, the same procedure was performed on virgin mordenite to evaluate the efficacy of these technologies as novel pre-treatment processes. As in the regeneration studies, toluene disproportionation was utilised as the probe reaction.

7.2. CATALYST TESTING

7.2.1. Toluene Conversion as a Function of Time

Virgin mordenite was pre-treated (as described in Section 4.1.3.) before the materials were subjected to toluene disproportionation. The activity represented as toluene conversion as a function of time has been plotted in Figures 7.1.-7.3.. The data for each pre-treatment has been plotted alongside virgin mordenite in order to assist in the visualisation of any differences which may have resulted.

As can be seen in Figure 7.1., the initial toluene conversion over the virgin catalyst was 60 %, which decreased over time. After 450 minutes, catalytic activity had dropped to a 10 % conversion and remained in a *pseudo*-steady state with activity only reducing a further 4 % after an additional 500 minutes. Rapid deactivation occurred between 180 minutes and 325 minutes at a rate of 0.30 % min^{-1}.

The activity data for a sample of mordenite which had undergone microwave pre-treatment is also shown in Figure 7.1.. The deactivation profile was significantly different from the virgin sample, where, in terms of toluene conversion, the sample did not undergo a rapid deactivation, but instead the profile displays a much more gradual deactivation with a rate of 0.087 % min^{-1}, over the measured period (77-458 mins). Initial toluene conversion was slightly reduced (56 %) compared with the virgin sample.
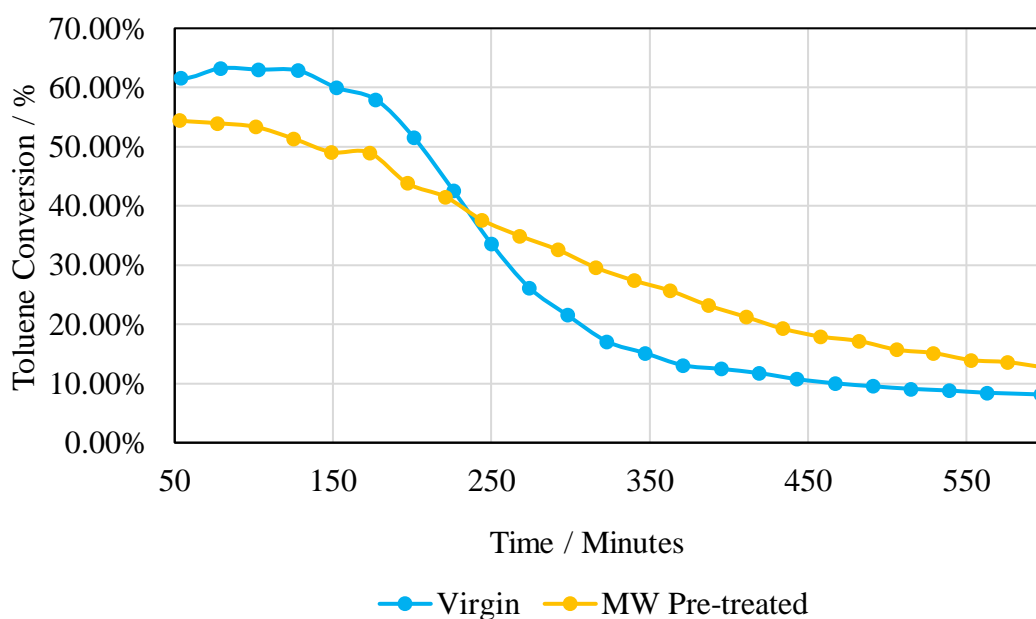
Figure 7.1. –Activity Plot of Virgin Catalyst Compared with Microwave Pre-treated Catalyst

The sample of mordenite which had undergone microwave plasma pre-treatment displayed an activity profile for toluene disproportionation (Figure 7.2.) very similar to the microwave pre-treated sample. The initial activity was slightly reduced compared with the virgin material (57 %) and the rate of deactivation over the measured period (175-561 mins) was calculated to be 0.087 % min^{-1}.

The sample of mordenite which had undergone DBD plasma pre-treatment (Figure 7.3.) proceeded to deactivate rapidly, similar in profile to the virgin catalyst. Rapid deactivation occurred between 153-275 minutes with a rate of deactivation of 0.33 % min^{-1}, reaching a *pseudo-*steady state where toluene conversion was 10 %.
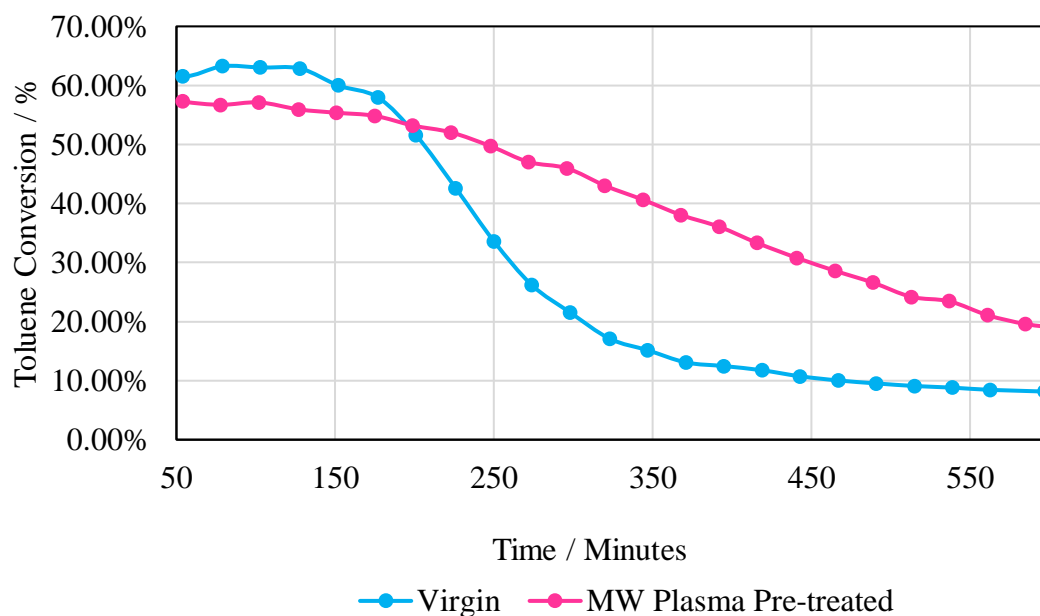
Figure 7.2.- –Activity Plot of Virgin Catalyst Compared with Microwave Plasma Pre-treated Catalyst
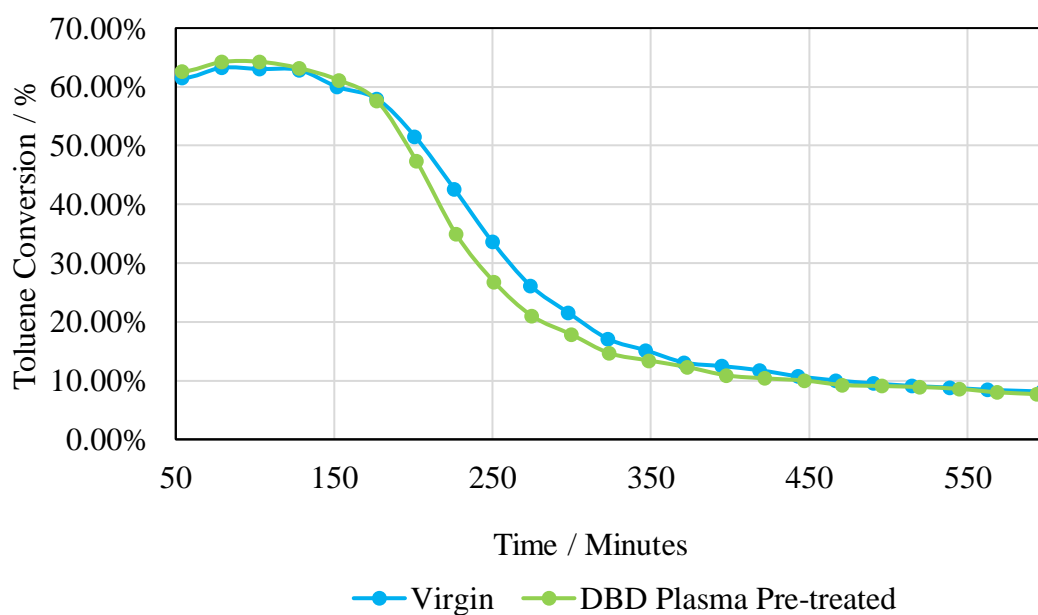
Figure 7.3.- –Activity Plot of Virgin Catalyst Compared with DBD Plasma Pre-treated Catalyst

7.2.2. Effect of Pre-treatment on Catalyst Selectivity

When investigating how the pre-treatments have affected catalyst selectivity, both the more desirable toluene disproportionation and the competing toluene dealkylation (cracking) need to be considered. Reaction selectivity between disproportionation and cracking can be studied through observation of the B/X, whereas the product selectivity of disproportionation can be

examined through xylene isomer selectivity, in terms of quantities of the individual isomers produced.

The B/X as a function of reaction time for the pre-treated catalysts is shown in Figure 7.4., excluding the initial data point, which is instead provided in Table 7.1.. As can be seen in Figure 7.4., the B/X decreases as a function of reaction time, reducing to a *pseudo*-steady state of ~0.2 for all samples. From Table 7.1. it can be seen that the initial B/X of the virgin and DBD Plasma pre-treated samples is significantly higher than their subsequent values, and therefore the reason the initial data point for each sample was excluded from Figure 7.4.. The virgin catalyst had an initial B/X of 0.57, whereas the pre-treated catalysts (with the exception of the DBD plasma pre-treated sample) had B/X values half of the virgin. In contrast the initial B/X of the DBD plasma pre-treated sample had virtually the same B/X of the virgin sample.

Table 7.1. - Initial B/X of Pre-treated Catalysts

Pre-treatment Method	Initial B/X
None (Virgin)	0.57
Microwave	0.27
Microwave Plasma	0.32
DBD Plasma	0.58
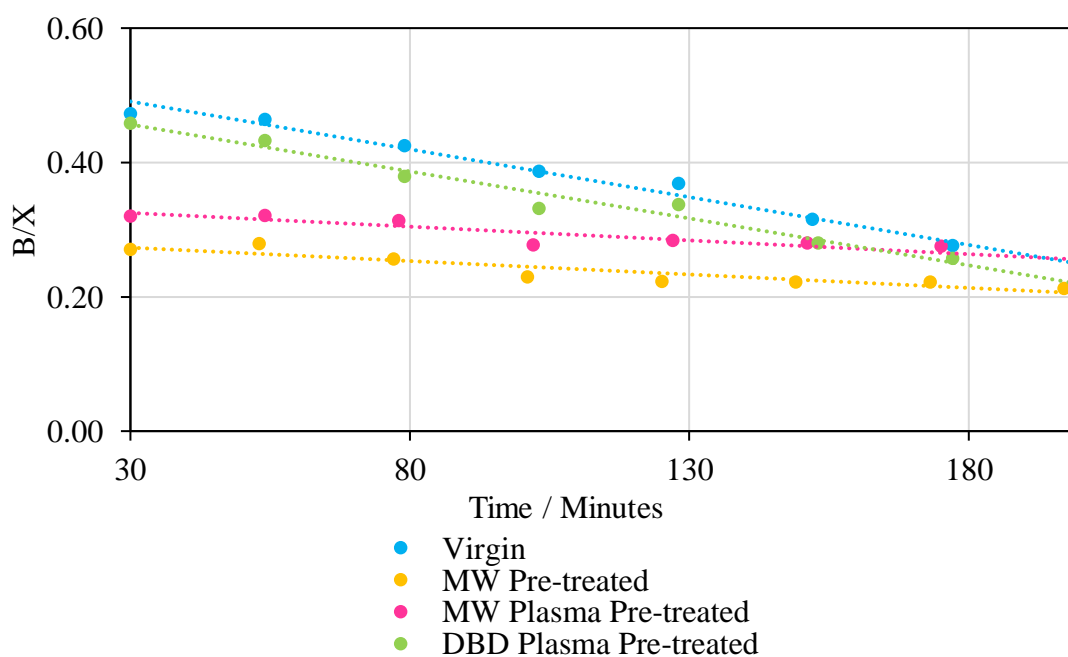
Figure 7.4. - B/X of Pre-treated Catalysts

The individual xylene isomer selectivities as a function of reaction time for the pre-treated catalysts are given in Figures 7.5. and 7.6.. The data has been plotted alongside the thermodynamic equilibrium (T.E.) and grouped by similarity of xylene selectivity profiles for ease of discussion and interpretation.

Figure 7.5. presents the individual xylene selectivities for a sample of virgin and a sample of DBD plasma pre-treated mordenite. Initial values of *p*- and *o*-xylene are slightly higher than the thermodynamic equilibrium. During the first 400 minutes, the amount of *p*- and *o*-xylene slowly decreases (whilst the amount of *m*-xylene correspondingly increases) towards thermodynamic equilibrium. However, after this period, the amount of *p*-xylene begins to move away from thermodynamic equilibrium, slowly increasing for the remainder of the reaction, whilst *m*- and *o*-xylene values slowly decrease accordingly.
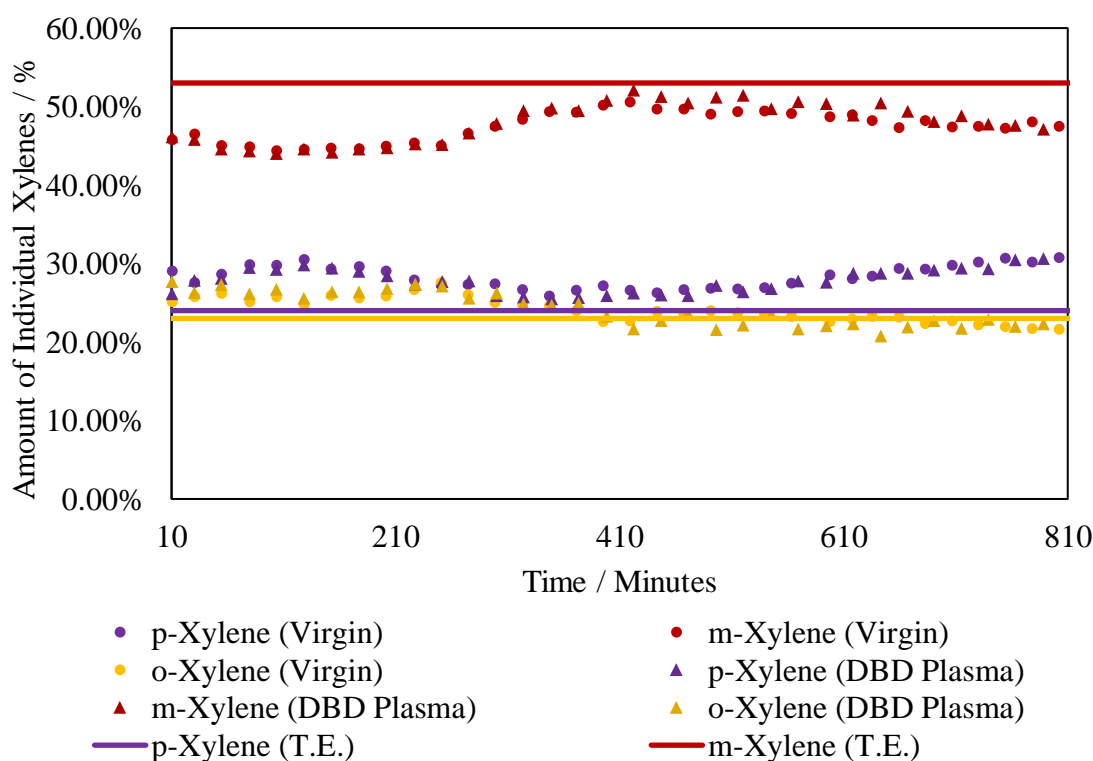
Figure 7.5. - Plot of Individual Xylene Selectivities for Virgin and DBD Plasma Pre-treated Catalysts
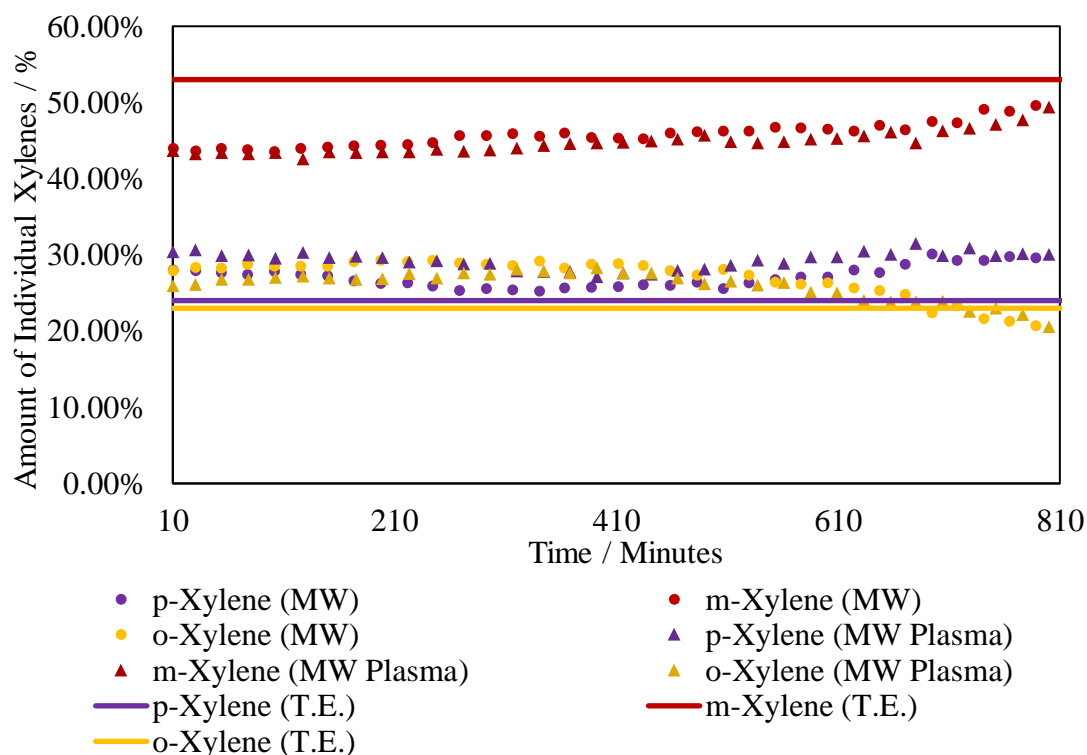
Figure 7.6. - Plot of Individual Xylene Selectivities for Microwave and Microwave Plasma Pre-treated Catalysts

Figure 7.6. presents the individual xylene selectivities for a sample of microwave pre-treated and a sample of microwave plasma pre-treated mordenite. Similar to the virgin and DBD Plasma pre-treated samples, the initial amounts of *p*- and *o*-xylene are slightly elevated compared with the thermodynamic equilibrium, whilst the amount of *m*-xylene is lower accordingly. In comparison to the virgin and DBD plasma pre-treated samples however, this increase is more gradual. Over the duration of the first 400 minutes, the amount of *p*-xylene decreases slightly, moving towards thermodynamic equilibrium, after which the amount of *p*- begins to move away from thermodynamic equilibrium, slowly increasing for the remainder of the reaction. *m*-Xylene increases throughout the duration of the reaction towards thermodynamic equilibrium, almost reaching it by 800 minutes, whilst the *o*-xylene value slowly decreases proportionately in accordance with changes in *p*- and *m*-xylene.

7.3. SURFACE AREA AND AMOUNT OF COKE

The surface area and coke present for each of the catalysts (as determined according to the methods described in Sections 4.2.2. and 4.2.4.) is given in Table 7.2..

Table 7.2. - Surface Area and Coke Present on Pre-treated Catalysts

	BET Surface Area / m^2g^{-1}		Coke Present
	Uncoked	Coked	/ weight %
Virgin	348	189	4.55
Microwave Pre-treated	188	153	1.32
Microwave Plasma Pre-treated	335	245	2.28
DBD Plasma Pre-treated	339	194	5.09

As can be seen from Table 7.2., the BET surface area of the catalysts is slightly reduced upon pre-treatment, with microwave pre-treatment possessing a surface area almost half of the surface area of virgin mordenite. Upon deactivation, a proportion of surface area is lost, ranging between 18.6-45.7 % depending on the pre-treatment method. Both the virgin and DBD plasma pre-treated catalysts lost the most surface area during deactivation, with a loss of over 40 %. The microwave plasma pre-treated sample only lost 27 % of its surface area upon deactivation, and the microwave pre-treated sample lost only 19 % of its surface area. With this said, the pre-treatment had considerably reduced the surface area of the microwave sample prior to deactivation (56 %) when compared to virgin.

The coke data given in Table 7.2. presents the amount of coke present on each of the pre-treated catalysts following their deactivation. The DBD plasma pre-treated sample possessed a higher amount of coke (5.09 % by weight) to the deactivated virgin sample (4.55 % by weight), whilst the microwave and microwave plasma pre-treated materials showed a considerable drop in the amount of coke present. The microwave plasma pre-treated sample had a coke value half of the virgin, and the microwave pre-treated sample possessed even less, with a value of 1.32 % by weight.

7.4. COKE COMPOSITION

The deactivation of the catalyst in this reaction is attributed to coking. Therefore, determination of the coke composition may offer an insight into whether the pre-treatment process affects the coking mechanism. Identification of carbonaceous species is often determined using solvent extraction (1). Studies have shown coke deposited during toluene disproportionation to consist of various hydrocarbons, some readily soluble and others insoluble to common solvents such as DCM (2). A typical solvent extraction performed on a zeolite can involve multiple extraction stages, ultimately leading to treatment with HF, resulting in the destruction of the zeolite (2). For this research, a milder solvent extraction involving DCM was performed, to investigate any difference in the proportion or type of DCM soluble coke species upon regeneration. The solvent extraction process was as follows: 100 mg coked catalyst was submerged in 20 mL DCM and vigorously shaken for a period of 72 hours. Following this, the samples were removed, and the effluent was injected into the GC-MS for analysis. Figure 7.7. gives a photograph of the effluent post-extraction, and Figure 7.8 gives the results of the GC-MS analysis.
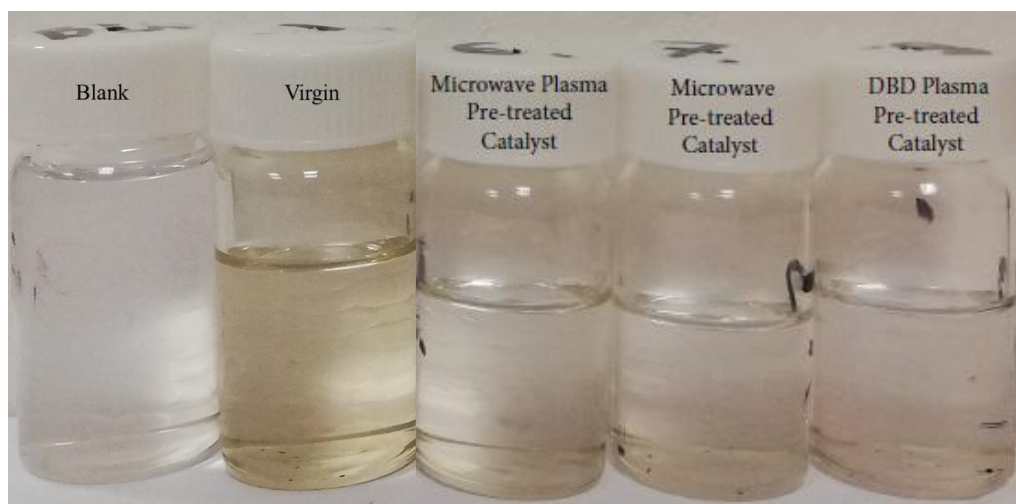
Figure 7.7. - Photo of the Effluent Post-Extraction

From Figure 7.7. the extracted effluents can be seen to have a slightly different colour compared with the blank, however only the virgin sample appears to have a considerable darker, yellow colour indicating the presence of DCM soluble coke.

Figure 7.8. presents the GC-MS data of the effluent, with relative abundance referenced to the solvent. The GC-MS programme used was the same used for the detection of TDP products on-stream during the deactivation process and the species elucidated were preliminarily identified through the NIST library.

There were no significant peaks below 15 minutes with the exception of the solvent. Of the samples, all appeared to have DCM soluble species. The virgin sample displayed the most peaks and had the earliest retention time of 15 and a half minutes, although maximum abundance of any single peak was only ~ 8 %. Similarly, the DBD plasma pre-treated sample had significantly less DCM soluble coke species than the other samples, where the maximum abundance of any single peak was <5 %. In contrast, the microwave and microwave plasma pre-treated samples had higher relative abundances of up to 15 and 22 % respectively. Whilst both had a considerable number of peaks, resolution declined in comparison to the virgin and DBD plasma pre-treated samples. The microwave pre-treated DCM soluble coke species began to elute just under 16 and a half minutes, whereas the microwave plasma pre-treated sample only eluted after 17 minutes.

The results of the NIST library search determined the DCM soluble coke structures to have 3 rings and molecular weights ranging from 165-340 g mol^{-1}. The NIST results were all very similar: polyaromatic ringed structures, similar to those reported by Magnoux et *al.* (3).
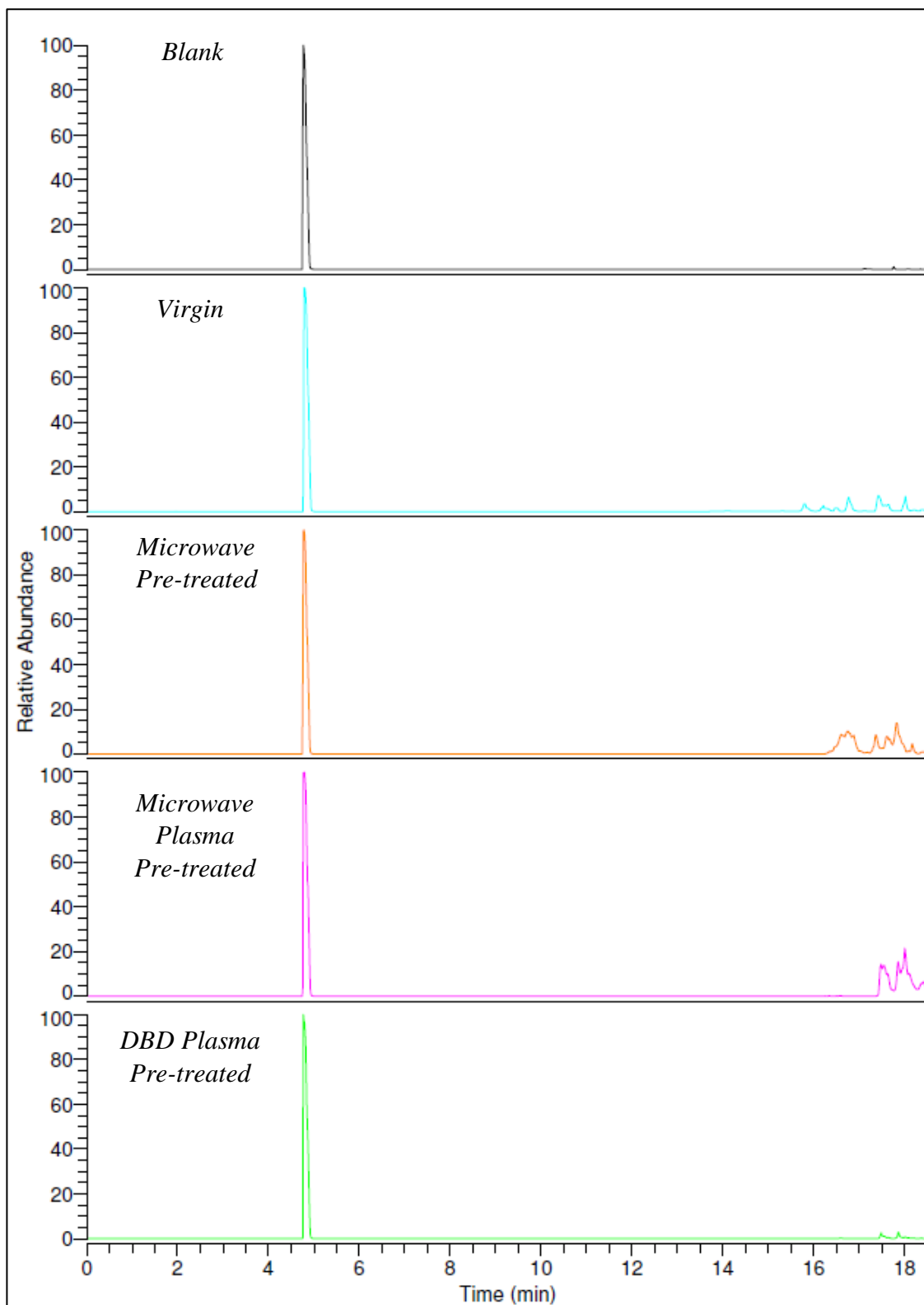
Figure 7.8. – Chromatogram of DCM Soluble Coke

7.5. XRD

XRD was carried out on the pre-treated samples to determine whether the microwave, microwave plasma and DBD plasma pre-treatment processes had any significant effect on the catalytic crystal structure. The results of this are given in Figures 7.9.-7.11., with the pre-treated samples laid over virgin mordenite to aid in visualisation of any changes which may have occurred.

All the diffractograms show the characteristic mordenite peaks (4), with very little peak broadening. There is some shift in peak position and loss of relative intensity in the microwave and microwave plasma pre-treated samples which is not present in the DBD pre-treated material. These changes indicate a change in unit cell coordinates and/or composition. However, further analysis would need to be performed, such as Rietveld refinement to confirm this.
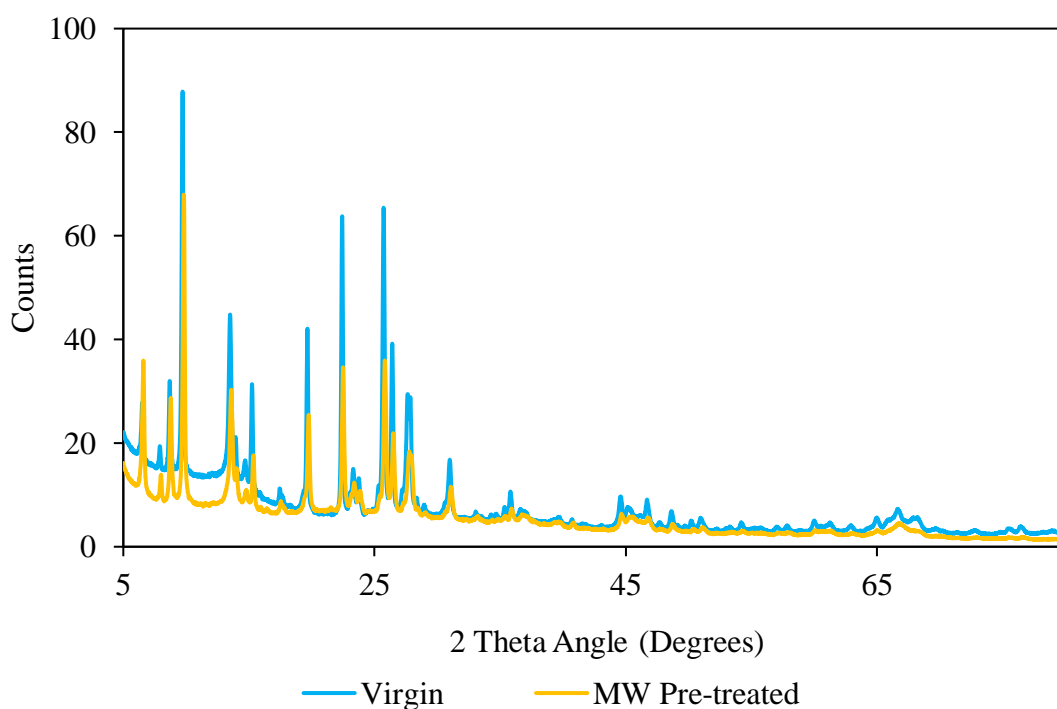
Figure 7.9. - XRD Diffractogram of Microwave Pre-treated Mordenite
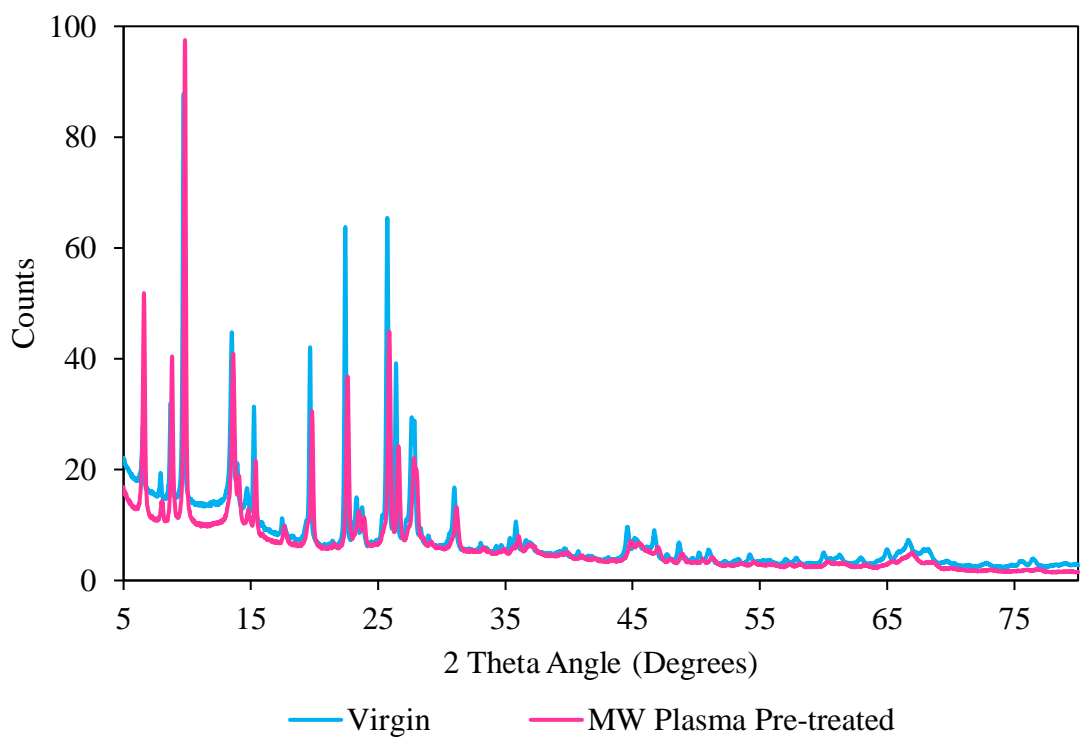
Figure 7.10. - XRD Diffractogram of Microwave Plasma Pre-treated Mordenite
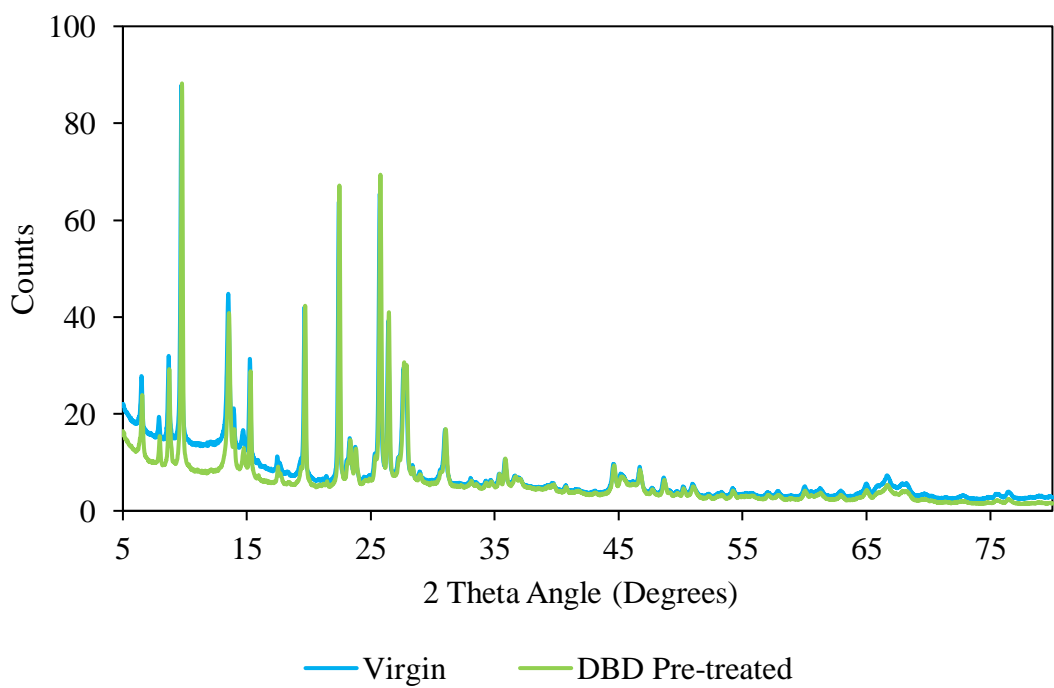
Figure 7.11. - XRD Diffractogram of DBD Pre-treated Mordenite

7.6. CATALYST ACIDITY

As an acid catalyst, the activity of mordenite is heavily linked to availability and strength of its acid sites. IR and NH$_3$ TPD studies were carried out to determine any impact the microwave or plasma pre-treatment processes may have had on catalytic acidity.

7.6.1. Infrared Spectroscopy

Results from the infrared studies using probe molecules are given in Figures 7.12.-7.17.. Figure 7.12. depicts the IR spectra of the virgin sample prior to and post pyridine adsorption in the 4000-3500 cm^{-1} region where the O-H stretching frequencies appear (5). Peaks of interest include 3742 cm^{-1}, 3653 cm^{-1} (Si-OH and Al-OH groups) and 3606 cm^{-1} (acidic Al-OH-Si groups). The additional peak at 3775 cm^{-1} is a result of the γ-Al$_2$O$_3$ in the binder. These peaks were also present in the pre-treated samples but were omitted for simplification.
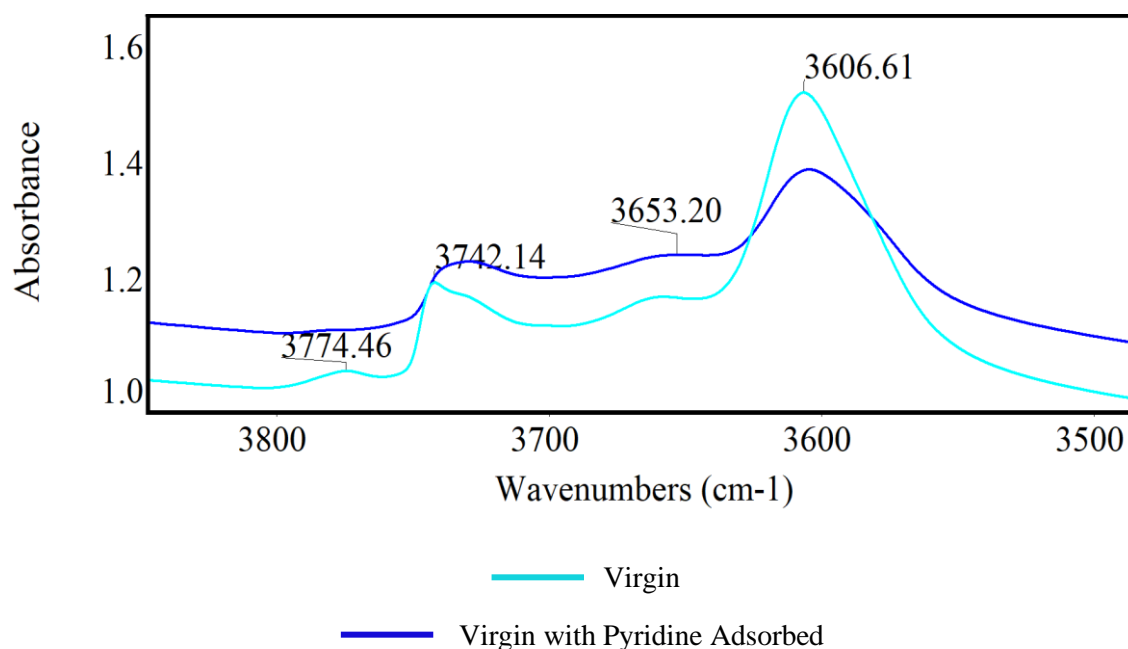
Figure 7.12. – IR Spectra of Virgin Sample Pre- and Post-Pyridine Adsorption

The subtraction result ((spectrum of the sample after pyridine adsorption) – (the spectrum of the activated sample prior to adsorption)) of the pre-treated samples is given in Figure 7.13.. The interaction of pyridine with the catalyst samples can be seen from the presence of negative peaks appearing at 3608 cm^{-1}, 3660 cm^{-1}, 3744 cm^{-1} and 3775 cm^{-1}.
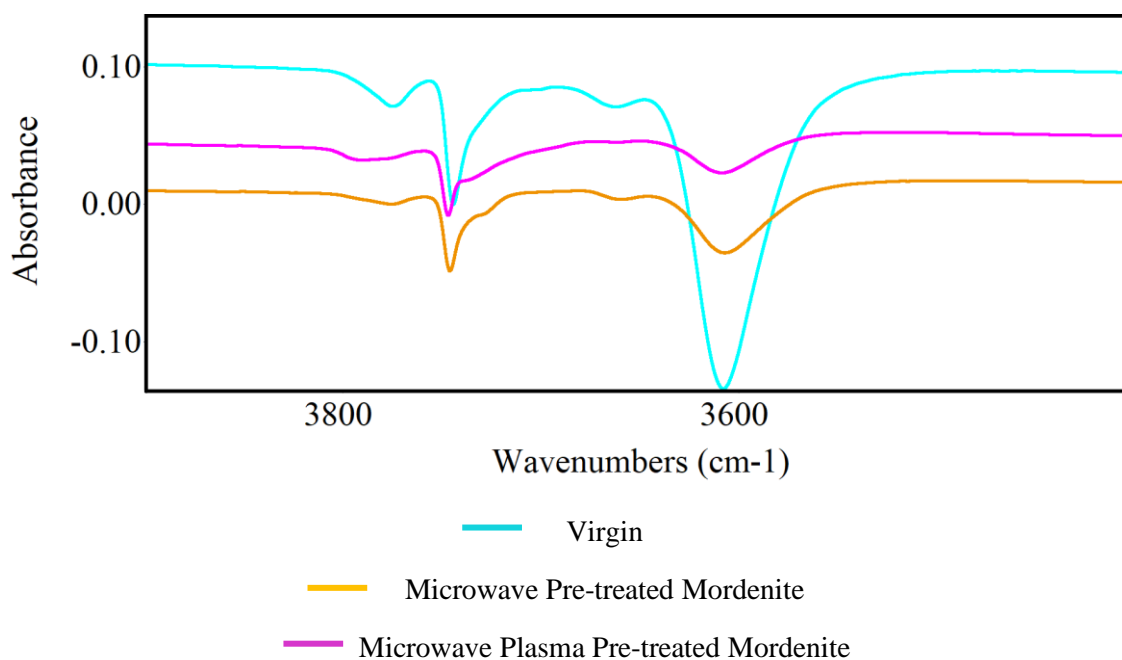
Figure 7.13. – IR Spectra Subtraction Result of Pyridine Adsorbed Pre-treated Catalysts

(4000-3400 cm^{-1})

Figure 7.14 depicts the IR subtraction result of the pre-treated catalysts in the 1700-1400 cm^{-1} region where the pyridine frequencies appear (5). Peaks of interest include 1454 cm^{-1} (strong LAS), 1489 cm^{-1} (BAS and LAS), 1544 cm^{-1} (BAS), 1621 cm^{-1} and 1633 cm^{-1}. The peaks at 1544 cm^{-1} and 1454 cm^{-1} were used to calculate the concentration of Brønsted and Lewis acid sites (as described in section 4.2.6.) respectively (Table 7.3.).
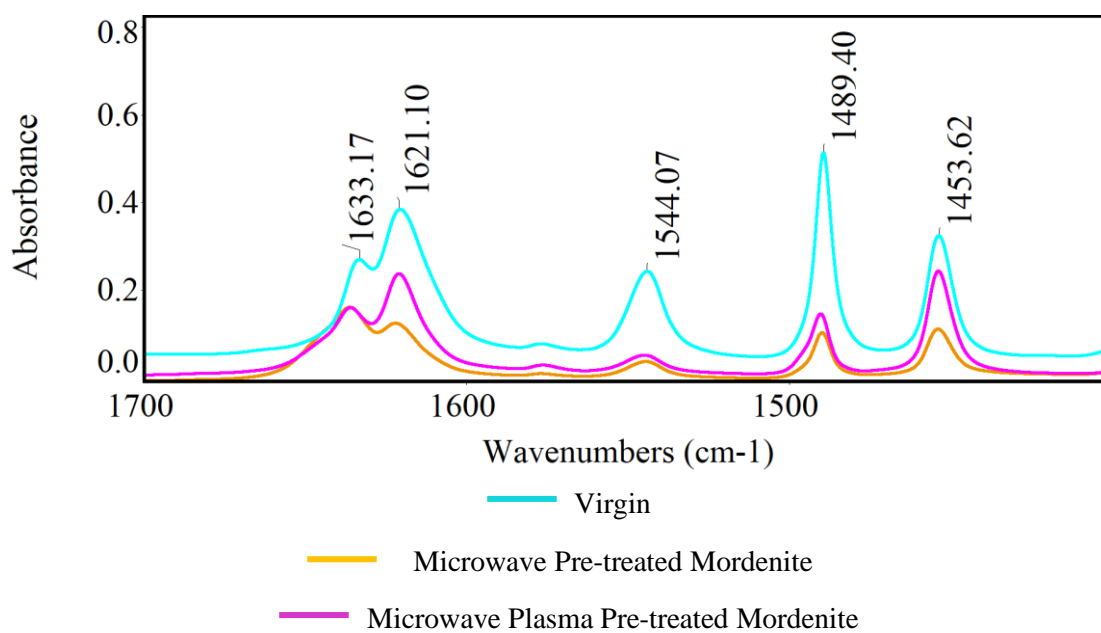
Figure 7.14. – IR Spectra Subtraction Result of Pyridine Adsorbed Pre-treated Catalysts

(1700-1400 cm^{-1})

Figure 7.15. depicts the IR spectra of the virgin sample prior to and post collidine adsorption in the 4000-3500 cm^{-1} region where the O-H stretching frequencies appear (5). Peaks of interest include 3743 cm^{-1}, 3657 cm^{-1} (Si-OH and Al-OH groups) and 3607 cm^{-1} (acidic Al-OH-Si groups). The additional peak at 3775 cm^{-1} is a result of the γ-Al$_2$O$_3$ in the binder.
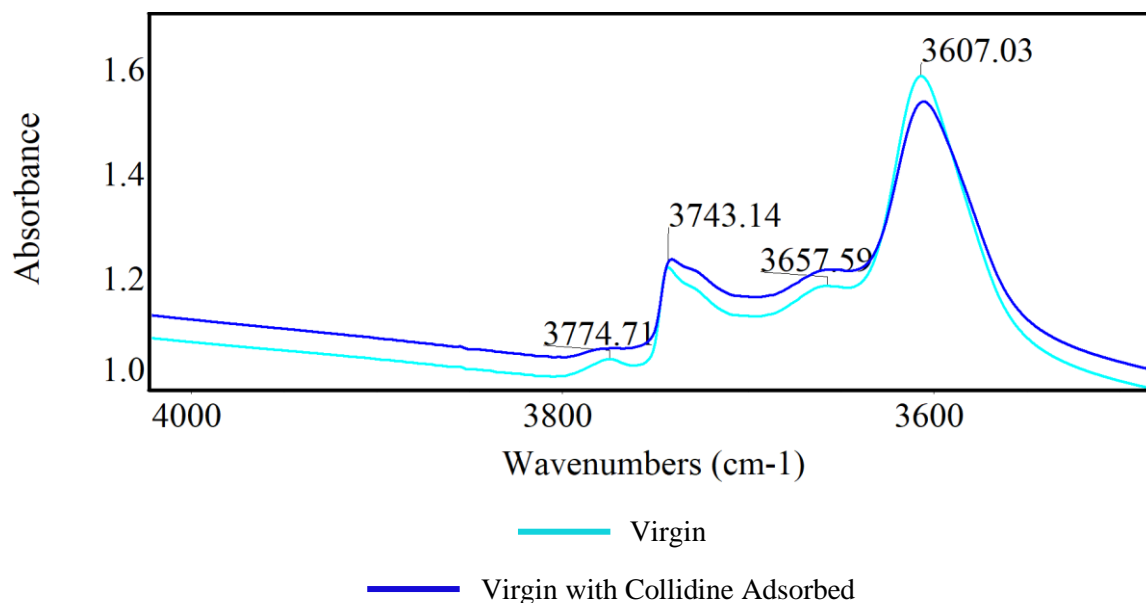
Figure 7.15. – IR Spectra of Virgin Sample Pre- and Post-Collidine Adsorption

The subtraction result of the pre-treated samples is given in Figure 7.16.. The interaction of collidine with the catalyst samples can be seen from the presence of negative peaks appearing at 3608 cm^{-1}, 3663 cm^{-1}, 3745 cm^{-1} and 3775 cm^{-1}.
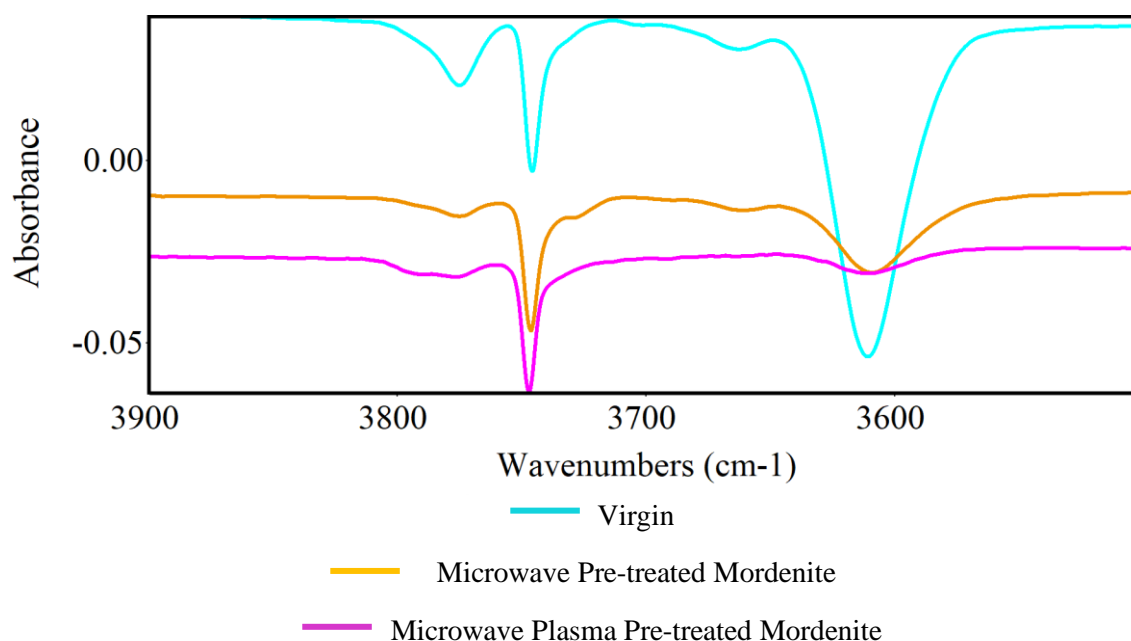
Figure 7.16. – IR Spectra Subtraction Result of Collidine Adsorbed Pre-treated Catalysts

(4000-3400 cm^{-1})

Figure 7.17. depicts the IR subtraction result of the regenerated catalysts in the 1800-1500 cm^{-1} region where the collidine frequencies appear (5). The peak of interest appears at 1636 cm^{-1}, corresponding to the BAS present (6). This peak was used (as described in Section 4.2.6.) to calculate the concentration of Brønsted acid sites (Table 7.3.)
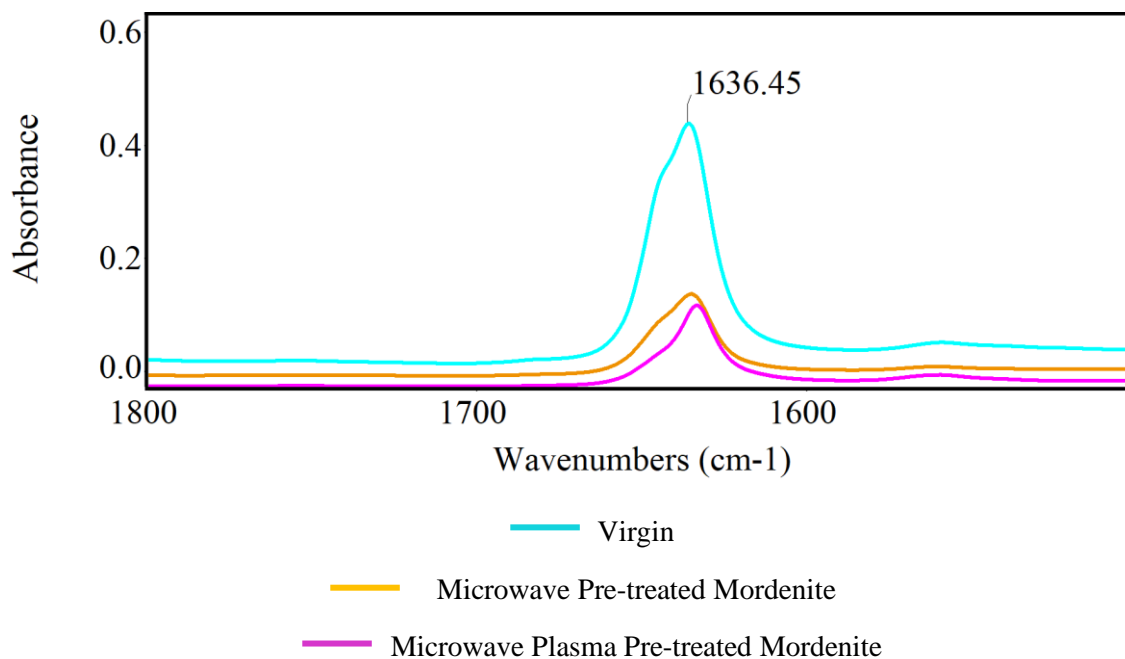
Figure 7.17. – IR Spectra Subtraction Result of Collidine Adsorbed Pre-treated Catalysts (1700-1400 cm^{-1})

The concentration of Brønsted and Lewis acid sites determined using the probe molecules is reported in Table 7.3., taking surface area into account. As can be seen from Table 7.3., virgin mordenite possessed the highest number of total Brønsted acid sites, followed by microwave and microwave plasma pre-treated mordenite. This trend was seen for both probe molecules, however the pre-treated samples had less than half the concentration of BAS of the virgin sample when using pyridine as the probe molecule. In terms of Lewis acidity, virgin possessed the highest concentration followed by microwave plasma and microwave pre-treated samples. In contrast to Brønsted acidity, the concentration of LAS decreases by a quarter in the pre-treated samples.

		Virgin	Microwave Pre-treated	Microwave Plasma Pre-treated
Pyridine	**BAS**	0.50	0.18	0.10
	LAS	0.45	0.33	0.37
	B/L	1.1	0.5	0.3
Collidine	**BAS**	0.24	0.17	0.07

7.6.2. Ammonia Temperature Programmed Desorption

Results of the NH$_3$ TPD studies of the pre-treated catalysts are given in Figures 7.18.-7.19., plotted alongside a sample of virgin mordenite to assist in the visualisation of any differences which may have arisen. Typically, relative acid site strength can be determined by peak temperature, where increasing temperatures are indicative of stronger acid sites (7).

The NH$_3$ TPD data for a sample of virgin mordenite, given in Figure 7.18., exhibits two peaks; the first at 225°C and the second at 560°C. The peak at 225°C possesses 7 µmoles g^{-1} min^{-1} ammonia, twice as much as the peak at 560°C displays.

The NH$_3$ TPD data for a sample of microwave pre-treated mordenite is also displayed in Figure 7.18.. Similar to the virgin sample, there are two peaks exhibited, the first at 225°C and the second at 530°C, slightly lower than the corresponding virgin peak at 560°C. Both of the microwave pre-treated peaks possess significantly lower intensities than the virgin sample. The peak at 225°C has a concentration of 3.5 µmoles g^{-1} min^{-1} ammonia, and the 530°C peak has an ammonia concentration of 1.25 µmoles g^{-1} min^{-1}.

The NH$_3$ TPD data for a sample of microwave plasma pre-treated mordenite is given in Figure 7.19.. In contrast to the virgin sample, the microwave plasma pre-treated mordenite exhibits a single peak at 225°C with a 3.5 µmoles g^{-1}min^{-1} concentration of ammonia. However, the peak also displays a broad shoulder which declines in intensity to 0 µmoles g^{-1}min^{-1} at 950°C.
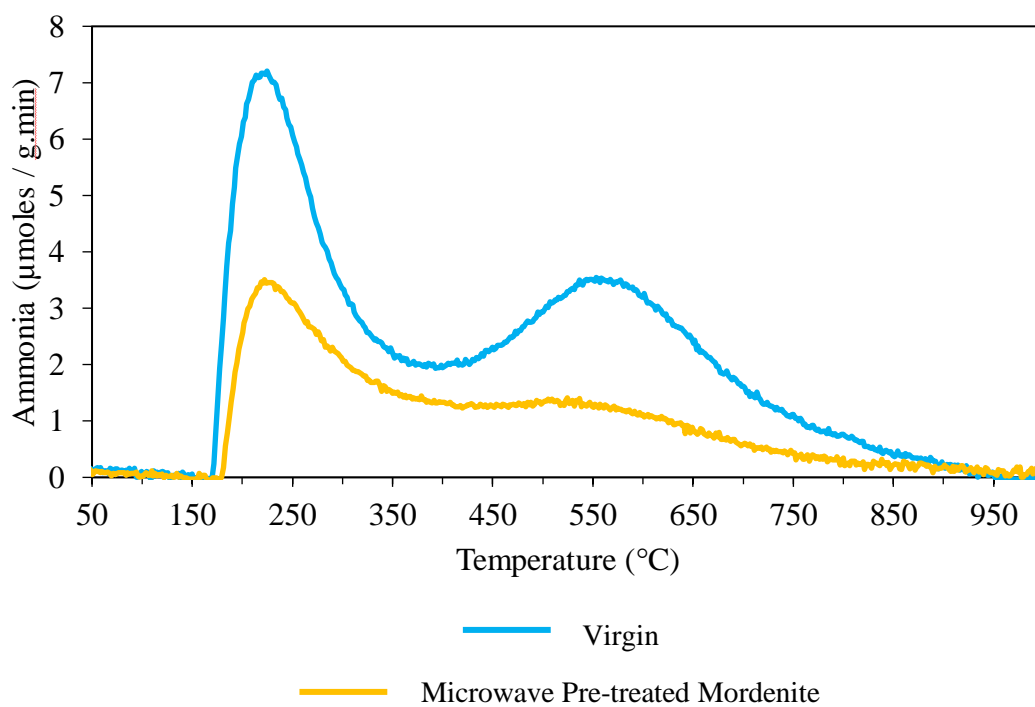
Figure 7.18. – NH₃ TPD Spectra of Virgin Catalyst Compared with Microwave Pre-treated Catalyst
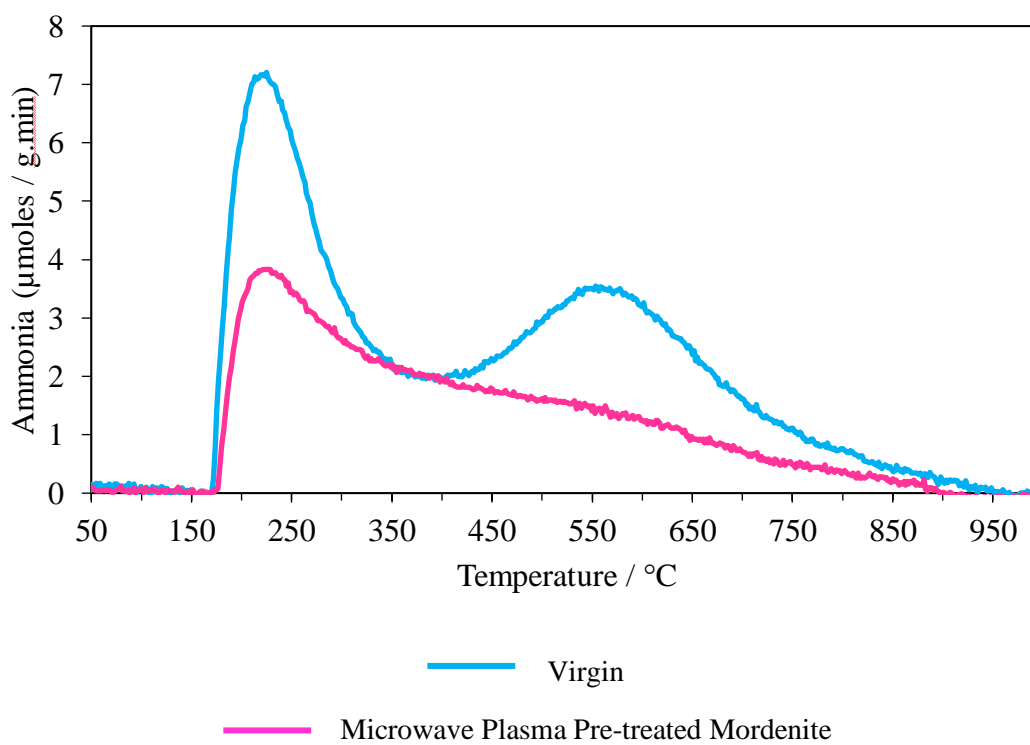
Figure 7.19. – NH₃ TPD Spectra of Virgin Catalyst Compared with Microwave Plasma Pre-treated

Catalyst

7.7. REFERENCES

(1) Abdullah HA, Hauser A, Ali FA, Al-Adwani A. Optimal Conditions for Coke Extraction of Spent Catalyst by Accelerated Solvent Extraction Compared to Soxhlet. Energy and Fuels 2006;20:320-323.

(2) Holmes SM, Garforth M, B., Dwyer J. A Solvent Extraction Method to Study the Location and Concentration of Coke Formed on Zeolite Catalysts. Applied Catalysis A: General 1997;151:355-372.

(3) Magnoux P, Canaff C, Machado F, Guisnet M. Coking Aging and Regeneration of Zeolites XIII. Composition of the Carbonaceous Compounds Responsible for the Deactivation of USHY Zeolite during Toluene Disproportionation. Journal of Catalysis 1992;134:286-298.

(4) Lafuente B, Downs RT, Yang H, Stone N. Mordenite R061118. 2015; Available at: http://rruff.info/Mordenite/R061118. Accessed 02/28, 2019.

(5) Hadjiivanov K. Identification and Characterisation of Surface Hydroxyl Groups by Infrared Spectroscopy. Advances in Catalysis 2014;57:99-318.

(6) Lonstad Bleken B, Mino L, Giordanino F, Beato P, Svelle S, Lillerud KP, et al. Probing the Surface of Nanosheet H-ZSM-5 with FTIR Spectroscopy. Physical Chemistry Chemical Physics 2013;15(32):13363-13370.

(7) Karge HG. Comparative Measurements on Acidity of Zeolites. In: Ohlmann G, Pfeifer H, Fricke R, editors. Catalysis and Adsorption by Zeolites. First ed. Amsterdam: Elsevier Science Publishers; 1991. p. 133-156.

CHAPTER 8: PRE-TREATMENT STUDIES II - DISCUSSION

8.1. SURFACE AREA AND CATALYST CRYSTALLINITY

Pre-treating the catalysts was performed to investigate the efficacy of microwave and plasma technologies for extending the catalytic life of mordenite for toluene disproportionation. However, the pre-treatment processes have been shown to cause a loss of crystallinity to varying degrees. The XRD results (Figures 7.9.-7.11.) displayed no loss of crystalline structure to the DBD plasma pre-treated sample, a minor loss of crystallinity to the microwave plasma pre-treated sample and a significant loss of crystal structure to the microwave pre-treated sample. The extent of the loss of crystallinity caused by the microwave pre-treatment was also seen visually by the fusion of the extrudate into an amorphous glass-like material (Figure 8.1.) and was also reflected in the change in surface area (188 m^2 g^{-1}), compared with the virgin sample (348 m^2 g^{-1}) (Table 7.2.). Similarly, the non-destructive properties of the DBD plasma pre-treatment on the crystal structure are seen by the absence of change in the surface area (339 m^2 g^{-1}) compared with the virgin sample, whereas the minor loss of crystallinity in the microwave plasma pre-treatment process did not appear to significantly impact the surface area of the catalyst, with only a 4 % reduction (335 m^2 g^{-1}) compared to the virgin sample (348 m^2 g^{-1}).

Figure 8.1 - Photo of Microwave Pre-treated Mordenite

8.2. COKE AMOUNT AND COMPOSITION

Upon deactivation, the surface area of the pre-treated catalyst samples reduced in accordance with the amount of coke deposited. Table 8.1. expresses the loss of surface area as a percentage for each of the pre-treated samples. The greater % loss of surface area is consistent with the samples where the most coke was deposited, and the sample with the least coke exhibited the smallest reduction of surface area.

Table 8.1 - Surface Area and Coke Deposited on Pre-treated Catalysts

	Loss of Surface Area / %	Coke Deposited / weight %
Virgin	46	4.55
Microwave Pre-treated	19	1.32
Microwave Plasma Pre-treated	31	2.28
DBD Plasma Pre-treated	43	5.09

In terms of coke composition, the solvent extraction results (Figure 7.8.) indicated no significant amount of DCM soluble coke on the DBD plasma pre-treated sample and minimal DCM soluble coke on the virgin sample. Alongside the TGA results (Table 8.1.), this indicates the majority of coke formed on the DBD plasma pre-treated sample is insoluble in DCM. In contrast, the microwave and microwave plasma pre-treated samples exhibited significantly stronger peaks with longer retention times. This is indicative of higher molecular weight aromatics, suggestive of the pre-treatment affecting the coke deposition mechanism. This difference is likely to be attributed to a change in the concentration, strength or a redistribution of the acid sites present.

8.3. CATALYST ACIDITY

8.3.1. Infrared Spectroscopy

The infrared spectroscopy data for both pyridine and collidine studies (Figures 7.12.-7.17.) provided an insight to the concentration of BAS and LAS present in the pre-treated catalysts. A preliminary inspection of the OH-stretching region (4000-3500 cm^{-1}) can identify which of the acid sites are available to the probe molecule, before quantification of the concentration of acid

sites is performed using the 1700-1400 cm^{-1} region where the pyridinium and collidinium ions appear.

OH Region

In the OH-stretching frequency region (4000-3500 cm^{-1}), the IR spectra of the samples (Figures 7.12.-7.17.), exhibited four peaks prior to the adsorption of the probe molecule. The peaks at ~3742 cm^{-1} and ~3655 cm^{-1} are readily identified as Si-OH and Al-OH groups respectively, and the ~3606 cm^{-1} peak corresponds to acidic Al-OH-Si groups (1). The ~3775 cm^{-1} peak is attributed to the γ-Al$_2$O$_3$ in the binder (1). Interactions of the probe molecule with the zeolite acid sites reduces the peak intensities. The extent of such interaction across the regenerated samples can be seen in the subtraction result (Figures 7.13. and 7.16.). The interaction between the probe molecules and the acidic Al-OH-Si groups (3600 cm^{-1}) of the pre-treated samples appears to be considerably weaker compared with the virgin sample. This may indicate a significant decrease in the presence of Brønsted acid sites in the pre-treated samples compared with the virgin sample.

Acid Site Concentration

The 1700-1400 cm^{-1} region of the IR spectra using pyridine as the probe molecule (Figure 7.14.) exhibited five peaks. The peaks appearing at 1633 cm^{-1} and 1544 cm^{-1} correspond to the pyridinium ion (PyH$^+$) and the peaks appearing at 1620 cm^{-1} and 1453 cm^{-1} correspond to pyridine co-ordinated to Lewis acid sites. The peak exhibited at 1489 cm^{-1} is a result of interactions between both PyH$^+$ and LAS. To calculate BAS and LAS concentration, the 1544 cm^{-1} and 1453 cm^{-1} peaks are used (as described in Section 4.2.6.). The results are given in Table 7.3..

The 1700-1400 cm^{-1} region of the IR spectra using collidine as the probe molecule (Figure 7.17.) exhibited a peak at 1636 cm^{-1}. This peak is attributed to the collidinium ion (CollH$^+$) (2) and is used to calculate the concentration of Brønsted acid sites (as described in Section 4.2.6.). The results are given in Table 7.3..

The results (Table 7.3.) display more BAS in the virgin sample and a significant decrease in BAS for the pre-treated samples, as suggested previously from the IR spectra in the OH-stretching

frequency (Figures 7.13. and 7.16.). Furthermore, the significant loss of BAS for the pre-treated samples has occurred both internally and externally, with the microwave pre-treated sample retaining a slightly higher concentration of BAS than the microwave plasma-pre-treated sample. Therefore, more coke deposition might be expected from the microwave pre-treated sample than the microwave plasma pre-treated sample, however this is not the case. A cause for this may be due to the significant loss of surface area from the microwave pre-treated sample, possibly reducing the availability of the acid sites.

8.3.2. Ammonia Temperature Programmed Desorption

The ammonia TPD results (Figures 7.18.-7.19.) of the pre-treated catalysts give an insight into possible changes of acid site strength due to the pre-treatment process. The virgin sample exhibited two peaks, one at a lower temperature (225°C) and one at a higher temperature (560°C), corresponding to l- (lower temperature) and h- (higher temperature) peaks (3). Whilst the h-peak is attributed to directly adsorbed ammonia on the zeolite, the l-peak is attributed to weakly adsorbed NH_4^+ species and is therefore not accurately quantifiable (3).

The microwave pre-treated sample exhibits two peaks in the same region as the virgin sample, however the peak maximum of both peaks is considerably lower. This is indicative of a decrease in acid site concentration, although as the peaks appear at the same temperatures as the virgin sample, the strength of the acid sites remaining can be considered the same (4). This supports the heavily reduced acid site concentration seen in the IR results (Table 7.3.).

In contrast, the microwave plasma pre-treated sample appears to exhibit only a single broadened peak, as the h-peak has a significantly reduced peak maximum. This makes it difficult to determine whether the acid site strength has changed compared to the virgin sample. However, the heavily reduced h-peak peak maximum indicates a significant reduction in acid sites, supporting the IR data (Table 7.3.).

8.4. CATALYST ACTIVITY

8.4.1. Dielectric Barrier Discharge Plasma Pre-treatment

The activity of the DBD plasma pre-treated catalyst (Figure 7.3.) was similar in both profile and deactivation rate to the virgin sample. There was no loss of crystalline structure seen from the XRD results (Figure 7.11.) and no considerable change to the surface area (Table 7.2.) of the catalyst. There was a slight increase in the amount of coke present, but this was not reflected in any change of B/X or individual xylene selectivity. Overall, the DBD plasma pre-treatment under the conditions used appears to have had no effect on the mordenite sample.

8.4.2. Microwave Pre-treatment

The microwave pre-treatment was shown to be a harsh process, destroying the crystal structure (Figures 7.9. and 8.1.), leading to a loss of surface area (Table 7.2.) and acidity (Table 7.3.). Therefore, the activity of the microwave pre-treated catalyst (Figure 7.1.) differed from the virgin sample, exhibiting a more gradual deactivation profile with a correspondingly much reduced deactivation rate. This is explained by the reduction of coke deposition seen in the TGA data (Table 7.1.) as a direct result of the heavily reduced concentration of BAS seen from the IR and NH_3 TPD data (Table 7.3. and Figure 7.18.). The decrease in acid site concentration meant there were less BAS available for cracking, resulting in the reduction of B/X compared with virgin by almost half (Table 7.1.).

As expected, the individual xylene selectivity did not favour any one isomer, as the absence of coke present would allow the rapid isomerisation of *p-* to *m-* and *o-*xylene on the catalyst surface. However, the absence of selectivity could also be attributed to the loss of pore structure, as *p-*xylene is known to rapidly diffuse out of the zeolite channels at a rate 1000 times faster than the other isomers due to steric effects (5). With the considerable destruction of the crystal structure, seen by the XRD (Figure 7.9.) and supported by the loss of surface area (Table 7.2.), the steric constraints may be significantly reduced, and would therefore increase the rate of diffusion for the *m-* and *o-* xylene isomers.

8.4.3. Microwave Plasma Pre-treatment

Similar to the microwave pre-treated sample, the activity of the microwave plasma pre-treatment (Figure 7.2.) exhibited a more gradual deactivation profile with a much-reduced deactivation rate than the virgin sample. This is likely due to the reduction of carbonaceous deposits seen on the catalyst, which can be attributed to the considerable loss of Brønsted acidity seen from the IR data and NH_3 TPD data (Table 7.3. and Figure 7.19.). A strong reduction in acidity would lead to less cracking which would in turn produce less coke. This is further supported by the reduced initial B/X (Table 7.1.).

In contrast to the microwave pre-treated sample, the microwave plasma pre-treated sample exhibited no significant loss to crystal structure (Figure 7.10.), which is reflected in the retention of surface area (Table 7.2.). Therefore, alongside a reduced amount of coke, a shift in individual xylene selectivity would not be expected, which is the case (Figure 7.6.).

8.5. SUMMARY

Overall, the pre-treatment of the mordenite samples under the conditions used has little to no impact on the catalyst properties in the case of the DBD plasma pre-treated sample. In the microwave pre-treated sample the impact was harsh, destroying crystallinity, surface area and acidity, whereas the microwave plasma pre-treatment was milder, only severely affecting acidity. In terms of activity, none of the pre-treatments shifted individual xylene selectivity towards any one particular isomer, although the destruction of acidity in the microwave and microwave plasma pre-treatments had an impact on the B/X, shifting the reaction in favour of toluene disproportionation. Finally, this loss of acidity also reduced the production of carbonaceous deposits, leading to the extended catalytic life which was seen in the microwave and microwave plasma pre-treated samples.

8.6. REFERENCES

(1) Hadjiivanov K. Identification and Characterisation of Surface Hydroxyl Groups by Infrared Spectroscopy. Advances in Catalysis 2014;57:99-318.

(2) Lonstad Bleken B, Mino L, Giordanino F, Beato P, Svelle S, Lillerud KP, et al. Probing the Surface of Nanosheet H-ZSM-5 with FTIR Spectroscopy. Physical Chemistry Chemical Physics 2013;15(32):13363-13370.

(3) Niwa M, Katada N, Okumura K. Solid Acidity of Zeolites. In: Hull R, Jagadish C, Osgood RM, Jr., Parisi J, Wang Z, Warlimont H, editors. Characterisation and Design of Zeolite Catalysts. First ed. Heidelberg: Springer; 2010. p. 9-28.

(4) Karge HG. Comparative Measurements on Acidity of Zeolites. In: Ohlmann G, Pfeifer H, Fricke R, editors. Catalysis and Adsorption by Zeolites. First ed. Amsterdam: Elsevier Science Publishers; 1991. p. 133-156.

(5) Tsai T, Liu S, Wang I. Disproportionation and Transalkylation of Alkylbenzenes Over Zeolite Catalysts. Applied Catalysis A: General 1999 5/17;181(2):355-398.

CHAPTER 9: POWER STUDIES I - RESULTS

9.1. INTRODUCTION

In previous chapters, the regeneration and pre-treatment of coked mordenite samples has been investigated, comparing thermal methods with a microwave plasma process amongst others. Further studies on microwave plasma regeneration, i.e. varying the input power, have been investigated and the results are provided in this chapter. The microwave plasma regenerations were performed as described in Section 4.1.2., varying only the microwave input power so as to create a specific wall temperature. The power input required for the wall temperatures is given in Table 9.1..

Table 9.1. - Microwave Power Required to Produce Set Wall Temperatures

Wall Temperature / °C	Microwave power / Watts
150	125
250	195
350	400
450	650

9.2. CATALYST TESTING

9.2.1. Toluene Conversion as a Function of Time

Regenerated mordenite was subjected to a second toluene disproportionation. The regenerated activity represented as toluene conversion as a function of time has been plotted in Figures 9.1.-9.4.. The data for each regeneration treatment has been plotted alongside virgin mordenite in order to assist in the visualisation of any differences which may have resulted.

As can be seen in Figure 9.1., the initial toluene conversion over the virgin catalyst was 55 %, which decreased over time. After 350 minutes, catalytic activity had dropped to a 5 % conversion and remained in a *pseudo*-steady state with activity only reducing a further 3 % after an additional

500 minutes. Rapid deactivation occurred between 118 minutes and 260 minutes at a rate of 0.29 % min^{-1}.

The activity data for a sample of mordenite which had undergone microwave plasma regeneration (MWPR) at a wall temperature of 150°C is also shown in Figure 9.1.. Whilst the catalyst exhibits a similar activity profile to the virgin material, the rate of deactivation is slightly higher (0.31 % min^{-1}), and the initial activity is slightly reduced (51 %).

In contrast, the deactivation profile of a sample of spent mordenite which had undergone MWPR at a wall temperature of 250°C (Figure 9.2.), was significantly different from the virgin and 150°C MWPR materials. Whilst the initial activity was the same as the virgin sample (55 %), in terms of toluene conversion, the sample did not undergo a rapid deactivation but instead the profile displays a more gradual deactivation with a rate of 0.16 % min^{-1}, over the measured period (98-324 mins).

The sample of mordenite which had undergone MWPR at a wall temperature of 350°C (Figure 9.3.) displayed a similar deactivation profile to the 250°C MWPR sample, with a deactivation rate of 0.035 % min^{-1}, and a reduced initial activity (22 %) compared to virgin (55 %). The sample of mordenite which had undergone MWPR at a wall temperature of 450°C (Figure 9.4.) had a significantly reduced initial activity (6 %) compared to virgin, which was reduced to 2 % as the reaction progressed (at a rate of 0.0069 % min^{-1}).
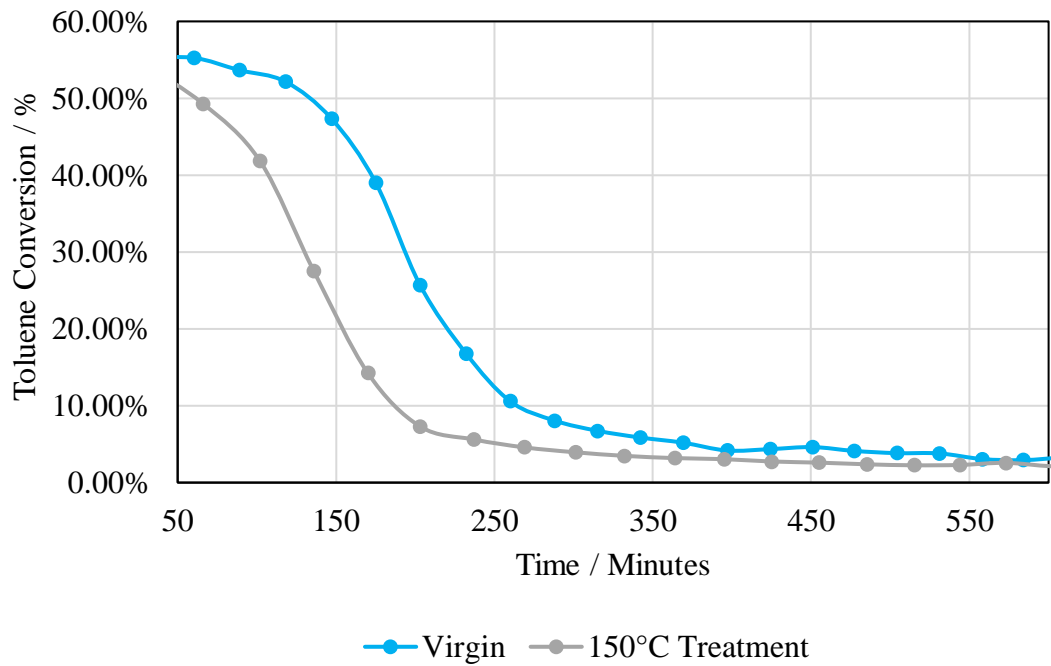
Figure 9.1. –Activity Plot of Virgin Catalyst Compared with 150°C Microwave Plasma Treated Catalyst
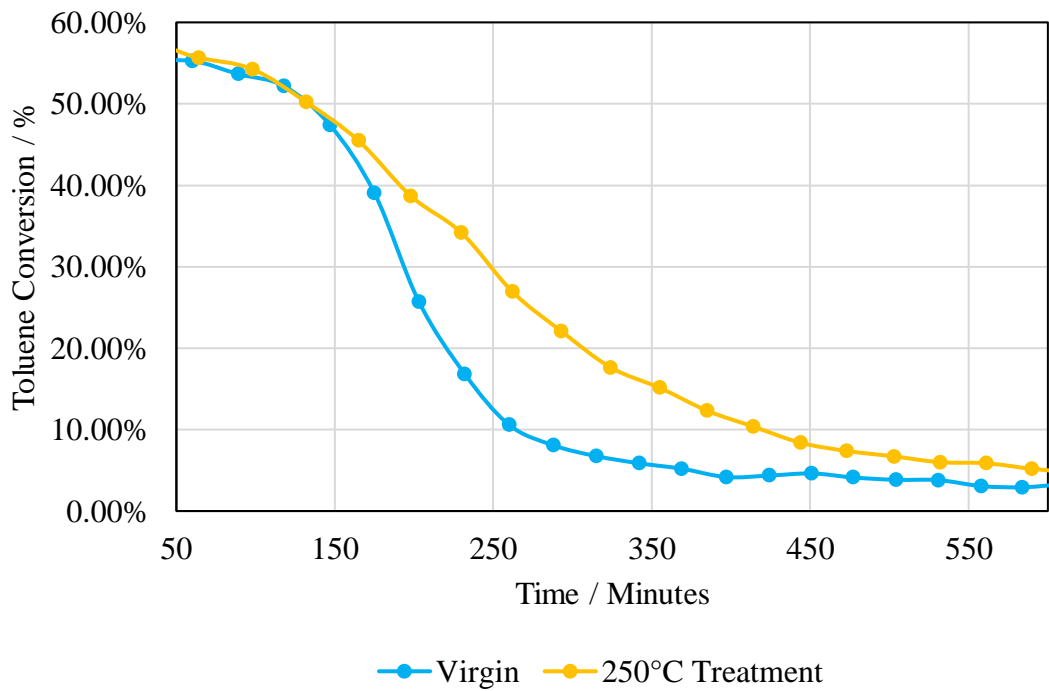
Figure 9.2. –Activity Plot of Virgin Catalyst Compared with 250°C Microwave Plasma Treated Catalyst
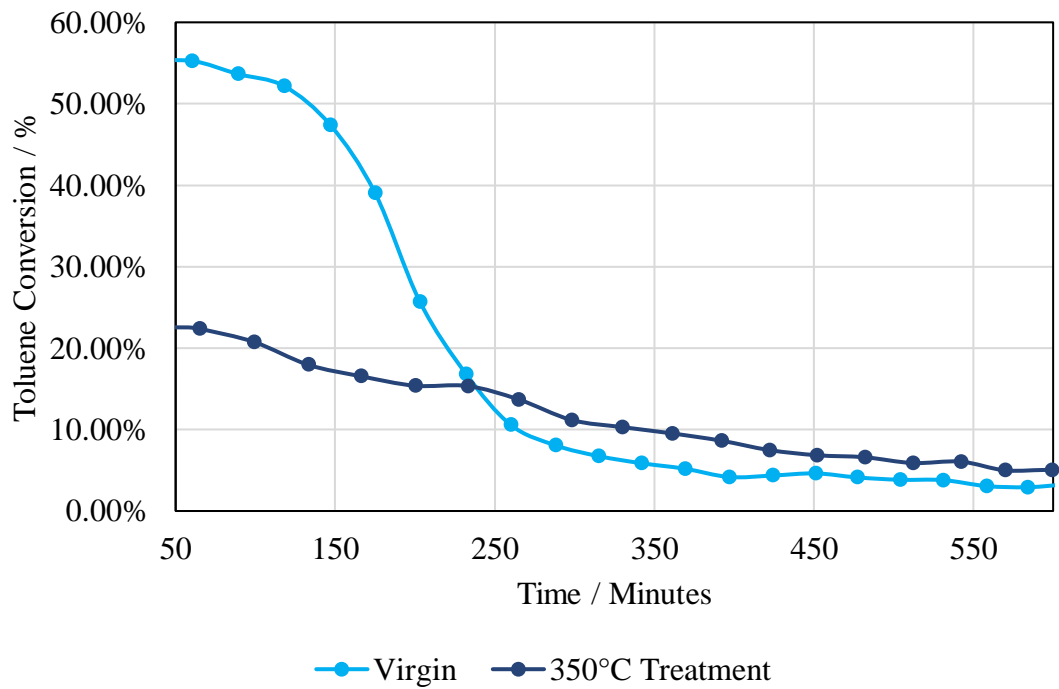
Figure 9.3. –Activity Plot of Virgin Catalyst Compared with 350°C Microwave Plasma Treated Catalyst
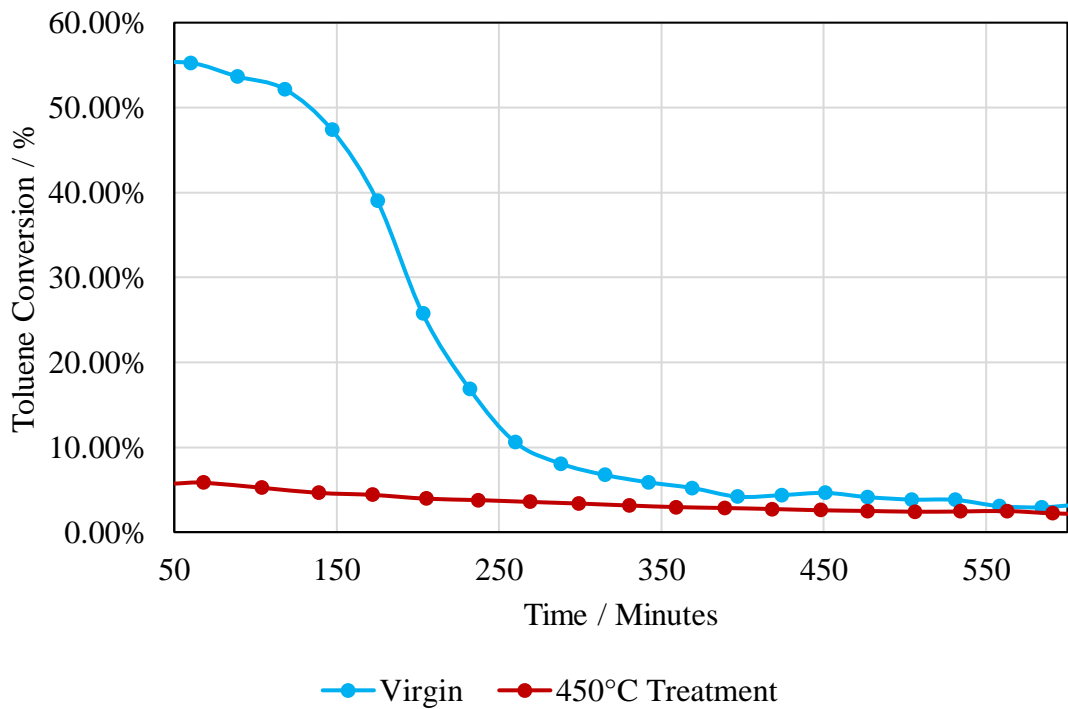
Figure 9.4. –Activity Plot of Virgin Catalyst Compared with 450°C Microwave Plasma Treated Catalyst

9.2.2. Effect of Power Used During Regeneration on Catalyst Selectivity

When investigating how the change in power used in the regeneration treatments have affected catalyst selectivity, the reaction selectivity between the more desirable toluene disproportionation and the competing cracking reactions can be studied through observation of the B/X.

The B/X as a function of reaction time for the regenerated catalysts is shown in Figure 9.5., excluding the initial data point, which is instead provided in Table 9.2.. As can be seen in Figure 9.5., the B/X of the virgin material decreases as a function of reaction time, reducing to a *pseudo*-steady state of 0.2. This is also seen for the B/X of the 150°C and 250°C MWPR samples although at a much-reduced gradient. The B/X for the 350-450°C MWPR samples appears as a constant value of 0.17 (350°C MWPR sample), and 0.25 (450°C MWPR sample).

From Table 9.2. it can be seen that the initial B/X of the virgin and MWPR samples between 150-250°C is significantly higher than their subsequent values, and therefore the reason the initial data point for each sample was excluded from Figure 9.5.. The virgin catalyst had an initial B/X of 0.74, whereas the regenerated catalysts had B/X values much reduced than the virgin.

Table 9.2. - Initial B/X of Microwave Plasma Treated Catalysts

Pre-treatment Method	Initial B/X
None (Virgin)	0.74
150°C Treatment	0.40
250°C Treatment	0.55
350°C Treatment	0.16
450°C Treatment	0.26
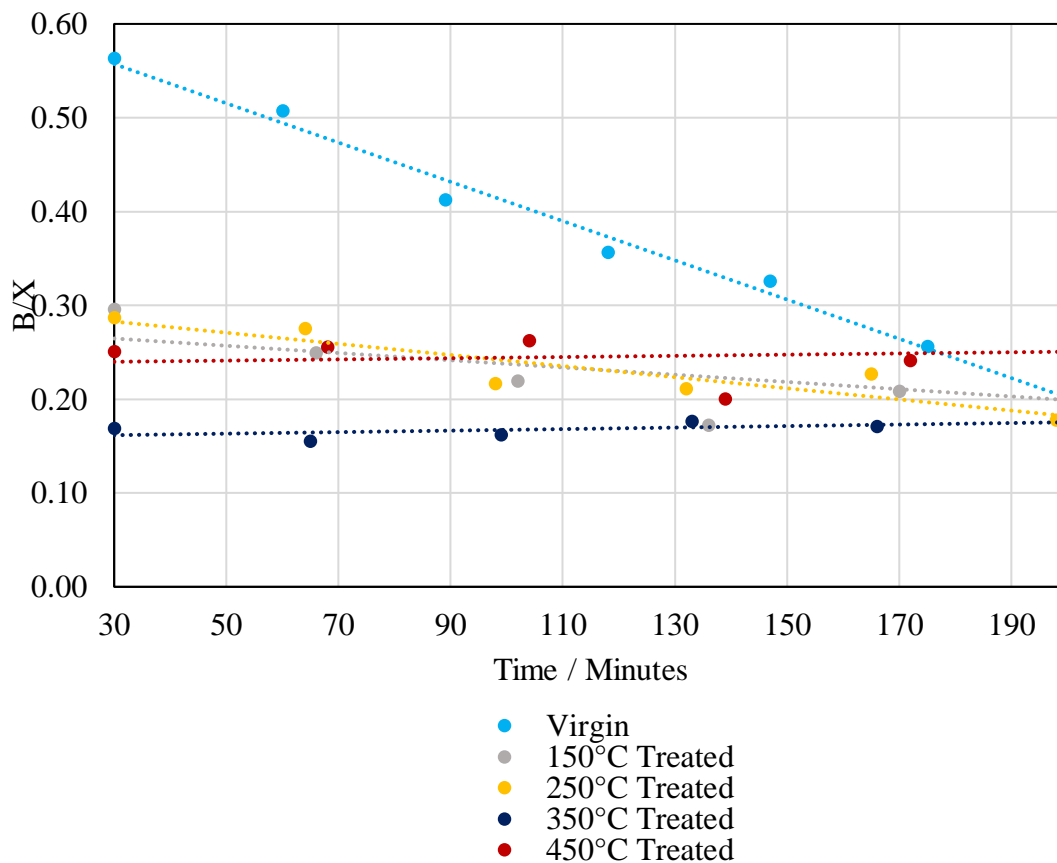
Figure 9.5. - B/X of Microwave Plasma Treated Catalysts

9.3. SURFACE AREA AND AMOUNT OF COKE

The surface area and coke present for each of the coked microwave plasma regenerated catalysts (as determined according to the methods described in Sections 4.2.2. and 4.2.4.) is given in Table 9.3..

Table 9.3. - Surface Area and Coke Present on Microwave Plasma Regenerated Catalysts[a]

	BET Surface Area / m^2g^{-1}	Coke Present / weight %
Virgin[b]	348	4.55
150°C Treated	212	3.15
250°C Treated	229	2.34
350°C Treated	159	0.15
450°C Treated	155	0.14

[a] *Surface areas given are prior to second deactivation*

[b] *Uncoked virgin BET Surface Area: 189 m^2 g^{-1}*

As can be seen from Table 9.3., the BET surface area of the microwave plasma treated catalysts regenerated with a wall temperature between 150-250°C displayed a higher surface area compared with the coked virgin sample. In contrast, the microwave plasma treated catalysts regenerated with a wall temperature between 350-450°C displayed a lower surface area compared with the coked virgin sample. All samples possessed a lower surface area than the uncoked virgin sample.

From the coke data given in Table 9.3., it can be seen that the amount of coke deposited on the regenerated catalysts decreased with regeneration wall temperature. Furthermore, in the regenerations at a temperature of 350°C-450°C, coke deposition is almost negligible.

9.4. X-RAY DIFFRACTION

XRD was carried out on the microwave plasma regenerated samples to determine whether the exposure of mordenite samples to microwave plasma regeneration at increasing energy input levels had any significant effect on the catalytic crystal structure. The results of this are given in Figures 9.6.-9.9., with the regenerated samples laid over virgin mordenite to aid in visualisation of any changes which may have occurred.

There is little difference in the diffractograms of the virgin and lower temperature MWPR treatments shown in Figures 9.6. and 9.7. (i.e. wall temperatures of 150°C and 250°C). The diffractograms show characteristic mordenite peaks (1), with negligible change in peak position and very little peak broadening. Any minor loss of intensity in these materials might be attributed to a systematic sample displacement and for the purpose of this analysis is insignificant.

There is however a considerable difference in the diffractograms of the higher temperature MWPR treatments shown in Figures 9.8. and 9.9. (i.e. wall temperatures of 350°C and 450°C) compared with the virgin material. These diffractograms display a significant decrease of peak intensity and although the main characteristic mordenite peaks can be seen, there is noticeable peak broadening, at the larger angles (i.e. 35-80°) in particular.
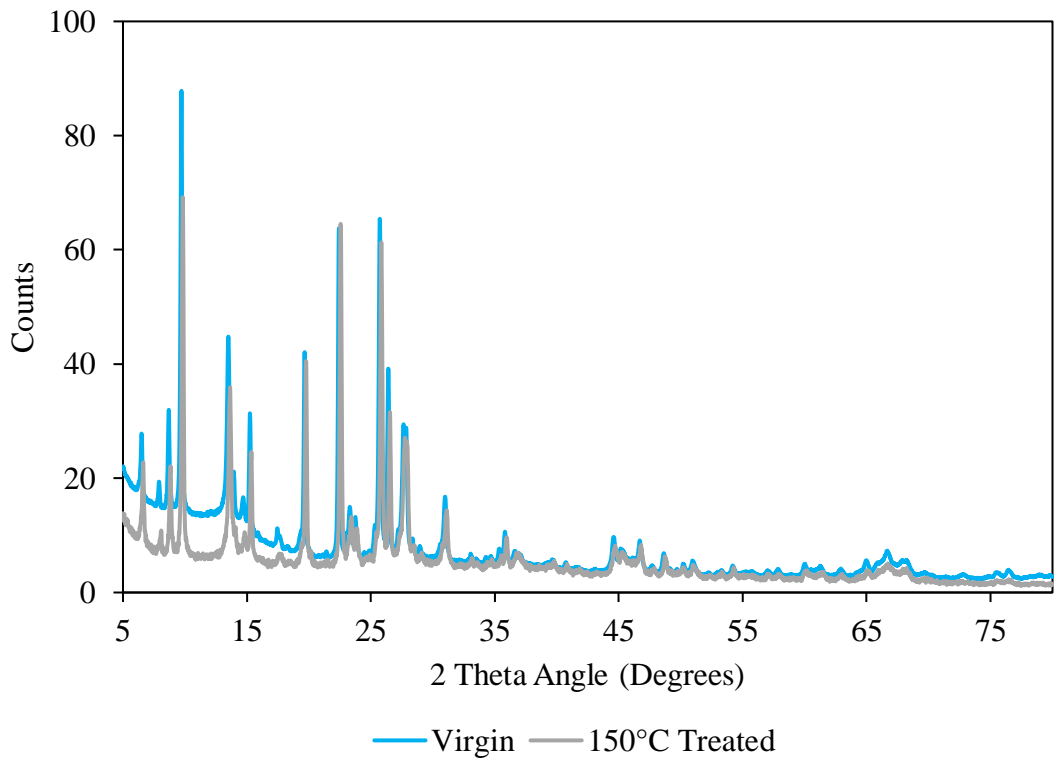
Figure 9.6. - XRD Diffractogram of MWPR Mordenite at a Wall Temperature of 150℃
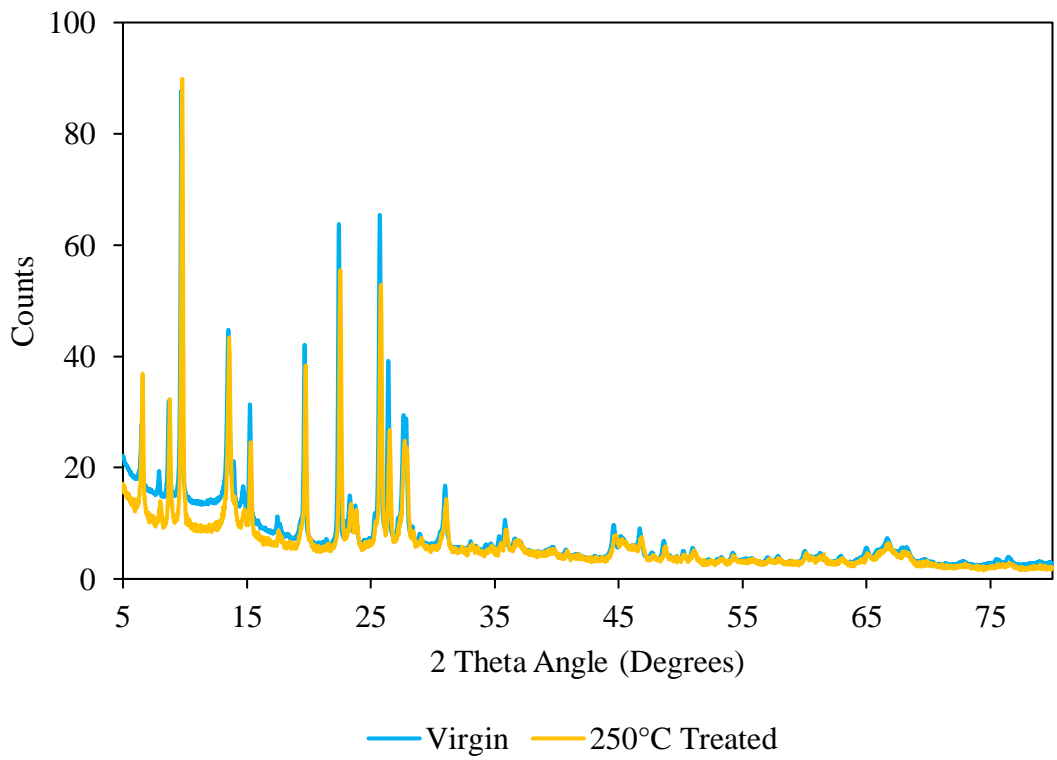
Figure 9.7. - XRD Diffractogram of MWPR Mordenite at a Wall Temperature of 250℃
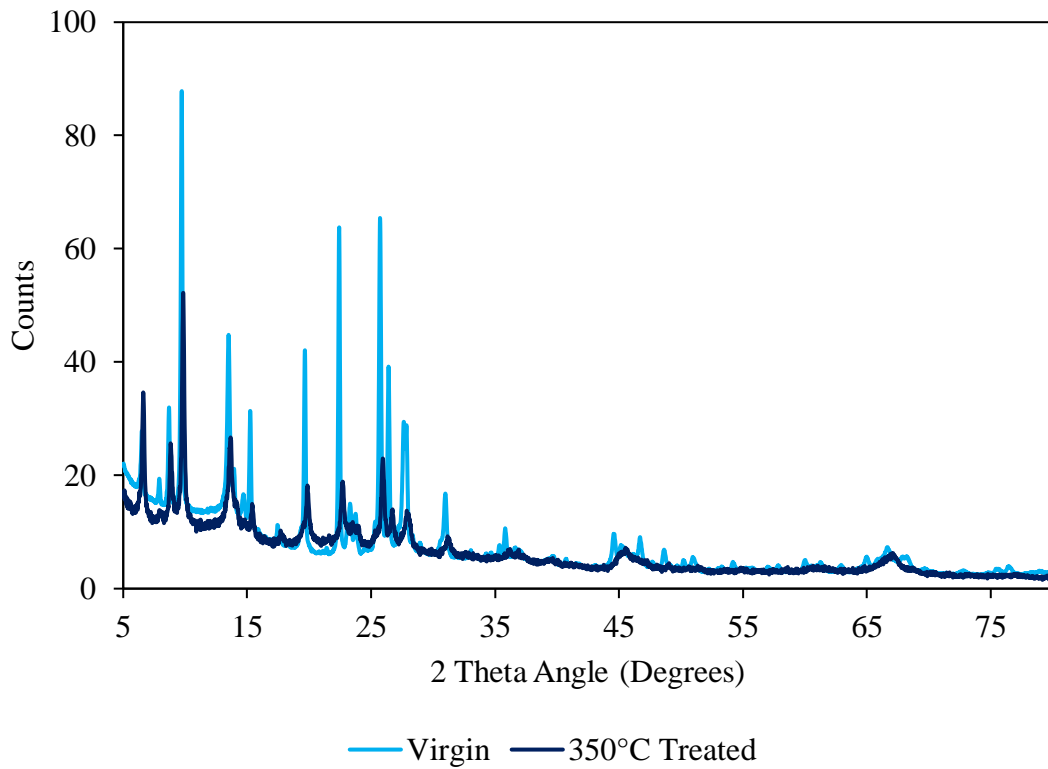
Figure 9.8. - XRD Diffractogram of MWPR Mordenite at a Wall Temperature of 350℃
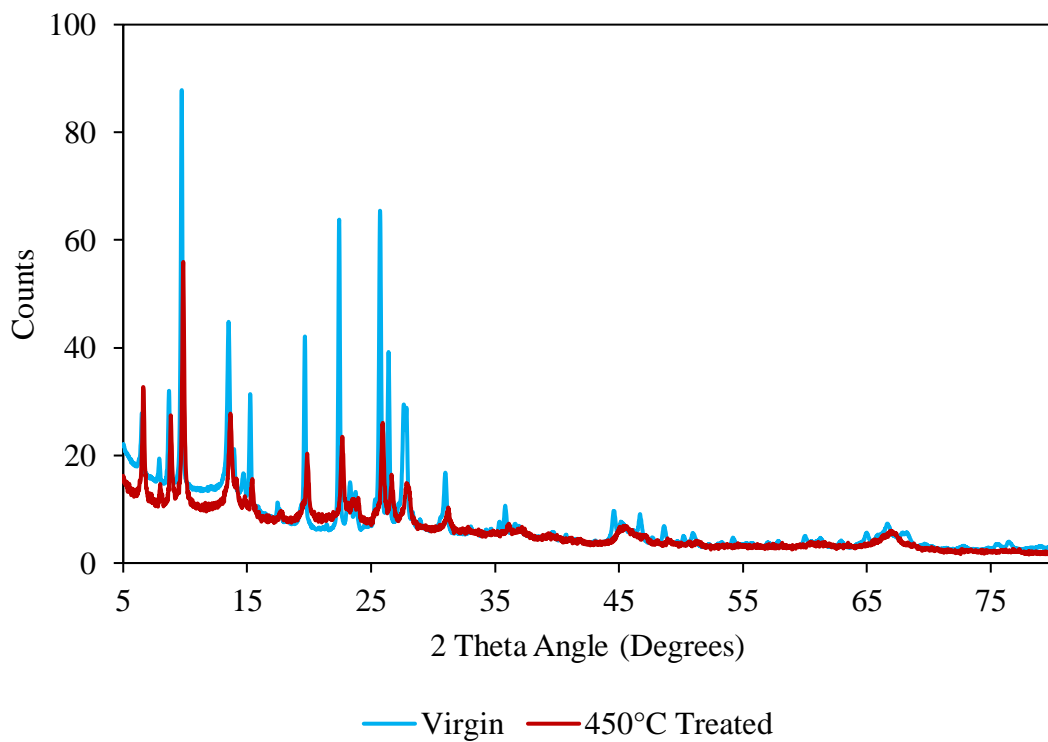
Figure 9.9. - XRD Diffractogram of MWPR Mordenite at a Wall Temperature of 450℃

9.5. SOLID STATE NUCLEAR MAGNETIC RESONANCE

ssNMR studies were performed to determine the impact the exposure of mordenite samples to microwave plasma regeneration at increasing energy input levels had on catalytic acidity. Figure 9.10. depicts the ^{27}Al ssNMR data of the MWPR materials treated, labelled by their respective wall temperatures.

The ^{27}Al NMR in Figure 9.10. displays two crucial peaks for each sample: 54 ppm and 0 ppm, representing framework and extra-framework aluminium (EFAl) respectively (2). The peaks seen at 100 ppm and -75 ppm are spinning side bands, and the broader peaks at 75 ppm 10 ppm are attributed to the aluminium in the γ-alumina binder. The EFAl is over-shadowed by the aluminium from the γ-alumina binder, therefore a magnified image of the EFAl peak at 0 ppm is given in Figure 9.11..

From Figure 9.11., a decrease in framework aluminium corresponding to increasing wall temperature can be seen. Figure 9.11. exhibits a significant decrease in EFAl for the MWPR catalysts, with no EFAL seen in the 350℃ and 450℃ samples.
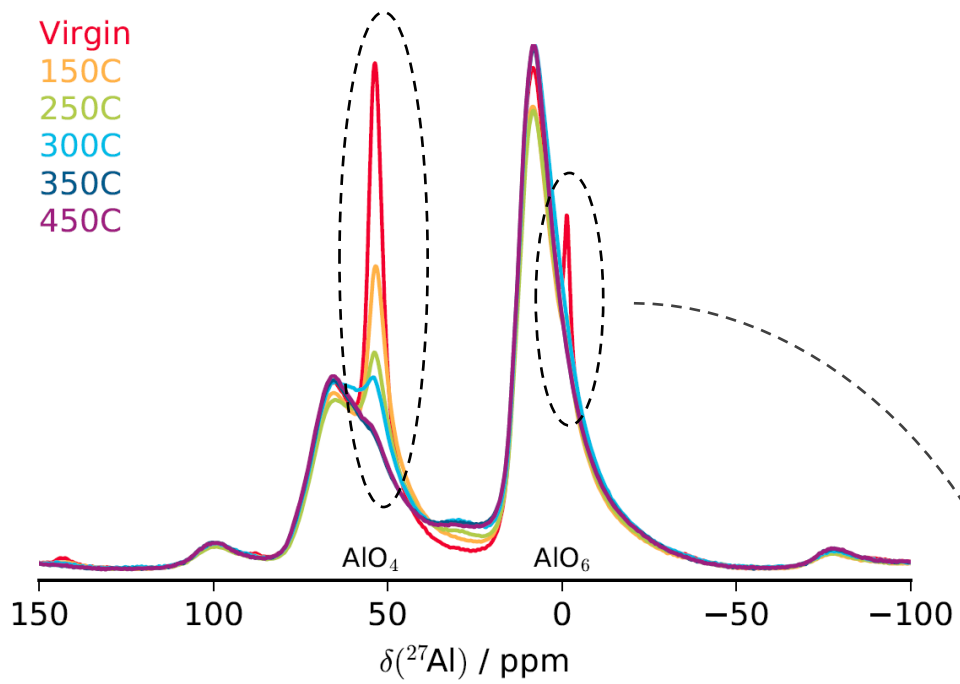
Figure 9.10. – ^{27}Al MAS ssNMR of MWPR Catalysts
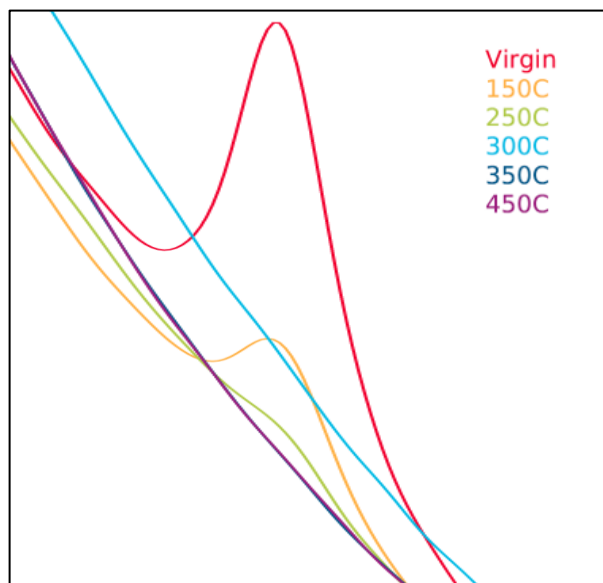
Figure 9.11. – Magnified 0 ppm Region of ^{27}Al MAS ssNMR of MWPR Catalysts

9.6. REFERENCES

(1) Lafuente B, Downs RT, Yang H, Stone N. Mordenite R061118. 2015; Available at: http://rruff.info/Mordenite/R061118. Accessed 02/28, 2019.

(2) Hannus I, Fonseca A, Kiricsi I, Nagy JB, Fejes P. ^{29}Si and ^{27}Al MAS NMR Investigation of H-mordenite Dealuminated with Phosgene. Studies in Surface Science and Catalysis 1995;94:155-162.

CHAPTER 10: POWER STUDIES II - DISCUSSION

10.1. INTRODUCTION

Studies on the application of plasma for the regeneration of catalysts is limited. The investigations which have been performed cite speed as a key advantage (1). The power studies performed explored the impact of increasing the input energy to determine whether power could be optimised for rapid and efficient regeneration of deactivated mordenite samples.

10.2. SURFACE AREA AND AMOUNT OF COKE

The deactivation of mordenite samples in toluene disproportionation can be produced via the deposition of carbonaceous material on the surface, in the channel intersections and cavities of the zeolite (2-4). Typically, the deposition of coke leads to a decrease in surface area (5-8), however this is not necessarily the only cause. The surface area and amount of carbonaceous deposits of coked MWPR mordenite samples are given in Table 9.3.. A deactivated virgin sample of mordenite exhibited a surface area of approximately 190 m^2 g^{-1}, with a deposition of approximately 4.5 % by weight of carbonaceous material. The MWPR coked samples of mordenite regenerated with a wall temperature of 150°C and 250°C, underwent less coking than the virgin deactivation, with approximately 3.2 and 2.3 % by weight of carbonaceous material, respectively. Correspondingly, these samples also exhibited a surface area higher than the deactivated virgin sample. In contrast, the MWPR coked samples of mordenite regenerated with a wall temperature of 350°C and 450°C exhibited a lower surface area compared with virgin, albeit these samples displayed negligible amounts of coke (< 0.2 %). The reason behind this can be seen from the X-ray diffraction data (Figures 9.6.-9.9.). Whilst the lower wall temperature MWPR catalysts (i.e. 150-250°C) exhibited little change in crystal structure, the higher wall temperature MWPR catalysts (i.e. 350-450°C) displayed a significant loss of intensity and some peak broadening. This demonstrates a considerable loss of crystallinity to the higher wall temperature MWPR catalyst samples, which would partially destroy the catalyst surface area. The

loss of zeolite structure and surface area would heavily suggest a loss of surface acidity, which would also account for the negligible amount of coke deposited on these samples.

10.3. SOLID STATE NUCLEAR MAGNETIC RESONANCE

The ^{27}Al MAS ssNMR performed on the MWPR catalysts (Figures 9.10. and 9.11.) display a shift in the amount of aluminium present compared with the virgin sample. Figure 9.10. exhibits two peaks arising from framework (54 ppm) and extra-framework (0 ppm) aluminium (9). There is a significant decrease in framework aluminium seen in the MWPR catalysts compared with the virgin sample, corresponding to increase in wall temperature. This is indicative of dealumination. Moreover, the higher wall temperature MWPR samples do not exhibit any tetrahedral framework aluminium. During dealumination, tetrahedral aluminium is removed and a proportion of it is known to be deposited in the pores as octahedral extra-framework species (10). However, the EFAl of the zeolite samples is overshadowed by the aluminium found in the γ-alumina binder making it difficult to determine the amount of EFAl species formed. Nevertheless, Figure 9.11. displays a higher amount of EFAl species for the virgin sample compared to the MWPR samples. There is some EFAl species present in the lower wall temperature MWPR samples, however no EFAl species can be identified for the higher wall temperature MWPR samples. Whilst the lack of EFAl species for the higher wall temperature MWPR samples could be attributed to the destruction of the zeolite structure seen from the XRDs (Figures 9.8. and 9.9.), it is somewhat surprising not to see more EFAl for the lower wall temperature MWPR samples. Further studies would need to be performed to explain this, e.g. XPS, Pyridine IR or NH$_3$ TPD.

10.4. CATALYST ACTIVITY

10.4.1. Sample of Mordenite Regenerated at a Wall Temperature of 150°C

The activity of the sample of mordenite which had undergone MWPR at a wall temperature of 150°C, had a similar activity profile as the virgin sample, although the rate of deactivation was higher, and the initial activity was reduced. These differences can be attributed to incomplete regeneration, which was seen visually from cross-sectioning the catalyst (Figure 10.1.). The shape

of the activity profile was unlikely to differ from the virgin sample as the XRD results (Figure 9.6.) and retention of surface area (Table 9.3.) illustrated the regeneration process had not damaged the crystal structure.

The initial B/X of the MWPR sample with a wall temperature of 150°C (Figure 9.1.) was

Figure 10.1. - Cross-Section of Mordenite Sample MWPR at a Wall Temperature of 150°C

approximately half the value of the virgin sample (Table 9.2.). This might be attributed to the significant loss of framework aluminium seen from the NMR results (Figure 9.10.), indicating a possible loss of acid sites. Fewer acid sites available for cracking, would reduce the B/X and would also explain the reduction in the coking rate seen by the TGA results (Table 9.3.). However, further studies would need to be performed to confirm this, e.g. Pyridine IR.

10.4.2. Sample of Mordenite Regenerated at a Wall Temperature of 250°C

The activity of the sample of mordenite which had undergone MWPR at a wall temperature of 250°C (Figure 9.2.), exhibited a different activity profile from the sample regenerated at a wall temperature of 150°C and the virgin sample (Figure 9.1.), with a much-reduced deactivation rate. The initial activity was the same as the virgin sample (55 %), indicating the microwave plasma treatment had fully regenerated the catalyst. As the surface area was retained (Table 9.3.) and XRD results (Figure 9.7.) exhibited no destruction of the crystalline structure, the reduction in deactivation rate is most likely attributed to a reduced concentration of acid sites, likely to be produced from the significant dealumination seen by the ssNMR results (Figure 9.10.). A reduction in acid sites would lead to the lower coking rate seen by the TGA (Table 9.3.), and the

reduction of the initial B/X compared with the virgin sample. As the sample which was MWPR at 250°C exhibited a greater amount of dealumination than the sample which was MWPR at 150°C, the initial B/X would be expected to be lower for the sample which had undergone more dealumination, i.e. MWPR at 250°C. However, the results show that the initial B/X of the 250°C MWPR sample was higher. The reason for this, is likely due to the incomplete regeneration of the 150°C MWPR sample, where the remaining coke could be blocking the acid sites, reducing their availability for cracking.

10.4.3. Sample of Mordenite Regenerated at a Wall Temperature of 350°C

The activity of the sample of mordenite which had undergone MWPR at a wall temperature of 350°C (Figure 9.3.), exhibited a similar activity profile to the sample of mordenite which had undergone MWPR at a wall temperature of 250°C (Figure 9.2.), although with a much-reduced initial activity. The heavily reduced surface area (Table 9.3.) and XRD results (Figure 9.8.) illustrate the destructive nature of the regeneration treatment on the crystal structure of the catalyst. The loss of crystallinity leads to destruction of the acid sites, seen from the significantly low B/X ratio compared with the virgin sample and corresponding lack of coke deposition seen from the TGA results (Table 9.3.). The NMR results support this, displaying a negligible amount of framework aluminium.

10.4.4. Sample of Mordenite Regenerated at a Wall Temperature of 450°C

Similarly, the destruction of the crystal structure seen in the sample of mordenite MWPR at a wall temperature of 350°C (Figure 9.3.) was echoed in the sample of mordenite MWPR at a wall temperature of 450°C (Figure 9.4.). However, in this case, the activity of the sample of mordenite which had undergone MWPR at a wall temperature of 450°C was effectively completely destroyed (toluene conversion <5 %).

10.5. REFERENCES

(1) Mok YS, Jwa E, Hyun YJ. Regeneration of C_4H_{10} Dry Reforming Catalyst by Nonthermal Plasma. Journal of Energy Chemistry 2013 MAY 2013;22(3):394-402.

(2) Bhatia S, Beltramini J, Do DD. Deactivation of Zeolite Catalysts. Catalysis Reviews: Science and Engineering 2008;31(4):431-480.

(3) Bibby D, Milestone NB, Patterson JE, Aldridge LP. Coke Formation in Zeolite ZSM-5. Journal of Catalysis 1986;97:493-502.

(4) Tsai TC, Chen WH, Lai CS, Liu SB, Wang I, Ku CS. Kinetics of Toluene Disproportionation Over Fresh and Coked H-Mordenite. Catalysis Today 2004 NOV 3 2004;97(4):297-302.

(5) Querini CA. Chapter 4 - Coke Characterization - 13 - Sorption Capacity: Surface Area and Pore Volume. In: Spivey JJ, Roberts GW, editors. Catalysis. First ed. United Kingdom: RSC; 2004. p. 197-199.

(6) Soni HS, Samuel V, Ramaswarmy AV. Locartion of Coke in ZSM-5 and HY Zeolite Catalysts used in Ethylation Reaction from Micropore Size Distribution Analysis. Indian Journal of Chemistry 1994;33:844-846.

(7) Gao Y, Zheng B, Wu G, Ma F, Lui C. Effect of the Si/Al Ratio on the Performance of Hierarachical ZSM-5 Zeolites for Methanol Aromatization. RSC Advances 2016;6(87):83581-83588.

(8) Chua LM, Hitchcock I, Fletcher RS, Holt EM, Lowe J, Rigby SP. Understanding the Spatial Distribution of Coke Deposition Within Bimodal Micro-/Mesoporous Catalysts Using a Novel Sorption Method in Combination with Pulsed-Gradient Spin-Echo NMR. Journal of Catalysis 2012;286:260-265.

(9) Hannus I, Fonseca A, Kiricsi I, Nagy JB, Fejes P. 29Si and 27Al MAS NMR Investigation of H-mordenite Dealuminated with Phosgene. Studies in Surface Science and Catalysis 1995;94:155-162.

(10) Debras G, Nagy JB, Gabelica Z, Bodart P, Jacobs PA. Determination of Silicon-Aluminium Orderings in Mordenite and its Aluminium Deficient Forms Using High-Resolution Magic-Angle-Spinning ^{29}Si-NMR. Chemistry Letters 1983;12(2):199-202.

CHAPTER 11: OVERALL DISCUSSION

11.1. INTRODUCTION

Results from the novel regeneration and pre-treatment methods were given and discussed in comparison to virgin and thermal methods in previous chapters. This chapter aims to discuss any differences between the novel regeneration and pre-treatment processes in comparison to one another. Through this, an understanding of the interactions the novel processes have on the catalysts with or without coke can be developed. For ease of comparison, the surface areas of the regenerated and pre-treated catalysts are given in Table 11.1., the coke present on the deactivated regenerated and pre-treated catalysts is given in Table 11.2., and the concentration of acid sites determined via pyridine and collidine IR is given in Table 11.3..

Table 11.1. - Surface Area ($m^{-2}\ g^{-1}$) of Regenerated and Pre-treated Catalysts

	Regeneration		Pre-treatment	
	Uncoked	**Coked**	**Uncoked**	**Coked**
Virgin	348	189	348	189
Thermal	352	190	N/A	
Microwave	259	210	188	153
Microwave Plasma	333	158	335	245
DBD Plasma	290	186	339	194

Table 11.2. – Coke Present (% by Weight) on Deactivated Regenerated and Pre-treated Catalysts

	Regeneration	Pre-treatment
Virgin	4.55	4.55
Thermal	3.37	N/A
Microwave	2.39	1.32
Microwave Plasma	3.05	2.28
DBD Plasma	4.49	5.09

Table 11.3. – Concentration of Acid Sites ($\mu mol\ m^{-2}\ g^{-1}$) on Deactivated Regenerated and Pre-treated

		Virgin	Thermally Regenerated	Microwave		Microwave Plasma	
				Regenerated	**Pre-treated**	**Regenerated**	**Pre-treated**
Pyridine	**BAS**	0.5	0.42	0.32	0.18	0.37	0.10
	LAS	0.45	0.47	0.43	0.33	0.50	0.37
	B/L	1.1	0.9	0.7	0.5	0.7	0.30
Collidine	**BAS**	0.24	0.18	0.15	0.17	0.13	0.07

11.2. DIELECTRIC BARRIER DISCHARGE PLASMA

11.2.1. Surface Area

The surface areas of the DBD plasma regenerated sample and the DBD plasma pre-treated sample are given in Table 11.1.. The difference between the surface area of the uncoked DBD plasma regenerated sample (290 m^2 g^{-1}) and DBD plasma pre-treated sample (339 m^2 g^{-1}) can be attributed to the presence of coke on the regenerated sample. Whilst the XRD data for the DBD plasma samples (Figure 11.1.) shows no difference between the two treatments, the DBD plasma regenerated sample was shown to retain 2.20 % by weight of coke (Table 5.2.) after regeneration, in comparison to the pre-treated sample which possessed no coke. Whilst it might therefore be expected that the DBD plasma regenerated sample would exhibit more coke upon deactivation than the DBD plasma pre-treated sample, this is not the case. Furthermore, the surface area of the deactivated DBD plasma regenerated sample (186 m^2 g^{-1}) compared with the deactivated DBD plasma pre-treated sample (194 m^2 g^{-1}) is surprisingly similar in comparison to their difference in coke deposited (4.49 and 5.09 % by weight, respectively). Whilst the cause of this is unknown, it might be due to the mechanism of coke deposition. Coke deposition is a shape selective process (1), and as there is already coke present on the DBD plasma regenerated catalyst, it may act as a barricade, blocking access to areas of the catalyst which might hamper further coke lay down.
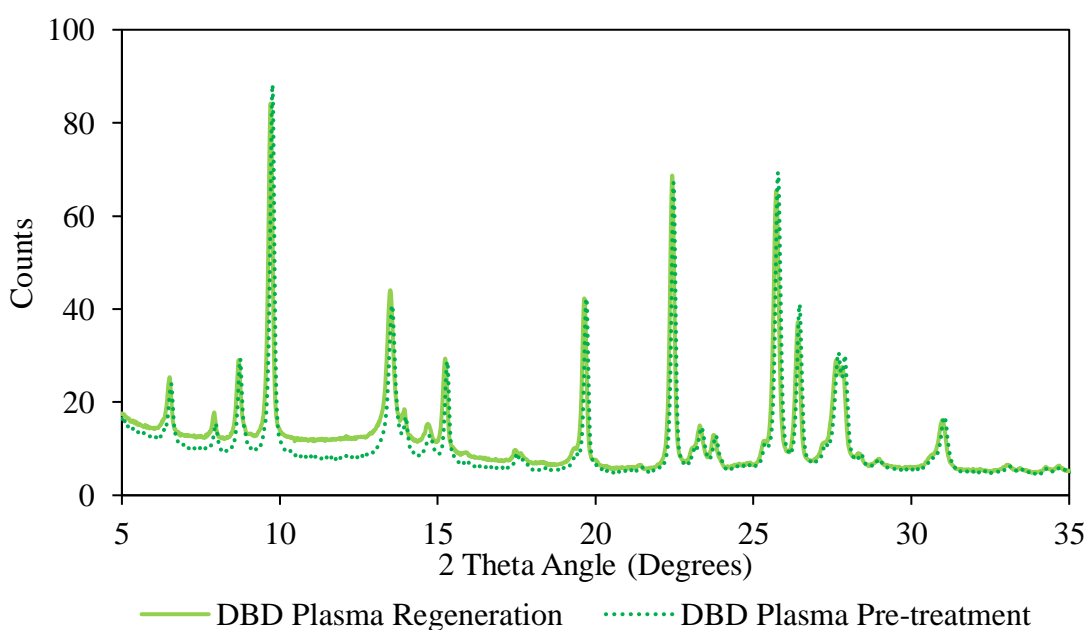
Figure 11.1. – XRD Diffractogram of DBD Plasma Regenerated and Pre-treated Catalysts

11.2.2. Catalyst Activity

The activity of DBD plasma regenerated and DBD plasma pre-treated samples of mordenite are given in Figure 11.2.. Virgin data was omitted as it was identical to the DBD pre-treatment. From Figure 11.2. it can be seen that the rate of deactivation of the regenerated sample (0.523 % min^{-1}) is much more rapid than the rate of deactivation of the pre-treated sample (0.33 % min^{-1}) (Table 11.4.). This is explained by the incomplete regeneration of the regenerated sample, as compared with the virgin sample (Figure 7.3.), the DBD pre-treated sample is almost identical. Furthermore, the initial B/X (Table 11.4.) of the DBD plasma treated samples is very similar, both to each other and the virgin (Tables 5.2. and 7.2.) indicating no change in acid sites, although this would need to be confirmed, e.g. NH$_3$TPD or pyridine/collidine IR studies.
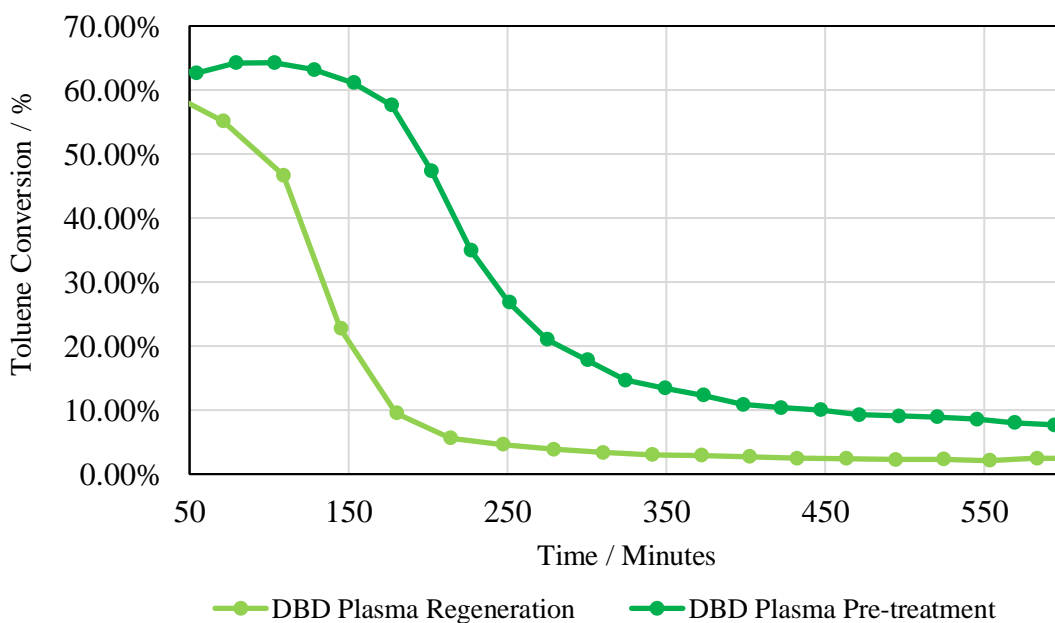
Figure 11.2. – Activity Plot of DBD Plasma Regenerated and Pre-treated Catalysts

Table 11.4. – Rate of Deactivation and Initial B/X of DBD Plasma Regenerated and Pre-treated Catalysts

	Regenerated	Pre-treated
Rate of Deactivation / % min^{-1}	0.52	0.33
Initial B/X	0.61	0.58

11.2.3. Summary

From the results of the DBD plasma treated catalysts, it can be seen that there is very little difference produced between them, and similarly compared with the virgin catalyst. The discrepancy between the amount of coke present on the regenerated and pre-treated samples is due to the incomplete regeneration of the DBD plasma regenerated catalyst, which also affected the surface area of the catalyst. The absence of change in initial B/X (Table 11.4.) suggests no change in acid sites, and the XRD results (Figure 11.1.) indicates no loss of crystalline structure. It appears, under the conditions used, that the DBD plasma treatments were insufficiently strong enough to penetrate the zeolite, leading to incomplete regeneration of the catalyst. In all other conditions, the zeolite remains effectively unchanged in comparison to the virgin catalyst.

11.3. MICROWAVE HEATING

11.3.1. Surface Area

There is a significant difference between the surface areas of both coked and uncoked mordenite samples exposed to microwave processes, as shown in Table 11.1.. The microwave regenerated catalyst retained more surface area (259 $m^2\,g^{-1}$) compared with the virgin catalyst (348 $m^2\,g^{-1}$) prior to deactivation, than the microwave pre-treated catalyst (188 $m^2\,g^{-1}$). This would suggest a more significant loss in the crystal structure for the pre-treated catalyst. However, whilst both microwave treatments have noticeably lost structural integrity compared with the virgin sample, seen from the XRD results (Figures 5.14. and 7.9.), there is no visible difference on the diffractogram to distinguish between the two microwave treatments (Figure 11.3.). With that said, observations during the experiments would suggest the pre-treatment was a harsher process, as catalyst sample was seen to fuse together (Figure 8.1.). This fusion of sample was not observed for the microwave regeneration. However, observations during preliminary microwave regeneration highlighted the non-uniformity of the microwave treatment (Figure 4.21.). Although best efforts were taken to analyse the extrudate which wasn't visibly sintered, the methods use only a fraction of the sample, assuming uniformity across the sample which was not the case. To

conclusively compare the microwave regeneration and microwave pre-treatments, these characterisation techniques would need to be repeated multiple times with the entirety of the sample.
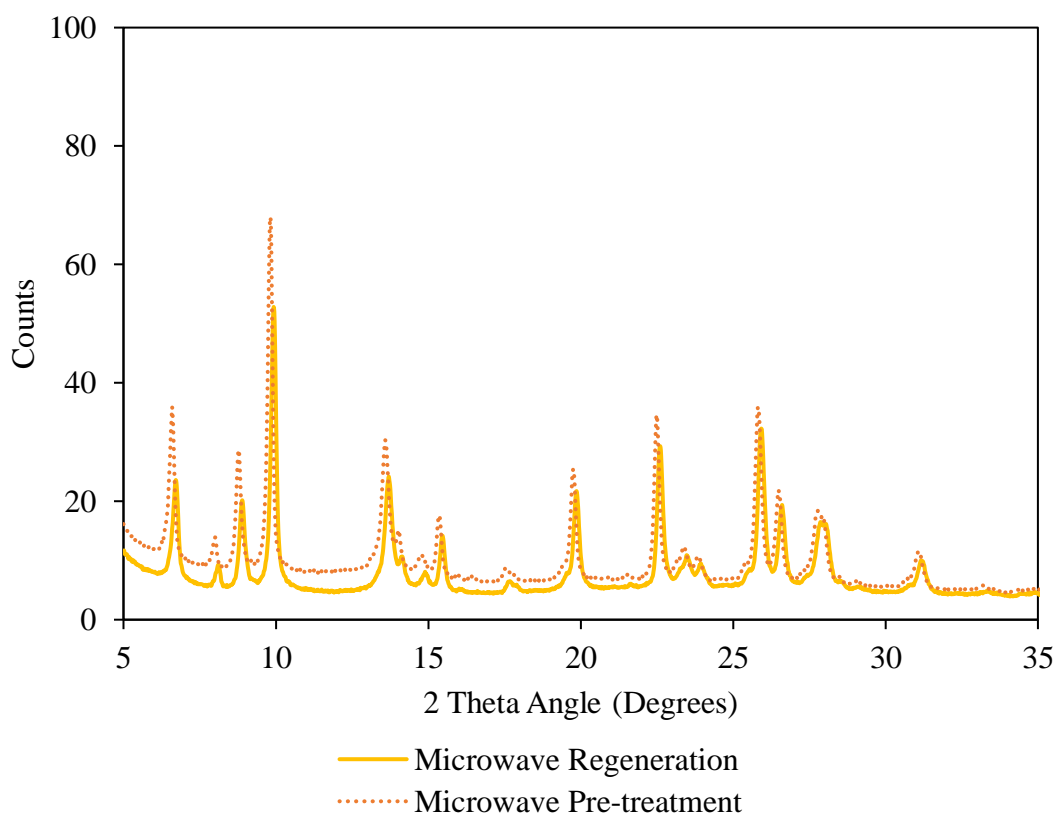
Figure 11.3. – XRD Diffractogram of Microwave Regenerated and Pre-treated Catalysts

11.3.2. Catalyst Acidity

The amount of coke present on the microwave treated catalysts (Table 11.2.), whilst lower than the virgin catalyst (4.55 % by weight) was significantly different. The microwave regenerated sample was subjected to a higher amount of coking (2.39 % by weight) than the microwave pre-treated sample (1.32 % by weight). The decrease in coking compared with the virgin was explained, in the previous discussions, as a result of sintering. However, the difference between the two microwave treatments can be seen from the acidity data. The IR results (Table 11.3.) display a higher concentration of BAS for the microwave regenerated sample ($0.32 \, \mu mol \, m^{-2} \, g^{-1}$) than the microwave pre-treated sample ($0.18 \, \mu mol \, m^{-2} \, g^{-1}$). The higher concentration of BAS seen in the microwave regenerated sample would produce more cracking, leading to a higher amount of coke deposited, compared with the microwave pre-treated sample. In contrast, the NH_3 TPD

results (Figure 11.4.), may suggest a lower concentration of acid sites in the microwave regenerated sample. However, the h-peak in the microwave sample is not clearly visible and could be seen as overlapping with the l-peak. Further studies would need to be undertaken to confirm the difference in acid sites between the two samples, e.g. ssNMR.
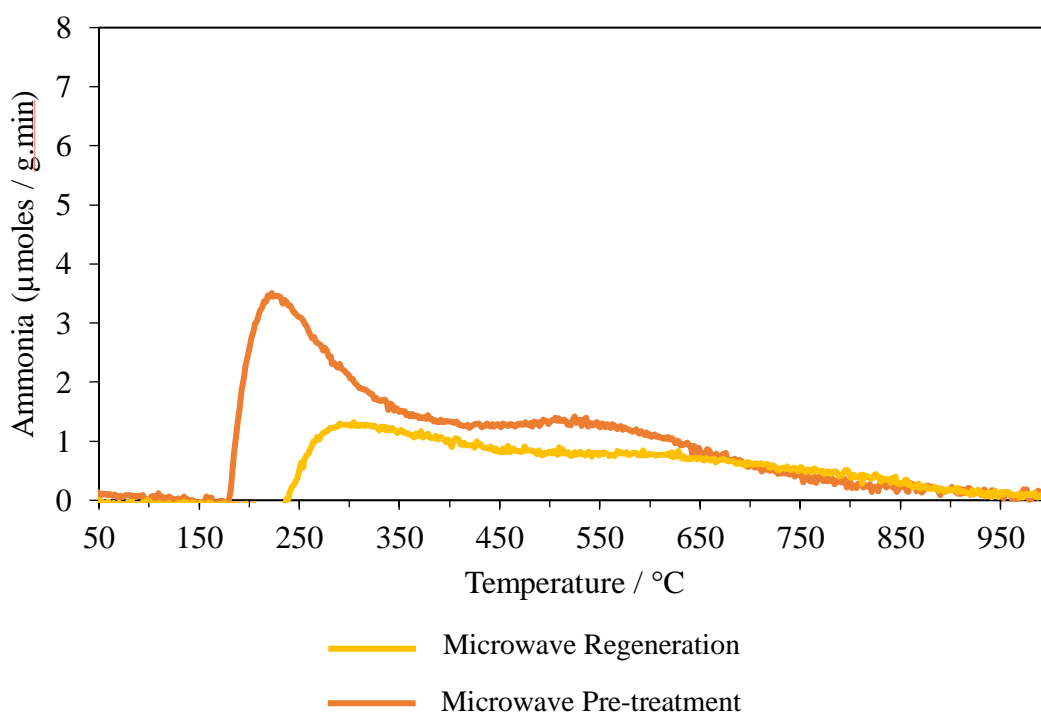
Figure 11.4. – NH₃ TPD of Microwave Regenerated and Pre-treated Catalysts

11.3.3. Catalyst Activity

The catalytic activity for samples of microwave regenerated and microwave pre-treated mordenite are given in Figure 11.5., with the rate of deactivation and initial B/X given in Table 11.5.. From this data it can be seen that the microwave pre-treated catalyst has a lower initial toluene conversion (54 %) compared with the microwave regenerated catalyst (63 %). This is most likely a result of the degree of sintering caused, where fewer active sites remain to catalyse the reaction. The rate of deactivation was the same for both samples, despite their difference in the amount of coke deposited (Table 11.2.). This is not unexpected as it would take less coke to block the fewer number of acid sites in the microwave pre-treated catalyst than in the microwave regenerated catalyst. This is furthermore supported, by the difference in the initial B/X (Table 11.5.).
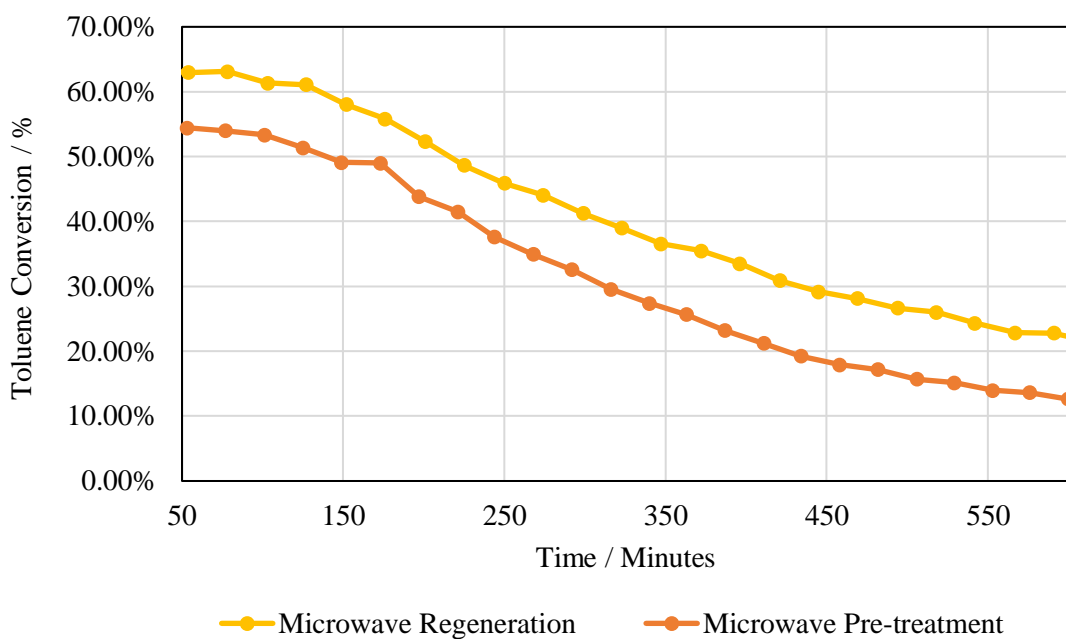
Figure 11.5. – Activity Plot of Microwave Regenerated and Pre-treated Catalysts

Table 11.5. – Rate of Deactivation and Initial B/X of Microwave Regenerated and Pre-treated

Catalysts

	Regenerated	Pre-treated
Rate of Deactivation / % min^{-1}	0.088	0.087
Initial B/X	0.36	0.27

11.3.4. Summary

The differences between microwave regenerated and microwave pre-treated samples of mordenite were discussed. There were differences in the surface areas of the catalysts, the amount of carbon deposited and the concentration of BAS. However, the activity of the catalysts was similar. The differences seen could be attributed to varying degrees of sintering caused by the harsh processes, where the microwave pre-treatment appeared to be harsher, seen from the lower surface area (Table 11.1.), lower concentration of BAS (Table 11.3.) and visually (Figure 8.1.). This might be expected, as the direct interaction of the microwaves with the catalyst, would not be reduced by the presence of coke. Ultimately, the use of microwaves as a method of pre-treatment or

regeneration of mordenite for toluene disproportionation, under the conditions used is too harsh to be considered viable.

11.4. MICROWAVE PLASMA

11.4.1. Surface Area

From Table 11.1. no significant changes can be seen in the surface areas of the uncoked microwave plasma regenerated (333 m^2 g^{-1}) and pre-treated (335 m^2 g^{-1}) samples. In contrast, there is a considerable difference between the surface areas of the coked microwave plasma samples. A third of the surface area is lost during toluene disproportionation in the pre-treated sample (245 m^2 g^{-1}), whereas the surface area of the regenerated sample decreased by half (158 m^2 g^{-1}). The change in surface area is reflected in the difference of coke deposited on the samples (Table 11.2.), with more coke present on the regenerated sample (3.05 % by weight), and less coke present on the pre-treated sample (2.28 % by weight). The retention of surface area of the microwave plasma samples prior to deactivation can be explained by the XRD results (Figure 11.6.). There is little difference seen between the diffractograms of the two samples, indicating no significant structural changes between the two samples, which was also true when compared with the virgin sample (Figures 5.15. and 7.10.).
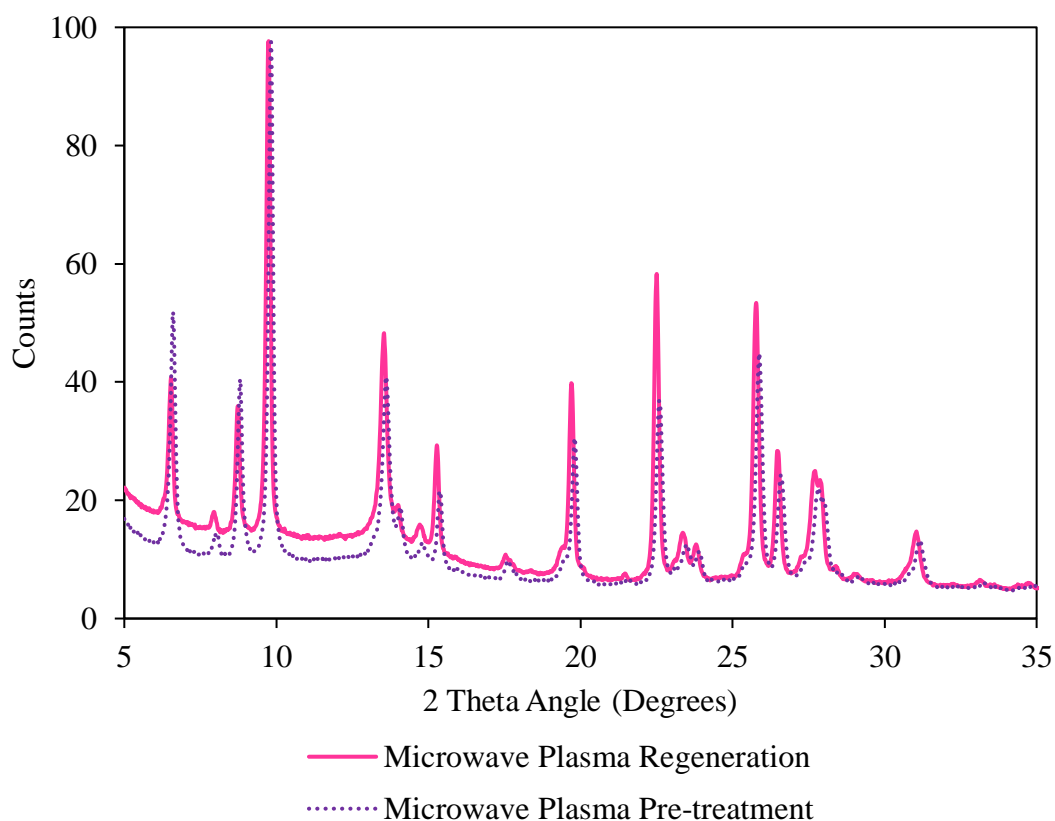
Figure 11.6. – XRD Diffractogram of Microwave Plasma Regenerated and Pre-treated Catalysts

11.4.2. Catalyst Acidity

The NH_3TPD and infrared studies reveal differences in acidity between the microwave plasma regeneration and pre-treatment processes. The NH_3TPD results (Figure 11.7.) exhibit a difference in the concentration of acid sites, with the reduced h-peak peak maximum of the microwave plasma pre-treated catalyst displaying fewer acid sites than the regenerated catalyst. Furthermore, the reduction of h-peak peak maximum of the microwave plasma pre-treated catalyst makes it difficult to determine whether a shift in the acid site strength has occurred. This was not the case for the microwave plasma regenerated sample (as seen in Figure 5.28.), where a minor shift towards weaker acid strength in comparison to the virgin sample was identified. The infrared studies further support a change between the microwave plasma processes, as shown in Table 11.3.. Whilst there is a considerable decrease of Brønsted acidity in the microwave plasma regenerated sample (0.37 µmol m^{-2} g^{-1}) compared to the virgin sample (0.5 µmol m^{-2} g^{-1}), this is much more exacerbated in the microwave plasma pre-treated sample (0.10 µmol m^{-2} g^{-1}).

Furthermore, whilst the loss of Brønsted acidity in the microwave plasma regenerated catalyst was shown to be surface specific (Table 6.2.), the microwave plasma pre-treatment was able to penetrate the catalyst with sufficient energy to destroy internal and external Brønsted acid sites alike. One plausible explanation for this is that during the microwave plasma regeneration treatment, the microwave plasma interacted with the carbon, oxidising it to carbon dioxide and water. In the microwave plasma pre-treatment however, there was no carbon involved, therefore the microwave plasma could only interact with the catalyst. Without the interaction of the microwave plasma with the coke, the catalyst was exposed to the full energy of the plasma, resulting in the destruction of both the internal and external BAS. In terms of the destruction of external BAS during the microwave plasma regeneration, the external surface area of the catalyst was most likely regenerated first. This meant that once the coke had been removed from the surface, the microwave plasma would interact directly with the external surface of the catalyst, causing the destruction of the external BAS. The destruction of the acid sites is most likely due to dealumination, as seen in the ssNMR for the microwave plasma regenerated catalyst (Figures 5.17. – 5.19.). Whilst ssNMR was not carried out on the pre-treated catalyst, the likelihood of dealumination can be speculated from the ssNMR carried out on the power studies (Figures 9.10.-9.11.), where an increase of input energy corresponded to an increased amount of dealumination.

It is the reduction in acidity between the microwave plasma regenerated and pre-treated catalysts which caused the change in the amount of coke deposition between the two samples. With more acid sites, the microwave plasma regenerated catalyst could produce more cracking than the microwave pre-treated sample. A higher cracking rate would be expected to lead to a higher amount of coke deposited, which is what is seen in Table 11.2..
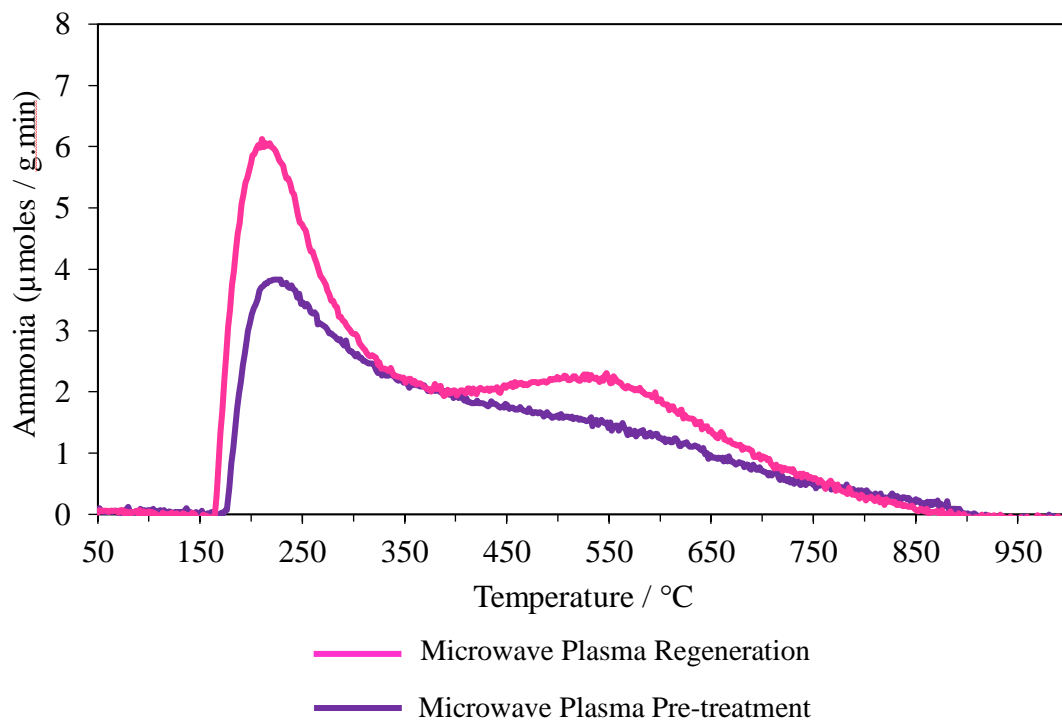
Figure 11.7. – NH₃TPD of Microwave Plasma Regenerated and Pre-treated Catalysts

11.4.3. Catalyst Activity

The activity data for a sample of microwave plasma regenerated and a sample of microwave plasma pre-treated mordenite is given in Figure 11.8.. From this it can be seen that the activity appears to be the same for both microwave plasma processes. This is confirmed by the rate of deactivation and initial B/X given in Table 11.6., where there is a negligible difference between the samples.
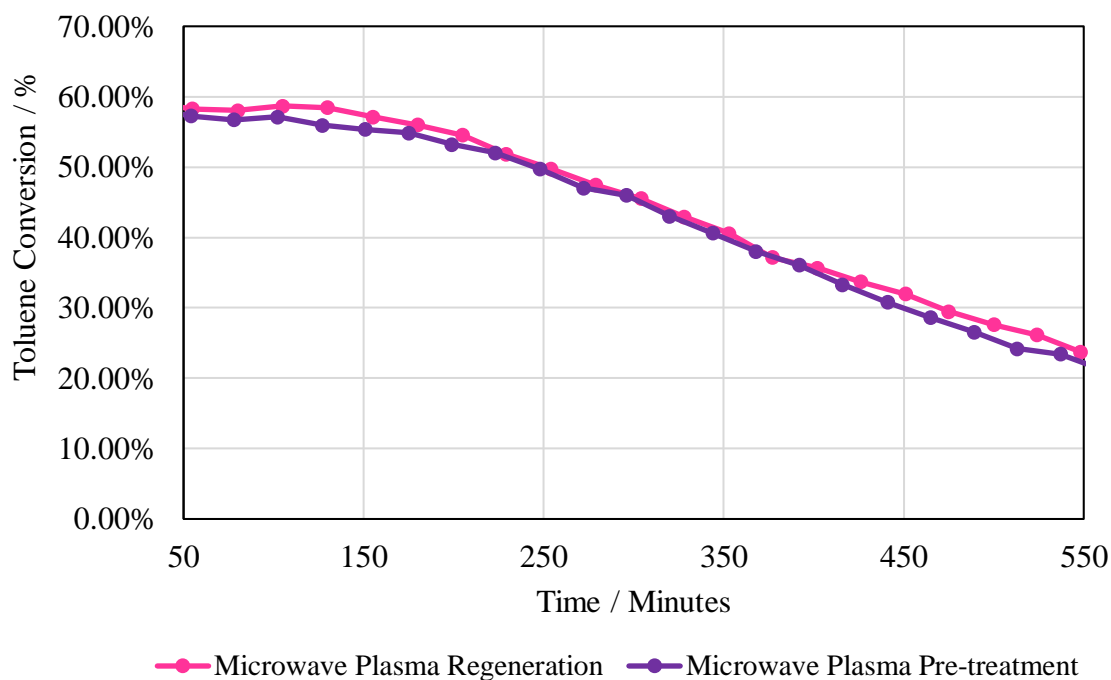
Figure 11.8. – Activity Plot of Microwave Regenerated and Pre-treated Catalysts

Table 11.6. - Rate of Deactivation and Initial B/X for Microwave Plasma Regenerated and Pre-treated Catalysts

	Regenerated	Pre-treated
Rate of Deactivation / % min^{-1}	0.085	0.087
Initial B/X	0.35	0.32

11.4.4. Summary

The results of microwave plasma regenerated mordenite and microwave plasma pre-treated mordenite samples were compared. From this it can be determined, that although coke deposited on the catalyst during toluene disproportionation reduces the activity of the catalyst, the difference in the amount of coke deposited on the microwave plasma regenerated and microwave plasma pre-treated samples has not had a significant impact. The plasma treatments have not destroyed any crystalline character of the mordenite samples, but they have significantly effected the Brønsted acidity of the catalysts. Whilst the microwave plasma regeneration only destroyed the BAS on the surface of the catalyst, the microwave plasma pre-treatment destroyed the internal BAS as well. This accounts for the difference in coke deposited, as cracking is known to occur

on BAS (2). However, it also demonstrates that the presence of strong BAS, even in diminishing numbers, is sufficient to produce a 60 % toluene conversion under the conditions used in this research. The destruction of BAS is beneficial for this reaction, under these conditions, as it reduces the amount of cracking and thus coking which occurs, seen from the decrease in B/X compared to virgin (Tables 5.1. and 7.1.), and the TGA results (Table 11.2.). The preferential formation of toluene disproportionation is desirable, especially with the extended catalytic life exhibited by the microwave plasma treated samples. However, under the conditions used, no individual xylene selectivity was seen. To preferentially produce the much-desired *p*-xylene isomer, structural modifications would be required. This might include changing the catalyst used, or as mentioned in Chapter 3, by selectively pre-coking the catalyst (3).

11.5. REFERENCES

(1) Bhatia S, Beltramini J, Do DD. Deactivation of Zeolite Catalysts. Catalysis Reviews: Science and Engineering 2008;31(4):431-480.

(2) Wu J, Leu L. Toluene Disproportionation and Transalkylation Reaction Over Mordenite Zeolite Catalysts. Applied Catalysis 1983;7:283-294.

(3) Tsai T, Liu S, Wang I. Disproportionation and Transalkylation of Alkylbenzenes Over Zeolite Catalysts. Applied Catalysis A: General 1999 5/17;181(2):355-398.

CHAPTER 12: CONCLUSIONS AND FUTURE WORK

12.1. CONCLUSIONS

The research contained within this thesis focused on the modifications of the zeolite mordenite as a result of microwave and plasma treatments. Structural modifications and changes to acidity were characterised using post-mortem techniques including XRD, IR and NH$_3$TPD amongst others. Catalytic activity was measured using toluene disproportionation as a probe reaction.

In Chapters 5 and 6, the regeneration of coked mordenite via novel microwave and plasma methods was explored. Under the conditions used, the results exhibited an extended catalytic life for microwave and microwave plasma regenerated samples, compared with virgin and thermally regenerated samples (Figures 5.1.-5.3.). In contrast, the DBD plasma regeneration, under the conditions used, was unsuccessful at removing all the coke (Table 5.2.) and therefore exhibited an accelerated deactivation rate compared with the virgin material (Figure 5.4.).

Following this, Chapters 7 and 8 employed these novel methods in the pre-treatment of mordenite. Under the conditions used, the results exhibited an extended catalytic life for microwave and microwave plasma pre-treated samples compared with the virgin catalyst; however, no change was seen for the catalyst treated with DBD plasma.

The development of extended catalytic life was seen in both regeneration and pre-treatment of mordenite samples via microwave and microwave plasma methods. The absence of this effect from the DBD plasma treatments indicated, under the conditions used, that the plasma was not sufficiently strong to remove all the carbonaceous deposits or penetrate the catalyst structure. That the effect was present in both microwave and microwave plasma regeneration and pre-treatment processes, revealed the presence of (residual) coke was not required to produce this effect, but that the extended life was a result of catalyst modification.

Characterisation of the catalyst samples demonstrated the extended life to be due to a change in the acidity of the mordenite samples, rather than a change in the crystalline structure. However,

structural changes were seen for the microwave treatments (Figures 5.14. and 7.9.), with heavily reduced surface areas (Tables 5.2. and 7.2.), where the processes had been too harsh and destroyed the integrity of the catalyst. This was observed visually in the pre-treatment (Figure 8.1.).

The Brønsted acidity of mordenite provides the active sites for toluene disproportionation but is also the site where cracking occurs. As cracking is one of the main processes for coke deposition in toluene disproportionation (1), the reduction in acid site concentration of the microwave and microwave plasma treated catalysts led to less cracking and hence less coke deposition. The diminished amount of coke deposited meant the catalyst pores were not blocked and therefore the acid sites remained available for toluene disproportionation, therefore extending the catalytic life cycle, as seen in the activity data (Figures 5.2.-5.3. and 7.1.-7.2.).

The strength of the acid sites in the microwave regeneration and pre-treatment appeared to become weaker, which would shift the reaction in favour of toluene disproportionation over cracking. However, the acid site strength did not appear to significantly change in the microwave plasma regeneration, and it was difficult to determine if the acid site strength had changed in the microwave plasma pre-treatment due to poor h-peak resolution.

The source of the loss of acidity was most likely dealumination of the catalyst, seen from the ssNMR data (Figures 5.17.-5.19.), and XPS results (Table 5.3.) of the microwave plasma regenerated catalyst. In the case of the microwave treated catalysts, the dealumination was certainly accompanied by sintering of the catalyst, seen in Figure 8.1.. However, ssNMR studies of the pre-treated samples and microwave regenerated sample would need to be run to confirm this.

Whilst the pre-treatment results illustrated that residual coke was not required to provide extended catalytic life, the microwave plasma pre-treatment demonstrated the benefit of treating a coked catalyst with microwave plasma treatment over a virgin sample. During the microwave plasma pre-treatment of the virgin catalyst, the internal and external BAS were destroyed (Table 7.3.). In contrast, the microwave plasma regeneration of a sample of coked mordenite only destroyed BAS on the surface of the catalyst (Table 6.2.). Whilst this may not have had an overall effect on the

catalytic activity of toluene disproportionation (Figure 11.8.), the surface specificity may have applications in other reactions or on other zeolites.

Chapters 9 and 10 explored the possibility of optimisation, by varying the microwave power input to produce the microwave plasma. The results illustrated a correlation between power input and dealumination (Figures 9.9.-9.10.), where too much power resulted in the destruction of the catalyst structure (Figures 9.6.-9.9.) and as a result, loss of catalytic activity (Figures 9.1.-9.4.).

In summary, under the conditions used, DBD plasma was not a viable method for complete regeneration of coked mordenite. Microwave and microwave plasma regeneration methods, under the conditions used, successfully regenerated the coked mordenite samples, restoring toluene conversion and led to an extended catalytic life. This was achieved by the destruction of BAS through dealumination, however in the microwave plasma regeneration, this destruction was surface specific. In terms of pre-treatment, the DBD plasma did not appear to have had any effect on the catalyst, under the conditions used. In contrast, the microwave and microwave plasma pre-treatments produced an extended catalytic life through the destruction of BAS, both internally and externally. Additionally, the microwave pre-treatment caused the catalyst to sinter. Under the conditions used, the microwave and microwave plasma treatments extended the catalytic life and decreased the concentration of acid sites, thereby shifting the reaction in favour of toluene disproportionation over cracking. However, whilst the heavily reduced coking rate extended catalytic life, it also meant there was no individual xylene selectivity. Finally, there potentially exists a matrix between the input power, concentration of oxygen, and pressure when using microwave plasma to regenerate a coked catalyst. Within the time constraints of this research, input power was exclusively investigated. From the preliminary studies performed varying the microwave input power, it was shown that there is a balance between dealuminating mordenite to extend the catalyst life cycle, and too much dealumination resulting in the destruction of the catalyst structure and its activity.

12.2. FUTURE WORK

The research contained within this thesis is built upon the phenomenon of extended catalytic life of mordenite in the toluene disproportionation reaction observed when a sample of coked mordenite was subjected to microwave plasma. Through the application of DBD plasma, microwave plasma and microwaves as novel regeneration methods, an understanding of the cause for the extended catalytic life was developed. This then led onto pre-treatment studies and the preliminary studies of microwave plasma optimisation. However, this research is still in its infancy with much more to explore. This chapter lists some of the future possibilities to continue developing this project.

12.2.1. Multiple Regenerations

The successful regeneration of a sample of coked mordenite using microwave plasma or microwaves may have extended the catalytic life of the catalyst, but eventually the zeolite would need regenerating once more. The indisputable questions which arise from this are:

- Does this extended life remain after a second microwave/microwave plasma regeneration?

- Would the extended life remain if this second regeneration was a conventional thermal regeneration?

- How many catalytic regeneration cycles would be possible before the catalyst structure was compromised, and activity was no longer restored?

Preliminary studies were performed on multiple catalytic regeneration using microwave plasma, although under different deactivation conditions from those described within this thesis. The results (provided in the Appendix) exhibited an even longer extended life upon a second regeneration, when compared to the first regeneration. In further studies, conditions would be identical to those contained within this thesis for reproducibility, repeatability and direct comparison with the other regeneration processes. Characterisation would include those

contained within this research, i.e. ssNMR, pyridine and collidine IR, BET, TGA, XPS, XRD and NH₃ TPD.

12.2.2. Further Characterisation

With additional time, characterisation would have included the following to develop an improved understanding:

- ssNMR for microwave regenerated, DBD plasma regenerated and pre-treated samples

    - *This would give an indication of the degree of dealumination occurring*

    - *From the data shown in this thesis, the expectation would be to see a higher degree of dealumination on the microwave regenerated sample than seen in the microwave plasma regenerated sample and little to no dealumination on the DBD plasma regenerated sample*

    - *More prominent dealumination would be expected for the pre-treated samples*

- Pyridine and collidine IR for the DBD plasma samples

    - *This would complete the data set and would show whether there was any change in acid site concentration.*

    - *From the data shown in this thesis, the expectation would be no change in acid site concentration*

- Raman for microwave and DBD plasma regenerated samples

    - *This would give a clearer impression of whether the coke deposited post microwave or DBD plasma regenerated changes*

    - *Is there a third peak as seen in the microwave plasma regenerated sample?*

- A more reliable and in-depth solvent extraction

    - *This would aid in building an understanding about whether the coke deposited on the microwave and plasma treated catalysts is different than on the virgin catalyst, e.g. is the coke less deactivating or spectator coke?*

- XPS on pre-treated samples and DBD plasma regenerated sample

  - *This would complete the data set for the regenerated samples, where the results would be expected to show very little difference for the DBD plasma regenerated sample*

  - *For the pre-treated samples, the results would most likely support the ssNMR studies which would be carried out (suggested above, showing the loss of aluminium from the structure)*

  - *Combined with the ssNMR, this could potentially be used in support of the IR results already displayed in this thesis*

- NH_3 TPD on DBD plasma samples

  - *This would complete the data set*

  - *Based on previous data, this would be expected to show little to no change in the acid site strength or concentration*

- Determination of TGA coke effluent via MS

  - *This would be a confirmatory test to demonstrate the combustion of coke into carbon dioxide and water*

12.2.3. Oxygen Concentration Studies

As mentioned previously, it is thought that a matrix involving oxygen concentration, pressure and power input exists when investigating microwave plasma regeneration. Optimisation studies would be performed to determine the efficiency and any additional effects of regenerating a sample of coked mordenite under increasing concentrations of oxygen. Theoretically this may lead to a faster regeneration process as there would be a higher concentration of oxygen radicals in the plasma.

12.2.4. Pressure Studies

Similar to the oxygen concentration studies, optimisation of pressure may affect the regeneration process of microwave plasma. Preliminary studies were performed ranging from 5 mbar – 50 mbar (included in the Appendix), which found pressure did not appear to have an effect on the

regeneration process. Characterisation on these catalyst samples, e.g. BET, XRD and pyridine and collidine IR, could be run to confirm this.

12.2.5. Dielectric Barrier Discharge Studies

Under the conditions used, the DBD plasma did not appear to have an effect on the catalyst. It also proved under these conditions, unsuccessful at removing all the coke from the mordenite sample. Further studies could be performed using a more energetic DBD plasma to endeavour to replicate the successful regeneration of the microwave and microwave plasma processes. If this was possible, DBD plasma may offer a more viable method of selective dealumination as it can be tuned more accurately than the microwave plasma.

12.2.6. Varying Coke Amounts

The extent of dealumination in the microwave plasma treated catalysts has been assumed, in this research, to arise from the coke species preferentially interacting with the plasma active species over the zeolite. The coke was suggested to protect the zeolite, leading to surface specific dealumination in the microwave plasma regenerated sample. To support or disprove this theory, experiments could be carried out by controlling the amount of coke deposited on the virgin zeolite, followed by microwave plasma regeneration. If true, an inverse correlation between the amount of coke and the degree of dealumination would be seen.

12.2.7. Different Zeolite

This study was exclusively performed on mordenite. However, the zeolite modification, by microwaves and microwave plasma, seen in this study might be extended to other zeolites. For example, ZSM-5 is a medium-pore zeolite which is also used in toluene disproportionation. It would be a natural extension to this research to repeat it using this zeolite.

12.2.8. Template Removal

Following optimisation of the microwave plasma, and repeating the experiment with a different zeolite, it might be possible to explore the viability of using the microwave plasma as a means of

selectively removing a template from a catalyst. If this could be performed by microwave plasma, with the conditions optimised to avoid damage to the catalyst structure, it may be a desirable alternative to conventional methods.

12.3. REFERENCES

(1) Wu J, Leu L. Toluene Disproportionation and Transalkylation Reaction Over Mordenite Zeolite Catalysts. Applied Catalysis 1983;7:283-294.

APPENDIX

TABLE OF CONTENTS

I. COPY OF SOLID STATE NUCLEAR MAGNETIC RESONANCE REPORTS

I.A. Comparison of Microwave Plasma Regenerated, Thermally Regenerated and Virgin Mordenite

JM Johnson Matthey
Inspiring science, enhancing life

Advanced Characterisation Department

Johnson Matthey Technology Centre

Blount's Court, Sonning Common, Reading, RG4 9NH

April 16, 2018

To: **Alice Halman** (UCLan)

WebALMS ⊚ **20180778**

---

^{1}H, ^{27}Al and ^{29}Si Solid State MAS NMR Analysis of Three Mordenite Zeolites

---

From: **Dr Nathan Barrow**

0118 924 2060

nathan.barrow@matthey.com

1 Introduction & Executive Summary

1.1 Summary

- Brønsted acid quantity was highest for Virgin, then Conventional, then Plasma samples.

- Framework aluminium quantity was highest for Virgin, then Conventional, then Plasma samples.

- A large amount of γ-alumina was seen.

- SAR was lowest for Virgin, then Conventional, then Plasma samples.

1.2 Aims & Background

We are looking at the modifications on coked H-mordenite caused by an exposure to an argon/oxygen plasma. By using the oxygen containing plasma to regenerate the catalyst, we have seen the activity (toluene disproportionation) of the catalyst is not only restored, but has increased. One possibility is that the plasma may have caused dealumination to occur. The virgin mordenite sample was provided by JM. The conventionally regenerated sample has been deactivated via toluene disproportionation (TDP) and regenerated in a furnace under air. This process was performed twice. The plasma regenerated sample has been deactivated via TDP and regenerated in an oxygen-containing plasma. This process was performed twice.

The samples covered by this requisition are given in table 1. The unique ID refers to the data location on the spectrometer as a folder name and experiment number. The date each experiment finished is also shown.

2 Results & Discussion

2.1 ^{1}H MAS NMR

The processed spectra are given in figure 1. The Plasma sample appeared to have a lower than expected intensity for some reason (spectra are normalised by mass and number of scans), but scaling all spectra to the SiOH peak allows a comparison to

Table I. Datasets and samples covered by this requisition.

Unique ID	Sample	Acquired On
W/1H/20180778/7	440-SP1 Mordenite virgin	2018-04-13
W/1H/20180778/8	440-SP2 Mordenite conventional regeneration	2018-04-13
W/1H/20180778/9	440-SP3 Mordenite plasma regeneration	2018-04-13
W/27Al/20180778/1	440-SP1 Mordenite virgin	2018-04-12
W/27Al/20180778/2	440-SP2 Mordenite conventional regeneration	2018-04-12
W/27Al/20180778/3	440-SP3 Mordenite plasma regeneration	2018-04-12
W/29Si/20180778/2	440-SP1 Mordenite virgin	2018-04-14
W/29Si/20180778/4	440-SP2 Mordenite conventional regeneration	2018-04-15
W/29Si/20180778/6	440-SP3 Mordenite plasma regeneration	2018-04-16

be made. Both Conventional and Plasma samples contained slightly more AlOH sites than the Virgin sample. The Virgin zeolite gave the most Brønsted acid sites, followed by Conventional and then Plasma. There did not appear to be a significant shift in Brønsted acid strength, but pyridine FTIR or ammonia TPD experiments would be more sensitive to that characteristic.

Saturation-recovery data fitted to stretched exponentials are given in figure 2. Whilst the Virgin and Plasma had similar rates the Conventional zeolite relaxed faster, which could indicate greater local disorder.

2.2 ^{27}Al MAS NMR

The processed spectra are given in figure 3. The framework and extra-framework zeolite peaks sit on top of a broad background of AlO_4 and AlO_6 environments, probably from γ-alumina. Nevertheless, the Conventional and Plasma samples showed less framework aluminium compared to the Virgin zeolite, which is consistent with dealumination. Interestingly, less EFAl was seen for the Plasma zeolite compared to the other samples.

2.3 ^{29}Si MAS NMR

The processed spectra are given in figure 4. Although the mordenite framework has four T-sites, they are appear close enough to each other that the spectra can be deconvoluted into three environments; **Si**$(OSi)_4$ (-114 ppm), **Si**$(OSi)_3$OAl
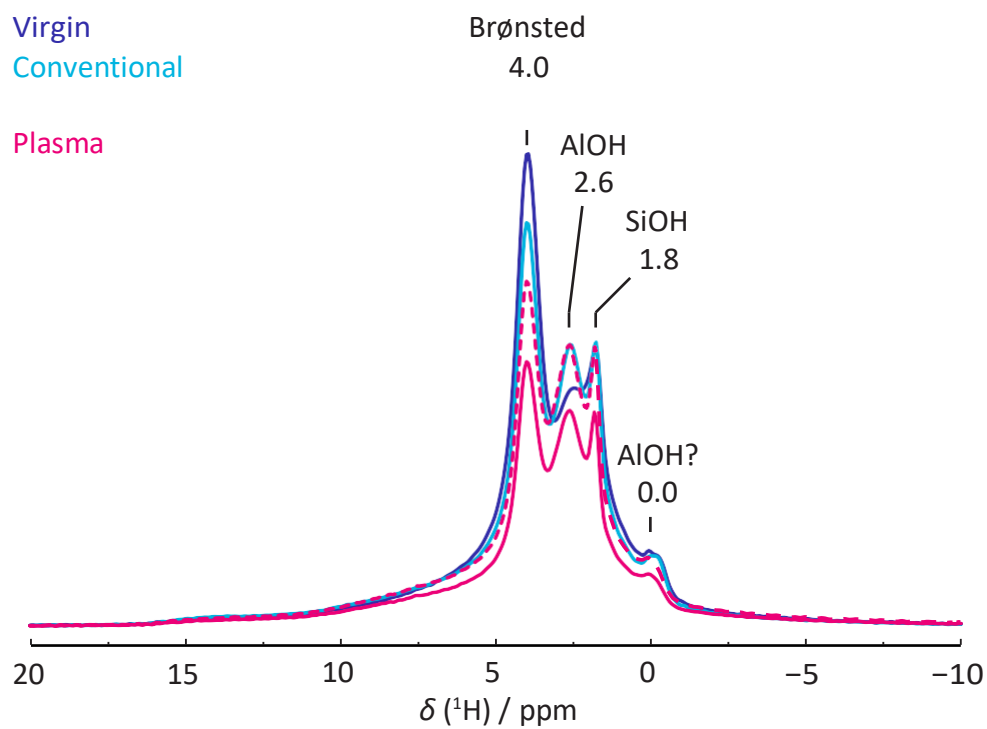
Figure 1. Normalised ^{1}H solid-state MAS NMR spectra. Dashed line is the "Plasma" scaled to the SiOH peak height of the other samples.
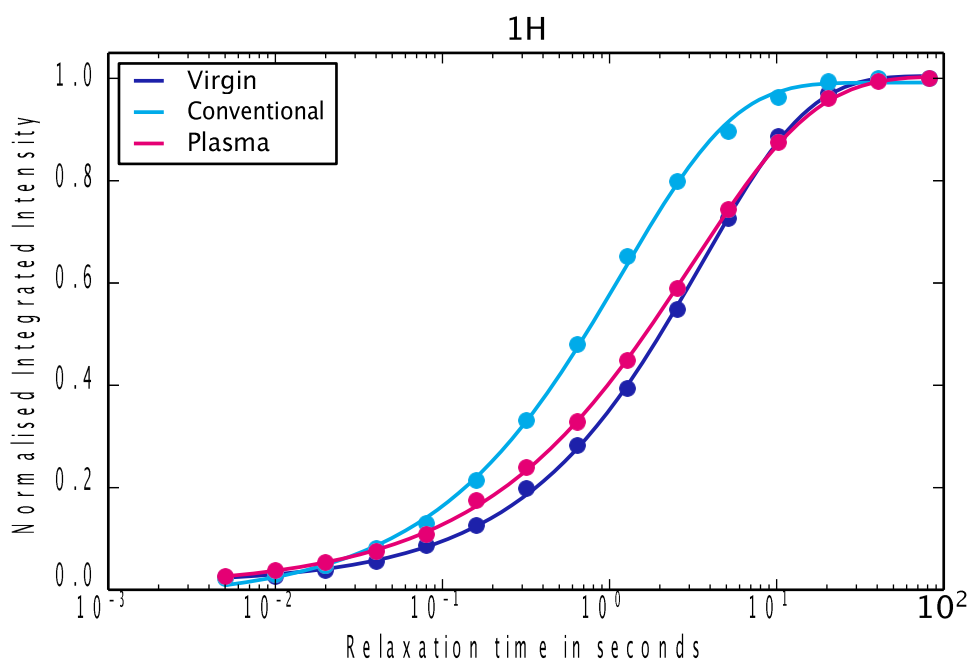
Figure 2. Saturation-recovery data fitted to stretched exponentials.
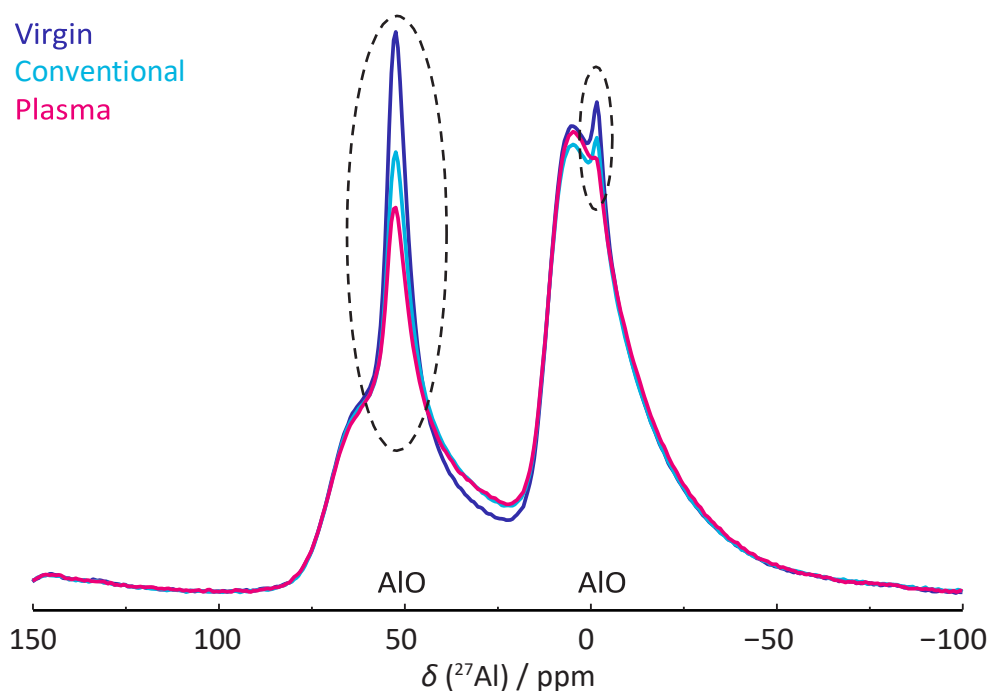
Figure 3. Normalised ^{27}Al solid-state MAS NMR spectra. Dashed ellipses highlight areas where zeolite signal appear.

(-108 ppm) and **Si**(OSi)$_2$(OAl)$_2$ (-100 ppm). The spectra were deconvoluted using DMFit, to three Gaussian lineshapes. Silica to alumina ratios (SAR) were found using equation 1. As **Si**(OAl)$_n$ and **Si**(OH)$_n$ sites may overlap, SAR values found using this method may be underestimated. An increase in SAR was observed, with Plasma having the highest, then Conventional, then Virgin. Again, this is consistent with dealumination. All ^{29}Si T_1 values were similar, around 1.7 s.

$$\frac{SAR}{2} = \frac{Si}{Al} = \frac{\sum_{n=0}^{4}\left(Si(nAl)\right)}{\sum_{n=0}^{4} 0.25n\left(Si(nAl)\right)} \tag{1}$$

3 Experimental Method

SSNMR spectra were acquired at a static magnetic field strength of 9.4 T ($v_0(^1H) = $ 400 MHz) on a Bruker Avance III console using TopSpin 3.1 software. For ^{1}H, the
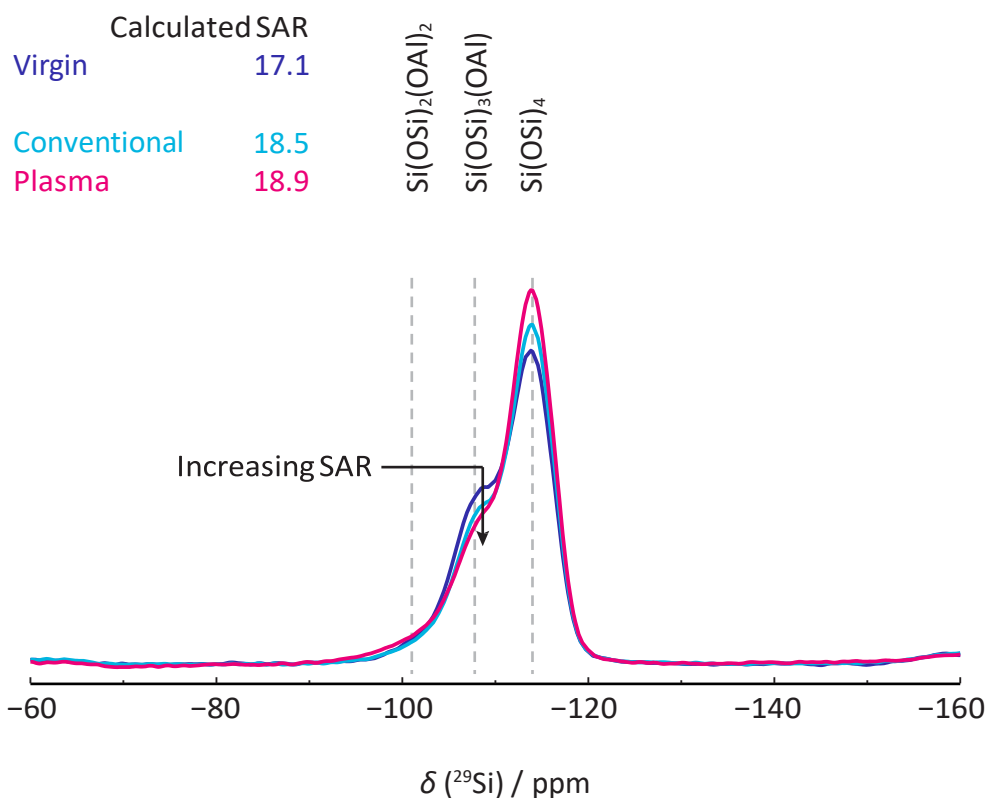
Figure 4. Normalised ^{29}Si solid-state MAS NMR spectra.

probe was tuned to 400.16 MHz and referenced to d16 adamantane at 1.73 ppm. For ^{27}Al, the probe was tuned to 104.27 MHz and referenced to YAG at 0.0 ppm. For ^{29}Si, the probe was tuned to 79.49 MHz and referenced to kaolinite at −91.2 ppm. Powdered samples were packed into zirconia MAS rotors with Kel-F caps, with before and after weighings providing the sample mass. The rotors were spun using room-temperature purified compressed air. Sample advised hazards were assessed. The total experiment time to acquire these spectra was 67 hours.

To enable reproducibility and quantification, the experimental parameters for each dataset are given in table 2. An explanation of the variables is available on myJM.

Table 2. Experimental parameters for solid-state MAS NMR experiments performed on a Bruker Avance III spectrometer.

Unique ID	Sample	MASR in Hz	D1 in s	Scans	Mass in mg
W/1H/20180778/7	Virgin (vacuum dried)	14 000	37.9	64	61.5
W/1H/20180778/8	Conventional (vacuum dried)	14 000	14.2	64	68.0
W/1H/20180778/9	Plasma (vacuum dried)	14 000	47.6	64	68.5
W/27Al/20180778/1	Virgin (hydrated)	14 000	0.1	8192	81.5
W/27Al/20180778/2	Conventional (hydrated)	14 000	0.1	8192	85.3
W/27Al/20180778/3	Plasma (hydrated)	14 000	0.1	8192	78.9
W/29Si/20180778/2	Virgin (dried 110 °C)	4000	18.3	4136	154.1
W/29Si/20180778/4	Conventional (dried 110 °C)	4000	12.3	6168	157.8
W/29Si/20180778/6	Plasma (dried 110 °C)	4000	14.6	5356	159.3

I.B. Microwave Plasma Regeneration Using Varying Amounts of Input Power

Table I. ^{27}Al quantification at 14.1 T. Total integral from 80 ppm to -15 ppm and AlO$_6$ integral from 15 ppm to -15 ppm.

Sample	Total Relative Intensity ($\pm$3%)	AlO$_6$ Intensity ($\pm$3%)
Virgin	100%	52%
150C	91%	52%
250C	87%	54%
300C	96%	56%
350C	91%	57%
450C	91%	57%
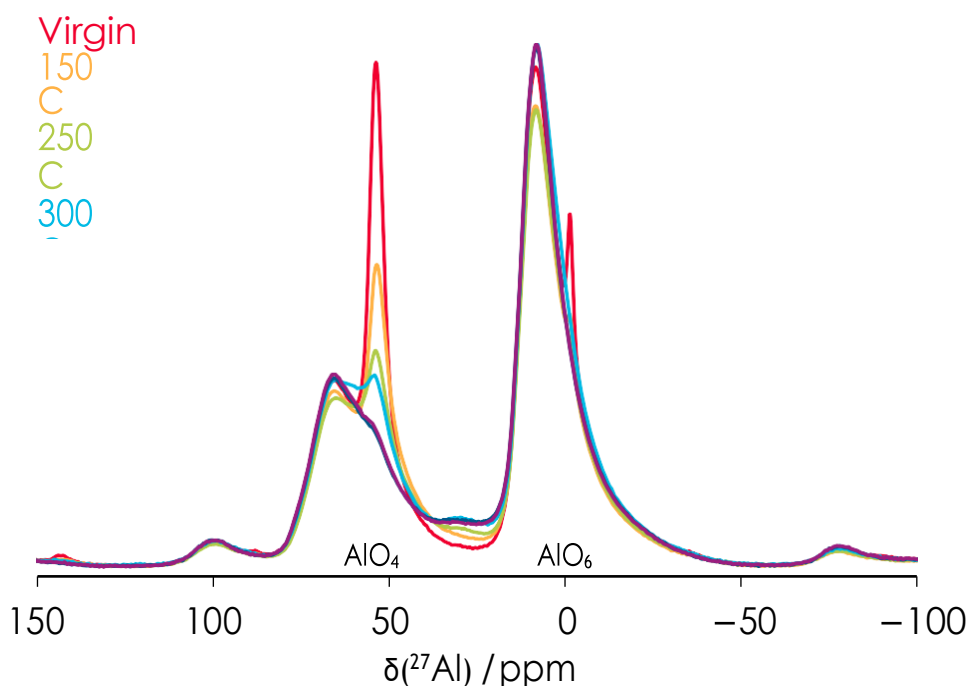
Figure I. Normalised ^{27}Al solid-state MAS NMR spectra.

The processed spectra are given in Fig. 1 and extra-framework aluminium "quantitation" is given in Tab. 1. Although steps were taken to avoid errors in quantitation (short pulse length, soft pulse power, long relaxation time, fast spinning), the sites still overlap. Furthermore, the intensity of the spinning sidebands from the 4-coordinated aluminium have been neglected. Hence, the "quantitation" is merely an integration of two areas of the spectra, which is thought to be physically meaningful.

JM

Johnson Matthey
Inspiring science, enhancing life

Advanced Characterisation

Johnson Matthey Technology Centre

Blount's Court, Sonning Common, Reading, RG4 9NH

April 27, 2018

To: **Steve Pollington, JMTC N**

WebALMS number: **20180777**

XPS Analysis of Zeolite Mordenite Samples

From: **Dr. Tuğçe Eralp Erden**
+44(0) 118 924 2163
eralpt@matthey.com

Overview

External and internal surfaces of three samples were studied, a general comparative study was carried out.

Samples submitted for XPS analysis

Req ID	Customer label	Description	Notes
1	RT/GB/18/SP/439-SP1	Virgin (V)	
2	RT/GB/18/SP/439-SP2	Conventional Regeneration (C)	
3	RT/GB/18/SP/439-SP3	Plasma Regeneration (P)	Dark and Light Int parts

Analysis Requested

Al : Si ratios and oxidation states, general surface quantification.

Sample Preparation and Area of Interest

The samples were placed onto carbon tape and thereby attached to a sample stub. Care was taken to avoid signals from the tape contributing to the study. Sample advised hazards were assessed prior to analysis.

Data Analysis

Energy scales were corrected to the aluminum $2p$ signals (74.5 eV).

Data Collection and Further Information

The data were collected using the standard method (see MyJM XPS Report page). For further information about the technique please see the MyJM XPS page.

Results and Observations

Quantification Tables

Table 1. Surface At%'s. 0.0* in the table represents At%'s < 0.05%.

Element	1V Ext	1V Int	2C Ext	2C Int	3P Ext	3P Int Ext	3P Int Int	Comments
Oxygen	60.5	60.2	59.2	59.5	60.4	59.4	58.7	Various
Aluminiu	25.5	27.8	24.9	27.2	22.7	28.0	27.2	Al-O
Silicon	7.9	6.4	8.5	7.1	11.6	6.1	7.3	Si-O
Carbon	3.5	3.5	4.4	3.9	3.7	3.8	4.1	C-C and C-
Fluorine	2.0	1.9	2.5	2.1	1.4	2.5	2.3	Inorganic
Nitrogen	0.2	0.2	0.3	0.3	0.2	0.2	0.2	Ammonium
Sodium	0.2	0.0	0.1	0.0	0.1	0.0	0.0	
Chlorine	0.1	0.1	0.1	0.1	0.1	0.1	0.1	
Al : Si	3.2	4.3	2.9	3.8	2.0	4.6	3.7	
Al : C	7.3	8.0	5.6	6.9	6.2	7.5	6.7	

Interpretation of Surface Chemistry

For all the samples, Al : Si ratios for the externals surface of the samples are lower compared to the internal surfaces (Table 1). There is sodium present on the surface of all the external surfaces for the samples but not for the internal surfaces. For the external surface of the plasma regeneration sample, Al : Si ratio is significantly lower indicating a higher silicon content compared to the other samples.

Aluminium 2p signals are used for binding energy scale correction (all the maxima shifted to 74.5 eV), they are due to aluminium-oxygen interactions (Figure 1).

Silicon 2p signals appear at around 103.0 eV and they are due to silicon-oxygen interactions (Figure 2). For the external surface of the plasma sample (3 ext), silicon signal's shifted to the lower binding energy side by 0.3 eV which could indicate a more negative charge around the silicon atoms compared to the other samples.

Oxygen signals are mainly due to aluminium-oxygen interactions with a contribution from silicon-oxygen and carbon-oxygen interaction (Figure 3). Carbon 1s signals are similar for all the samples indicating carbon-carbon (main) and carbon-oxygen interactions.

For general quantification of the elements present on the surface, please see Table 1.
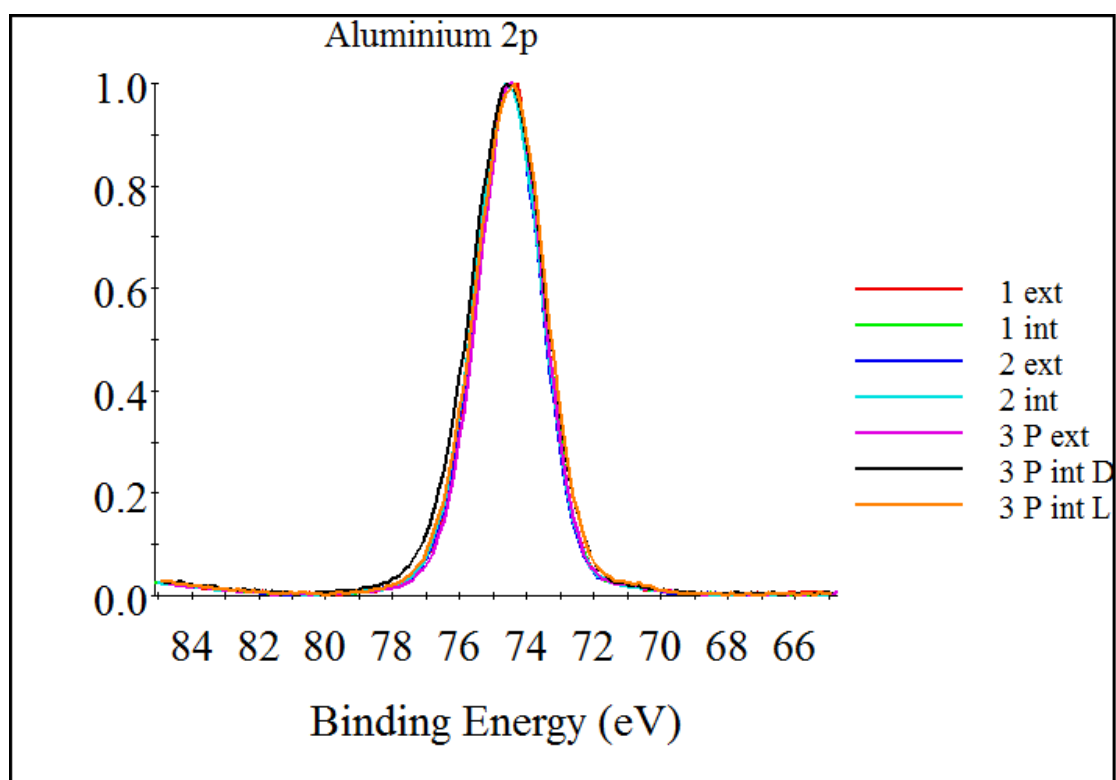
Figure 1. Aluminum $2p$ spectra from the samples. Intensities are normalised. Binding energy scales are corrected.
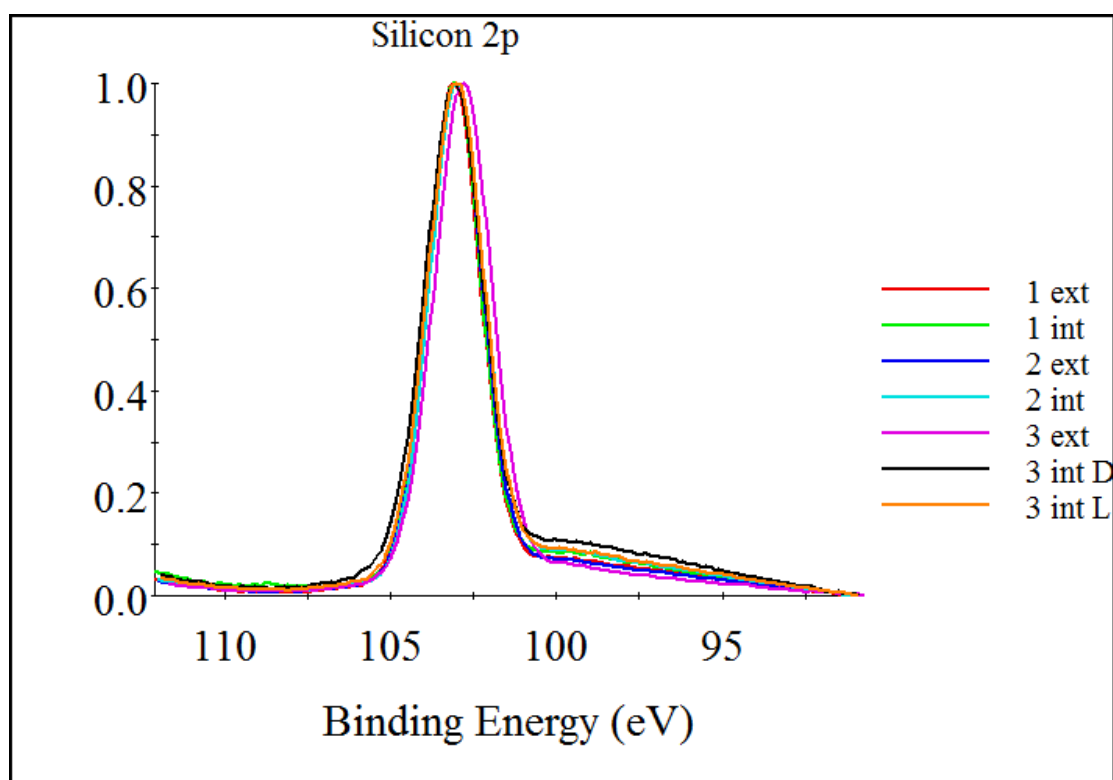
Figure 2. Silicon $2p$ spectra from the samples. Intensities are normalised. Binding energy scales are corrected.
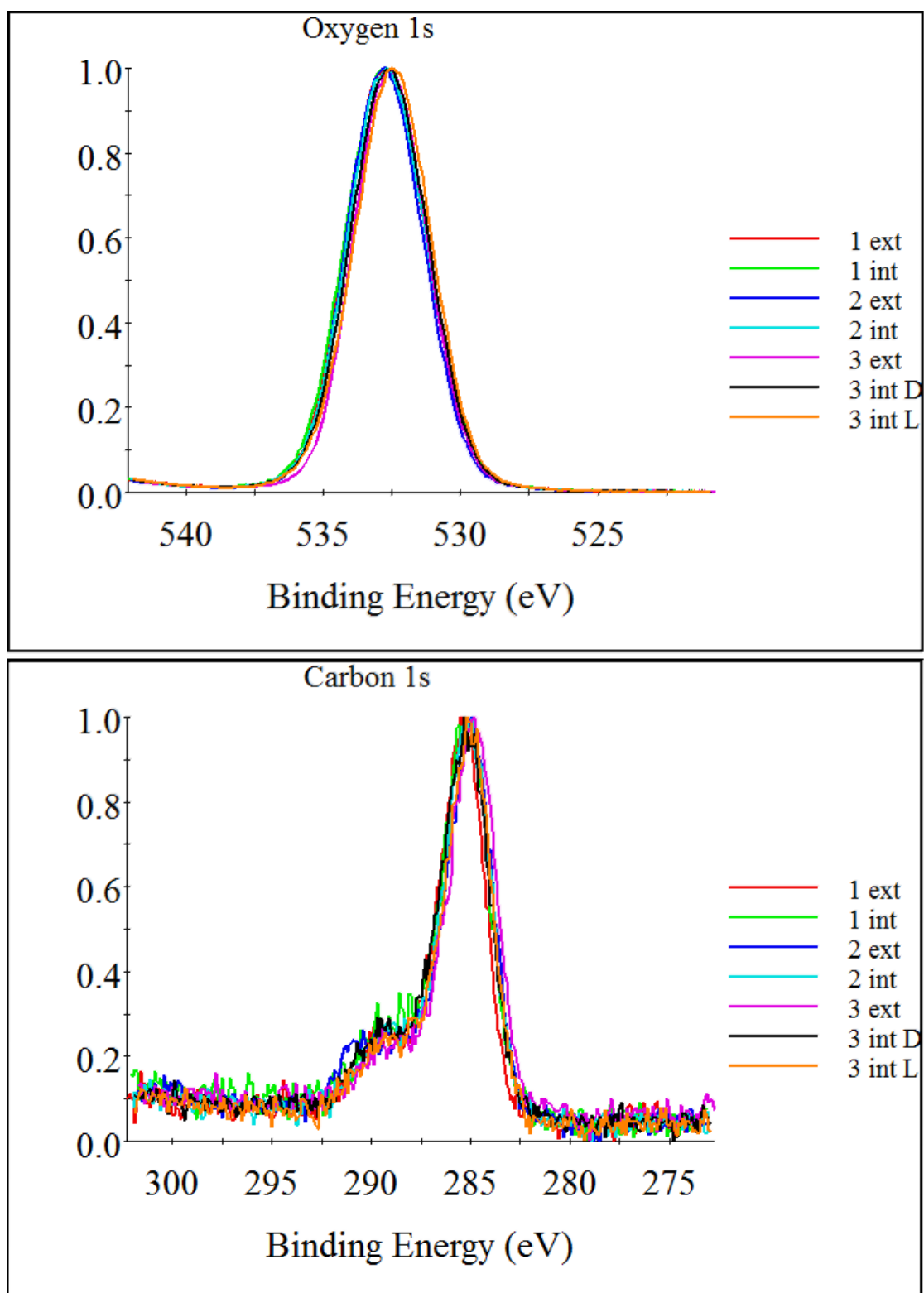
Figure 3. Oxygen 1*s* and carbon 1*s* spectra from the samples. Intensities are normalised. Binding energy scales are corrected.

III. ADDITIONAL RESULTS

III.A. ACTIVITY PROFILES OF MULTIPLE REGENERATIONS

Multiple regeneration describes the repeated deactivation of virgin mordenite samples by toluene disproportionation and their regeneration using either thermal or microwave plasma methods (as described in Section 4.1.2.). The activity profile given was produced from coked mordenite samples which had been regenerated a total of two times and were subjected to a third toluene disproportionation. This experiment was carried out under the same conditions as contained within the main body of the thesis, except the toluene reservoir was not kept under ice bath conditions, but instead was heated with a water bath to a constant temperature of 35°C.
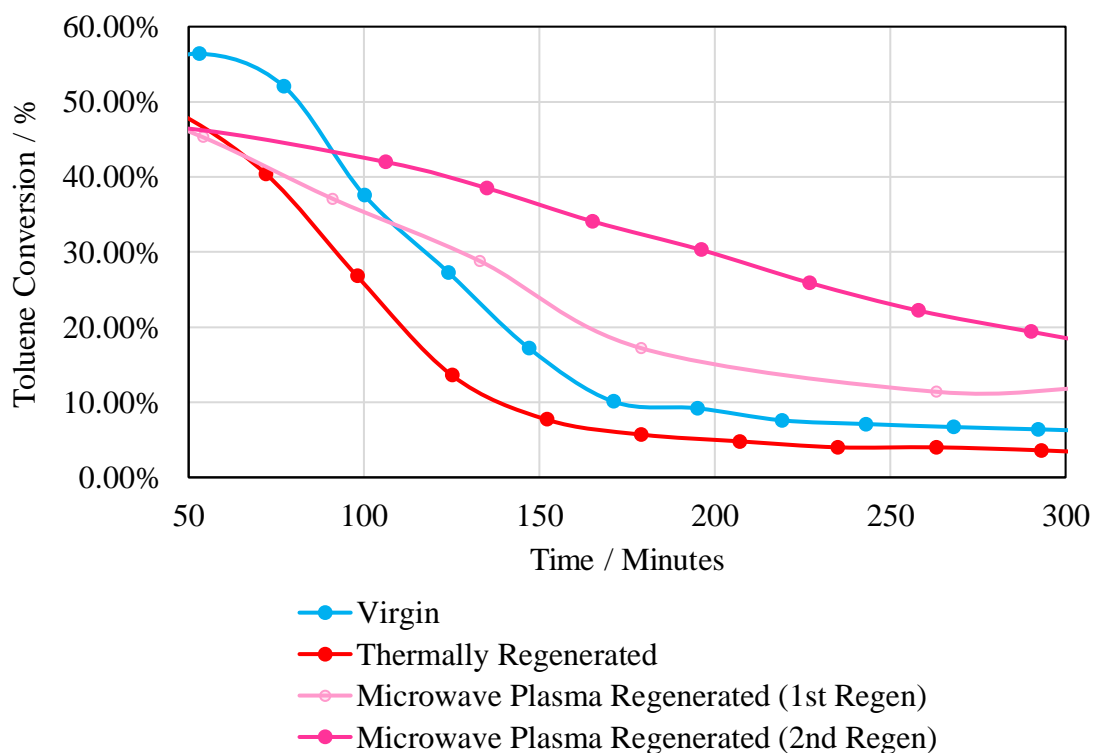
III.B. ACTIVITY PROFILES OF VARYING PRESSURE

Microwave plasma regeneration under the conditions set out within Section 4.1.2. were carried out, varying the pressure between 5 mbar and 50 mbar. The activity profile given displays the results of a second toluene disproportionation after regeneration.